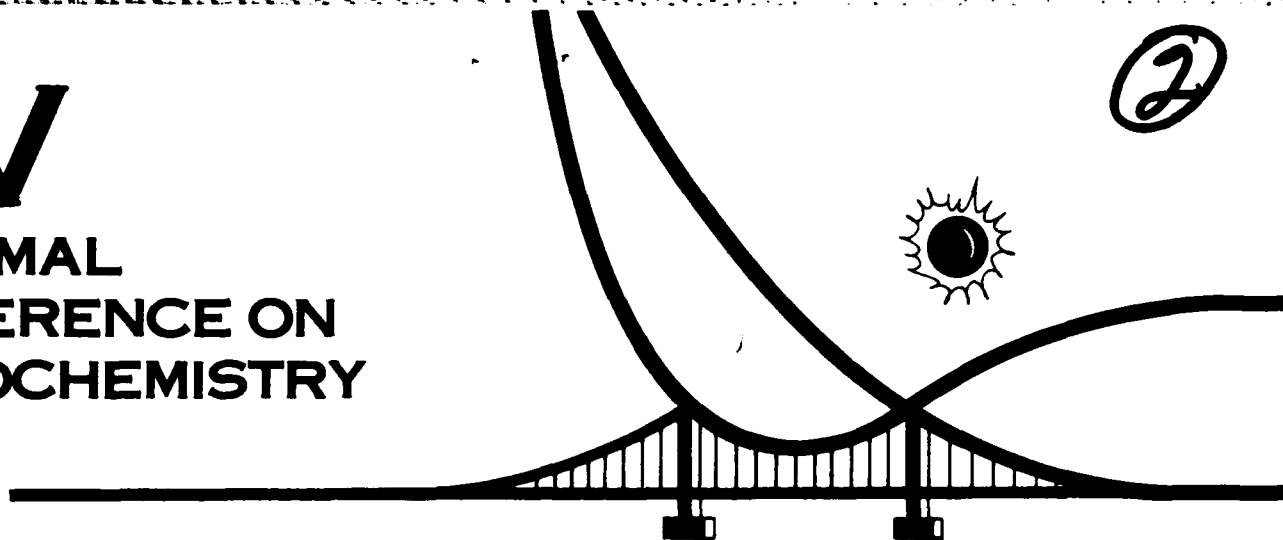


XV

INFORMAL CONFERENCE ON PHOTOCHEMISTRY

②



AD A 1 3 0 6 7 7

ABSTRACTS

STANFORD, CALIFORNIA
JUNE 27 - JULY 1, 1982

DTIC FILE COPY

DTIC
ELECTE
JUL 1 1 1983
S E

83 07 08 055



CO-CHAIRMAN: D. M. GOLDEN & T. G. SLANGER

This document has been approved
for public release and sale; its
distribution is unlimited.

**XVTH INFORMAL CONFERENCE
ON PHOTOCHEMISTRY**

Stanford, California June 27 - July 1, 1982

**We gratefully acknowledge sponsorship of this
conference by:**

**NATIONAL AERONAUTICS AND SPACE ADMINISTRATION
(Upper Atmosphere Program)**

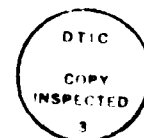
**ARMY RESEARCH OFFICE
(Chemistry Division)**

**NATIONAL SCIENCE FOUNDATION
(Atmospheric Chemistry Division)**

OFFICE OF NAVAL RESEARCH

**Co-Chairmen: Tom G. Slanger
David M. Golden**

Accession For	
NTIS GRA&I	<input checked="checked" type="checkbox"/>
DTIC TAB	<input type="checkbox"/>
Unannounced	<input type="checkbox"/>
Justification	
By _____	
Distribution/ _____	
Availability Codes	
Dist	Avail and/or Special
A	



XV INFORMAL CONFERENCE ON PHOTOCHEMISTRY

Stanford, California - June 27-July 1, 1982

SCHEDULE

All sessions in Terman Engineering Bldg.

Sunday	Posters	7:00-9:00
Monday	Unimolecular Reactions	8:00-12:00
	Atmospheres	1:30-5:10
	Posters	7:45-9:45
Tuesday	Bimolecular Reactions	8:30-12:00
	Bimolecular Reactions	1:30-3:00
Wednesday	Condensed Phase	8:15-9:45
	Energy Transfer	10:15-12:45
	Posters	1:45-3:45
Thursday	Photophysics	8:15-9:45
	Spectroscopy	10:15-12:45

Sunday June 27

Poster Session I - 7-9 p.m.

- A-1 Alkyl Nitrate Formation from the NO_x - Air Photo-oxidation of C_2 - C_8 n-Alkanes
Roger Atkinson, Sara M. Aschmann, William P. L. Carter, A. M. Winer and J. N. Pitts, Jr.
- A-2 The Determination of Specific Rate Constants for Triplet-Triplet Annihilation in Rigid Solutions of 1,2-Benzanthracene Using Pulsed Laser Excitation and Triplet-Triplet Absorption
R. D. Burkhart
- A-3 Laser Fluorescence Spectroscopy of NCO.
Brian J. Sullivan, Gregory P. Smith, and David R. Grosley
- A-4 Preparation and Characterization of Vibrationally Excited Molecular Ions in Thermal Energy Charge Transfer Reactions
G. Mauclaire, R. Deraï, and R. Marx
- A-5 Rare-Gas Oxide Van der Waals Molecule Formation by Photodissociation of Triatomic Molecules Trapped in Rare Gas Matrices at Low Temperature
J. Fournier, D. Maillard, H. H. Mohammed, C. Girardet, J. Deson
- A-6 CO_2 Laser Induced Multiple Photon Dissociation of Molecular Ions
J. S. Chou, Y. Haas, H. Reisler, D. Sumida, and C. Wittig
- A-7 Direct Rate Measurement on the Reaction: $\text{D} + \text{OH} \rightarrow \text{OD} + \text{H}$ Between 300 K and 515 K.
Mark J. Howard and Ian W. M. Smith
- A-8 Kinetics of the Reaction $\text{O} + \text{HO}_2 \rightarrow \text{OH} + \text{O}_2$ From 229 to 372 K
Leon F. Keyser
- A-9 The $\Pi^* \rightarrow n$ Spectrum of Jet-Cooled Acetaldehyde
Marcus Noble, Eric C. Apel, Edward K. C. Lee
- A-10 Unimolecular Decay of Toluene
R. J. Buss, D. J. Krajnovich and Y. T. Lee
- A-11 Predicting the Rate of OH-Addition to Aromatics Using σ^- -Electrophilic Substituent Constants for Mono- and Polysubstituted Benzene
Cornelius Zetzsch

- A-12 Kinetic Studies of F-Atom Reactions and of Vibrational Relaxation of HF (v_6) by Time-Resolved Infrared Chemiluminescence Following Pulsed Laser Photolysis
Martin K. Osborn, Ian W. M. Smith and David J. Wrigley
- A-13 The Chemistry of the Gaseous Ethynyl Radical: Direct Observation of the $A^2\Pi$ State
T. A. Watson, F. Shokoohi, H. Reisler, and C. Wittig
- A-14 Rate Constants for the Recombination Reactions
 $OH + OH(+M) \rightarrow H_2O_2(+M)$ ($M = N_2$) and $OH + H + M \rightarrow H_2O + M$ ($M = He$)
R. Zellner, K. Erler, R. Paschke and G. Wagner

Monday June 28

8:00	Conference Opening	D. M. Golden
8:10	Welcome	W. F. Miller, President SRI International
8:20	Remarks	T. G. Slanger

THIS REPORT DEALS WITH: Unimolecular Reactions, I

Chairman, T. G. Slanger

8:30	B-1	Thermal Unimolecular Reactions H. M. Frey
9:00	B-2	Two-photon Photodissociation Dynamics of NO ₂ R. J. S. Morrison and <u>E. R. Grant</u>
9:15	B-3	Rotationally Excited CO From Formaldehyde Photodissociation <u>Pauline Ho</u> and Arlee V. Smith
9:30	B-4	Photochemistry of Acetylene at 1849Å H. Okabe
9:45	B-5	Thermal Decomposition of Oxetan and Oxetan-D ₂ Zs. Huntyadai-Zoltán, L. Zalotai, T. Bérces and <u>F. Márta</u>
10:00		Coffee Break

Unimolecular Reactions II

Chairman - J. Heicklen

10:30		W. A. Noyes, Jr. - A Remembrance - J. Heicklen
10:40	C-1	Unimolecular Reactions with Non-Thermal Activation J. Troe
11:10	C-2	Photofragment Spectroscopy of Ultracold NO ₂ at 355nm: Internal Energy Distributions of NO A. P. Baronavski, <u>Benjamin M. DeKoven</u> , and H. Helvajian
11:25	C-3	A Search for Mode-Selective Chemistry: The Unimolecular Dissociation of t-Butyl Hydroperoxide Induced by Vibrational Overtone Excitation David W. Chandler, <u>William E. Farneth</u> , and Richard N. Zare
11:40	C-4	Molecular Beam Study of Glyoxal Predissociation From the S ₁ State <u>J. W. Hepburn</u> , L. J. Butler, R. J. Buss and Y. T. Lee

- 11:45 C-5 Laser Induced Photochemistry in a Supersonic Expansion
Michael Heaven, Terry A. Miller, and V. E. Bondybey
- 12:10 Lunch
- Atmospheres I
Chairman - R. T. Watson
- 1:30 M. A. A. Clyne - A Remembrance - R. T. Watson
- 1:40 D-1 Tropospheric Chemistry: A Kineticist's View
A. R. Ravishankara
- 2:10 D-2 Observations of Free Radicals in the Earth's Stratosphere:
Recent Advances in Studies of ClO and OH
J. G. Anderson and R. M. Stimpfle
- 2:25 D-3 Sensitivity of an Urban Photochemical Model to Changes in
Meteorology
Joyce E. Penner
- 2:40 D-4 The Photolysis of Acetaldehyde Under Atmospheric Conditions
H. Meyrahn, G. K. Moortgat and P. Warneck
- 2:55 D-5 Atmospheric Sources of Nitrous Oxide-Solar Resonant Excitation
of Metastables OH(A) and N₂(A)
Sheo S. Prasad and Edward C. Zipf
- 3:10 Coffee Break
- Atmospheres II
Chairman - W. B. DeMore
- 3:30 E-1 The Role of Atmospheric Photochemistry In Biogeochemical
Cycles
P. J. Crutzen
- 4:00 E-2 Product Identification and Quantum Yield Determination in
N₂O₅ Photolysis at Several Discrete Wavelengths Between 249 nm
and 300 nm
Peter S. Connell, Frank Magnotta, Diane Swanson, and Harold
Johnston
- 4:15 E-3 ClONO₂ Photolysis: Direct Detection of Primary Products
James J. Margitan
- 4:30 E-4 An FTIR Study of the Cl-Atom and HO-Radical Reactions of
CH₃OOH
Hiromi Niki, P. D. Maker, C. M. Savage, and L. P. Breitenbach
- 4:45 E-5 Atmospheric Photodissociation and Related Experimental
Parameters
Marcel Nicolet

Poster Session II - 7:45-9:45 p.m.

- F-1 Reversible Electron Transfer Reactions of the $\text{RuL}_3^{2+}/\text{Cu(II)}$ System in Various Solvents
B. A. DeGraff, Pat Morris, Phil Britt, and J. N. Demas
- F-2 Absolute Rate Constants for the Reactions of $\text{CH(X}^{2\Pi})$ with NO , N_2O , NO_2 and N_2
S. S. Wagal, T. Carrington, S. V. Filseth, and C. M. Sadowski
- F-3 Radiative and Predissociative Lifetimes of the $v'=0$ Level of the $\text{A}^2\Sigma^+$ State of SH and SD from Chemical and Spectroscopic Studies
Randall R. Friedl, Wm. H. Brune, and J. G. Anderson
- F-4 Rotationally Resolved Laser Excitation Spectra of Pb_2 , Sn_2 and Se_2
M. C. Heaven, V. E. Bondybey, and Terry A. Miller
- F-5 Photodissociation Dynamics of Pulsed Molecular Beams
Richang Lu, Joshua B. Halpern and William M. Jackson
- F-6 Background Reactivity Estimates for Atmospheric Modeling Studies
J. P. Killus
- F-7 Photodissociation Processes of CS_2 at 1060-1520 Å
R. L. Day, Masako Sutoh, and L. C. Lee
- F-8 Multiphoton Excitation of Diethyl Ether
L. Butler, R. J. Buss, R. Brudzynski and Y. T. Lee
- F-9 Statistical Limit Quenching of S_1 Pyrimidine
G. Loge
- F-10 Vacuum Ultraviolet Photolysis of H_2O and NO_2
J. B. Nee and J. G. Anderson
- F-11 The Reaction of OH with CO. The Pressure Dependence of the Rate Constant
G. Paraskevopoulos and R. S. Irwin
- F-12 Low-Temperature Chemistry of a 1,3-Biradical
John H. Penn, Detlef Döhnert, and Josef Michl
- F-13 The Reaction of Hot H Atoms with CO_2
C. R. Quick, Jr. and J. J. Tjee
- F-14 Quenching of $\text{CF} (^1\text{B}_1)$ and $\text{CF}_2 (^3\text{B}_1)$ Emission in the Reaction of Ozone with Tetrafluorethene
S. Toby and F. S. Toby
- F-15 The Reaction of Methyl Radicals with Oxygen at Low Pressure
K. D. Bayes, E. A. Schultz, M. J. Pilling, M. MacPherson, and M. Smith

Tuesday June 29

Bimolecular Reactions I *Sc. 1. X*
Chairman - C. Zetzsch

- 8:30 G-1 The Transition State Model for Bimolecular Reactions. Loose and Tight Complexes
S. W. Benson
- 9:00 G-2 Rates and Product Channels of the Reactions of HO₂ with O- and H-Atoms at 298 K
U. C. Sridharan, L. X. Qui, and F. Kaufman
- 9:15 G-3 CO₂ Laser Photolysis of C₆F₅X Compounds - A Useful Source of Free Radicals for Chemical Kinetic Studies
Irene R. Slagle and David Gutman
- 9:30 G-4 A Laser-Photolysis/Resonance Fluorescence Study of the Rate of The Reactions of OH with HNO₃, PH₃, C₂H₄O, C₆H₆ and Naphthalene
K. Lorenz and R. Zellner
- 9:45 G-5 Vinylidene Radicals: Long May They Live
A. H. Laufer
- 10:00 Coffee Break

Bimolecular Reactions II
M. C. Castex - Chairman

- 10:30 H-1 Non-Thermal Bimolecular Reactions
J. Wolfrum
- 11:00 H-2 Chemiluminescence of PH₃, AsH₃ and SbH₃ With Ozone
Donald H. Stedman and Mark E. Fraser
- 11:15 H-3 Effect of Ring Strain on Gas Phase OH Radical Reaction Rate Constants with Bi- and Tri-Cycloalkanes at 299 ± 2 K
Roger Atkinson, Sara M. Aschmann and W. P. L. Carter
- 11:30 H-4 Arrhenius Parameters for the Gas Phase Reactions of C₃ With Selected Olefins Over the Temperature Range 300-650 K
H. Helvajian, H. H. Nelson, L. Pasternack and J. R. McDonald
- 11:45 H-5 Abstraction vs Exchange in the Reaction of D + HCl
John C. Miller and Robert J. Gordon
- 12:00 Lunch

Bimolecular Reactions III

Chairman - G. P. Smith

- 1:30 I-1 Theoretical and Experimental Studies of the Reaction:
 $\text{Mg}(^1\text{P}_1) + \text{H}_2 \rightarrow \text{MgH}(\text{v},\text{N}) + \text{H}$
W. H. Breckenridge, N. Adams, and H. Umemoto
- 1:45 I-2 Recent Applications of Flash Photolysis Resonance
Fluorescence to Stratospheric Chemical Kinetics
Michael J. Kurylo
- 2:00 I-3 Kinetics of Hydroxyl Radical Reactions with Alkanes
Larry G. Anderson and Robert D. Stephens
- 2:15 I-4 Laser Initiated Chain Reactions of Br_2 and Cl_2 with HI
David A. Dolson and Stephen R. Leone
- 2:30 I-5 Temperature Dependence of Rate Constants for the Reaction
 $\text{OH} + \text{SO}_2 + \text{M} \rightarrow \text{HOSO}_2 + \text{M}$
Ming-Taun Leu
- 2:45 I-6 Lifetimes of Acetaldehyde ($^3\text{A}''$) and its Deuterated Analogues
in the Vapor Phase
Merlyn D. Schuh, Mark P. Thomas, T. John Trout, and
Warren F. Beck

Wednesday June 30

Condensed Phase,
Chairman - R.D. Burkhart

- 8:15 J-1 Picosecond Intermediates of Chemical Reactions
P. Rentzepis
- 8:45 J-2 Fluorescence Quenching of Aromatic Liquids at Energies Above
and Below The Photoionization Threshold
Frederick P. Schwarz and Michael Mautner
- 9:00 J-3 Non-Linear Photoreduction of Ytterbium (III) and Samarium
(III)
Terence Donohue
- 9:15 J-4 Photochemical Generation of $(HO_2)_2$ and $H(C=O)OO$ from
Formaldehyde and Glyoxal in an O_2 Matrix
Tai-Ly Tso, Michael Diem and Edward K. C. Lee
- 9:30 J-5 Photoionization Versus Bond Homolysis in Polyatomic Molecules
in Condensed Phase
Michel J. Rossi
- 9:45 Coffee Break

Energy Transfer; *Go to XV*
Chairman - G. Black

- 10:15 K-1 Large Molecule Intermolecular Energy Transfer in the
Electronic Ground State: New Techniques for Non-Reactive
Systems
J. R. Barker
- 10:45 K-2 Vibrational Energy Relaxations in Small Molecules
I. W. M. Smith
- 11:15 K-3 Vibrational Excitation of Molecules by Collisions with "Hot"
Hydrogen Atoms
R. E. Weston, Jr., C. R. Quick, Jr., S. D. Ghosh,
G. W. Glynn, J. Chu
- 11:30 K-4 Vibrational Redistribution in S_1 p-Difluorobenzene
R. A. Coveleskie, D. A. Dolson, S. C. Munchak, and
C. S. Parmenter
- 11:45 K-5 Inelastic and Reactive Scattering of Metastable Rare Gas
Atoms
K. M. Johnson, R. Pease and J. P. Simons

12:00 K-6 Orange Chemiluminescence from NO₂
R. D. Kenner and E. A. Ogryzlo

12:15 Lunch

Poster Session III - 1:45-3:45 p.m.

- L-1 Laboratory Studies of Hydrogen-Oxygen, Radical-Radical Reactions with Combined Laser Magnetic Resonance, Resonance Fluorescence and Atomic Absorption Detection
Wm. H. Brune, J. J. Schwab, and J. G. Anderson
- L-2 The UV Spectrum of SiF, SiCl and CCL
H. Bredohl, L. Dubois, Y. Houbrechts and F. Melen
- L-3 Multiphoton Ionization of the Trifluoromethyl Radical, CF₃
Michael T. Duignan, Jeffrey W. Hudgens and Jeffrey R. Wyatt
- L-4 Intensity Effects in Infrared Multiphoton Absorption and Decomposition
D. K. Evans, and Robert D. McAlpine
- L-5 Gas Phase Reactions of the Vinyloxy Radical with NO and O₂
H. H. Nelson and D. Gutman
- L-6 Time-Resolved Resonance Raman Investigation of Photostimulated Electron Transfer from and to Trans-Stilbene
W. Hub, S. Schneider, F. Doerr, F. T. Simpson, F. Oxman, F. D. Lewis
- L-7 Comparison of the O(³P) + Trimethylene Sulfide Reaction with Photolysis of Trimethylene Sulfoxide
D. L. Singleton
- L-8 Photodissociation Processes of SO₂ at 1060-1330 Å
M. Sutoh, R. L. Day, and L. C. Lee
- L-9 Multiphoton Laser-Induced Fluorescence Studies of Atomic and Simple Molecular Species
J. J. Tise, M. J. Ferris, G. Loge and F. B. Wampler
- L-10 Formation of Radiative Exciplex in the Quenching of Excited Uranyl Ion (UO₂²⁺) by Organic Molecules
Kunihiko Tokumura
- L-11 Enhancement of Smog by the Presence of Chlorine
G. Z. Whitten
- L-12 Kinetics of Cl(²P) Reactions with Several Chloro-Substituted Ethanes
P. H. Wine, D. H. Semmes, and A. R. Ravishankara

- L-13 Unknown Radical Sources in Environmental Chambers
William P. L. Carter, Roger Atkinson, Arthur M. Winer and
James N. Pitts, Jr.
- L-14 The Kinetics of Alkyl Radicals Reacting with Ozone
R. Paltenghi, E. A. Ogryzlo, and K. D. Bayes

Thursday July 1

Photophysics
Chairman - D. K. Evans

- 8:15 M-1 The Photophysics of Unimolecular Reactions: Product VRT Energy Disposal
C. Wittig
- 8:45 M-2 Superfluorescence from Chemically Pumped Iodine Molecules
F. J. Comes, K.-H. Stephan-Rossbach
- 9:00 M-3 Surface Photochemistry: The Photophysics of Pyrene Adsorbed on Silica Gel, Alumina and CaF_2
Richard K. Bauer, Paul de Mayo, William R. Ware, and Kam C. Wu
- 9:15 M-4 Anomalies in IR Multiphoton Excitation of Cl_2CS : Theoretical Insight
D. M. Brenner, M. N. Spencer and J. I. Steinfeld
- 9:30 M-5 Near Threshold Dissociation of Tetramethyldioxetane (TMD) Using a TEA CO_2 Laser
O. Aner, Y. Haas and S. Ruhman
- 9:45 Coffee Break

Spectroscopy
Chairman - R. P. Saxon

- 10:15 N-1 Vibrationally Excited Formaldehyde and Acetylene
E. Abramson, H. L. Dai, R. W. Field, J. L. Kinsey, C. Kittrell, D. E. Reisner, and P. H. Vaccaro
- 10:45 N-2 Visible Electronic Absorption Spectrum of Vinyl Radical
H. E. Hunziker, H. Knepe, A. D. McLean, P. Siegbahn, and H. R. Wendt
- 11:00 N-3 Spectral and Kinetic Study of Rare Gas/ Cl_2 Mixtures Excited with Synchrotron Radiation
M. C. Castex, J. Le Calve, D. Haaks, B. Jordan, G. Zimmerer
- 11:15 N-4 Multiphoton Excitation of Halogen Molecules
T. Ishiwata, T. Shinzawa, and I. Tanaka
- 11:30 N-5 Vibration-Rotation and Pure Rotational Spectra of the CH_2 Radical in its ground, $\tilde{X}^3\text{B}_1$, Electronic State, Implications Regarding the Singlet-Triplet Splitting in CH_2
T. J. Sears, P. R. Bunker, A. R. W. McKellar, K. M. Evenson, D. A. Jennings and J. M. Brown

- 11:45 N-6 Experimental Determination of Absorption Cross Sections and
Band Oscillator Strengths of the Schumann-Runge Bands of O_2
in the Wavelength Region 175-205 nm
D. E. Freeman, K. Yoshino, and W. H. Parkinson
- 12:00 N-7 Photoabsorption Spectrum of OH in the Vacuum Ultraviolet
Region
R. L. Day and L. C. Lee
- 12:15 Adjourn

ABSTRACT A-1

ALKYL NITRATE FORMATION FROM THE NO_x -AIR PHOTOOXIDATION OF C_2 - C_8 n-ALKANES

Roger Atkinson, Sara M. Aschmann, William P. L. Carter, A. M. Winer and J. N. Pitts, Jr., Statewide Air Pollution Research Center, University of California, Riverside, CA 92521

The higher alkanes are important constituents of many types of fuels currently in use, and are hence emitted into the atmosphere in substantial quantities. However, relatively little work has been carried out on the products and mechanisms of their NO_x -air photooxidation. The atmospheric photooxidation mechanism of the larger alkanes ($\geq \text{C}_4$) differs from that of the smaller alkanes in two respects: the larger alkoxy radicals can undergo unimolecular isomerization and/or decomposition, while the larger peroxy radicals appear to be more likely to undergo an alternate reaction with NO forming alkyl nitrates,



competing with the "usual" chain propagating reaction



The isomerizations and decompositions of alkoxy radicals have been discussed previously but relatively little work has been done concerning the implications of alkyl nitrate formation from reaction (1), and how its importance depends on the structure of the alkyl peroxy radical. While the alkoxy radical isomerization and decomposition reactions affect primarily the nature of the organic products formed, the reaction pathway involving alkyl nitrate formation is potentially more important, since it is radical terminating and removes NO_x from the system, and thus affects the NO_x chemistry, O_3 formation, and radical levels.

In this work the alkyl nitrate yields have been determined during the NO_x -air photooxidations of the C_2 through C_8 n-alkane series. Experiments were carried out in an ~75-liter FEP Teflon cylindrical reaction chamber surrounded by 24 GE F15T8-BL 15-watt blacklamps.

Two chemical systems were used to generate RO_2 radicals: either reaction of OH radicals (generated by photolysis ($\lambda > 290$ nm) of methyl nitrite

in air) or Cl radicals (from photolysis of Cl_2) with the n-alkane being studied. Reactant (CH_3ONO or Cl_2 , NO, and the n-alkanes) concentrations were ~1 part-per-million (ppm, 1 ppm = 2.37×10^{13} molecule cm^{-3} at 299 K, 735 torr total pressure), and the n-alkane and alkyl nitrate yields were quantitatively monitored by gas chromatography with flame ionization detection.

In all cases the total alkyl nitrate yields increased linearly with the amount of alkane consumed, and the fractional yields, after correction for the small amount removed by reaction with OH radicals [1], are given in Table 1. The distributions of isomeric alkyl nitrates formed were very similar to those expected on the basis of the kinetics of OH + n-alkanes [2], showing that the alkyl nitrates were indeed formed from RO_2 radical reactions. These observations, together with a consideration of other possible competing reactions, confirm that the fractional yields of alkyl nitrates shown in Table 1 correspond to the rate constant ratio $k_1/(k_1 + k_2)$.

Table 1. Fractional yields of alkyl nitrates in the NO_x -air photooxidation of C_2 through C_8 n-alkanes.

n-Alkane	$\Delta[\text{alkyl nitrate}]/-\Delta[\text{n-alkane}]^{\text{a)}}$
Ethane	0.010
Propane	0.036
n-Butane	0.077
n-Pentane	0.128
n-Hexane	0.22
n-Heptane	0.31
n-Octane	0.33

^{a)} Corrected for loss processes of alkyl nitrates due to reaction with OH radicals

The dependence of the rate constant ratio $k_1/(k_1 + k_2)$ on the carbon numbers in the n-alkane is shown in Figure 1, indicating a rapid increase in importance of this chain-terminating reaction with the size of the alkyl peroxy radical.

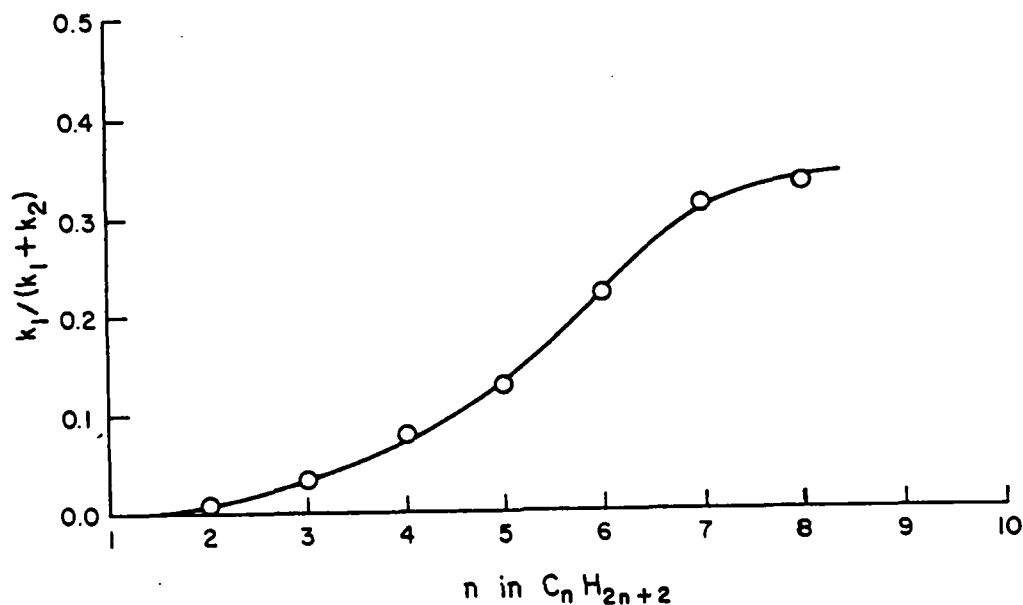


Figure 1. Plot of the rate constant ratio $k_1/(k_1 + k_2)$ against carbon number in the n-alkane series studied.

References

1. R. Atkinson, S. M. Aschmann, W. P. L. Carter and A. M. Winer, *Int. J. Chem. Kinet.*, in press (1982).
2. R. Atkinson, S. M. Aschmann, W. P. L. Carter, A. M. Winer and J. N. Pitts, Jr., *Int. J. Chem. Kinet.*, in press (1982).

Acknowledgments

This work was supported by the California Air Resources Board Contract No. A1-030-32.

ABSTRACT A-2

The Determination of Specific Rate Constants for Triplet-Triplet Annihilation in Rigid Solutions of 1,2-Benzanthracene Using Pulsed Laser Excitation and Triplet-Triplet Absorption

R. D. Burkhart
Department of Chemistry
University of Nevada
Reno, Nevada 89557

Using pulsed UV laser excitation, 1,2-benzanthracene triplets in thin polymer films may be produced at concentrations up to $10^{-3}M$. An analyzing beam having a wavelength of 485 nm is a sensitive detector of these triplets since ϵ_{T-T} is $23,400 M^{-1} cm^{-1}$ at this wavelength. Earlier work involving the kinetics of delayed luminescence decay and time-resolved optical anisotropy has demonstrated that solute molecules in these films are distributed heterogeneously. The current studies using triplet-triplet absorption have made it possible to determine the specific rate constants for triplet-triplet annihilation (k_2). In a system of heterogeneously distributed solute molecules one would expect k_2 to decrease with time as remaining triplets are found in less densely populated regions. Furthermore, k_2 values should increase with increasing solute concentration since rates of triplet excitation hopping depend on average intermolecular separation distances.

Both of these predicted characteristics of k_2 are observed experimentally in the present work. Furthermore, k_2 depends upon the average intermolecular separation distance, \bar{x} , and upon the excitation hopping frequency, $n(\bar{x})$. The well known relation of Dexter, Inokuti and Hirayama can be used to calculate $n(\bar{x})$ as a function of \bar{x} . Thus, the dependence of \bar{x} on time may be determined from the time-dependent values of k_2 and, of course, they increase with time.

The detailed time-dependence of $\bar{\epsilon}$ naturally depends upon the solute distribution function. Therefore, these results, along with earlier studies of the time dependence of the optical anisotropy of delayed fluorescence and phosphorescence, provide a unique two-pronged route to the characterization of these non-random distributions.

ABSTRACT A-3

LASER FLUORESCENCE SPECTROSCOPY OF NCO. Brian J. Sullivan, Gregory P. Smith, and David R. Crosley, SRI International, Menlo Park, CA 94025.

Laser-induced fluorescence of the NCO $A^2\Sigma^+ - X^2\Pi$ and the $B^2\Pi - X^2\Pi$ systems was investigated between 440-398 nm and 316-314 nm, respectively. Excitation spectra, fluorescence spectra, radiative lifetimes, and quenching rate constants were studied.

NCO has been proposed as an intermediate in the oxidation of nitrogen-containing fuels, and has recently been observed in the reaction zone of a CH_4/N_2O flame.¹ The present work provides some of the spectroscopic characteristics necessary for semi-quantitative estimates of NCO concentrations from LIF signals in flames.

NCO is produced by the gas-phase reaction $F + HNCO$ and/or $HOCN$. The acid vapor is formed in a small reaction vessel containing KOCN and stearic acid at $\sim 100^\circ C$, and is injected into a glass flow system of moderate pumping speed. F-atoms are created using a microwave discharge on CF_4 or SF_6 in ~ 1 torr He.

The exciting radiation for the A-X excitation is provided by a Nd:YAG-pumped tunable dye laser which has been frequency-shifted by stimulated Raman frequency conversion in ~ 10 atm of H_2 . Coumarin dyes and second-order anti-stokes shifted radiation from rhodamine dyes were used. The laser has a bandwidth of $\sim 0.15\text{ cm}^{-1}$ and pulse length of ~ 8 nsec. For the B-X excitation, we use a frequency doubled dye laser containing rhodamine 640.

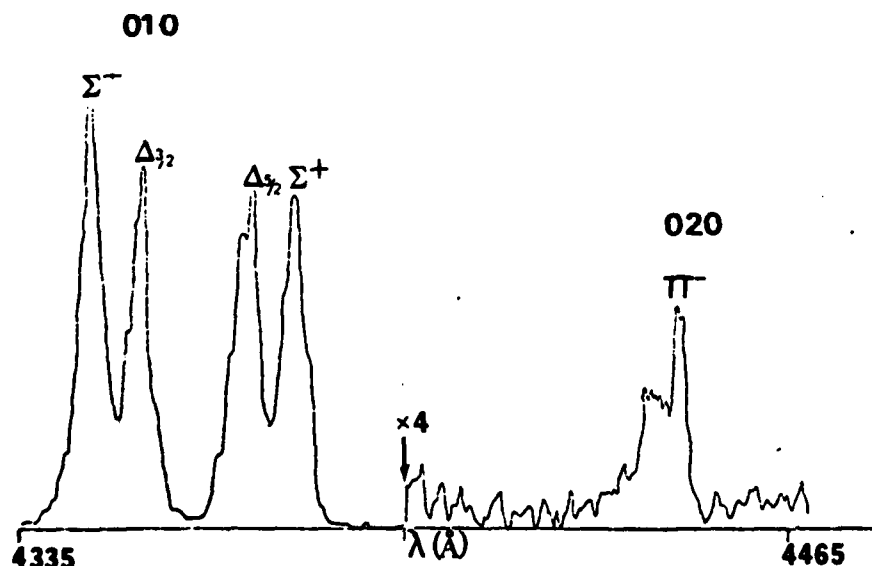
The fluorescence emitted at right angles to the laser beam is focussed onto the slits of a .35 m monochromator with a 40 Å bandpass for excitation spectra, and a 1-10 Å bandpass for several runs in which the fluorescence spectra at fixed excitation wavelength were measured. A boxcar integrator and a chart recorder, with 2 second (20 pulse) averaging time, were used for signal processing.

Transitions from the ground (0,0,0) level of the $X^2\Pi$ state to five vibrational levels (0,0,0; 0,1,0; 1,0,0; 0,2,0; 0,0,1) of the $A^2\Sigma^+$ state were pumped; excitation scans (fixed fluorescence detection wavelength while the laser is tuned) have been obtained for such upper state vibration level

studies. These spectra can be rotationally assigned following Dixon's analysis.²

Emission lifetimes were measured for such vibrational levels, both with and without added gases, to obtain radiative lifetimes (τ) and collisional quenching rates. The radiative lifetime is 410 nsec and is relatively insensitive to vibrational level. Our measured radiative lifetimes agree well with those of Reisler, Mangir, and Wittig³, but is considerably longer than the value of 180 nsec in an Ar matrix⁴ study. Collisional quenching rate constants for the 0,0,1 level are 3.0×10^{-11} and $1.1 \times 10^{-10} \text{ cm}^3 \text{ sec}^{-1}$ for N_2 and O_2 , respectively. Similar rates were measured for the other levels. Helium was found to have a small collisional quenching rate ($\leq 1.5 \times 10^{-12} \text{ cm}^3 \text{ sec}^{-1}$). The fluorescence spectra also indicate no significant collisional population of other vibrational levels of the A-state prior to quenching or fluorescence.

Fluorescence spectra (laser-fixed, monochromator-scanned) were obtained for excitation at band heads in all levels. The wavelengths of the observed bands agree with previous determinations of $\text{X}^2\Pi$ vibrational level energies.^{4,5} The $\text{A}^2\Sigma^+(0,1,0) \rightarrow \text{X}^2\Pi(0,0,0)$ transition is electronically forbidden, but weakly allowed due to vibronic interaction. Figure 1 shows a portion of the



high resolution (1 Å) spectra of the $A^2\Sigma^+(0,1,0) \rightarrow X^2\Pi_1(v_1, v_2, v_3)$ fluorescence. The four vibronic components, which are due to Renner-Teller and spin-orbit interactions, of the 0,1,0 level of the ground state, were easily seen. The lack of observable $A^2\Sigma^+(0,1,0) \rightarrow X^2\Pi_{1/2}(0,0,0)$ fluorescence indicates this transition is at least an order of magnitude weaker than the $A^2\Sigma^+(0,1,0) \rightarrow X^2\Pi(0,1,0)$ transition. Several $A^2\Sigma^+(0,1,0) \rightarrow X^2\Pi_1(v_1, 2, v_3)$ fluorescence bands were also observed, but only emission to the Π^- vibronic component was seen. Fluorescence from the 0,0,0 level of the $A^2\Sigma^+$ state shows similar behavior. Possible explanations for this phenomenon are being pursued.

An excitation spectrum of the (0,0,0)-(0,0,0) band of the $B^2\Pi_1 - X^2\Pi_1$ system was obtained between 3156-3142 Å. The rotational structure is very congested⁶, and only the R_1 and R_2 heads are easily discernible. A radiative lifetime of 63 nsec was measured for the $B^2\Pi_1$ state, considerably shorter than the $A^2\Sigma^+$ state lifetime. No fluorescence to the A-state, or A-X emission upon B-state excitation was observed. Quenching rate constants for N_2 and O_2 are 1.3×10^{-10} and $2.0 \times 10^{-10} \text{ cm}^3 \text{ sec}^{-1}$, respectively. The fluorescence spectra show long progressions in the ground-state stretching modes. Derived ground-state vibration constants are: $\omega_1^0 = 1286 \text{ cm}^{-1}$, $\omega_3^0 = 1925 \text{ cm}^{-1}$; $X_{11} = -10.3 \text{ cm}^{-1}$, $X_{33} = -11.6 \text{ cm}^{-1}$, $X_{13} = -27.8 \text{ cm}^{-1}$. Attempts are underway to derive potential surface information from the fluorescence spectrum intensities.

This work was supported by the U.S. Army Research Office.

References

1. J. A. Vanderhoff, R. A. Beyer, W. R. Anderson, and A. J. Kotlar, Thirty-Sixth Symposium on Molecular Spectroscopy, Columbus, Ohio, June 1981; W. R. Anderson, J. A. Vanderhoff, A. J. Kotlar, L. J. Decker, and R. A. Beyer, Eastern Section Meeting of the Combustion Institute, Pittsburgh, Pennsylvania, October 1981.
2. R. N. Dixon, Phil. Trans. Roy. Soc., London, A262, 165 (1960).
3. H. Reisler, M. Mangir, and C. Wittig, Chem. Phys., 47, 49-58 (1980).
4. V. E. Bondybey and J. H. English, J. Chem. Phys., 67, 2868 (1977).
5. D. E. Milligan and M. E. Jacox, J. Chem. Phys., 47, 5157 (1967).
6. R. N. Dixon, Can. J. Phys., 38, 10 (1960).

ABSTRACT A-4

PREPARATION AND CHARACTERIZATION OF VIBRATIONALLY EXCITED MOLECULAR IONS IN THERMAL ENERGY CHARGE TRANSFER REACTIONS

G.MAUCLAIRE, R.DERAI and R.MARX

Laboratoire de Résonance Electronique et Ionique, Bât 350
Université de Paris-Sud, 91405 ORSAY, France

Charge transfer reactions have been widely used to deposit a given amount of energy in an ion, for example to determine breakdown curves. However we have recently shown that most of the non dissociative reactions occurring at thermal energy are not energy resonant: the available energy, which in this case is the recombination energy of the primary ion, is partitioned into kinetic and internal energies of the products (1). By measuring the kinetic energy, we can deduce from energy balance the internal energy of the products. Most of the time the molecular ion formed is in excited vibrational levels of the ground state with a rather selective population extending from one level for diatomic ions (e.g. CO^+) to four for polyatomic ions (e.g. NH_3^+). By reaction of various primary ions with a given molecule, it is possible to form molecular ions with different vibrational energies in levels which are often not available either by photon or by electron impact (2). For example, in charge transfer of NH_3 with several primary ions (Ar^+ , Kr^+ , Xe^+ , O_2^+ , CO^+ , N_2^+ , CO_2^+), the NH_3^+ ions are produced in the $\tilde{\text{X}}$ state with seven different vibrational energies covering the range 0 to 5 eV and can then be used to study their reactivity as a function of internal energy (3).

- 1) G.MAUCLAIRE, R.DERAI, S.FENISTEIN and R.MARX, J.Chem.Phys. 70, 4017 (1979);
R.DERAI, G.MAUCLAIRE and R.MARX, 3rd Symposium on Atomic and Surface Physics, Maria Alm, Austria (1982), book of contributions p.278
- 2) R.DERAI, G.MAUCLAIRE and R.MARX, Chem.Phys.Lett., 86, 275 (1982)
- 3) P.R.KEMPER, M.T.BOWERS, D.PARENT, G.MAUCLAIRE, R.DERAI and R.MARX, to be published

ABSTRACT A-5

Rare-gas oxide Van der Waals molecule formation by photodissociation of triatomic molecules trapped in rare gas matrices at low temperature

J. Fournier, D. Maillard,^{*} H. H. Mohammed,
C. Girardet,^{**} J. Deson
E.S.P.C.I., Equipe 57, C.N.R.S.,
10 rue Vauquelin, 75005 Paris

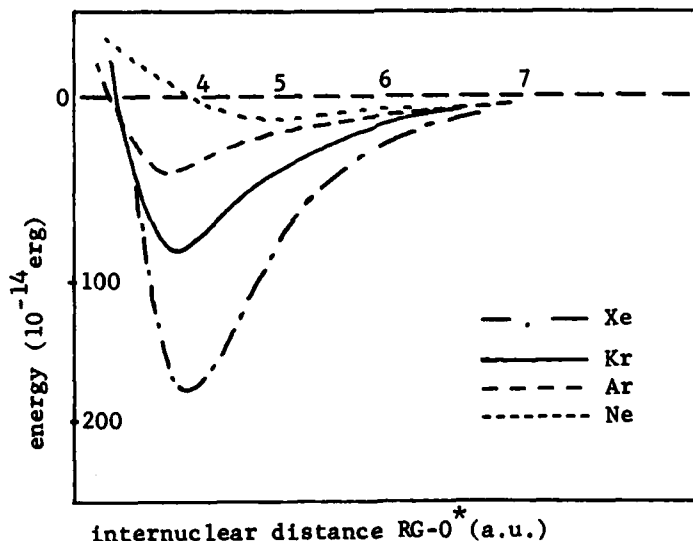
The far UV dissociation of small oxygenated molecules leads to $O(^1D)$ atom formation. In argon, krypton and xenon matrices this atom is trapped and forms with the matrix a rare gas excimer. The potential energy curves of these complexes are calculated using a modified Buckingham potential

$$V = Ae^{-\alpha R} - \left(\frac{C_6}{R^6} + \frac{C_8}{R^8} + \frac{C_{10}}{R^{10}} \right),$$

minimized to find the equilibrium position.

It can be shown that the minimum of the potential is deeper in krypton than in argon. After the process of dissociation, the rare gas oxide excimer absorbs photon energy (8.7 eV) continuously to form the $RG O(^1S)$ molecule, and $RG O(^1S) \rightarrow RG O(^1D)$ emission is observed during irradiation. During warming up after cessation of irradiation, the formation of $O_2(A^3\Sigma_u^+)$ is observed due to $O(^3P) + O(^3P)$ recombination.

In a neon matrix the potential is always repulsive and no excimer formation is detected. Only $O(^1D) \rightarrow O(^3P)$ emission and excited O_2 emission are observed. These mechanisms are in good agreement with our calculations.¹



^{*}Laboratoire de Spectrochimie Moléculaire

⁴ place Jussieu, 75005 Paris.

^{**} Université de Besancon, Faculté des Sciences,
Besancon.

¹D. Maillard, J. Fournier, H. H. Mohammed, J. P. Perchard,
Phys. Rev. Lett. (submitted for publication).

ABSTRACT A-6

CO₂ LASER INDUCED MULTIPLE PHOTON DISSOCIATION OF MOLECULAR IONS

J.S. Chou, Y. Haas, H. Reisler, D. Sumida, and C. Wittig

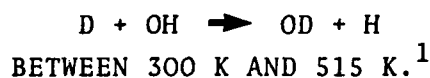
University of Southern California

Los Angeles, CA 90007

Several quantitative aspects of infrared laser multiphoton dissociation can be better observed with ions than with neutrals. Both parents and daughters can be counted, sequential processes are readily followed, and low densities are easily monitored. We present results on the IR multiphoton dissociation of ions prepared by photoionization, usually multiphoton ionization. Substrates include hydrocarbons, nitrogen and sulfur containing organic compounds, and some inorganic compounds (such as UF₆). It is shown that in some cases all of the parent ions can be dissociated with rather modest CO₂ laser fluences. Sequential absorption in daughter ions leads to fragmentation down to small molecular units. The results can be understood in terms of the initial vibrational excitation in the nascent ions, and the potential energy surfaces of molecular ions. Fragmentation efficiency depends on the CO₂ laser frequency, showing that even vibrationally excited molecules maintain a non uniform spectral structure over the CO₂ laser tuning range.

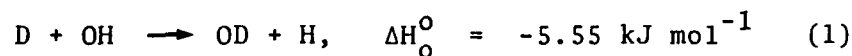
ABSTRACT A-7

DIRECT RATE MEASUREMENTS ON THE REACTION :



Mark J. Howard[†] and Ian W.M. Smith,
Department of Physical Chemistry,
University Chemical Laboratories,
Lensfield Road, Cambridge CB2 1EP, England.

As part of our continuing work¹⁻⁴ on radical-radical processes, we have measured the rate of



between 300 and 515 K in direct experiments combining discharge-flow and pulsed laser photolysis techniques. Although reaction (1) has no practical terrestrial importance, it appears that it - and similar processes with virtually no activation barrier - are the only important processes involving uncharged species in interstellar gas clouds.⁵ Reaction (1) is also theoretically interesting as it presumably proceeds via a collision complex (DOH^{\dagger}) for which it should be possible to calculate an accurate ab initio surface. Its rate has only been measured once before. Margitan et al,⁶ using resonance fluorescence to observe removal of OH in a double discharge-flow apparatus, obtained $k_1 = (1.3 \pm 0.3) \times 10^{-10} \text{ cm}^3 \text{ molecule}^{-1} \text{ s}^{-1}$ at room temperature.

[†] Present address : Department of Chemistry,
University of Minnesota, Minneapolis,
Minnesota 55455, U.S.A.

Our experiments were performed in the apparatus illustrated in Fig. 1. D atoms were generated by microwave

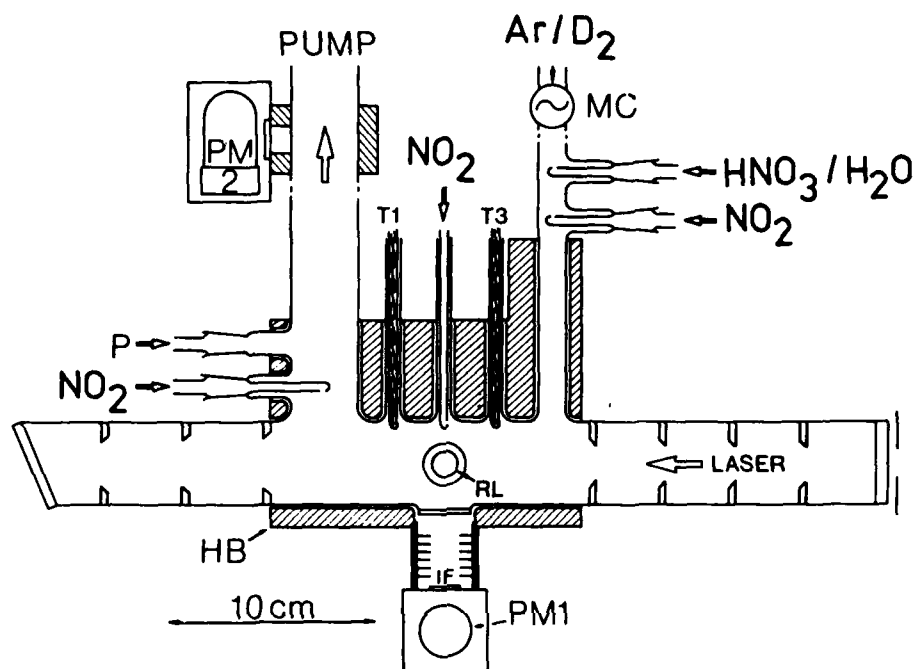


FIG. 1. - Diagram of the apparatus for laser flash photolysis / time-resolved resonance fluorescence measurements. The OH resonance lamp shines out of the plane of the paper.

discharge through a dilute mixture of D_2 ($<1\%$) in Ar and their steady-state concentration was determined by titration with NO_2 . The DNO^* afterglow served as indicator and secondary reactions were allowed for in comprehensive computer modelling.¹

OH radicals were produced by pulsed photolysis using an excimer laser operating on either (i) the ArF line ($\lambda = 193$ nm, ca 200 mJ per pulse) to dissociate HNO_3 , or (ii) the F_2 transition ($\lambda = 157$ nm, ca 4 mJ per pulse) to dissociate H_2O . The concentration of OH which was produced was typically 10% of the D atom concentration in experiments with HNO_3 as photolytic precursor and 3% in those utilising H_2O . First-order decays of OH were observed by accumulating time-resolved resonance fluorescence from 1024 or 2048 shots.

Fig. 2 shows plots of the derived first-order constants (k_{1st}) plotted against D-atom concentration for all our experimental conditions. At each temperature, k_1 was calculated

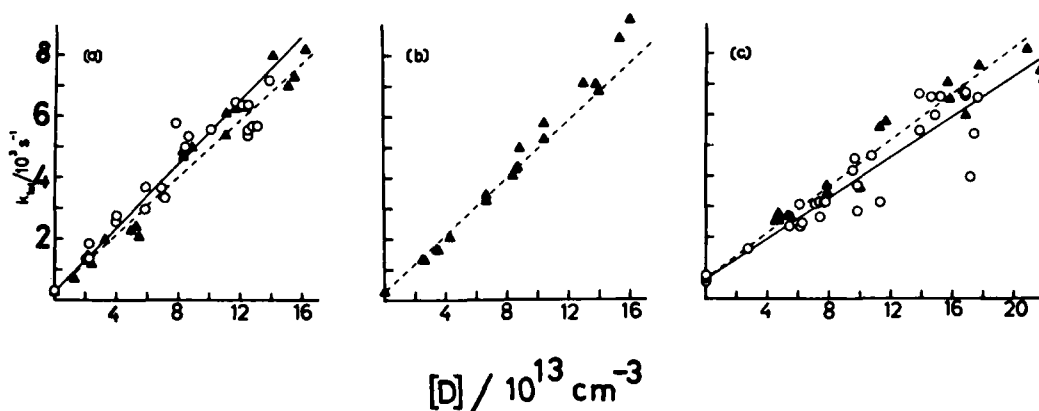


FIG. 2. - First-order decay constants plotted against concentrations of D atoms using photolysis of HNO_3 (\blacktriangle) and H_2O (\circ) to generate OH radicals: (a) at (300 ± 5) K, (b) at (390 ± 5) K, and (c) at (500 ± 5) K with HNO_3 and (515 ± 5) K with H_2O .

by averaging the values of $(k_{1st} - k_b)/[D]$, where k_b is the small, 'background', first-order rate constant for OH removal in the absence of D atoms. Fitting the results to the form AT^{-n} yields:

$$k_1 = (1.9 \pm 0.3) \times 10^{-9} T^{-(0.63 \pm 0.05)} \text{ cm}^3 \text{ molecule}^{-1} \text{ s}^{-1}.$$

where the errors are 95% confidence limits within our temperature range.

The discrepancy between our value of k_1 at 300 K ($5.3 \times 10^{-11} \text{ cm}^3 \text{ molecule}^{-1} \text{ s}^{-1}$) and that of Margitan *et al*⁶ lies well outside the combined error limits. We shall discuss possible sources of systematic error in both sets of experiments.

It is also interesting to compare the experimental values of k_1 with estimates based on models developed by Quack and Troe.^{7,8} The rate constant (k_c) for formation of DOH^\ddagger complexes

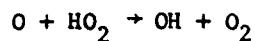
can be estimated via their maximum free energy/transition state model.⁷ We find $k_c = 1.2 \times 10^{-10} \text{ cm}^3 \text{ molecule}^{-1} \text{ s}^{-1}$ at 300 K and $1.45 \times 10^{-10} \text{ cm}^3 \text{ molecule}^{-1} \text{ s}^{-1}$ at 500 K. The rate constant (k_c) for redissociation of these complexes can be estimated using methods⁸ designed to find the equilibrium constant, $K_c = k_c/k_{-c}$, for $\text{D} + \text{OH} \rightleftharpoons \text{DOH}^\ddagger$. The redissociation process competes with dissociation of the complexes 'forward' to the $\text{H} + \text{OD}$ products of the reaction. The rate constant (k_p) for this channel is estimated via a new procedure based on locating a transition state at a position associated with a minimum number of states - in keeping with the microcanonical transition state theory expression⁹ for a specific rate constant : $k(E) = N^*(E+)/h$ (E). The results of these calculations indicate that, in this nearly thermoneutral system, at least part of the negative temperature dependence may reflect the fact that $k_c/(k_c + k_p)$, i.e. the fraction of complexes which redissociate to reagents rather than dissociate to products, increases as the temperature is raised.

References

1. To be published shortly in J.C.S. Faraday II.
2. M.J.Howard and I.W.M.Smith, Chem. Phys. Letters, **69**, 40 (1980).
3. M.J.Howard and I.W.M.Smith, J.C.S. Faraday II, **77**, 997 (1981)
4. M.J.Howard and I.W.M.Smith, Prog. Reac. Kinetics, in press (1982)
5. A.Dalgarno and J.H.Black, Rep. Prog. Phys., **39**, 573 (1976).
6. J.J. Margitan, F.Kaufman and J.G.Anderson, Chem. Phys. Letters, **34**, 485 (1975)
7. M.Quack and J.Troe, Ber. Bunsenges. Phys. Chem., **81**, 329 (1977).
8. J. Troe, J. Chem. Phys., **66**, 4758 (1977)
9. I.W.M.Smith, Kinetics and Dynamics of Elementary Gas Reactions (Butterworths, London 1980).

ABSTRACT A-8

KINETICS OF THE REACTION



FROM 229 TO 372K*

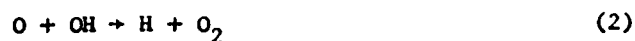
Leon F. Keyser

Molecular Physics and Chemistry Section
Jet Propulsion Laboratory
California Institute of Technology
Pasadena, California 91109

The reaction of atomic oxygen with the perhydroxyl radical (eq. 1) plays an important role in the chemistry of the mesosphere



and upper stratosphere. Reaction (1) along with the reaction of atomic oxygen with the hydroxyl radical (eq. 2) are the major paths



by which odd oxygen (O, O_3) is converted to O_2 in these regions of the atmosphere. Moreover, the relative concentrations of mesospheric OH and HO_2 are almost entirely determined by the rate constant ratio, k_1/k_2 .

In the present study absolute measurements of k_1 have been made from 229 to 372K using resonance fluorescence detection of radical and atomic species. Pseudo-first-order conditions were used with $[\text{HO}_2] \gg [\text{O}]$. To test for interference from secondary reactions, both the HO_2 and the atomic oxygen were generated by two entirely different techniques. The rate constant was determined directly from the slopes of $\ln[\text{O}]$ vs. time plots.

* Work supported by NASA at California Institute of Technology, Jet Propulsion Laboratory.

In addition relative rate measurements have been carried out at 299K using $[O] \gg [HO_2]$. The rate constant ratio, k_1/k_2 was determined from the quasi-steady state concentrations of OH and HO_2 .

At 299K the absolute measurements of k_1 yield a value of $(6.1 \pm 0.6) \times 10^{-11} \text{ cm}^3 \text{ molecule}^{-1} \text{ s}^{-1}$. The temperature dependence expressed in Arrhenius form is $(3.1 \pm 0.3) \times 10^{-11} \exp[(+200 \pm 28)/T]$. The error limits given are twice the standard deviation; overall experimental error is estimated to be $\pm 25\%$. The steady-state experiments yield a value of 2.1 ± 0.3 for k_1/k_2 at 299K. This result is in good agreement with the present absolute measurement of k_1 and with recent measurements of $k_2^{1,2}$.

The present results will be discussed in terms of their effect on our understanding of atmospheric chemistry.

References

1. R. S. Lewis and R. T. Watson, J. Phys. Chem. 84, 3495 (1980).
2. M. J. Howard and I. W. M. Smith, J. Chem. Soc., Faraday Trans. 2, 77, 997 (1981).

ABSTRACT A-9

"THE $\pi^* + n$ SPECTRUM OF JET-COOLED ACETALDEHYDE"

Marcus Noble, Eric C. Apel, Edward K.C. Lee

Department of Chemistry
University of California
Irvine, California 92717

The $\pi^* + n$ ultraviolet spectrum of acetaldehyde has been observed as part of our current study into molecular complexes formed in supersonic jet expansion. Using laser induced fluorescence many vibronic bands have been observed corresponding to the acetaldehyde monomer. The first observed feature is a doublet at 29768 cm^{-1} and $29798\text{ cm}^{-1} \pm 2\text{ cm}^{-1}$. This is 916 cm^{-1} above the previously assigned origin (Hubbard et al., 1981).¹ In a polyatomic molecule with such low excited state symmetry it seems likely that this observed origin is the true electronic origin of the system.

The most striking feature of this spectrum in contrast, for example, to the $\pi^* + n$ spectrum of CF_3NO (DeKoven et al., 1981)² is that there appears to be a doubling in the torsional progression, in addition to the expected a-e splitting of ν_{15}' (methyl torsion) = 186 cm^{-1} . This seems to indicate the presence of two excited state geometries.

1. L.M. Hubbard, D.F. Bocian and R.R. Birge, J. Am. Chem. Soc. 103, 3313 (1981).
2. B.M. DeKoven, K.H. Fung, D. Levy, L.D. Hoffland and K.G. Spears, J. Chem. Phys. 74, 4755 (1981).

* This research has been supported by the National Science Foundation grant CHE-79-25451.

ABSTRACT A-10

UNIMOLECULAR DECAY OF TOLUENE

R. J. Buss, D. J. Krajnovich and Y. T. Lee

Materials and Molecular Research Division
Lawrence Berkeley Laboratory and
Department of Chemistry
University of California
Berkeley, California 94720 USA

ABSTRACT

The dynamics of unimolecular decay processes can now be studied in great detail with the combined techniques of laser preparation of isolated molecules of exact excitation energy in beams and detection of products under collision-free conditions. Of particular interest is the range of applicability of statistical theories in the calculation of specific rate constants and product energy partitioning.

We have investigated the unimolecular decay of toluene in a molecular beam, having prepared the molecule with known excitation energy by the isomerization of cycloheptatriene (CHT) irradiated with a KrF excimer laser at 248 nm. After single photon absorption, CHT is known to undergo rapid internal conversion to the ground electronic state followed by rapid isomerization to toluene. The toluene contains 147 kcal/mole of vibrational energy and might decay by any of several energetically feasible pathways. Previous studies¹ of similarly excited toluene in a gas cell have identified H + benzyl radical products under near collision-free conditions and derived reliable information on the rate of decomposition.

We have observed two primary decomposition reactions yielding H + benzyl radical and CH₃ + phenyl radical, and have obtained angular distributions, shown in the figure, and velocity distributions of the products with a rotatable quadrupole mass spectrometer. The product

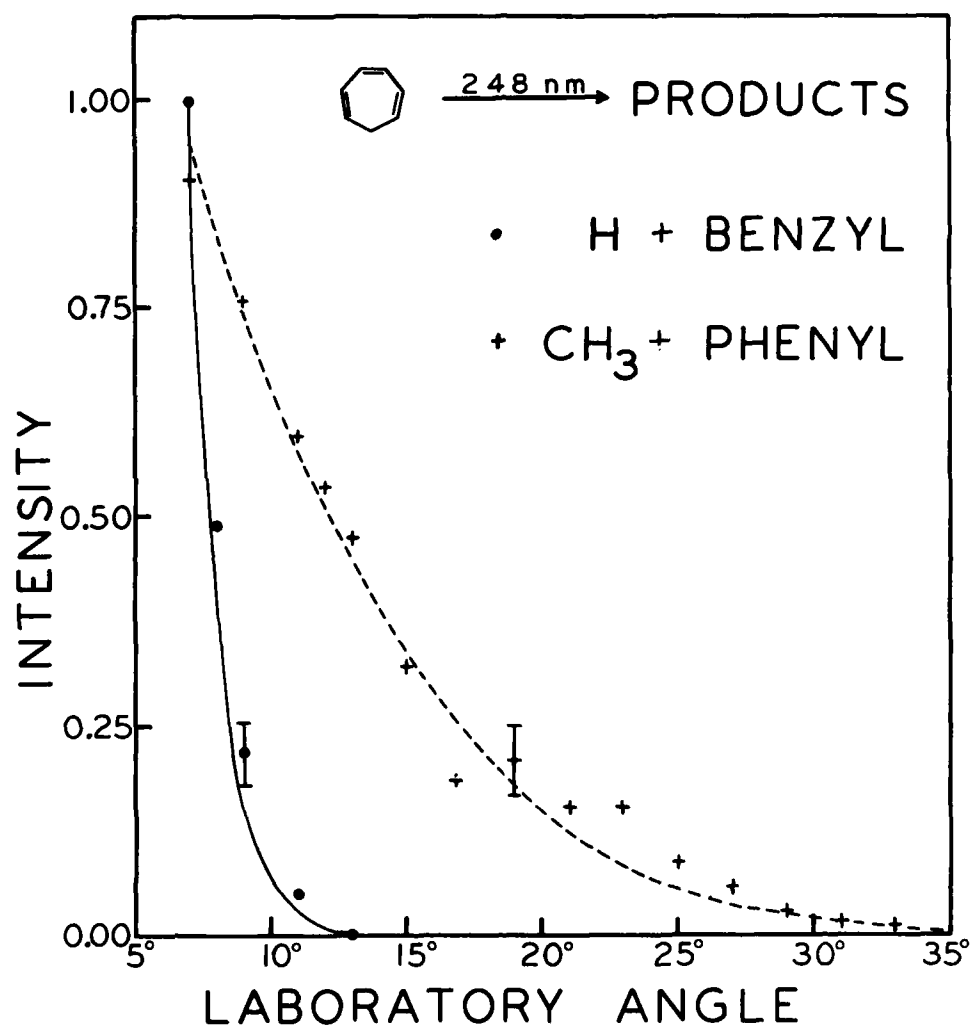
translational energy distributions for the two channels agreed reasonably well with those calculated by statistical theory. The RRKM calculation was found to somewhat underestimate the high energy product for the H atom elimination. The explanation for this deviation may lie in dynamical effects coupling the C-H bending motion to the C-H bond cleavage.

Although it is impossible to accurately determine the relative importance of the H atom and CH_3 radical elimination reactions from our data accumulated so far, it appears that CH_3 elimination is a minor channel of the order of 10% at this excitation energy. A statistical calculation, using reasonable values for the critical configuration parameters, predicts that 2-20% of the excited toluene molecules will dissociate via CH_3 elimination. No evidence for undissociated toluene was observed in experiments with the detector directly viewing the beam, showing that the lifetime of excited molecules is much less than the 0.28 msec flight time to the detector. This is in agreement with the rate constants for unimolecular decay to $\text{H} + \text{benzyl}$ measured by Hippler et al. of $3 \times 10^6 \text{ sec}^{-1}$.

This work was supported by the Office of Naval Research under Contract No. N00014-75-C-0671.

References

1. H. Hippler, V. Schubert, J. Troe and H. J. Wendelken, Chem. Phys. Lett. 84, 253 (1981).



XBL 824-9135

Fig. 1. Angular distributions of products from the KrF laser excitation of cycloheptatriene. Lines are statistical calculations. Typical 1 σ error bars are shown.

ABSTRACT A-11

PREDICTING THE RATE OF OH-ADDITION TO AROMATICS USING σ^+ -ELECTROPHILIC SUBSTITUENT CONSTANTS FOR MONO- AND POLYSUBSTITUTED BENZENE

Cornelius Zetzsch

Universität Bochum, Physikalische Chemie, Postfach 102148

4630 Bochum 1, W. - Germany

Rate constants were determined for the reactions of OH with aromatics at room temperature in the gas phase: biphenyl, chlorobenzene, benzonitrile, and nitrobenzene. The reactions were studied using the pulsed flash photolysis-resonance fluorescence technique.

Reactants were dosed under slow flow conditions by means of a gas saturation system. Concentrations of reactants and water vapor were calculated from known vapor pressure equations. Verification by freezing the vapors in cold traps always yielded agreement within better than 5%. This technique enables us to dose very low-volatile substances; substances with vapor pressures down to 10^{-2} torr (at room temperature) have been dosed successfully.

Rate constants were determined under pseudo first order conditions. Flash energies ranging from 3-25 J were applied, the former corresponding to initial concentrations of OH $\sim 5 \times 10^{10} \text{ cm}^{-3}$. The rate constants obtained were independent of flash energy, water concentration, or inert gas pressure (above 100 torr Ar or He). Rate constants, k , are obtained from linear regressions of the decay rate, τ^{-1} , vs the reactant concentrations; three standard deviations, 3σ , are given in the following Table I to indicate the reproducibility of the measurements:

Tab. I : Rate constants determined in the present study

Aromatic	$(k \pm 3 \sigma) / 10^{-12} \text{ cm}^3 \text{ s}^{-1}$
Biphenyl	5.8 ± 0.8
Chlorobenzene	0.67 ± 0.05
Benzonitrile	0.33 ± 0.03
Nitrobenzene	0.21 ± 0.05

The reactivities of various substituted aromatics increase rapidly with decreasing ionization potential of the reactant molecules.

Table II contains a summary of the data¹⁻⁵⁾, in the case of differing values an average value was chosen. The rate constants from Table II can be correlated to the ionization potential⁶⁾, yielding the equation

PREVIOUS PAGE
IS BLANK

$\log(k/\text{cm}^3\text{s}^{-1}) = 0.74 - 1.36 \text{ (IP/eV)}$ with a correlation coefficient of $r = 0.95$, if the data points for benzaldehyde, the cresols and chlorinated aromatics are omitted⁷⁾.

A somewhat more general correlation is obtained in the present work when using the electrophilic substituent constants, σ^+ , after Brown and Okamoto⁸⁾ with the following additional rules:

1. Steric hindrance is neglected, the electrophilic substituent constant of the ortho-position is set equal to the constant for the para-position.
2. The total substituent constant, $\Sigma\sigma_i^+$, is the sum of all substituent constants, σ_i , of the substituents, i , connected to the aromatic ring.
3. The OH radical adds to the position with the most negative value for $\Sigma\sigma_i^+$, preferably a free position.
4. If all positions are occupied, the ipso-position is treated like a meta-position.

The result of this treatment of the data in Table II is shown in Figure 1. Using rule 1 the equation

$$\log(k/\text{cm}^3\text{s}^{-1}) = 11.7 - 1.41 \sigma^+ \quad (\text{I})$$

is obtained for the monosubstituted aromatics (dashed line in Figure 1), using rules 1-4 the equation

$$\log(k/\text{cm}^3\text{s}^{-1}) = 11.6 - 1.39 \Sigma\sigma_i^+ \quad (\text{II})$$

is obtained for all aromatics contained in Table II (solid line in Figure 2), the only omitted data set being benzaldehyde, where the main reaction step might be abstraction of the aldehydic H.

Equation II is found to predict aromatic reactivities against OH within a factor of 2, as shown in the diagram, Figure I.

Acknowledgement

This work was supported by the Bundesminister für Forschung und Technologie and by the Fonds der Chemischen Industrie. The author wishes to thank the students M. Ramdohr †, U. Meier, R. Vogelsang, and J. Hurley for performing the measurements.

References

1. R. Atkinson, K.R. Darnall, A.C. Lloyd, A.M. Winer, and J.N. Pitts, Jr., *Advances Photochem.* **11**, 375 (1979)
2. J.N. Pitts, Jr., A.M. Winer, K.R. Darnall, A.C. Lloyd, and G.J. Doyle, *Proceedings Internat. Conf. on Photochem. Oxidant Pollution and its Control*, Dimitriadis Ed., EPA-600/3-77-001b, Paper 14-2 (1977)
3. H. Niki, P.D. Maker, C.M. Savage, and L.P. Breitenbach, *J. Phys. Chem.* **82**, 132 (1978)
4. M. Rinke and C. Zetzsch, *Abstr. Regionales Photochemiker-Treffen, Schriftenreihe Inst. f. Strahlenchemie, Mülheim/Ruhr* **1**, 15 (1980)
5. A. Wahner and C. Zetzsch, *Proc. Sec. Europ. Sympos. Physico-Chemical Behaviour of Atmospheric Pollutants*, Varese, Italy 1981, B. Versino, H. Ott Eds., Reidel, Dordrecht, p. 138 (1982)
6. H.M. Rosenstock, K. Draxl, B.W. Steiner, and J.T. Herron, *J. Phys. Chem. Ref. Data* **6**, Suppl. 1 (1977)
7. M. Rinke, A. Wahner, and C. Zetzsch, *J. Photochem.* **17**, 142 (1981)
8. H.C. Brown, Y. Okamoto, *J. Am. Chem. Soc.* **80**, 4979 (1958)

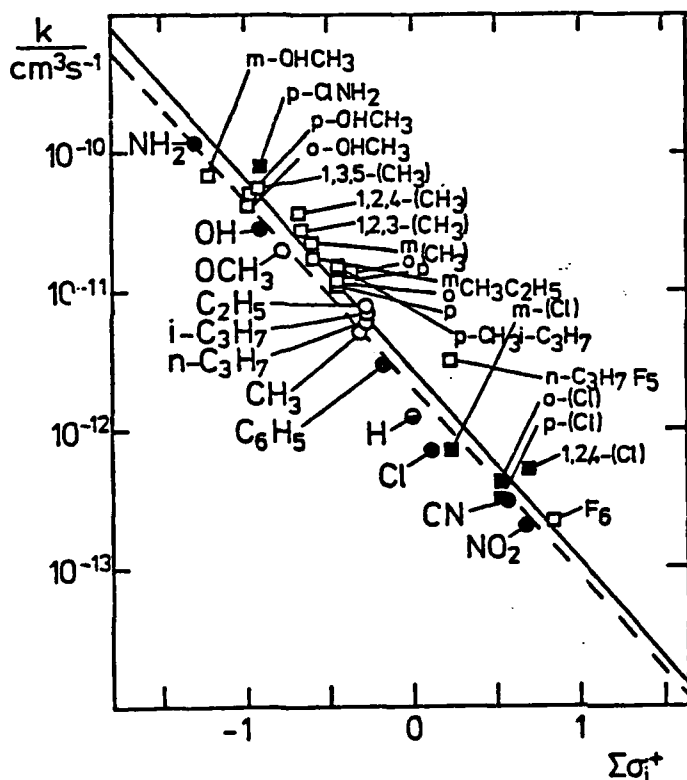


Fig. 1:
Hammett equation correlation for rate constants of OH in the gas phase using σ^+ -constants after Brown and Okamoto. Circles, monosubstituted (dashed line), squares, polysubstituted benzene. Filled symbols are work from our laboratory, the solid line includes all data points shown in the figure

Tab. II: Rate constants, k , for the reactions of OH with aromatics at room temperature, electrophilic substituent constants, σ_1^+ , and ionization potentials, IP

Aromatic	σ_1^+	σ_1^+	$\Sigma\sigma_1^+$	IP/eV	$k/10^{-12} \text{ cm}^3 \text{ s}^{-1}$	Ref.
1 Aniline	-1.3	(pNH ₂)	-1.3	7.69	120	4
2 p-Chloroaniline	-1.3	(pNH ₂)	-0.901	7.77	81	5
3 Anisol	-0.778	(pOCH ₃)	-0.778	8.21	20	1
4 Biphenyl	-0.179	(pC ₆ H ₅)	-0.179	8.23	5.8	this work
5 1,2,4-Trimethylbenzene	-2x0.311	(pCH ₃)	-0.688	8.27	35	1
6 1,3,5-Trimethylbenzene	-3x0.311	(pCH ₃)	-0.933	8.40	52	1
7 p-Xylene	-0.311	(pCH ₃)	-0.377	8.45	12	1
8 1,2,3-Trimethylbenzene	-2x0.311	(pCH ₃)	-0.688	8.48	27	1
9 Phenol	-0.92	(pOH)	-0.92	8.50	28	4
10 m-Xylene	-2x0.311	(pCH ₃)	-0.622	8.56	22	1
11 o-Xylene	-0.311	(pCH ₃)	-0.377	8.56	12	1
12 n-Propylbenzene	-0.295	(pC ₂ H ₅)	-0.295	8.72	5.8	1
13 i-Propylbenzene	-0.28	(p iC ₃ H ₇)	-0.28	8.73	6.7	1
14 m-Ethyltoluene	-0.295	(pC ₂ H ₅)	-0.606	-	18	1
15 o-Ethyltoluene	-0.064	(mC ₂ H ₅)	-0.375	-	13	1
16 p-Ethyltoluene	-0.064	(mC ₂ H ₅)	-0.375	-	12	1
17 p-Cymene	-0.151	(p iC ₃ H ₇)	-0.462	-	15	2
18 m-Cresol	-0.92	(pOH)	-1.231	8.75	67	1
19 Ethylbenzene	-0.295	(pC ₂ H ₅)	-0.295	8.76	7.8	1
20 Toluene	-0.311	(pCH ₃)	-0.311	8.82	5.5	1
21 o-Cresol	-0.92	(pOH)	-0.986	8.93	47	1
22 p-Dichlorobenzene	+0.114	(pCl)	+0.513	8.94	0.33	5
23 p-Cresol	-0.92	(pOH)	-0.986	8.97	52	1
24 Chlorobenzene	+0.114	(pCl)	+0.114	9.06	0.67	this work
25 o-Dichlorobenzene	+0.114	(pCl)	+0.513	9.07	0.42	5
26 1,2,4-Trichlorobenzene	+2x0.114	(pCl)	+0.627	9.10	0.52	4
27 m-Dichlorobenzene	+2x0.114	(pCl)	+0.228	9.12	0.69	5
28 Benzene	0		0	9.24	1.2	1
29 Benzaldehyde	+0.36	(mCHO)	+0.36	9.53	16	3
30 Benzonitrile	+0.562	(mCN)	+0.562	9.71	0.33	this work
31 Hexafluorobenzene	-3x0.073	(pF)	+0.837	9.90	0.22	1
32 Nitrobenzene	+0.674	(mNO ₂)	+0.674	9.90	0.21	this work
33 n-Propylpentafluorobenzene	-0.295	(pC ₂ H ₅)	+0.19	-	3.1	1

ABSTRACT A-12

KINETIC STUDIES OF F-ATOM REACTIONS AND OF VIBRATIONAL RELAXATION OF HF($v \leq 6$) BY TIME-RESOLVED INFRARED CHEMILUMINESCENCE FOLLOWING PULSED LASER PHOTOLYSIS.

Martin K. Osborn, Ian W.M. Smith and David J. Wrigley[†]
Department of Physical Chemistry,
University Chemical Laboratories,
Lensfield Road, Cambridge CB2 1EP, England.

Although steady-state, infrared chemiluminescence experiments have provided information about the rovibrational state distributions of HF produced in many reactions of F atoms,¹ it has not been easy to obtain accurate overall rate constants for these reactions. It has also proved difficult to determine the rate constants for vibrational relaxation of HF in levels $v > 1$ - which are for example, required for modelling HF chemical lasers.² We shall describe experiments which can simultaneously provide both types of information.

In these experiments, F atoms are generated by photolysis of F₂ with the 4th harmonic output ($\lambda = 266$ nm) of a repetitively pulsed (10 Hz) Nd:YAG laser. They then react with a hydrogen-containing molecule (HX) to form HF in vibrational levels up to some maximum determined by the exothermicity of the reaction (see Table 1). The mixture of F₂ and HX is diluted in Ar and flowed slowly through the reaction cell to prevent accumulation of products.

[†] Present address : Department of Chemistry, University of Toronto, 80, St. George Street, Toronto, Canada M5S 1A1.

Reaction	$-\Delta H_o^0/\text{kJ mol}^{-1}$	v_{max}	$10^{11}k/\text{cm}^3\text{ molecule}^{-1}\text{s}^{-1}$
$\text{F}+\text{HCl} \rightarrow \text{HF}+\text{Cl}$	138	3	0.70 ± 0.03
$\text{F}+\text{HBr} \rightarrow \text{HF}+\text{Br}$	203	4	6.2 ± 0.5
$\text{F}+\text{HI} \rightarrow \text{HF}+\text{I}$	271	6	$5.6^{+0.6}_{-0.2}$
$\text{F}+\text{H}_2\text{O} \rightarrow \text{HF}+\text{OH}$	69	1	
$\text{F}+\text{NH}_3 \rightarrow \text{HF}+\text{NH}_2$	107	2	
$\text{F}+\text{HCN} \rightarrow \text{HF}+\text{CN}$	53	1	

Chemiluminescence is observed only from the highest accessible level, v_{max} . In the cases of $X = \text{Cl}, \text{Br}, \text{I}$, the (3,0), (4,0) and (6,2) overtone bands are monitored using a photomultiplier and appropriate filtering. With the other reagents, vibrational chemiluminescence is observed in the infrared, again with filtering, if necessary to isolate emission from $\text{HF}(v_{\text{max}})$. Signals are digitised, accumulated in a signal averager and punched on paper tape. Data from each experiment are fitted to a function of the form :

$$\exp(-k'_{1st}t) - \exp(-k''_{1st}t).$$

Here, the two first-order constants correspond to $k_{\text{reac}}[\text{HX}]$ and $\sum k_{v_{\text{max}}}^Q [Q]$, where $k_{v_{\text{max}}}^Q$ is the second-order

rate constant for

relaxation of $\text{HF}(v_{\text{max}})$ by component Q of the gas mixture, but there is no direct way of knowing which is which. However, when HX is varied and k'_{1st} and k''_{1st} plotted against HX , as in Fig. 1(a) for $\text{HX} = \text{HBr}$, one line shows an intercept and this rate constant is assigned to the relaxation process. Furthermore, addition of non-reactive relaxants to the systems increase one rate first-order constant but leaves the other unaltered (see Fig. 1(b)). Hence, rate constants for reactions and individual relaxation processes can be obtained from the gradients of lines like those shown in Fig. 1.

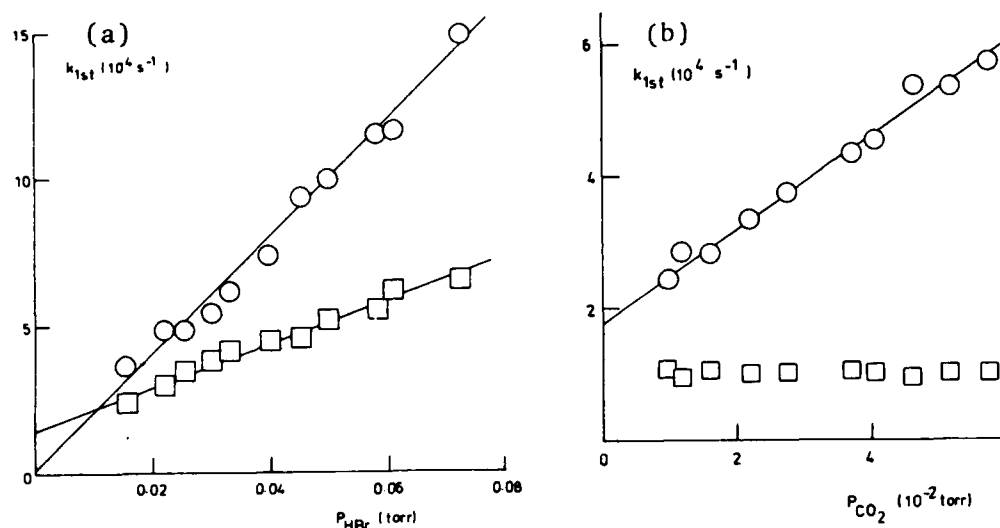


Fig.1. First-order constants derived from an analysis of the HF(4,0) chemiluminescence excited in the F + HBr reaction : (a) plotted against [HBr] ; (b) plotted against [CO₂] added, the concentration of HBr being kept constant.

Rate constants for reaction of F with HCl, HBr and HI are listed in Table 1. With HI, some difficulty was experienced because of 'pre-reaction' between F₂ and HI at a significant rate and because HI itself is photolysed by radiation at 266 nm, and this explains the wider error limits assigned to the rate constant for this reaction. These results, which have been published,³ are in quite good agreement with the only other time-resolved measurements⁴ on these reactions, although they differ by amounts outside the small quoted limits of uncertainty. New preliminary results on the other three reactions in Table 1 will be presented at the meeting.

Rate constants for relaxation of HF($v=1,2,3,4$ and 6) obtained by this method will also be presented and compared with (a) the considerable body of data available for HF($v=1$) from laser-induced vibrational fluorescence experiments,² and (b) the much smaller number of results obtained for higher levels of HF using direct optical pumping techniques.⁵⁻⁷

References

- ¹ B.E.Holmes and D.W.Setser in Physical Chemistry of Fast Reactions. Vol. 2: Reaction Dynamics, ed I.W.M.Smith (Plenum, New York, 1980) chap.2.
- ² R.T.Bailey and F.R.Cruickshank, Gas Kinetics and Energy Transfer, vol. 3, ed. P.G.Ashmore and R.J.Donovan (Chem. Soc., London, 1978) chap. 4.
- ³ I.W.M.Smith and D.J.Wrigley, Chem. Phys., 63, 321 (1980).
- ⁴ E.Wurzberg and P.L. Houston, J.Chem. Phys., 72, 5915 (1980).
- ⁵ J.F.Bott, J. Chem. Phys., 65, 4239 (1976); J.F.Bott and R.F.Herdner, J. Chem. Phys., 72, 3211 (1980).
- ⁶ D.J.Douglas and C.B.Moore, Chem. Phys. Letters, 57, 485 (1978); J. Chem. Phys., 70, 1769 (1979).
- ⁷ J.K.Lampert, G.M.Jurisch and F.F. Crim, Chem. Phys. Letters, 71, 258 (1980); G.M.Jurisch and F.F.Crim, J. Chem. Phys., 74, 4455 (1981).

ABSTRACT A-13

THE CHEMISTRY OF THE GASEOUS ETHYNYL RADICAL:
DIRECT OBSERVATION OF THE $A^2\Pi$ STATE

T.A. Watson, F. Shokoohi, H. Reisler, and C. Wittig
University of Southern California
Los Angeles, CA 90007, USA

ABSTRACT

The ethynyl radical, C_2H , although known to be an important intermediate in many chemical environments, has proven very difficult to monitor directly due to its lack of absorption features from the near infrared to the ultraviolet. Because of this, reactions of C_2H have been inferred from the appearance of products, and the initial energy content of the radical has been poorly defined. Recent theoretical and experimental studies have confirmed the existence of an electronically excited state of C_2H (C_2H^*) lying just 0.47 eV above the ground state. We will report on the direct observation of time and wavelength resolved emissions from C_2H^* , and discuss the role of this species in several reactive environments.

C_2H^* is prepared by passing the collimated 193 nm output (15 mJ cm⁻²) of a Lumonics ArF excimer laser through a cell containing either acetylene or bromoacetylene. Time resolved IR fluorescence is monitored at right angles to the laser beam with a LN₂ cooled InSb detector. After two stages of amplification,

the signals are digitized, averaged for a suitable number of excimer laser firings, and sent to an X-Y recorder. Interference filters and circular variable filters are used to observe the wavelength dependence of the emission.

The observed emission is quite broad, covering the region 2.5 - 5.0 μm , with the long wavelength limit determined by the wavelength response of the detector. Further studies using near infrared interference and cutoff filters will allow determination of the short wavelength limit. The fluorescence is characterized by a slow decay ($k_{\text{rad}} \leq 2 \times 10^4 \text{ s}^{-1}$) throughout the observed spectral region. While this is consistent with vibrational emission, the breadth of the emission and its presence at wavelengths shorter than 2.5 μm make such an assignment quite unlikely. The use of additional precursors should allow the unambiguous assignment of the emission to C_2H . Measurements of removal rates by H_2 , O_2 , CH_4 , C_2H_2 , and other reactants are underway and will be presented in detail. The results of these measurements will be compared with previously measured reaction rate coefficients for C_2H .

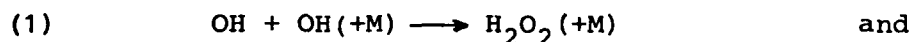
ABSTRACT A-14

RATE CONSTANTS FOR THE RECOMBINATION REACTIONS $\text{OH} + \text{OH}(+M) \rightarrow \text{H}_2\text{O}_2(+M)$ $(M = \text{N}_2)$ AND $\text{OH} + \text{H} + M \rightarrow \text{H}_2\text{O} + M$ $(M = \text{He})$ *

R. Zellner, K. Erler, R. Paschke and G. Wagner

Institut für Physikalische Chemie, Universität Göttingen,
3400 Göttingen, F.R.G.

The interest in radical recombination reactions yielding well known stable products is twofold: i) they compliment dissociation data and hence provide formidable examples to test unimolecular rate theory at the low temperature end and ii) they are important in modeling complex radical-radical reaction systems, in particular at higher pressures. Rate data on reactions



are extremely scarce [1,2] because of enhanced difficulties in establishing experimental conditions where these reactions can be studied in isolation. In view of this we have chosen two different experimental arrangements. i) Reaction (1) was studied in a conventional flash photolysis system, using H_2O photolysis as a source of OH. This system has been described previously [3,4]. Absolute OH concentrations were determined by quantitative absorption spectrometry using the Q_1 line of the A-X (0,0) band transition. Effective absorption coefficients at low pressures were

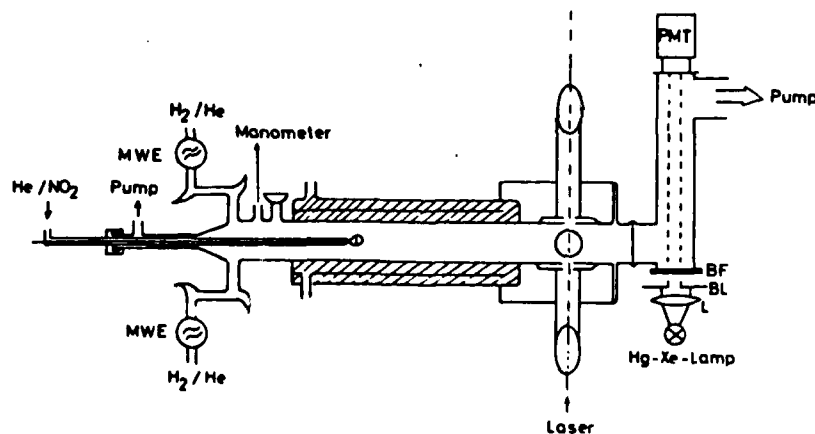


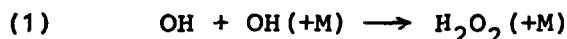
Fig. 1 Flow system arrangement with OH detection by LIF for studies of the reaction $\text{OH} + \text{H} + M \rightarrow \text{H}_2\text{O} + M$

*) submitted to: XVth Int. Conference on Photochemistry, Stanford, USA, 1982

those of ref. [3], but corrections due to homogeneous line broadening at pressures above 100 Torr were fully accounted for. The accessible pressure range for studies of the OH recombination in N_2 was 20 - 800 Torr. ii) Reaction (2) cannot be studied by the same technique. Rather we have used a flow system in which an excess concentration of H atoms can easily be established and the kinetics of the OH decay can be monitored under pseudo-first order conditions. For enhanced detection sensitivity ($\sim 10^{10} \text{ cm}^{-3}$) OH laser induced fluorescence of the (0,0) band coupled with box car integration was used. The H atom concentration was determined by NO_2 titration and HNO^* chemiluminescence [5]. The experimental arrangement is shown schematically in Fig. 1.

1. The reaction $OH + OH(+M) \rightarrow H_2O_2(+M)$

Rate measurement for this reaction were made for $M = N_2$ in the pressure range 20 - 800 Torr at three different temperatures (253, 298 and 353 K). Initial OH concentrations were of the order of 10^{14} cm^{-3} . Under these conditions the OH decay (followed over several msec) was found to be second order and due to the following reactions



with the effective decay constant k_{eff} equal to $2k_1^M + 3k_{1a}$. The validity of this simple analysis was tested using a computer code including reactions such as $OH + H_2O_2$, $OH + HO_2$ and $OH + H + M$. After correction for the pressure independent term ($3k_{1a}$) where k_{1a} was taken from our recent study of this reaction ($k_{1a} = (3.2 \pm 0.8)10^{-12} \exp(-242/T) \text{ cm}^3/\text{molecule s}$ [3]) k_1^M is found to show a 'fall-off' behaviour. From an analysis of the data using a symmetrical Kassel integral formalism [6] the following rate constants were deduced in the limits of low (k_1^0) and high (k_1^∞) pressure.

T/K	$k_1^0/\text{cm}^6 \text{ molecule}^{-2} \text{ s}^{-1}$	$k_1^\infty/\text{cm}^3 \text{ molecule}^{-1} \text{ s}^{-1}$
253	$(9.1 \pm 2.0)10^{-31}$ 3.5	$(1.3 \pm 0.4)10^{-11}$
298	$(6.9 \pm 1.5)10^{-31}$ 2.8	$(0.9 \pm 0.4)10^{-11}$
353	$(6.8 \pm 1.5)10^{-31}$ 2.8	$(0.9 \pm 0.4)10^{-11}$

Whereas the temperature variation of k_1^0 (corresponding to $T^{-0.8}$) is expected to be real, the different values of k_1^∞ are almost certainly a reflection of the uncertainty associated with the k_1^∞ extrapolation. A temperature independent value of $k_1^\infty = (1.0 \pm 0.4)10^{-11} \text{ cm}^3/\text{molecule s}$ is probably a better representation.

To our knowledge there has been no previous determination of the high pressure limit of reaction (1). The value reported here is, however, in the range expected from comparable reaction (i. e. $\text{OH} + \text{NO} \rightarrow \text{HONO}$). The only previous direct study of k_1 in the low p limit is due to Trainor and von Rosenberg [1]. Their value ($k_1(298\text{K}) = 2.5 \times 10^{-31} \text{ cm}^6/\text{molecule}^2\text{s}$) is more than a factor of two lower than ours, which we attribute predominantly to the 'fall-off' behaviour, which was not noticed in TR's experiments.

2. The reaction $\text{OH} + \text{H} + \text{M} \rightarrow \text{H}_2\text{O} + \text{M}$

This reaction was studied for $\text{M} = \text{He}$ over the pressure range 2.0 - 10.5 Torr at 300 K using a large excess of H and hence pseudo-first order conditions for the decay of OH . Initial OH concentrations were kept below $2 \times 10^{11} \text{ cm}^{-3}$, such that reaction second order in OH were entirely negligible. First order decay constants, however, were found to show a complicated dependence on H atom concentration (Fig. 2). We attribute this effect to an

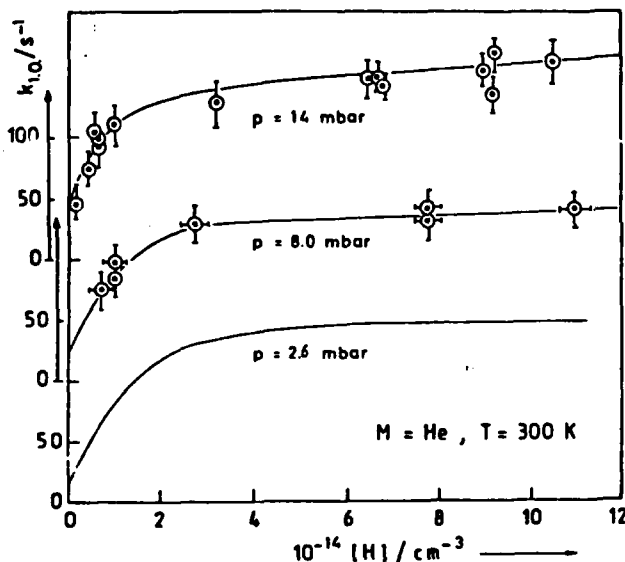
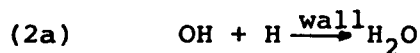


Fig. 2: Dependence of first order OH decay constants on H atom concentration

interference of the homogeneous recombination reaction (2) with an H atom catalyzed wall recombination of OH :



where the rate determining H -atom (surface) concentration ($[\text{H}]_{\text{ads}}$) is determined by the corresponding adsorption isotherm (Rideal mechanism). For $[\text{H}] > 4 \times 10^{14} \text{ cm}^{-3}$ the rate of reaction (2a) is found to be independent on $[\text{H}]$ and hence the homogeneous reaction (2) can be separated. We obtain at 300 K $k_2(\text{M} = \text{He}) = (8.2 \pm 2.5) \times 10^{-32} \text{ cm}^6/\text{molecule}^2\text{s}$. This value is almost a factor of two smaller than our previous data [2]. The difference is explained by an incomplete account of a complex surface reaction, which had been noted in our previous study but which was differently interpreted. The present result is in good agreement with a theoretical prediction [6].

1. D. W. Trainor, C. W. von Rosenberg, Jr., J. Chem. Phys. 61, 1010 (1974)
2. R. Zellner, K. Erler, D. Field, 16th Symp. (Int.) Combustion, p. 939 (1977)
3. G. Wagner, R. Zellner, Ber. Bunsenges. Phys. Chem. 85, 1128 (1981)
4. V. Handwerk, R. Zellner, Ber. Bunsenges. Phys. Chem. 82, 1161 (1978)
5. K. Erler, Ph.D. Dissertation, University of Göttingen 1981
6. K. Luther, J. Troe, 17th Symp. (Int.) Combustion, p. 535 (1979)

ABSTRACT B-1

THERMAL UNIMOLECULAR REACTIONS. H. M. Frey, Chemistry Department, Reading University, Reading, England.

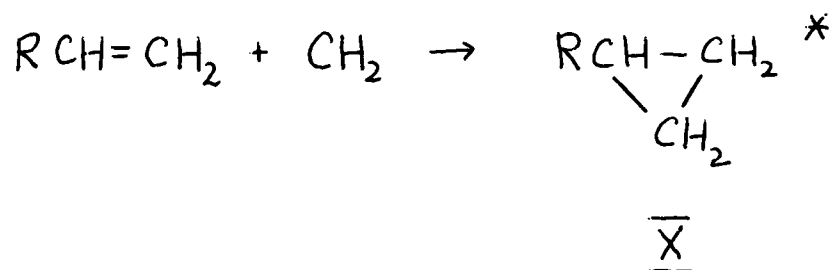
Quantitative studies are usually carried out to,

- I Determine accurate high Pressure Arrhenius Parameters,
- II Determine "fall off" curves and if possible low pressure Arrhenius parameters.

These may be applied in a number of ways as noted below.

- I (i) They yield input data required for many applications of Unimolecular Reaction Rate Theory to other (non thermal systems). Thus the calculation of the rate of decomposition of a monoenergetic species formed by chemical activation requires A and E_a to be known.

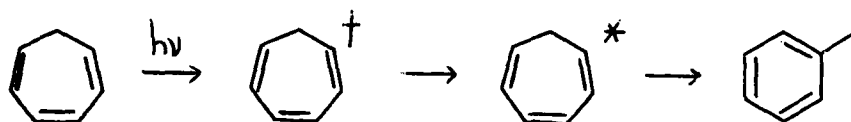
A large number of such systems have involved CH_2 reactions viz



To calculate the rate of isomerization of the highly energised species $\bar{\text{X}}$ (note $\Delta H \approx -450 \text{ kJ mol}^{-1}$) the Arrhenius parameters for the thermal unimolecular isomerization of the appropriate cyclopropane need to be available.

Highly vibrationally excited essentially monoenergetic species have been produced in many chemical activation systems and they are in no way limited to cyclopropanes or indeed methylene reactions.

- I (ii) Similarly excited species produced photochemically often undergo unimolecular isomerizations or decompositions. When the molecule decomposing results from internal conversion to the ground state then the appropriate thermal data allow the calculation of rate parameters to be carried out. An example of such a system is the photochemically induced isomerization of cycloheptatriene (and its alkyl derivatives)



(where + indicates electronic excitation and * vibrational excitation)

- I (iii) Studies provide much of the important primary data for determining bond strengths and heats of formation of radicals and biradicals. Use of thermochemical and thermochemical kinetic arguments can extend such data to many systems. It is difficult to overestimate the extent to which all branches of kinetics use such information.
- I (iv) Related to (iii) but in many instances somewhat different in both approach and objective, the determination of Arrhenius Parameters for a series of related compounds can lead to the formulation of a fairly detailed description of the activated complex. This in turn may lead to some simple additivity relationships that allow the effect of substituents and structure on the kinetic parameters to be rationalised.
- II (i) Fall off curves especially if available from the high pressure to the 2nd order region provide a direct though not searching test of unimolecular reaction theory. They also allow efficiencies of energy transfer between energised molecules and the "bath gas" molecules to be evaluated. Perhaps the most thoroughly studied system in this context is the thermal isomerization of methylisocyanide (Rabinovitch and co-workers) for which extensive data are available.
- II (ii) The change in Arrhenius parameters as a function of pressure in the fall off region provides a moderately good test of the vibrational assignment of the activated complex which goes beyond that available from the high pressure values alone. If data are available for isotopically substituted molecules (usually D for H) they can be used to make vibrational assignments with real precision.

II (iii) For molecules undergoing unimolecular transformations by two channel processes, data in the fall off region, if sufficiently precise and extensive can allow not only relative efficiencies of energy transfer to be obtained but assuming certain models about the distribution function for such transfer it may also be possible to estimate the amount of energy transferred per collision. Studies of the thermal decomposition of 1,1,2,2-tetrafluorocyclobutane have yielded information of this type. Such studies are also likely to produce results of use in unscrambling some of the data obtained by infra-red multiphoton excitation experiments.

It is hoped to discuss some recent experimental results relating to I (i) obtained by a study of the reactions of methylene with oxetane and 3,3-dimethyloxetane. Also results relating to I (iv) from studies on the thermal decomposition of several alkyl substituted cyclobutanones. Other studies on systems relating to II (i) and (ii), namely the thermal isomerizations of oxetanones will be presented and finally we will report data on thermal isomerizations yielding information under heading II (iii).

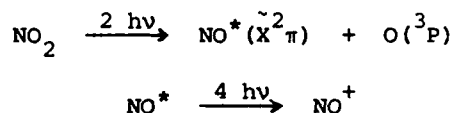
ABSTRACT B-2

TWO-PHOTON PHOTODISSOCIATION DYNAMICS OF NO₂ IN THE REGION OF 45,000 cm⁻¹

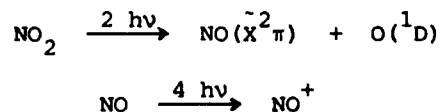
Richard J.S. Morrison and Edward R. Grant

Department of Chemistry
Baker Laboratory
Cornell University
Ithaca, New York 14853

In a recent paper we reported a survey of the visible multiphoton ionization spectrum of NO₂.¹ We showed that the appearance of this spectrum in the blue is dominated by photodissociation processes that occur at the level of the second photon. For excitation frequencies that in two photons reach beyond the origin of the NO₂ \tilde{B}^2B_2 state (40,000 cm⁻¹), but fall short of the threshold for production of O(¹D) (41,000 cm⁻¹), we see a multiphoton ionization spectrum not of the parent, but rather that characteristic of vibrationally and rotationally hot NO:



Above the two-photon threshold for O(¹D) formation, this spectrum changes dramatically. For two-photon frequencies greater than 43,000 cm⁻¹ the NO produced from NO₂ is substantially colder. This is consistent with a shift in the photolysis pathway to the production of electronically excited O(¹D), which leaves far less of the photolysis energy available for vibrational and rotational excitation of the diatomic fragment.



Using a molecular beam, we have re-examined the spectrum of nascent NO from supersonically cooled NO₂, again using the same laser pulse to pump NO₂ and probe for NO. By observing NO⁺ photofragment spectra at wavelengths corresponding to the A(²T⁺) ← X(²π_{1/2,3/2}) sequence band regions v'-v''=0, near 450 nm, and v'-v''=1, near 430 nm, we have been able to characterize the NO internal energy distribution with greater precision.

We have found for the most part that the internal energy distribution in the nascent NO resulting from photodissociation of NO₂ at the two photon level via the O(¹D) pathway qualitatively resembles that which has been observed in the one photon dissociation of NO₂ via the O(³P) pathway^{2,3} for a similar excess energy above threshold. As shown by Figure 1, for two

photon photolysis near 450 nm, we observe the production of both NO spin-orbit components. Vibrational and rotational excitation in the nascent NO are consistent with dissociation from the bent \tilde{B}^2B_2 upper state of NO_2 .

However, in the neighborhood of 427 nm, the NO internal state distribution, indicated by the spectrum in Figure 2, is dramatically different. For NO in $v''=1$, observed by means of the resonance: $\tilde{A}^2\Sigma^+(v'=2) \leftarrow \tilde{X}^2\Pi(v''=1)$, we find that the photoproduct rotational distribution is ice-cold, limited by the rotational temperature of our supersonic molecular beam, and that a spin-orbit component, $^2\Pi_{1/2}$, is missing. Our data thus indicates that the dissociation dynamics are radically different in this spectral region, suggesting a linear or near-linear dissociation geometry that imparts very little torque to the departing NO photofragment, and places strict symmetry requirements on its spin-orbit state.

In this report we present an analysis of the MPI spectrum of jet-cooled NO_2 that characterizes the anomalous behavior of the 427 nm region. We consider the source of this behavior and offer an interpretation that traces its cause to participation of a theoretically calculated⁴ but never observed linear state of NO_2 lying above the origin of \tilde{B}^2B_2 .

Acknowledgement

This work has been supported by the U.S. Army Research Office.

References

1. R.J.S. Morrison, B.H. Rockney and E.R. Grant, J. Chem. Phys. 75, (1981).
2. G.E. Busch and K.R. Wilson, J. Chem. Phys. 56, 3626 (1972).
3. H. Zacharias, M. Geilhaupt, K. Meier and K.H. Welge, J. Chem. Phys. 74, 218 (1980).
4. G.D. Gillispie, A.U. Khan, A.C. Wahl, R.P. Hosteny and M. Krauss, J. Chem. Phys. 63, 3425 (1975).

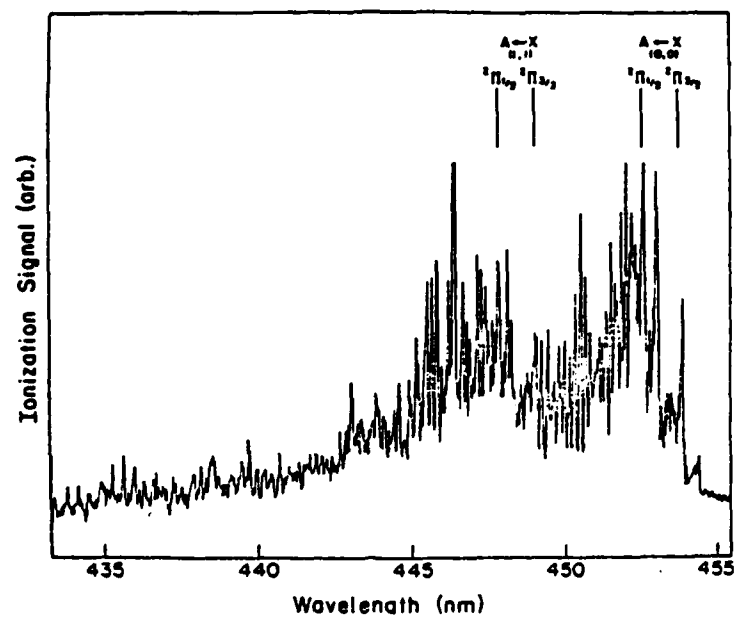


Figure 1: Molecular beam MPI spectrum of NO^+ from NO_2 in the 450 nm sequence region.

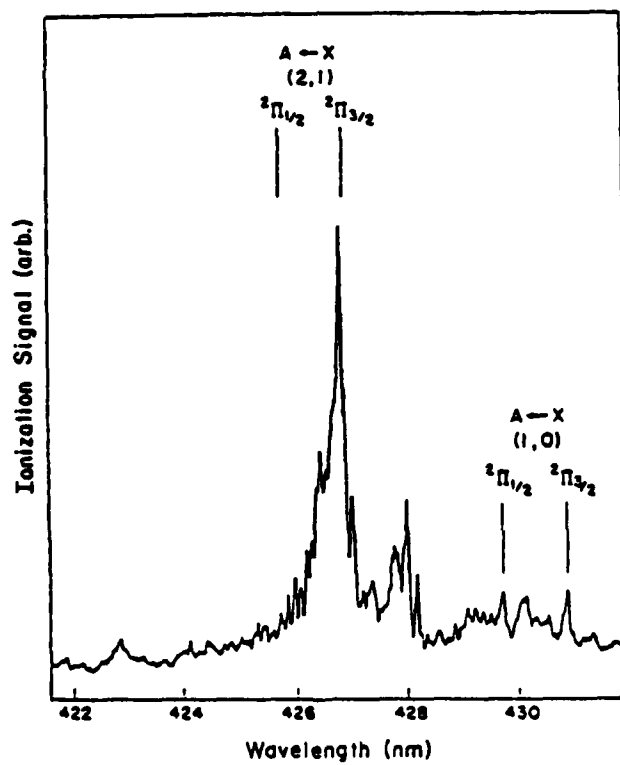


Figure 2: Molecular beam MPI spectrum of NO^+ from NO_2 in the 430 nm sequence region.

ABSTRACT B-3

ROTATIONALLY EXCITED CO FROM FORMALDEHYDE PHOTODISSOCIATION*

Pauline Ho and Arlee V. Smith
Sandia National Laboratories
Albuquerque, NM 87185

The mechanism of formaldehyde photodissociation has been the subject of extensive experimental and theoretical study.¹ Previous experiments² showed that the appearance rate of the CO product in low rotational levels was much slower than the corresponding disappearance of excited formaldehyde, and that these appearance rates were proportional to pressure. This led to the hypothesis that the H_2CO dissociation mechanism included a long-lived intermediate state which collisionally dissociated to $\text{H}_2 + \text{CO}$. Other experiments, notably low-pressure measurements of $\text{H}_2\text{CO}(\text{S}_1)$ decay rates³⁻⁵ and a molecular beam photofragmentation experiment⁶, showed that H_2CO dissociates in the absence of collisions, in apparent contradiction to the appearance rate results.

The present study resolves the question of the intermediate in formaldehyde photodissociation. $\text{CO}(J = 25-62)$ produced by 355 nm photolysis of H_2CO was observed by VUV laser-excited fluorescence. The temporal behavior of $\text{CO}(J = 36)$ indicates that H_2CO dissociates promptly giving CO in high rotational levels which

*This work performed at Sandia National Laboratories supported by the U. S. Department of Energy under contract number DE-AC04-76DP00789.

then collisionally relaxes to the lower rotational levels observed in the previous CO appearance rate measurements. Thus, rotationally excited CO fills the role of the long-lived intermediate.

References

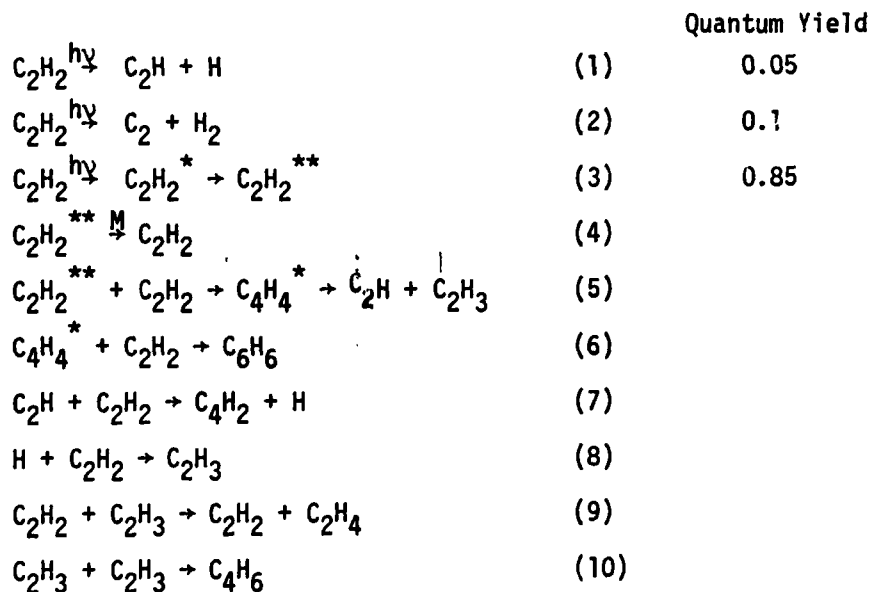
1. W. M. Gelbart, M. L. Elert and D. F. Heller, Chem. Rev. 80, 403 (1980), and references therein.
2. P. L. Houston and C. B. Moore, J. Chem. Phys. 65, 757 (1976).
3. J. C. Weisshaar, D. J. Bamford, E. Specht and C. B. Moore, J. Chem. Phys. 74, 226 (1981).
4. K. Shibuya, P. W. Fairchild and E. K. C. Lee, J. Chem. Phys. 75, 3397 (1981).
5. W. E. Henke, H. L. Seizle, T. R. Hays and E. W. Schlag, J. Chem. Phys. 76, 1327 (1982).
6. P. Ho, D. J. Bamford, R. J. Buss, Y. T. Lee and C. B. Moore, J. Chem. Phys., in press.

ABSTRACT B-4

Photochemistry of Acetylene at 1849Å

H. Okabe
Molecular Spectroscopy Division
National Bureau of Standards
Washington, D.C. 20234

The quantum yield of diacetylene, the major product in the photolysis of acetylene at 1849Å, has been measured as a function of pressure. The yield is 0.05 at the low pressure limit and increases with pressure to a maximum of 0.7 at 10 torr (see Fig. 1). The quantum yield of diacetylene formation is 0.2 at 1 torr of pure acetylene and it decreases to a limiting value of 0.05 with an increase of the partial pressure of He or N₂ (see Fig. 2). The quantum yield of H₂ in C₂H₂ photolysis is 0.1. The results may be explained on the basis of the following mechanism.



where $C_2H_2^*$ signifies the B ¹B_u state and $C_2H_2^{**}$ is a metastable (triplet) state.

Diacetylene is formed from reaction (1) followed by (7) and reaction (3) followed by (5) and (7). The addition of N_2 or He quenches $C_2H_2^{**}$ so that the quantum yield of 0.05 corresponds to that of reaction (1).

The reaction rates of C_2H with C_2H_6 and C_3H_8 relative to that with C_2H_2 have been measured by the decrease of diacetylene when the partial pressure of C_2H_6 (or C_3H_8) was increased. The results are shown in Table 1,

Table 1

Reaction	Ratio	Rate Constant	
		$(10^{-11} \text{ cm}^3 \text{ molec}^{-1} \text{ s}^{-1})$	
$C_2H + C_2H_6 \rightarrow C_2H_2 + C_2H_5$	0.240 ± 0.015	0.72 ± 0.05	0.65 ± 0.04^a
$C_2H + C_3H_8 \rightarrow C_2H_2 + C_3H_7$	0.469 ± 0.041	1.4 ± 0.1	
$C_2H + C_2H_2 \rightarrow C_4H_2 + H$	1	3	3.1 ± 0.2^b
			5^c

^aA. H. Laufer, J. Phys. Chem. 85, 3828 (1981).

^bA. H. Laufer and A. M. Bass, J. Phys. Chem. 83, 310 (1979).

^cW. Lange and H. G. Wagner, Ber. Bunsenges, Physik, Chem. 79, 165 (1975).

In the Jovian Atmosphere acetylene acts as a catalyst to decompose H_2 and CH_4 in the spectral regions where only acetylene absorbs ($> 1500\text{\AA}$).

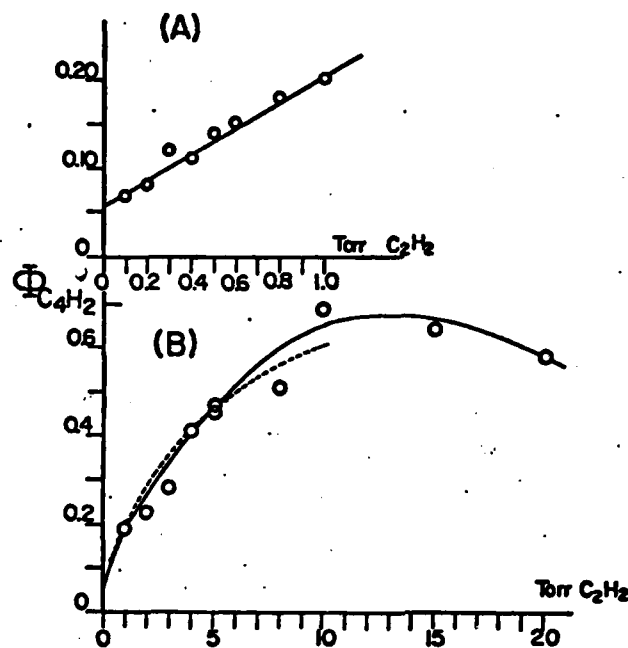


Figure 1. The quantum yield of diacetylene formation as a function of C_2H_2 pressure at 1849 Å.

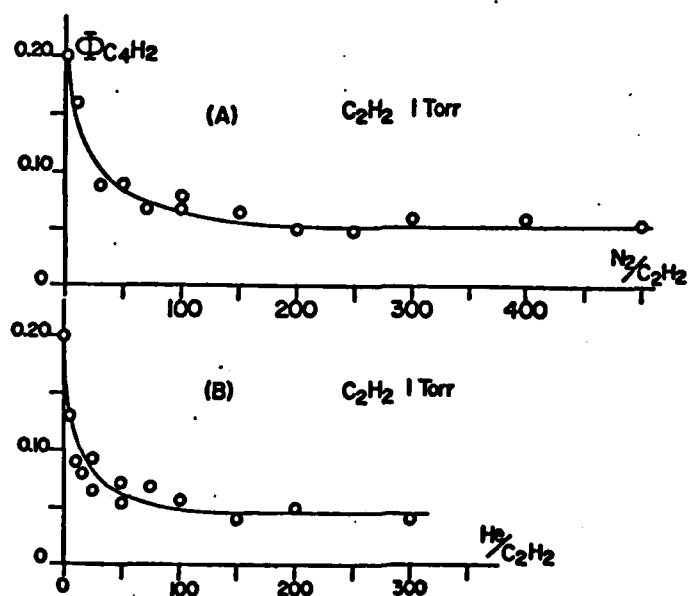


Figure 2. The quantum yield of diacetylene formation at 1 torr of C_2H_2 as a function of partial pressure of N_2 or He, incident wavelength 1849 Å.

ABSTRACT B-5

THERMAL DECOMPOSITION OF OXETAN AND OXETAN-D₂

Zs. HUNYADI-ZOLTÁN, L. ZALOTAI, T. BÉRCES and F. MÁRTA

Central Research Institute for Chemistry,
Hungarian Academy of Sciences, Budapest, Hungary

Kinetic data for oxetan and various substituted oxetans are available today. However, the reported Arrhenius parameters seem to involve certain inconsistencies. "Low" Arrhenius parameters /i.e. A factors around $10^{14.5} \text{ s}^{-1}$ and activation energies less than 250 kJ mol^{-1} / as well as "high" kinetic parameters /i.e. A factors of about $10^{15.5} \text{ s}^{-1}$ and activation energies around or above 250 kJ mol^{-1} / were published. The order of magnitude difference in the A factors is difficult to elucidate, provided that all compounds decompose by the same mechanism.

The decomposition of oxetan and oxetan-2, 2-d₂ were investigated at "high pressures" and in the pressure dependent range. The experimental results were analysed by unimolecular reaction rate theories.

Oxetan and oxetan-d₂ were found to decompose in clean unimolecular reactions into ethylene and formaldehyde. "High pressure" first order rate coefficients were deter-

mined at pressures of $p_0 \geq 6$ kPa over the temperature range of 670-760 K. A least-squares treatment of the oxetan decomposition data yields

$$\log/k_{\infty}/s^{-1}/ = 15.42 \pm 0.31 - /259.5 \pm 3.8/ \text{ kJ mol}^{-1} \ln 10$$

The rate coefficients for oxetan-d₂ decomposition fits the equation

$$\log/k_{\infty}/s^{-1}/ = 15.54 \pm 0.16 - /262.8 \pm 1.9/ \text{ kJ mol}^{-1}/\text{FT} \ln 10$$

The "high pressure" kinetic results obtained for oxetan decomposition in this study are compared with literature data in the following Table.

$\log/A^{\infty}/s^{-1}/$	$E_A^{\infty}/\text{kJ mol}^{-1}$	$10^4 \times k_{\infty}/s^{-1}$ at 713 K	Reference
15.42 ± 0.31	259.5 ± 3.8	2.56	This work
15.71 ± 0.31	263.7 ± 3.5	2.46	Holbrook and Scott /1/
14.79	251.0	2.52	Bittker and Walters /2/

/1/ K.A. Holbrook and R.A. Scott, J.C.S. Faraday I. 71,
1849 /1975/

/2/ D.A. Bittker and W.A. Walters, J.Amer.Chem.Soc., 77,
2326/1955/

The rate coefficients originating from the three sources

show remarkable good agreement, however, this is not the case for the Arrhenius parameters. It is obvious that all available theoretical and experimental information other than rate coefficient measurements as a function of temperature are required. Such information can be expected from the interpretation of the pressure dependence of the first order rate coefficient and of the kinetic isotope effect.

Experimental fall-off curves were determined at various temperatures in the pressure range from 7 kPa down to 10 Pa both for oxetan and for oxetan-d₂ decomposition. Interpretation of the fall-off plots by the RRK theory required the Kassel parameters of $s_K = 18$, $s_K = 19$ and $s_K = 17$ if Arrhenius parameters obtained in this work, reported by Holbrook and Scott /1/ and published by Bittker and Walters /2/, respectively, were used. Since there is no accurate theoretical method available which could predict the Kassel parameter, the RRK theory is not suitable either to support or to reject any of the reported Arrhenius parameters.

Hereupon a more sophisticated treatment known as RRKM /Marcus/ theory was used in the analysis of the fall-off data. Transition state models were constructed by fitting

the Arrhenius parameters for oxetan decomposition obtained in this work, reported by Holbrook and Scott /1/ and published by Bittker and Walters, respectively. Based on these three transition state models, RRKM fall-off curves were calculated. Comparison of the theoretical and experimental results proved that the transition state model which was constructed to fit the Arrhenius parameters determined in this work gave excellent agreement with the experimental fall-off data obtained in a pressure range of three orders of magnitude at eight temperatures.

The results of RRKM calculations were found to reproduce also the experimental kinetic isotope effect and its pressure dependence.

The high-pressure Arrhenius parameters evaluated are in accordance with the biradical mechanism. On the basis of experimental results obtained in this study, kinetic data were determined for the individual decomposition paths yielding various biradicals.

ABSTRACT C-1

Unimolecular-Reactions with Non-thermal Activation

J. Troe

Institut für Physikalische Chemie der Universität Göttingen

Tammannstr. 6

3400 Göttingen/Germany

Abstract

Apart from thermal collisional activation, unimolecular reactions can be initiated by a large group of non-thermal activation processes such as chemical activation, photochemical activation, electron impact, charge exchange, photoionization or exothermic precursor reactions. These experiments allow for the observation of various quantities. Yield-pressure relationships in chemical and photochemical activation lead to ratios of specific rate constants $k(E)$ and "effective" rate constants for collisional stabilization. Fragment distributions or product vibrational and translational energy distributions lead to ratios of specific rate constants for various chemically or energetically different channels. Multiphoton activation studies are characterized by the competition between optical pumping and unimolecular processes.

Direct, time-resolved measurements of specific rate constants $k(E)$ have frequently been performed for the fragmentation of molecular ions over the last 15 years. With the availability of intense lasers, such direct measurements of $k(E)$ have recently also become possible for neutral molecules after photoactivation. Also, direct measurements of collisional energy transfer for molecules high up in the vibrational quasi-continuum have become possible. This allows for a reinterpretation of earlier Stern-Volmer quenching curves for photochemical activation, or of yield curves for chemical activation, to give absolute values of specific rate constants $k(E)$. The present review summarizes recent advances in such direct determinations of specific rate

constants $k(E)$ for unimolecular processes after energy-selective, non-thermal excitation.

The experimental results for $k(E)$, so far, all can very well be represented by statistical theories. For rigid activated complex cases the RRKM theory provides a satisfactory formalism. Simple bond fission reactions only formally can be reproduced by this theory. With a more careful account for angular momentum restrictions, such as done in our statistical adiabatic channel model, one has formally to introduce "coordinates" which neither are harmonic oscillators, nor free or hindered rotors. Such angular momentum effects will become even more important when energy E - and angular momentum J - selected specific rate constants $k(E, J)$ are accessible experimentally. At present such effects often are compensated in RRKM treatments by fit with the many free parameters of the model.

The important problem of the general applicability of statistical descriptions to unimolecular processes has been approached recently by photoexcitation experiments with well localized initial excitations. An influence of the site of the initial excitation so far has only by chemical activation experiments been shown for processes occurring on a ps-time scale. Experimental evidence for effects on longer time scales from photoexcitation so far was very spurious or not present at all. This appears to be in some conflict with ample evidence for non-randomization effects from classical trajectory calculations.

ABSTRACT C-2

Photofragment Spectroscopy of Ultracold NO_2 at 355nm: Internal Energy Distributions of NO

A. P. Baronavski, Benjamin M. DeKoven,* and H. Helvajian*

Chemistry Division, Naval Research Laboratory
Washington, D.C. 20375 USA

*NRL/NRC Postdoctoral Research Fellow

Dual laser photofragment spectroscopy has been shown to be an extremely sensitive and informative technique to obtain internal energy distributions of fragments formed by photodissociation. Most experiments to date have been performed in static or flowing gases in which the internal energy content of the parent molecule is initially a Boltzmann distribution corresponding to the ambient temperature of the experiment. Theoretical studies have pointed out the advantage of preparing the parent molecule in as few states as possible prior to photodissociation. In this way, a more direct correlation between the parent and fragment angular momentum distributions can be deduced. One technique to accomplish this is a supersonic expansion of the parent gas. Quite simply, a reservoir of gas maintained at high pressure is expanded into an evacuated chamber through an orifice which has a diameter large compared to the mean free path of the expanding gas. Random thermal energy of the gas is converted to directed mass flow with a concomitant cooling of the internal degrees of freedom of the gas. Rotational and vibrational temperatures of 1-50 K are readily achieved resulting in significant population of only a few rotational levels of the parent. Such cooling occurs in both cw and pulsed expansions with pulse durations as short as 10 μsec . The latter is particularly advantageous since only modest size chambers and pumps are required and since most photofragment studies are performed with pulsed lasers. Only recently has dual laser photofragment spectroscopy been carried out on molecules such as HN_3 and H_2S , which have been cooled initially to a few degrees Kelvin using supersonic expansions [1,2]. From these early studies it is evident that fragment angular momentum distributions can be substantially simplified when the parent molecule initially contains little, if any, rotational and vibrational energy. These experiments can also provide an excellent test of photodissociation theories. The incentive for carrying out these experiments is obvious.

In this paper we present the resulting nascent internal energy distributions of the NO photofragment following the 355nm photolysis of ultra-cold NO_2 . The experimental configuration used has been previously described [1]. A 10% mixture of the parent NO_2 molecule seeded in He is expanded at a stagnation pressure of ~ 5 atm. At approximately 20 nozzle diameters downstream, the molecular beam is crossed perpendicularly by both the photolysis (355 nm) and photofragment probe lasers. The laser beams originating from a single YAG laser (Quanta International) collinearly counter-propagate through the chamber. Therefore, the delay between photolysis and probe lasers is on the order of a few nanoseconds, ensuring observation of nascent photofragment distributions. NO populations in the $X(^2\Pi)$ manifolds are monitored by single photon laser induced fluorescence (LIF) of $\text{NO}(A \leftrightarrow X)$. The lower and upper traces of Fig. 1 show the LIF spectra of NO with and without the 355nm photolysis laser, respectively. Following photolysis most of the NO population resides in $^2\Pi_{1/2}$ and $^2\Pi_{3/2}$, all $v'' = 0$. The upper trace of Fig. 1 represents the NO background in NO_2 after several freeze-pump purifications. Under the conditions of our experiment the NO_2 is found to be initially at $T_{\text{rot}} 4\text{K}$. However, due to the fact that the NO impurity is quite cold ($J \leq 7^{1/2}$) and NO_2 photolysis results in population of higher NO J levels, we are able to probe the NO ($v'' = 0, 1$) state populations resulting from photolysis. This experiment is nearly intractable at ambient temperatures, due to NO background as pointed out by Zacharias *et al* [3].

In the ambient temperature studies Zacharias *et al*, [3] using a 337 nm photolysis laser, observed an inverted vibrational population distribution. This is in contrast to our experiment, at 355 nm, where most of the NO is in $v'' = 0$ even though $v'' = 1$ is energetically accessible. In this paper we also present and discuss the spin orbit, vibrational, and rotational populations in the NO photofragment. In the supersonic expansion, NO_2 initially contains less 10 cm^{-1} of rotational energy, while in ambient conditions ($T = 300\text{K}$) NO_2 contains in excess of 300 cm^{-1} of rotational energy. Such prepared NO_2 populations allow comparison to existing theories on angular momentum distributions in photolysis. Comparisons to similar experimental studies will also be made.

References

1. Benjamin M. DeKoven and A. P. Baronavski, Chem. Phys. Letts. 86 392 (1982).
2. W. G. Hawkins and D. L. Houston, J. Chem. Phys. 76 729 (1982)
3. H. Zacharias, M. Geilhaupt, K. Meier, and K. H. Welge, J. Chem. Phys. 74 218 (1981).

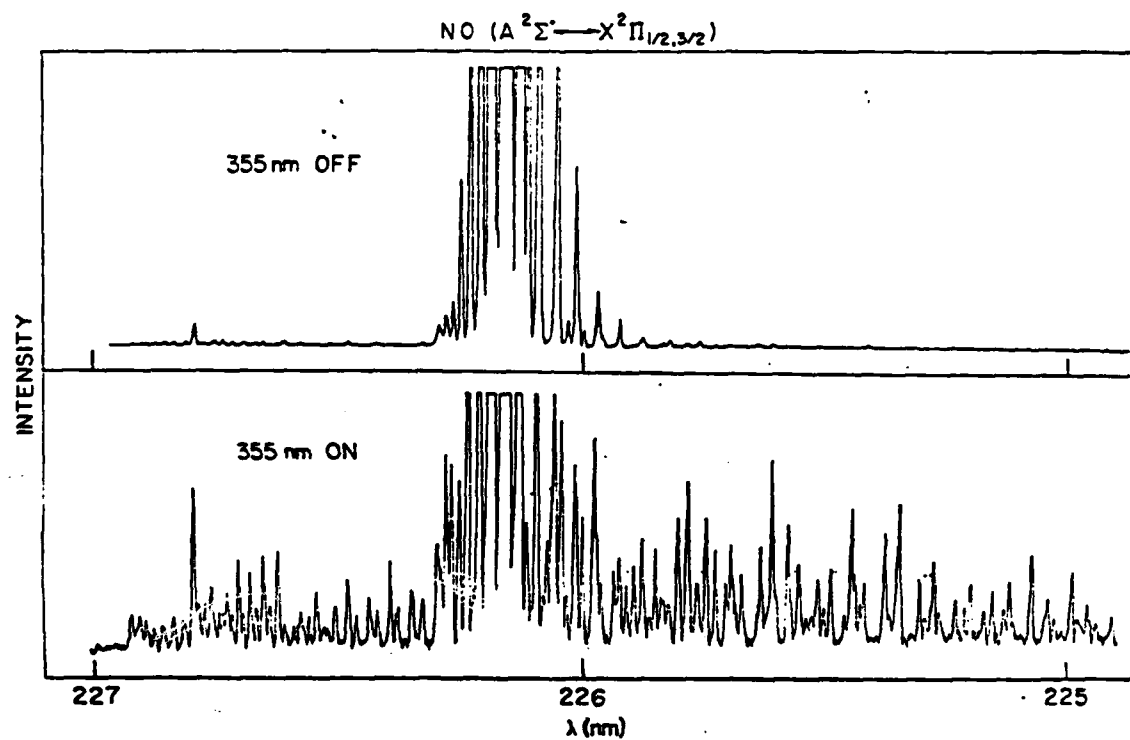


Figure 1. A portion of the Laser Induced Fluorescence Spectrum of NO ($A \leftrightarrow X$) from the photolysis of NO_2 at 355 nm (lower) and from background NO in the supersonic beam (upper).

ABSTRACT C-3

A Search For Mode-Selective Chemistry: The Unimolecular Dissociation of t-Butyl Hydroperoxide Induced by Vibrational Overtone Excitation

David W. Chandler, William E. Farneth^a, and Richard N. Zare

Department of Chemistry, Stanford University, Stanford, California 94305

^aOn quarter leave, September-December, 1981; present address:

Department of Chemistry, University of Minnesota, Minneapolis,
Minnesota 55455

ABSTRACT

One of the most provocative questions in chemical dynamics over the last three decades has been the range of validity of ergodic theories of unimolecular reaction.¹ A driving force for this continuing investigation is the presumption that given a sufficiently selective activation method and a sufficiently short reaction time scale, deviations from ergodic behavior must become apparent.

The experiment which we wish to report examines this question using vibrational overtone excitation as the activation method. We have chosen t-butyl hydroperoxide as the unimolecular reactant. This molecule possesses a number of features which make it attractive for experiments of this kind:

(1) It contains both O-H and C-H oscillators. Because of the high frequency and anharmonicity of these local modes², they might both be expected to have reasonable intensity in $\Delta v = 5,6$ as required to exceed the threshold energy for decomposition (43 kcal/mole).³

(2) It has a low energy reaction pathway that involves a simple reaction coordinate. The Arrhenius parameters for $(\text{CH}_3)_3\text{COOH} \rightarrow (\text{CH}_3)_3\text{CO}^\cdot + \text{OH}^\cdot$ have been well documented.

(3) The bulk of the vibrational state density involves displacements of the hydrocarbon portion of the molecule. Excitation of the O-H stretching overtone initially deposits energy remote from this energy sink and separated from it by the O-O bond. Therefore, the competition between non-ergodic reaction and intramolecular relaxation may be different for excitation into pure O-H, C-H or combination band overtones.

Our experiments are carried out using an intracavity opto-acoustic cell for both spectroscopy⁴⁻⁶ and photochemistry. Overtone pumping of the reactant t-BuOOH initiates the chemistry, and overtone probing of the O-H transition of the product, t-butyl alcohol (tBuOH), is used to monitor the rate of product formation. These techniques allow the reaction to be followed continuously and nondisruptively.

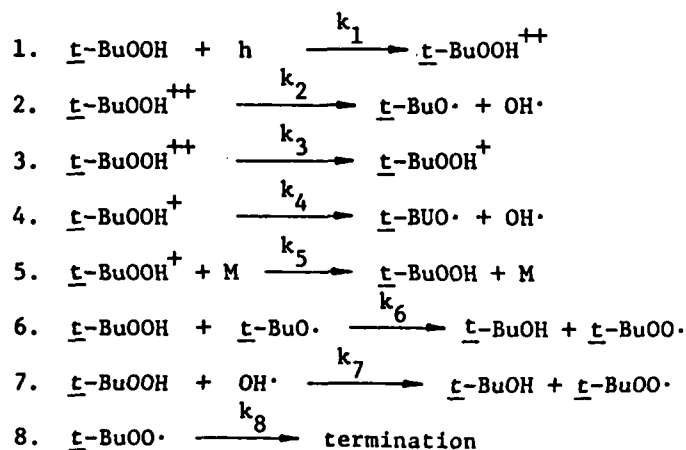
Overtone absorption spectra for t-BuOOH and t-BuOH were obtained by intracavity opto-acoustic methods at the room temperature vapor pressure of the compounds. For the hydroperoxide, bands maximizing at 619.0 nm and 531.9 nm are members of a sequence in the O-H manifold that can be described by the Birge-Sponer relationship⁷, $E_{n,o} = n(A + nB)$, where $E_{n,o}$ is the n -o transition energy, and $A(3692 \text{ cm}^{-1})$ and $B(-92.2 \text{ cm}^{-1})$ are constants related to the harmonic and anharmonic features of the potential surface, respectively. 619.0 nm corresponds to the 5-0 transition of the O-H stretch and 531.9 the 6-0 transition. Bands that can be assigned as members of a C-H sequence, and bands that appear to be O-H stretching plus skeletal bending combinations have also been observed. O-H stretching overtones for the product, tButyl alcohol, were similarly characterized.

Absolute absorption cross-sections are obtained from a comparison of signal intensities in benzene/hydroperoxide or benzene/alcohol mixtures.⁸ For the photochemical experiments, Ar⁺-pumped dye laser is tuned to 619.0 nm or 609.5 nm, absorption maxima of the pure 5-0 OH, or combination bands. The opto-acoustic cell is mounted within the dye laser cavity and irradiation is carried out continuously for fixed time intervals. During irradiation, laser power in the cavity is monitored by a photodiode. Prior to, and following a photolysis period, the pump laser beam is chopped and opto-acoustic spectra are taken over an appropriate wavelength range. The progressive growth of the t-BuOH absorption centered at 606.4 nm is followed.

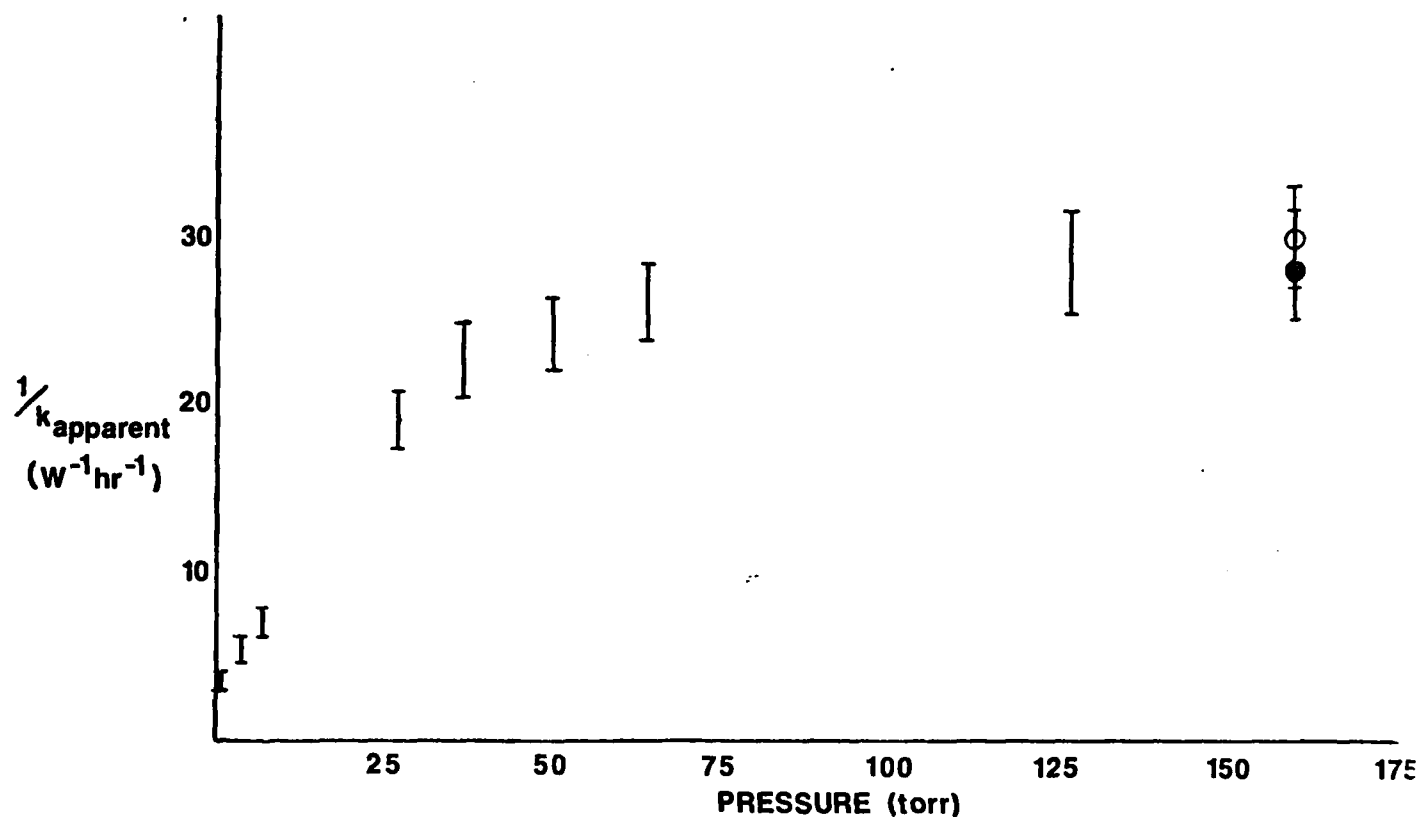
An apparent rate constant for growth of alcohol could be determined from $k_{\text{apparent}} = \Delta[\text{t-BuOH}]/[\text{t-BuOOH}]\tau[h\nu]$. τ is the time increment. $\Delta[\text{t-BuOH}]$ is the change in integrated area of the alcohol 5-0 OH band suitably corrected for the amount of dark reaction. $[\text{t-BuOOH}]$ is the integrated area of t-BuOOH peak at 609.5 nm, and $[h\nu]$ is the number of density of photons in the photolysis vessel calculated from the measured intracavity laser power and geometric factors.

At each pressure, k_{app} is obtained at several reaction times and laser powers. Figure 1 displays this data in the form of a Stern-Volmer plot where the reciprocal of k_{app} is plotted against the total pressure in the reaction cell. No systematic variation is found at a given total pressure with any of these variables. In particular, data at one torr t -BuOOH and 160 torr SF_6 (open circle) and 7 torr t -BuOOH and 153 torr SF_6 (closed circle) overlap within their uncertainties. The error limits represent one standard deviation from the mean at each pressure. In a few runs with other bath gases (toluene or 1,4 cyclohexadiene) once more no obvious change in k_{app}^{-1} is observed at a given total pressure. Similarly, variation of laser power by a factor of 3 causes no change in the apparent rate constant outside of experimental error limits. Irradiation at frequencies outside the overtone band profiles gives no reaction above background. Complementary data for excitation in the combination band will also be described.

These data will be discussed in light of the mechanism below, which for steps 1-5 is in essence that suggested by Rabinovitch and co-workers for chemical activation experiments.⁹



This mechanism distinguishes two pathways to product: reaction (k_1) from a vibrationally excited hydroperoxide molecule whose energy is not totally randomized, $t\text{-BuOOH}^{++}$, and reaction (k_4) that follows internal energy randomization (k_3). At low pressures reaction 4 is the principle source of product. But at high temperatures reaction 1 becomes an increasingly important contributor. RRKM calculations have been performed and the theoretical fit to this data and existing photochemical¹⁰ and thermal⁴ rate data will be described.



References

1. P. J. Robinson and K. A. Holbrook, "Unimolecular Reactions", Wiley-Interscience, London (1972) and references therein.
2. B. R. Henry, *Accnts. Chem. Res.* 10, 207 (1977).
3. W. Benson and G. N. Spokes, *J. Phys. Chem.* 72, 1182 (1972).
4. K. V. Reddy, R. G. Bray and M. J. Berry, in: *Advances in Laser Chemistry*, ed. A. H. Zewail (Springer, Berlin, 1978), p. 48.
5. K. V. Reddy and M. J. Berry, *Chem. Phys. Lett.* 72, 29 (1980).
6. G. Stella, J. Geltand, and W. H. Smith, *Chem. Phys. Lett.* 39, 146 (1976).
7. R. L. Swotford, M. E. Long, and A. C. Albrecht, *J. Chem. Phys.* 65, 179 (1976).
8. R. G. Bray and J. J. Berry, *J. Chem. Phys.* 71, 4909 (1979).
9. I. Oref and B. S. Rabinovitch, *Accnts. Chem. Res.* 12, 166 (1979).
10. T. R. Rizzo and F. F. Crim, *J. Chem. Phys.* 76, 2754 (1982).

ABSTRACT C-4

MOLECULAR BEAM STUDY OF GLYOXAL PREDISSOCIATION FROM THE S_1 STATE

J. W. Hepburn, L. J. Butler, R. J. Buss and Y. T. Lee

Materials and Molecular Research Division
Lawrence Berkeley Laboratory and
Department of Chemistry, University of California
Berkeley, California 94720 USA

ABSTRACT

A recent study undertaken in our lab has elucidated the primary photochemistry of several low lying vibronic states of the S_1 electronic state of glyoxal, without any interference from collisions. The method used for these experiments was molecular beam photofragment translational spectroscopy, a method recently applied to studies on ketene¹ and formaldehyde² photolysis.

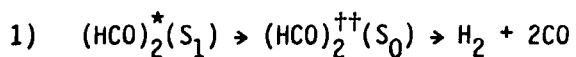
After formaldehyde, glyoxal has been the most studied aldehyde, with an extensive literature on its spectroscopy, photophysics and photochemistry.³ However, as Loge and Parmenter reported⁴ at the last meeting in this series, in spite of tremendous effort, the primary photochemistry of the S_1 state of glyoxal was still quite unclear.

In Fig. 1, the energetically allowed decomposition channels are shown, as well as the energies of their vibrational states discussed in this paper. The hydroxymethylene product shown has never been directly observed, and the energy shown is a calculated one.⁵ Results of gas bulb studies⁴ and matrix isolation studies⁶ have implied that all three energetically allowed channels are involved in glyoxal predissociation.

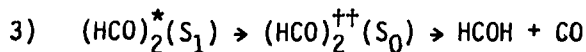
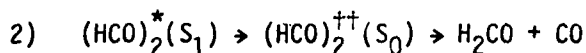
In a recent theoretical study reported by Osamura et al.³ the transition state for the $(\text{CHO})_2^{++} \rightarrow 2\text{CO} + \text{H}_2$ decay channel was investigated.

The results of the calculations suggested that the decomposition was a concerted 3 body process, not a sequential one as postulated by Loge et al.⁷.

Our results show quite clearly that there are in fact three different dissociation channels involved in the predissociation of the S_1 state of glyoxal. One of these is the channel studied by Osamura et al., viz:



The other two channels are:



The predissociation of the zero point level and the 2', 4', 5' and 8' levels was studied in these experiments and, neglecting variations in total fragmentation quantum yield, the photochemistry of all these vibrational levels was found to be the same.

As well as determining the primary products of the predissociation, our results also measure the partitioning of energy in the photofragments. The data indicate that less than half of the available energy goes into translation in channel (2); and in channel (1), most of the energy is released after the H_2 has departed from the two CO molecules.

This work was supported by the Office of Naval Research under Contract No. N00014-75-C-0671.

References

1. C. C. Hayden, D. M. Neumark, K. Shobatake, R. K. Sparks and Y. T. Lee, J. Chem. Phys. 76, 3607 (1982).
2. P. Ho, D. J. Bamford, R. J. Buss, Y. T. Lee and C. B. Moore, J. Chem. Phys. 76, 3630 (1982).
3. For example see the references for: Y. Osamura, H. F. Schaefer, D. Dupuis and W. A. Lester, J. Chem. Phys. 75, 5828 (1981).
4. G. Loge and C. Parmenter, Abstracts of the 14th Informal Conference on Photochemistry (1980), M2-1.
5. J. D. Goddard and H. F. Schaefer, J. Chem. Phys. 70, 5117 (1979).
6. M. Diem, B. G. MacDonald and E. K. C. Lee, Abstracts of the 14th Informal Conference on Photochemistry (1980), M3-1.
7. G. W. Loge, C. S. Parmenter and B. F. Rordorf, Chem. Phys. Lett. 74, 309 (1980).

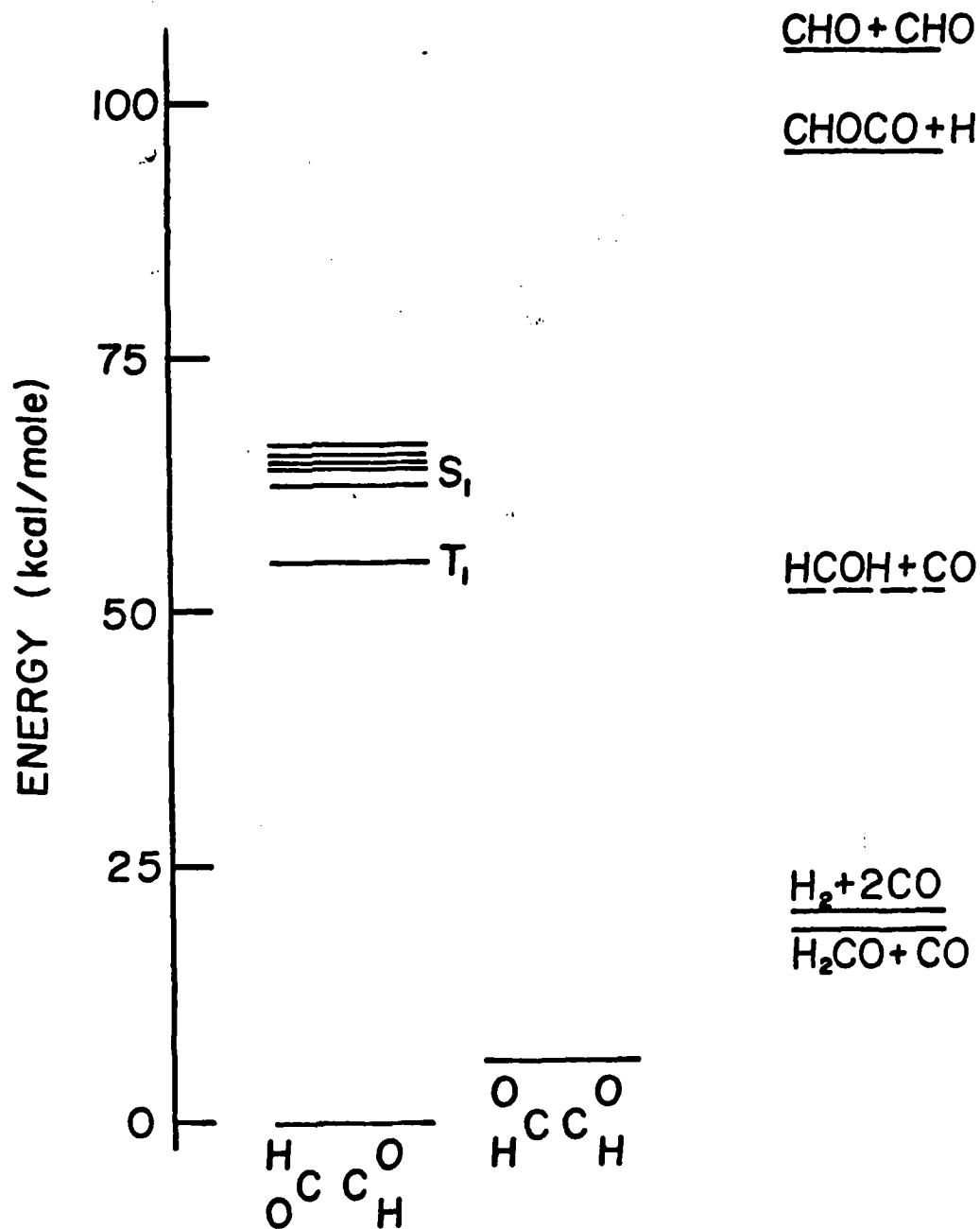


Fig. 1. Energetics of glyoxal predissociation. Energy levels for glyoxal molecule shown on left, with product channels on the right. Vibrational states shown in the S_1 state are: zero point, 5', 8', 4' and 2'.

ABSTRACT C-5

Laser Induced Photochemistry in a Supersonic Expansion

by

Michael Heaven, Terry A. Miller, and V. E. Bondybey
Bell Laboratories
Murray Hill, N.J. 07974

ABSTRACT

Recently there has been tremendous progress in the laser spectroscopy of molecules cooled by supersonic free jet expansions. This work has been extremely successful in providing greatly simplified and therefore interpretable spectra of large molecules,¹ as well as in obtaining spectra of Van der Waals molecules.

However, free jet cooled laser spectroscopy has been largely confined to stable molecules and their Van der Waals adducts. The only exceptions appear to be the very recent photolytic production²⁻⁴ of free jet cooled free radicals, followed by laser characterization, and the electron impact emission spectra of molecular ions,^{5,6} for which no laser probing was possible.

Pulsed laser photolysis or multiphoton ionization of stable molecules provides a versatile means for producing radicals and ions in the free jet expansion. At Bell Laboratories, we have been using a commercial excimer laser (operating on ArF at 193 nm) to generate transient species in a Campargue type expansion. The transients are detected by laser induced fluorescence (LIF), excited by a pulsed dye laser. Figure 1 shows the apparatus used in these experiments. The beams from the excimer laser and the dye laser traverse the vacuum chamber in an antiparallel fashion.

We have performed two types of experiments with this apparatus. In the first instance, the photolysis and probe beams are spatially overlapped, and the beams are positioned in the downstream portion of the expansion. The distribution of internal energy in the photofragments is mapped by LIF probing immediately after dissociation. Interpretation of this data is simplified because of the internal cooling of the parent molecule prior to excitation.

In the second type of experiment, the photolysis beam is positioned close to the nozzle. The probe beam is positioned several mm downstream from the photolysis beam, and the probe pulse is delayed with respect to the photolysis pulse. This delay allows the photolytically produced radicals to undergo collisional cooling, and flow into the probe beam path. Thus, greatly simplified spectra of radicals and ions can be obtained.

An additional advantage can be obtained when photolysis occurs close to the nozzle. Because of the high gas density in this region, rapid secondary photochemical reactions can occur, and have been observed in our experiments. The secondary reactions can be deliberately exploited for the production of radicals.

Production of CN radicals by photolysis of BrCN has been investigated. The CN fragment was detected by laser excitation of the B-X system. Probing the CN immediately after photolysis reveals a rotational temperature of approximately 4000K, and significant vibrational excitation. Collisional cooling of CN was investigated, and rotational relaxation to a distribution corresponding to $T_R \approx 80^\circ\text{K}$ achieved.

SH radicals have also been studied. These are produced by photolysis of H_2S and detected by excitation of the A-X system. Slight rotational excitation of the SH fragment is observed, ($T_R \approx 400^\circ\text{K}$), but the distribution of population between the spin-orbit components of the ground state is essentially statistical. SH is efficiently cooled by collisions with Ar, and rotational distributions corresponding to $T_R < 10^\circ\text{K}$ have been observed.

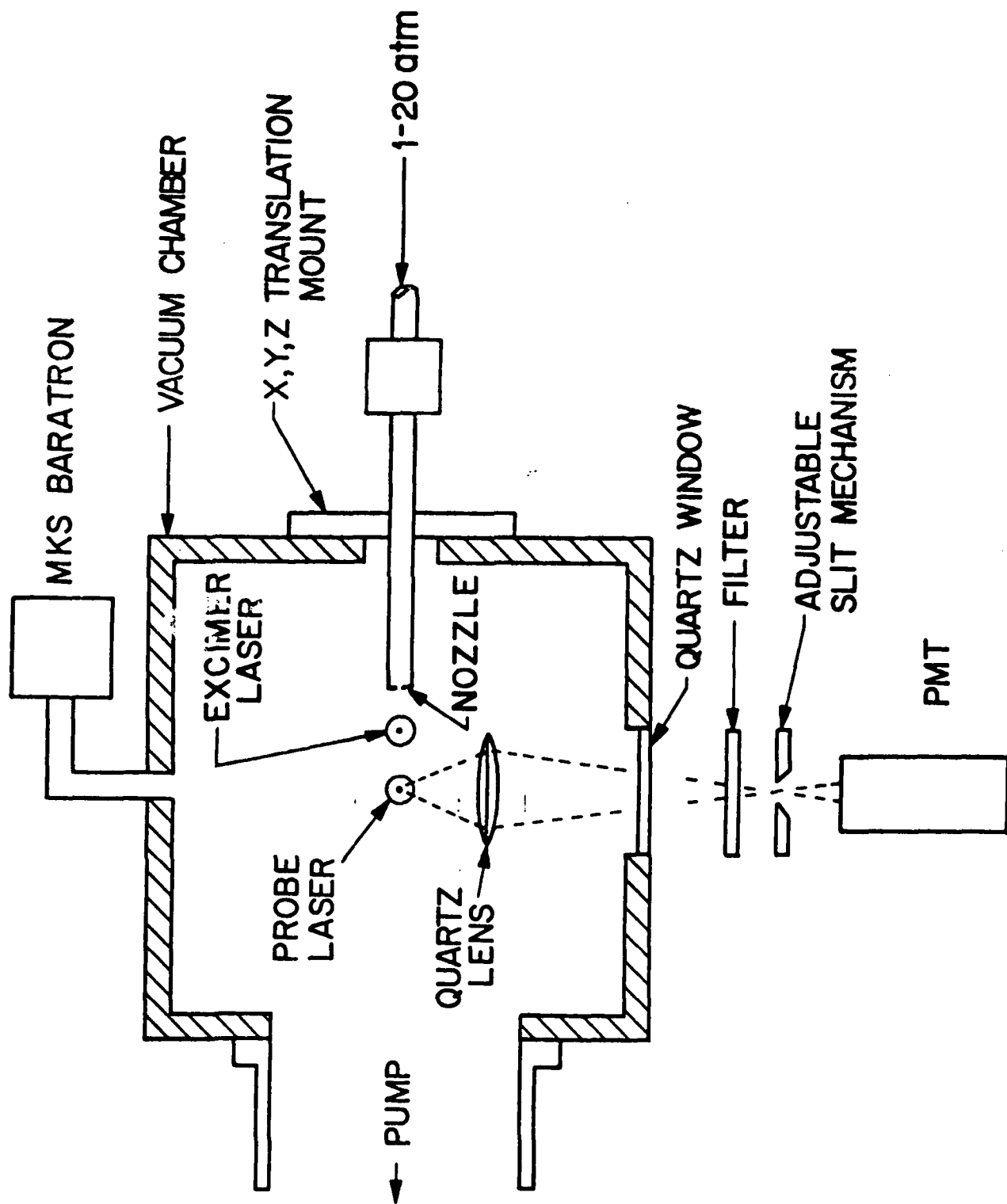
Photolysis of H_2S in a region of high gas density leads to the formation of S_2 via secondary photochemical reactions. Extensive rotational cooling of the S_2 is observed. Excitation spectra of the B-X system show strong satellite transitions, and we report the observation of a pair of new satellite branches.

Halobenzene radical cations have been produced in the expansion by two photon ionization of the neutral species. So far we have observed LIF from the cations of hexafluorobenzene, pentafluorobenzene, 1,3,5-trifluorobenzene, and 1,3,5-trichlorobenzene. In all cases, the LIF spectra indicate that the ions are extremely cold, and the observed linewidths of the vibronic bands are limited by the 1 cm^{-1} laser linewidth.

The ions form strong Van der Waals bonds, and extensive clustering of the ions is observed. Details of the ion and ion cluster spectra will be presented, and the mechanism of two photon ionization in the jet will be discussed.

References

1. See, for example, D. H. Levy, Am. Rev. Phys. Chem. 31, 197 (1980).
2. D. L. Monts, T. G. Dietz, M. A. Duncan, and R. F. Smalley, Chem. Phys. 45, 133 (1980).
3. D. E. Powers, J. B. Hopkins, and R. E. Smalley, J. Phys. Chem. 85, 2711 (1981).
4. M. Heaven, T. A. Miller, and V. E. Bondybey, Chem. Phys. Letts. 84, 1 (1981).
5. T. A. Miller, B. R. Zegarski, T. J. Sears, and V. E. Bondybey, J. Phys. Chem. 84, 3154 (1980).
6. A. Carrington and R. Tuckett, Chem. Phys. Letts. 74, 19 (1980).



ABSTRACT D-1

TROPOSPHERIC CHEMISTRY: A KINETICIST'S VIEW

A. R. Ravishankara

Molecular Sciences Group

Engineering Experiment Station

Georgia Institute of Technology

Atlanta, Georgia 30332

The troposphere encompasses ~85% of Earth's atmosphere and controls to a large degree life on this planet. The chemistry of the troposphere is essentially the chemistry of its minor constituents (such as CH_4 , CO , O_3 , H_2O , . . .) and is driven by sunlight. Thus gas phase photochemistry and chemical kinetics are major parts of tropospheric research. During the last two decades, in an effort to understand and predict the effect of man's activities on the composition of the troposphere, a great deal of work has been carried out to elucidate its chemistry. In this long, hard, and on-going saga of laboratory experiments, field measurements, and computer modeling there have been many successes and just as many surprises. We will describe a 'success story' - the elucidation of CH_4 oxidation cycle and then a 'surprise finding' - the effects of O_2 and H_2O on measured rate coefficients.

Methane Oxidation Cycle:

Figure 1 shows a reasonably complete scheme involved in oxidation of methane. CH_4 , introduced into the atmosphere from the biosphere, is oxidized stepwise via reactions with transient and stable trace species of the troposphere, finally leading to CO_2 and H_2O . In this process of conversion many new species are created. It is this myriad of reactions, all occurring at the same time and different rates which control the concentration of many important reactive species such as OH and HO_2 and lead to the formation of ozone. Until recently, our understanding of atmospheric methane degradation was limited to the knowledge that $\text{OH} + \text{CH}_4$ reaction followed by formation of CH_3O_2 initiates the CH_4 cycle. However, during the past few years, most of the photochemical and kinetic parameters

needed to model this cycle have been measured in the laboratory. One such study, that of $\text{CH}_3\text{O}_2 + \text{NO}$ reaction, was carried out in our laboratory using the technique of pulsed laser photolysis - CW laser induced fluorescence. The rate coefficient was measured as a function of temperature and the NO_2 product yield was determined. This study serves as an example of the current emphasis on not only measuring the reaction rate coefficients but also determining reaction products. This work will be described. A major remaining uncertainty in the hydrocarbon oxidation scheme centers around the rates of formation and removal of CH_3OOH . The rate coefficient for OH reaction with CH_3OOH is being measured in our laboratory, and will be discussed.

Effect of O_2 on Rates of Reactions:

Until late 1970's the reaction of OH with CO was thought to be a simple metathesis reaction, and the bimolecular rate coefficient for this reaction was thought to be well known. A few years back, however, Stuhl and co-workers discovered that the measured rate coefficient was pressure and oxygen concentration dependent. The exact course of this reaction under high pressure and in the presence of O_2 (or other impurities) is still not known. Our recent efforts at understanding this reaction by following the decay in OH reactant concentration and growth in H atom product concentration will be described.

Once it was discovered that O_2 could enhance the rate of certain reactions, it became imperative to closely examine the applicability of many laboratory measurements under tropospheric conditions. The finding that the presence of water vapor dramatically increases the rate of certain HO_2 reactions has further heightened this concern. Therefore, to ascertain the prevalence of O_2 and H_2O effects, there is currently a push to directly measure reaction rate coefficients under conditions of atmospheric pressures and compositions. We have, in fact, recently found evidence to confirm the hypothesis of Cox and co-workers that the reaction of OH with CS_2 , known to be very slow in the absence of O_2 is extremely fast in the

presence of O_2 and high pressures of diluent gas. The measured increase in rate coefficient upon addition of O_2 (a few orders of magnitude) will make this reaction very important in the atmosphere. A concise account of this work will be presented.

Lastly, it is to be noted that the laboratory kinetic studies will be presented mainly to give a flavor of the research in this area. Important problem areas in tropospheric chemistry, as currently perceived, will also be discussed.

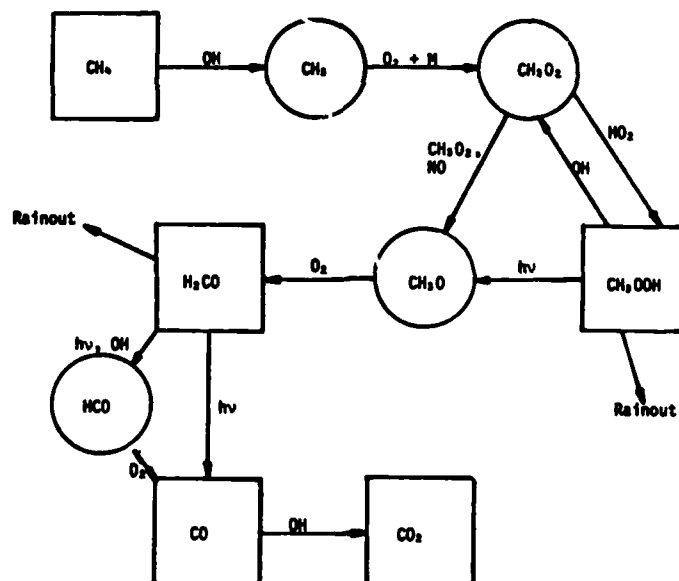


Figure 1. Methane Oxidation Scheme

ABSTRACT D-2

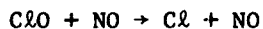
Observations of Free Radicals in the Earth's Stratosphere: Recent Advances in Studies of ClO and OH

J. G. Anderson and R. M. Stimpfle

Department of Chemistry and
Center for Earth and Planetary Physics
Harvard University
Cambridge, Massachusetts 02138

Within the last year, several significant advances have been made in techniques used for the detection of ClO and OH in the Earth's stratosphere. As a result, several important questions have been raised and the prospects for a far more thorough understanding of the photochemistry of these two key radicals within the next two years appears promising.

Five techniques for the detection of ClO have now been used. Two of these employ rotational transitions in the millimeter wavelength region; emission data have been obtained at 204 GHz from balloon-borne experiments (Waters et al., 1981) and at 204 and 273 GHz from the ground (Parrish et al., 1981). Heterodyne radiometers operating in the 10 μ region have been used to detect ClO in absorption using the sun as a source. Using an isotope doped CO₂ laser as a local oscillator, spectral resolution of 10⁻⁴ cm⁻¹ has been obtained from balloon-borne experiments (Menzies, 1982) and ground-based observations (Rodgers et al., 1982); the latter study reports two observations with an upper limit significantly below that of the other techniques. Finally, results from an in situ technique (see Anderson et al., 1980; Weinstock et al., 1981) using atomic resonance fluorescence to detect atomic chlorine following chemical conversion of ClO to Cl by the rapid bimolecular reaction

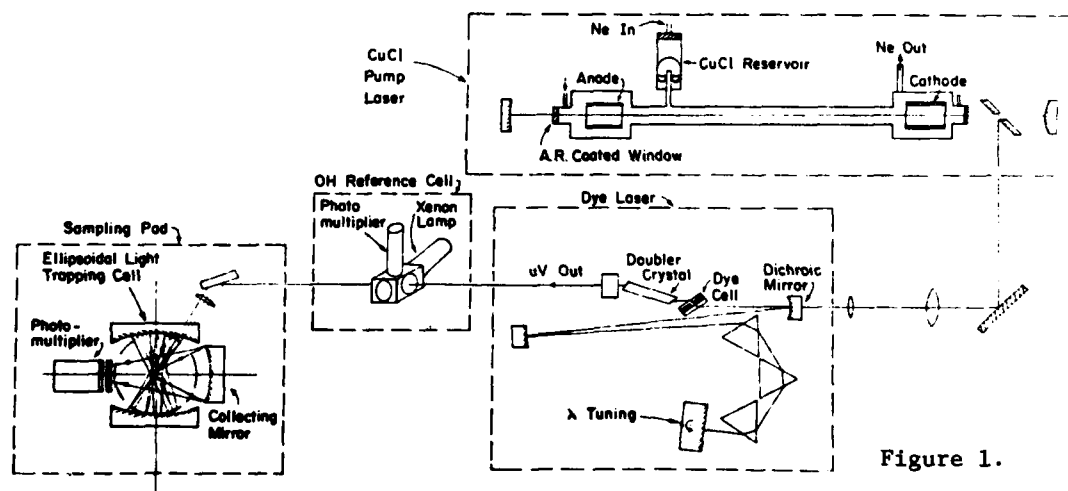


are reviewed. Emphasis is given to the differences which appear in the five developing data sets. Results are interpreted in terms of recent model calculations with emphasis on predictions of global ozone changes into the next century.

The observation of OH in the stratosphere by in situ molecular resonance fluorescence (Anderson et al., 1982) and by ground-based total column absorption methods (Burnett and Burnett, 1981) are reviewed. Ground-based observations over the past five years have revealed important trends in total column OH as a function of solar activity and a clear dependence on solar zenith angle.

It is demonstrated that the use of current OH measurements to constrain models of global ozone reduction are unsuccessful because of the absence of data on [OH] below 30 km in the stratosphere. It is demonstrated that the absence of detailed knowledge of the absolute concentration of OH in the middle and lower stratosphere is the single greatest impediment to our understanding of the chemical partitioning in the reactive nitrogen and halogen systems. In response to this need, a new laser-induced fluorescence experiment for the *in situ* detection of stratospheric OH and HO₂, shown schematically below, has been developed. The heart of the system is an atomic copper vapor laser operating at 20,000 Hz which simultaneously provides (a) high average power for correspondingly low detection thresholds ([OH] ~ 10⁴ cm⁻³), and (b) low peak power to eliminate both saturation effects and photochemical interference. First tests of the system in the stratosphere are scheduled for July, 1982.

LASER OH OPTICAL SCHEMATIC



Need for the development of this high repetition rate approach to the detection of OH in the stratosphere (and troposphere) is demonstrated through the use of a time-dependent calculation and the state-to-state kinetics during and after the interrogation of the atmospheric sample. A detailed model was used with three objectives in mind: First, since there are a large number of chemical species and quantum states involved, with characteristic time constants on the order of the laser pulse length, details of the temporal development are essential. A thorough understanding of the energy transfer rates and photochemical interference terms can only be achieved by a detailed

comparison between calculated and observed behavior. Second, it is possible, with the aid of the calculation, to define the minimum aggregate of experimental parameters which comprise a complete description of a given experiment. There has been considerable controversy created regarding tropospheric OH observations which results directly from incomplete specification of experimental quantities. What we will show is that the results of the fully time-dependent model can be condensed into an analytical expression which affords rapid analysis of photochemical interference effects for any tropospheric laser-induced fluorescence experiment if the minimum set of experimental parameters are provided. Third, the model provides direct guidance for maximizing the design of the experimental hardware.

The kinetic model follows the time evolution of the laser flux, the concentration of twenty specific internal energy states of the OH radical including those formed by the reaction of $O(^1D)$ with H_2O , the $O(^1D)$ concentration, and the fluorescence emission rate from each state under a variety of experimental conditions.

The laser pulse is simulated by a time-dependent Gaussian function with variable amplitude and width. The time-dependent populations and photon emission rates for each of the quantities noted in the schematic below are calculated with ~ 10 psec time resolution.

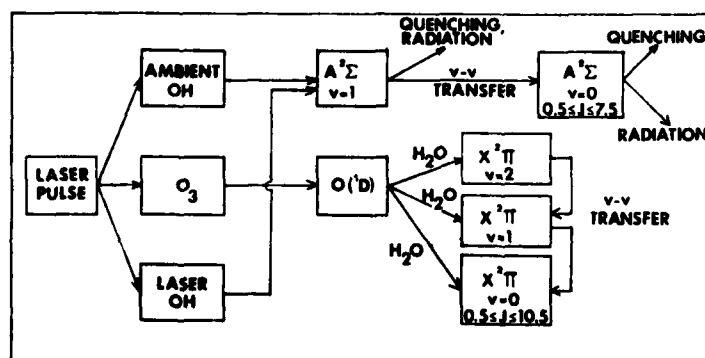


Figure 2.

The results from a series of calculations carried out with a fixed laser pulse width of approximately 15 nsec and three different pressure regimes in the absence of O_3 and H_2O are shown in Figure 3.

These three pressure regimes summarize the points that (a) at ground level the $A^2\Sigma$ v-v transfer rates occur on a time scale short compared with the pulse length, as does electronic quenching; (b) at the tropopause, electronic quenching is on the order of the laser pulse length and v-v transfer into the ground vibrational level of the $A^2\Sigma$ state shifts the population peak

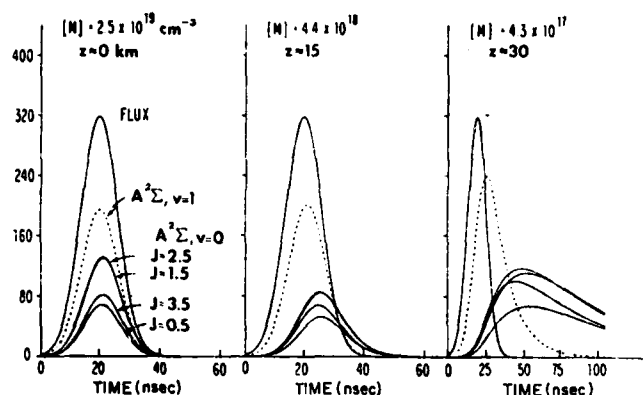


Figure 3.

of the $v=0$ state toward the trailing edge of the pulse; and, finally, (c) at the mid-stratosphere, the quenching and $v-v$ transfer rates are significantly longer than the laser pulse length.

Inclusion of O_3 and H_2O into the model allows one to determine the temporal development of fluorescence from ambient and photochemically induced OH.

These calculations will be compared with laboratory data obtained with the balloon-borne system.

References:

1. Waters, J.W., J.C. Hardy, R.F. Jarnot and H.C. Pickett, Chlorine monoxide radical, ozone and hydrogen peroxide: stratospheric measurements by microwave limb sounding, *Science*, **214**, 61, 1981.
2. Parrish, A., R.L. de Zafra, P.M. Solomon, J.W. Varrett and E.R. Carlson, Chlorine oxide in the stratospheric ozone layer: ground-based detection and measurement, *Science*, **211**, 1158-1161, 1981.
3. Menzies, R.T., Laboratory spectra of ClO have demonstrated that the previous observations (see R.T. Menzies, *Geophys. Res. Lett.*, **6**, 151, 1978) using this technique incorrectly identified the transition. A reanalysis of the data is forthcoming. Private communication, April, 1982.
4. Rodgers, J.D., M.J. Mumma, T. Kostuik, D. Deming, J.J. Hillman, J. Faris and D. Zipoy, Is there any chlorine monoxide in the stratosphere?, submitted to *Science*, April 12, 1982.
5. Anderson, J.G., R.E. Shetter, H.J. Grassel and J.J. Margitan, Stratospheric free chlorine measured by balloon-borne *in situ* resonance fluorescence, *J. of Geophys. Res.*, **85**, 2869, 1980.
6. Weinstock, E.M. M.J. Phillips and J.G. Anderson, *In situ* observations of ClO in the stratosphere: a review of recent results, *J. of Geophys. Res.*, **86**, 7273, 1981.
7. Anderson, J.G., The measurement of trace reactive species in the stratosphere: a review of recent results, in *Causes and Effects of Stratospheric Ozone Reduction: An Update*, National Academy Press, 1982.
8. Burnett, C.E. and E.B. Burnett, Spectroscopic measurements of the vertical column abundance of hydroxyl [OH] in the earth's atmosphere, *J. of Geophys. Res.*, **86**, 5185, 1981.

ABSTRACT D-3

Sensitivity of an Urban Photochemical Model to Changes in Meteorology*

Joyce E. Penner

University of California, Lawrence Livermore National Laboratory

Livermore, California 94550

Complex urban-scale photochemical models are increasingly being used to predict air quality and the impacts of alternative emission control strategies. For air quality planning purposes, one or two historical days in which high oxidant values were observed are usually picked for study. The cost of data acquisition is large for these models, and, therefore, most communities have had to restrict the amount of data gathered. In the San Francisco Bay Area, for example, meteorology fields are developed from a sparse network of surface wind observations and one early morning and afternoon radiosonde observation of the temperature profile. This situation allows a great deal of flexibility in specifying the meteorology input to models, especially the mixing depth. In this study we explored the sensitivity of a complex urban photochemical model to changes in mixing depth, wind speed, and direction.

The model used in this study is a two-dimensional grid-based model with one layer in the vertical whose height extends from the surface to the bottom of the mixed layer. The mixed layer depth may vary with time and space. Mass flux fields are developed from observations of surface winds and estimates of the mixing height using an algorithm that ensures mass conservation for each grid element.

Joyce E. Penner

Four experiments were studied in order to test the effect on afternoon O_3 concentrations. These experiments were: (1) the afternoon inversion base height was increased from 380 m to 1900 m, (2) the horizontal convergence was decreased by adjusting observed wind directions, (3) afternoon wind speeds were decreased by 25%, and (4) the inversion base height at night was increased by 40%. The magnitude of each change tested was consistent with the uncertainty of the adjusted parameter in each case. Maximum layer-average ozone in the area of the observed high changed by -11%, -4%, +11%, and +13% in each of the four cases, respectively. Thus, the predicted maximum layer average ozone was uncertain by approximately 2.5 ppm. The chemical and physical processes leading to this observed sensitivity will be discussed.

*This work was performed under the auspices of the U. S. Department of Energy by the Lawrence Livermore National Laboratory under contract No. W-7405-ENG-48.

ABSTRACT D-4

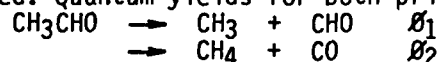
THE PHOTOLYSIS OF ACETALDEHYDE UNDER ATMOSPHERIC CONDITIONS.

H. MEYRAHN, G.K. MOORTGAT and P. WARNECK

Max-Planck-Institut für Chemie, Air Chemistry Division
Saarstrasse 23, Mainz. F.R.G.

Abstract

The photodecomposition of mixtures of 100-200 ppm CH_3CHO in 1 atm of air or purified N_2 has been studied at 300 K and the quantum yields of CO and CH_4 determined in the spectral range 250-340 nm. The quantum yields are nearly identical in both systems. ϕ_{CO} increases monotonically from zero at 330 nm to near 0.8 at 250 nm. ϕ_{CH_4} remains near zero at $\lambda > 285$ nm and increases sharply to 0.5 at 250 nm. A pressure dependence of ϕ_{CO} was observed at several wavelengths, indicating that some quenching occurs. No H_2 was observed. Quantum yields for both primary steps



are derived. Measured CO production rates in sunlit $\text{CH}_3\text{CHO}/\text{Air}$ and N_2 mixtures produce noontime dissociation rates of $3 \times 10^{-6} \text{ sec}^{-1}$ at 30° zenith angle. This is a magnitude lower as the currently accepted value of Meagher et al. (1976).

1. Introduction

The photooxydation of acetaldehyde in the atmosphere can occur by two routes: one is direct photodecomposition, the other is the reaction with OH radicals which abstracts the aldehydic hydrogen and leads to the formation of acetyl radicals. Then they add oxygen to form peroxyacetyl which is the precursor of peroxyacetylnitrate (PAN), an air pollutant having important physiologic effects. PAN probably occurs also naturally in small concentrations. The relative contributions of the two oxidation pathways are critical for an assessment of PAN formation in the natural atmosphere, but have remained uncertain because photodecomposition quantum yields for acetaldehyde under natural conditions had remained undetermined. We have measured CO and CH_4 product quantum yields in mixtures of about 100 ppm of acetaldehyde in air and report the results here.

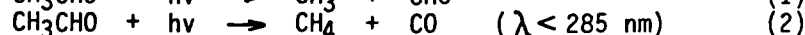
2. Experimental

Two Xe arc-monochromator set-ups (A,B) with different light throughput (A= Jobin-Yvon, f/2 and B= Spex, f/4) were used. Mixtures of acetaldehyde in air or N_2 were prepared in a Hg and grease-free handling system and then expanded simultaneously into 3 identical quartz gas cells (25 cm^3 , i.d.= 18 mm): one was used for the determination of the CO/ CH_4 background, one served as blank cell (kept in dark during the photolysis), and one as the photolysis cell proper. A calibrated thermopile and/or acetone actinometry ($\phi_{\text{CO}} = 1$ at 125 °C) was used to measure the photon fluxes. In the analysis CO was converted to CH_4 by means of a Ni-catalyst. All the gas samples were analysed gas-chromatographically.

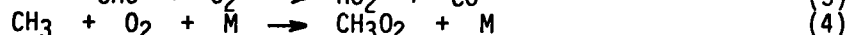
3. Quantum Yields

It made no difference in the quantum yields observed whether irradiations were performed with mixtures of acetaldehyde in air or nitrogen. Although prepurified nitrogen was used, its oxygen content probably was still about 1 ppmv which would not have been enough to change the prevalent reaction sequence. Figure 1 shows the variation of CO and CH_4 quantum yields versus wavelength with the total pressure fixed at one atmosphere. ϕ_{CO} increases monotonically from zero at 330 nm to near 0.8 at 250 nm. ϕ_{CH_4} remains near zero at wavelengths greater than 285 nm, then increases sharply

towards shorter wavelengths. The threshold energy corresponds to 420 kJ/mole. Within experimental error there was no dependence on quantum yield with light intensities varying within a factor of four (5.10^{13} - 2.10^{14} photons/cm².s). Hydrogen was not found in significant amounts, indicating that the primary process $\text{CH}_3\text{CHO} + h\nu \rightarrow \text{CH}_2\text{CO} + \text{H}_2$ does not occur. Also Blacet and coworkers (1942) working with pure CH_3CHO did not detect H_2 as a photolysis product. Consequently, also $\text{CH}_3\text{CHO} \rightarrow \text{CH}_3\text{CO} + \text{H}$ cannot be an important process. The CO quantum yield remained unchanged at higher acetaldehyde partial pressures. However, CO_2 appears then as a product, which is probably due to secondary attack of radicals formed in the photolysis. Other products were not searched for. Therefore, under our experimental conditions, the main reactions are



followed by



On the assumption that no CO nor CH_4 are produced from secondary reactions, the primary quantum yields at atmospheric pressure are given by

$$\phi_1 = \phi_{\text{CO}} - \phi_{\text{CH}_4}$$

$$\phi_2 = \phi_{\text{CH}_4}$$

and are displayed in Fig. 2(a + b).

Separate experiments done at 270, 304 and 313 nm indicate that the CO quantum yields both in air and N_2 mixtures increase as the total pressure is lowered. The data follow a Stern-Volmer type dependence

$$1/\phi_{\text{CO}} = 1 + \alpha(p, \lambda) \cdot p$$

with a quenching constant 2.90×10^{-4} , 1.87×10^{-3} and 3.49×10^{-3} torr⁻¹ at 270, 304 and 313 nm respectively.

4. Photodissociation rates

The quantum yield data can be readily applied to the troposphere. At ground level, radiation at wavelengths below 295 nm is absent due to the filtering effect of stratospheric ozone. As a consequence, the production of methane from photodecomposition of acetaldehyde can be neglected. According to our present knowledge, CO appears to be the only stable product resulting from the processes (1) and (3). The corresponding acetaldehyde photodissociation and CO production rates are then identical.

Photodissociation coefficients may be calculated from

$$J_{\text{CH}_3\text{CHO}} = \int \phi_{\text{CO}}(\lambda) \cdot \sigma(\lambda) \cdot I_0(\lambda) \cdot d\lambda$$

where $\phi_{\text{CO}}(\lambda)$ and $\sigma(\lambda)$ are the quantum yield and absorption cross section, respectively, both as function of wavelength as determined by us. $I_0(\lambda)$ is the solar radiation intensity as a function of zenith angle. We have used data from Peterson (1976) for middle latitudes. The integral was evaluated and is shown in Fig. 3. The calculated photoproduction rates were further compared with experimental values obtained from the acetaldehyde photodecomposition in sunlight. For this purpose several quartz bulbs filled with mixtures of 100 ppm CH_3CHO in air or N_2 were exposed to sunlight during noon hours in July 1981. The photodissociation coefficients were derived from the production rates are also shown in Fig. 3 and give an average value $J_{\text{CH}_3\text{CHO}} = 3 \cdot 10^{-6} \text{ s}^{-1}$. Stratospheric photodissociation coefficients calculated from a radiative transfer model also will be presented.

5. Relative importance of Acetaldehyde photodecomposition in the atmosphere.

All aldehydes react very rapidly with OH radicals. The measured rate coefficient of the reaction with acetaldehyde is $k = 1.6 \times 10^{-11} \text{ cm}^3/\text{molec.s}$ (Atkinson and Pitts, 1978). If we assume a noon value for the OH concentration

of 10^6 molecules/cm³, one obtains a removal rate for acetaldehyde due to photolysis. Weaver et al. (1976) assumed additional CO formation due to chemical quenching of triplet acetaldehyde and deduced a photodissociation coefficient of $1.2 \times 10^{-5} \text{ s}^{-1}$, which is about equal to the removal of OH. Our results suggest that acetaldehyde is predominantly removed by reaction with OH whereas photolysis amounts to less than 20 % of the total. Accordingly, the acetaldehyde in the lower troposphere is predominantly converted to acetylperoxy radicals leading to the subsequent formation of PAN.

6. References

- ATKINSON R. and PITTS, Jr. J.N., J. Chem. Phys., **68**, 3581 (1978).
 BLACET, F.E. and HELDMAN, J.D., J. Am. Chem. Soc. **64**, 889 (1942).
 BLACET, F.E. and LOEFFLER, D.E., J. Am. Chem. Soc. **64**, 893 (1942).
 PARMENTER, C.S. and NOYES, Jr. W.A., J. Am. Chem. Soc. **85**, 416 (1963).
 PETERSON, J.T., Rept. EPA-600/4-76-025. U.S. Environ. Prot. Agency, Research Triangle Park, N.C. (NTIS PB 255819).
 WEAVER, J., MEAGHER, J. and HEICKLEN, J., J. Photochem., **6**, 111 (1976/77)

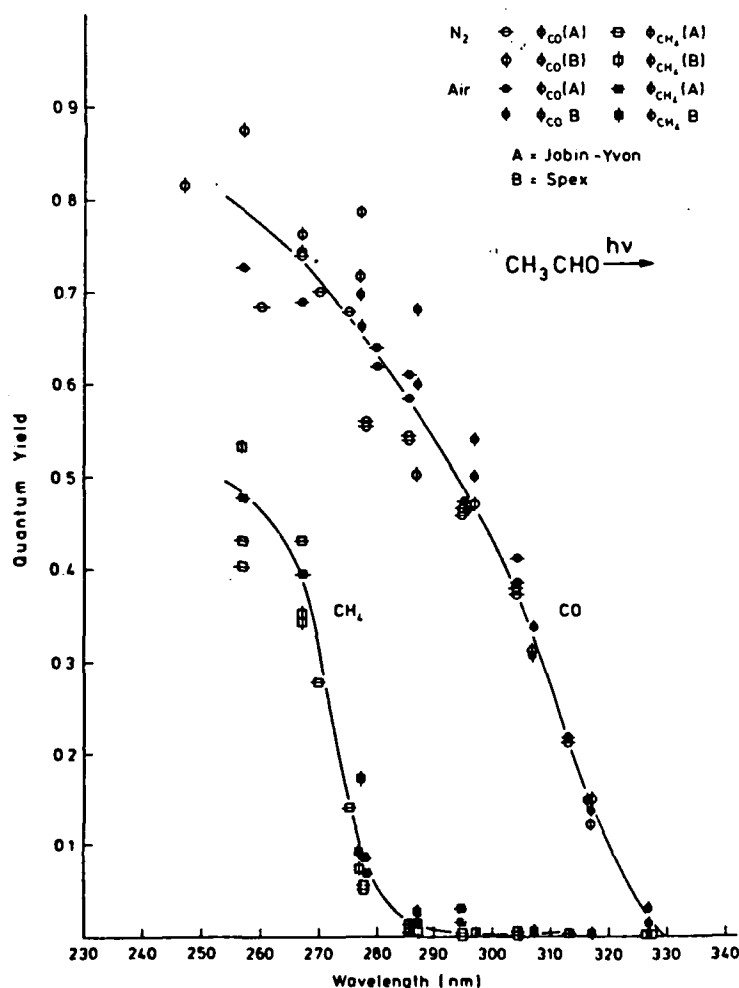


Fig.1 CO and CH₄ quantum yields as a function of wavelength (about 100 ppm acetaldehyde in air and N₂ at 1 atm.)

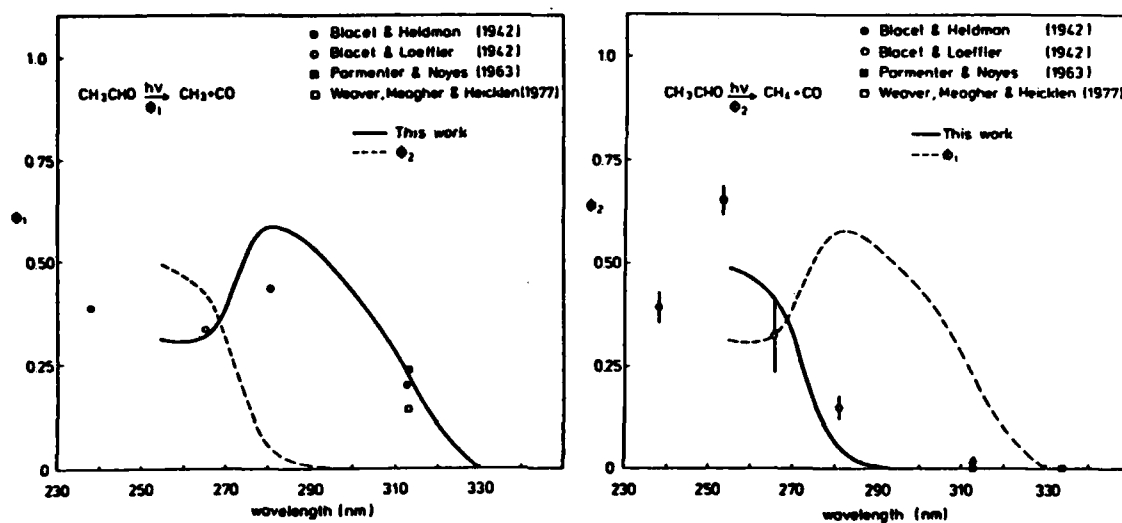


Fig. 2(a and b). Primary quantum yields at atmospheric pressure
 $\phi_1 = \phi_{\text{CO}} - \phi_{\text{CH}_4}$; $\phi_2 = \phi_{\text{CH}_4}$

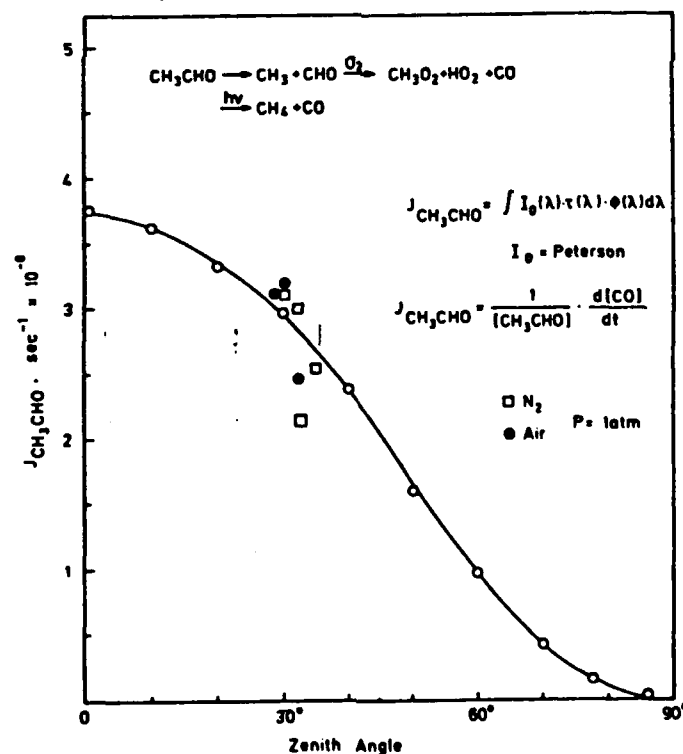


Fig.3. Calculated (o) and measured (●, ■) acetaldehyde photodissociation coefficients as a function of zenith angle.

ABSTRACT D-5

ATMOSPHERIC SOURCES OF NITROUS OXIDE-SOLAR RESONANT EXCITATION OF METASTABLES OH(A) AND N₂(A)

Sheo S. Prasad
Jet Propulsion Laboratory (183-601), California Institute of Technology,
Pasadena, CA 91109

and
Edward C. Zipf
Department of Physics and Astronomy, University of Pittsburgh,
Pittsburgh, PA 15260

Potential chemical roles of electronically excited metastables produced by solar resonant excitation will be discussed. This is a relatively unexplored area of atmospheric chemistry with many interesting possibilities. In particular, the production of nitrous oxide¹⁾ by excited OH(A) via reactions 1 and 2a



maximizing at 42 km in the stratosphere is especially important. Introduction of this non-biogenic atmospheric source of N₂O implies either weaker transport of N₂O from troposphere to stratosphere, or to the existence of unknown photochemical sinks of N₂O in the upper stratosphere, or both. Metastable N₂(A^{3Σ}) pumped by solar UV would produce a considerable amount of nitrous oxide in the earth's present mesosphere if the reaction N₂(A) + O₂ → N₂O + O has a rate coefficient of the order reported by Zipf²⁾. Iannuzzi et al.³⁾ have reported a factor of 30 smaller rate coefficient for this reaction. The origin of this difference is not understood, but a large body of irradiation experiments⁴⁾ support the higher yield of N₂O. It is possible that an overestimate of N₂(A) in Iannuzzi et al.'s experiment and a contribution from potentially important reactions O₂* + N₂ → N₂O + O and O₃* + N₂ → N₂O + O₂ involving excited oxygen and ozone⁵⁾ in irradiation experiments might be partly responsible for the present uncertainties over the efficiency of N₂O formation from N₂(A). Laboratory studies on the possibility of N₂O formation from excited molecular oxygen and ozone are therefore needed. In any case, an important point is that even if the smaller rate coefficient is correct, N₂(A) was an important source of fixed nitrogen nutrient to support primitive life some 3.5 billion years ago⁶⁾.

- 1) E. C. Zipf, Manuscript under preparation.
- 2) E. C. Zipf, Nature, 287, 523, 1980.
- 3) M. P. Iannuzzi, J. B. Jeffries, and F. Kaufman, 1982. Preprint submitted to Chem. Phys. Lett.
- 4) P. Harteck and S. Dondes, J. Chem. Phys., 24, 619, 1956. Also, D. J. Malcombe-Lewis, Nature, 247, 540, 1974.
- 5) S. S. Prasad, Nature, 289, 386, 1981.
- 6) E. C. Zipf and S. S. Prasad, Nature, 295, 133, 1982.

*Work supported by NASA at Caltech-JPL and at the University of Pittsburgh.

ABSTRACT E-1

The Role of Atmospheric Photochemistry in Biogeochemical Cycles

by

Paul J. Crutzen

Max-Planck-Institut f. Chem., D-6500 MAINZ / F.R.G.

to be presented at the XV Informal Photochemistry Meeting 1982

Abstract

We review the most important photochemical processes which take place in the atmosphere and the cycles of many C, N, and S containing constituents. We emphasize the essential role of tropospheric ozone and how the distribution of this gas is influenced by photochemical interactions between carbon and nitrogen containing compounds, which are changing substantially due to man's activities.

There is a large potential for tropospheric ozone formation of which at most only 10% is realized due to generally low NO_x concentrations. The input of NO_x in the troposphere may be dominated by anthropogenic sources so that tropospheric ozone may have increased in the industrial era.

The budgets (sources and sinks) of many compounds are derived and presented (e.g. see attached table and figures). It is shown that these are mostly dominated by tropospheric reactions. However, several gases are inert in the troposphere and their photochemical breakdown in the stratosphere leads to products which influence stratospheric ozone and sulfate aerosol. There often remain large uncertainties in the quantitative aspects of the atmospheric cycles of trace constituents.

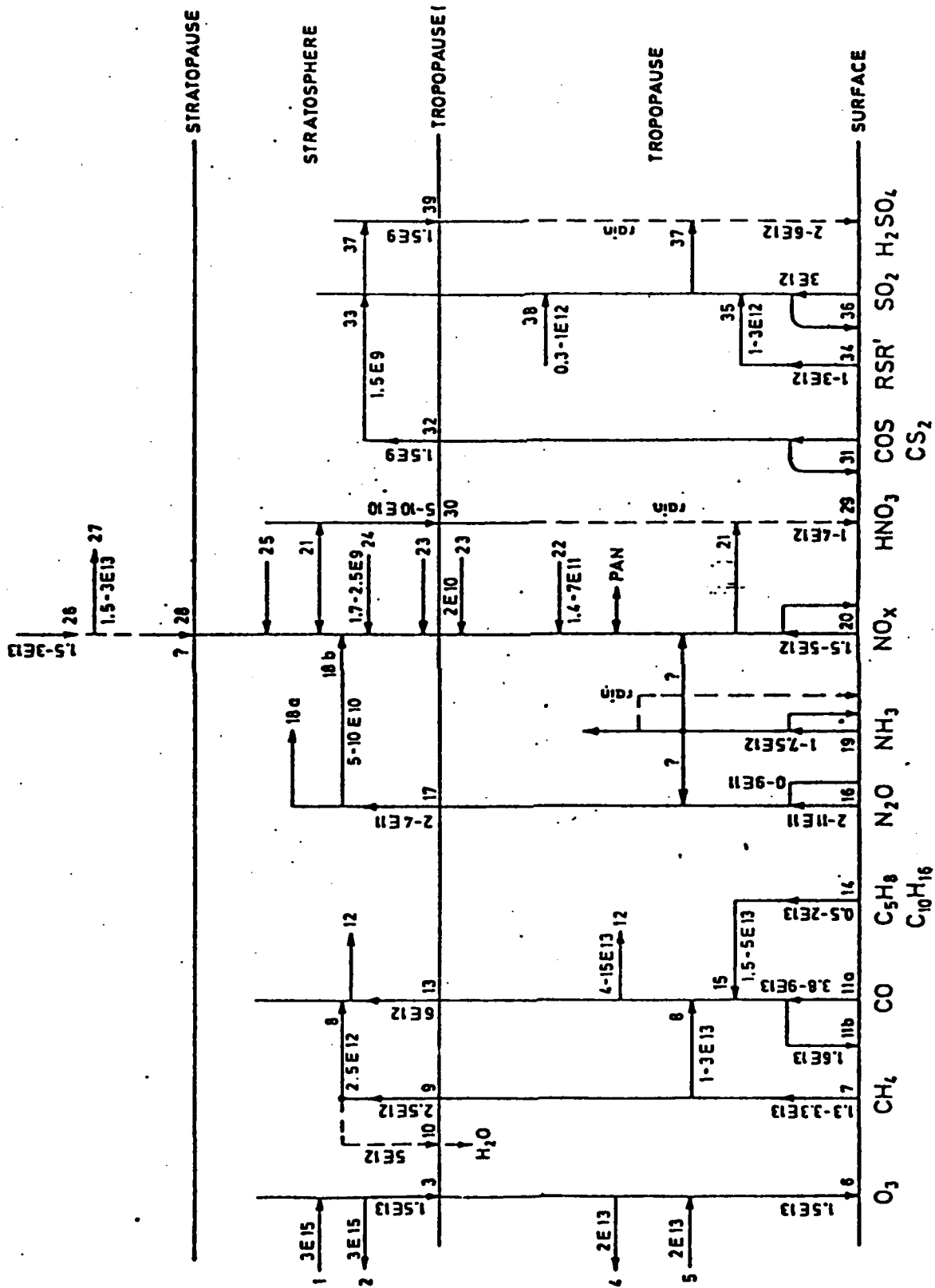
encl.

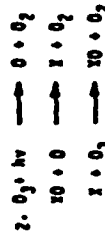
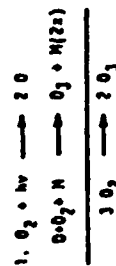
Gas	Direct source/year Source identification	Secondary source/year Source identification	Removal by	Atmospheric lifetimes	Transport distances $\Delta x, \Delta y, \Delta z$ (km); volume mixing ratios in unpolluted tropo- sphere
CO	4-16 x 10 ¹⁴ g CO biomass burning	3.7 - 9.3 x 10 ¹⁴ g CO methane oxidation	30 x 10 ¹⁴ g CO OH	2 m.	4000, 2500, 10 50-200 ppbv
	6.4 x 10 ¹⁴ g CO industry 0.2-2 x 10 ¹⁴ g CO vegetation	4-13 x 10 ¹⁴ g CO C ₅ H ₈ , C ₁₀ H ₁₆ oxidation	4.5 x 10 ¹⁴ g CO uptake by soils		
CH ₄	0.7-1.2 x 10 ¹⁴ g CH ₄ rice paddy fields		4 x 10 ¹⁴ g CH ₄ OH	7 yrs	global 1.5 - 2.0 ppmv
	0.3-2.2 x 10 ¹⁴ g CH ₄ natural wetlands				
	0.6 x 10 ¹⁴ g CH ₄ ruminants				
	1.5 x 10 ¹⁴ g CH ₄ termites				
C ₅ H ₈ C ₁₀ H ₁₆	0.3-1.1 x 10 ¹⁴ g CH ₄ biomass burning				
	0.2 x 10 ¹⁴ g CH ₄ gas leakage				
	8.3 x 10 ¹⁴ g C trees		8.3 x 10 ¹⁴ g C OH	10 hrs	400, 200, 1 0-10 ppbv

Table 1: Budgets of carbon species; Atmospheric lifetimes in hours, months, or years; Diffusion distances in E-W, S-N and vertical directions (in km) over which concentrations are reduced to 30% by chemical reactions. Lifetimes and removal rates calculated with (OH) = $7 \times 10^5 \text{ cm}^{-3}$; 1 ppmv = 10^{-6} ; 1 ppbv = 10^{-9} ; 1 pptv = 10^{-12} . Table 1 continued on next two pages for nitrogen and sulfur compounds.

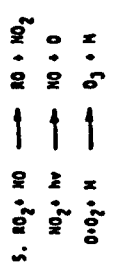
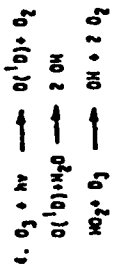
NO_x ($\text{NO} + \text{NO}_2$)	12-20 x 10^{12} g N industry 10-40 x 10^{12} g N biomass burning 1-10 x 10^{12} g N lightning 0-15 x 10^{12} g N soils 0.15 x 10^{12} g N ocean 0.25 x 10^{12} g N jet aircraft	1.0-1.5 x 10^{12} g N oxidation of N_2O	25-85 x 10^{12} g N oil deposition on soils and oceans	1.5 d	1500, 400, 1.0 1-100 pptv
HNO_3		15-85 x 10^{12} g N $\text{NO}_2 + \text{OH}$	rain	3 d	3000, 600, 1.5 10-300 pptv
N_2O	1.8 x 10^{12} g N fossil fuel burning 1-2 x 10^{12} g N biomass burning 0-10 x 10^{12} g N oceans, estuaries 1-3 x 10^{12} g N cultivation natural soils <3 x 10^{12} g N fertilized fields ? natural soils		6-11 x 10^{12} g N stratospheric photolysis	~100-200 yrs	global ~300 pptv

NH ₃	10-20 x 10 ¹² g N domestic animals 2-6 x 10 ¹² g N wild animals ≤ 3 x 10 ¹² g N fertilized fields ≤ 30 x 10 ¹² g N natural fields 4-12 x 10 ¹² g N coal burning ≤ 60 x 10 ¹² g N biomass burning	rain	< 9 d	< 9000, 1000, 3 0-3 ppbw
SO ₂	64 x 10 ¹² g S coal burning 26 x 10 ¹² g S petroleum burning 11 x 10 ¹² g S non-ferrous ores 10-30 x 10 ¹² g S. volcanoes	OH rain	5 d	5000, 700, 2.5 10-200 pptv
H ₂ S (CH ₃) ₂ S CH ₃ SH.	< 4 x 10 ¹² g S agricultural fields 31-42 x 10 ¹² g S. open ocean 10 x 10 ¹² g S coastal waters 16 x 10 ¹² g S (?) tropical forests 24 x 10 ¹² g S (?) wetlands	OH	2 d	2000, 500, 1.5 0-100 pptv

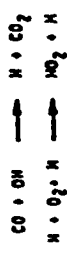




3. Downward flux to troposphere, small difference between 1. and 2.

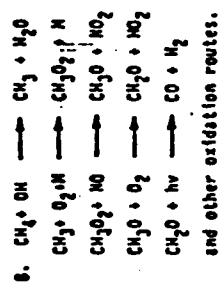


R = H, CH₃ etc. from CO and hydrocarbon oxidation



6. Ozone destruction at ground; difference between 3, 4 and 5.

7. Release of CH₄ at ground by variety of sources with range 1.3 - 3.3 E13 moles/year (E13=10¹³), 2.5 E13 with average OH concentration of 7 E5/cm³



9. Flux of CH₄ to the stratosphere and other oxidation routes.

10. Flux of H₂O to the troposphere from methane oxidation

11a. Release of CO from variety of sources, mostly man-made.

11b. Uptake of CO by microbiological processes in soils.

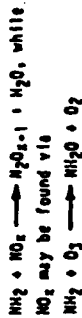
12. CO + OH \longrightarrow H + CO₂
Global loss of CO of 4-15 E 13 moles/year; 7 E 13 calculated with (OH) = 7 E 5.

15. Isoprene and terpene oxidation to CO following reaction with OH; oxidation mechanism and CO yield not well known.

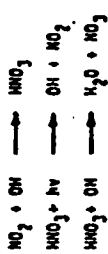
16,17. Release of H₂O to atmosphere by variety of sources; no significant sinks of H₂O in troposphere discovered; stratospheric loss estimated by model calculations.



19. Release of NH₃ by variety of sources to atmosphere; redeposition at the ground; most ammonia removed by rain, but some NO_x loss and H₂O formation possible by reactions



20. Release of NO_x at ground by variety of sources - redeposition at ground



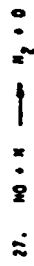
22. NO_x produced from lightning.

23. NO_x produced by subsonic aircraft.

24. NO_x from galactic cosmic rays.

25. NO_x from sporadic solar proton events; maximum production recorded in August 1972 event: 1 E10 moles.

26. NO production by fast photoelectrons in thermosphere and by auroral activity.



28. Downward flux of NO to stratosphere; small difference between 26 and 27, may be important.

31, 32. CO₂ destruction in stratosphere calculated with model; uptake of CO₂ in oceans and hydrolysis may imply an atmospheric lifetime of only a few years and a source of a few times E10 moles per year. There is very little knowledge on the sources and sinks of CO₂ and CS₂.



34. Release of H₂S, CH₃SCN and CH₃SH by biological processes in soils and waters.

35. Oxidation of H₂S, CH₃SCN and CH₃SH to SO₂ after initial attack by OH.

36. Industrial release of SO₂.

37. SO₂ oxidation to H₂SO₄ on aerosols, in cloud droplets, and by gas phase reactions following attack by OH.

38. Volcanic injections of SO₂ average over past centuries.

ABSTRACT E-2

PRODUCT IDENTIFICATION AND QUANTUM YIELD DETERMINATION IN N_2O_5 PHOTOLYSIS AT SEVERAL DISCRETE WAVELENGTHS BETWEEN 249 nm AND 300 nm*

Peter S. Connell,[†] Frank Magnotta,[†]
Diane Swanson, and Harold S. Johnston

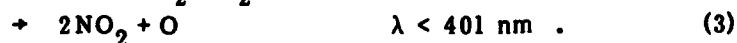
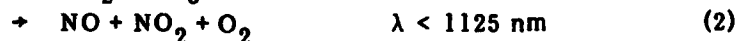
Department of Chemistry, University of California, Berkeley, California
and
Materials and Molecular Research Division,
Lawrence Berkeley Laboratory, Berkeley, California

April 1982

ABSTRACT

The photochemical decomposition of nitrogen pentoxide (N_2O_5) was first studied over 60 years ago,¹ but has received little attention since the first investigation and has remained poorly characterized. The available experimental data^{2,3} indicate variable quantum yields smaller than unity for the uv continuum absorption in the range 260 nm to 280 nm. No direct information on the products of photodecomposition was obtained. The potential importance of N_2O_5 in atmospheric chemistry as a member of the NO_x family and possible precursor in the formation of HNO_3 , depends on its lifetime with respect to thermal and photolytic decomposition and on the product channel of its photodissociation.

Alternative channels with the associated thermodynamically derived wavelength cutoffs for N_2O_5 photolysis include:



All three pathways are energetically accessible for absorption of ultraviolet radiation in the first electronic absorption band of N_2O_5 . The spectrum of N_2O_5 shows absorption commencing near 380 nm, the cross section increasing with decreasing wavelength to 210 nm. At 0.87 nm resolution the absorption is structureless.⁴

*This work was performed under the auspices of the U. S. Department of Energy by the Lawrence Berkeley Laboratory under contract No. W-7405-Eng-48.

[†]Present address: Lawrence Livermore National Laboratory, Livermore, CA.

In the present study, highly sensitive direct detection of N_2O_5 photolytic loss by long path infrared absorption and, in a separate apparatus, direct detection of the potential photofragments $O(^3P)$ and NO by resonant fluorescence (RF) following laser flash photolysis (LFP) have been combined to establish the photochemical mechanism. Detection of products in the LFP/RF study occurs on a time scale sufficiently short ($\sim 10^{-4}$ s) to escape interference from subsequent reactions involving the primary products, while knowledge of the temperature and pressure dependences of the rate constants of secondary reactions allows them to be exploited to study the primary photolysis process in the multi-pass ir cell experiments.

The values obtained for the quantum yield of N_2O_5 disappearance in the ir cell at 252 K and a nitrogen buffer pressure of ~ 0.1 torr are plotted in Fig. 1 as a function of N_2O_5 number density. Also plotted are the quantum yields for $O(^3P)$ production in the LFP/RF experiments at 298 K with a buffer nitrogen pressure of 10 torr. At the low pressure and temperature of the ir cell experiments, thermal decomposition of N_2O_5 is smaller than 0.1% of the photodecomposition rate.⁵ The associative reaction of NO_2 with NO_3 is however still rapid enough at the pressure used to reform N_2O_5 at rates comparable to the photodissociative rate. The good agreement observed between the ir N_2O_5 disappearance and LFP/RF $O(^3P)$ production data shows that the quantum yield for channel (1), NO_3 production, must be small. NO was not observed as a product by resonant fluorescence, allowing an upper limit of about 0.11 to be placed on the quantum yield of channel (2).

Results consistent with the predominance of channel (3), $O(^3P)$ production, and inconsistent with either of the other possibilities have also been observed comparing quantum yields for N_2O_5 disappearance in an atmosphere of nitrogen at 252 K and 295 K, for which $\phi_{295K}/\phi_{252K} = 2.2 \pm 0.3$, and in nitrogen and oxygen buffers at 295 K, $\phi_{N_2}/\phi_{O_2} = 2.1 \pm 0.3$. The errors quoted are estimated to represent 1 σ limits.²

From Fig. 1, the primary quantum yield under the experimental conditions employed is smaller than unity and a strong function of N_2O_5 number density, tending toward unity as the concentration of N_2O_5 goes to zero. A much weaker dependence on buffer gas pressure is also observed, Fig. 2. This pressure dependence of primary quantum yield suggests the existence of a relatively long-lived N_2O_5 excited state, which can be collisionally quenched before

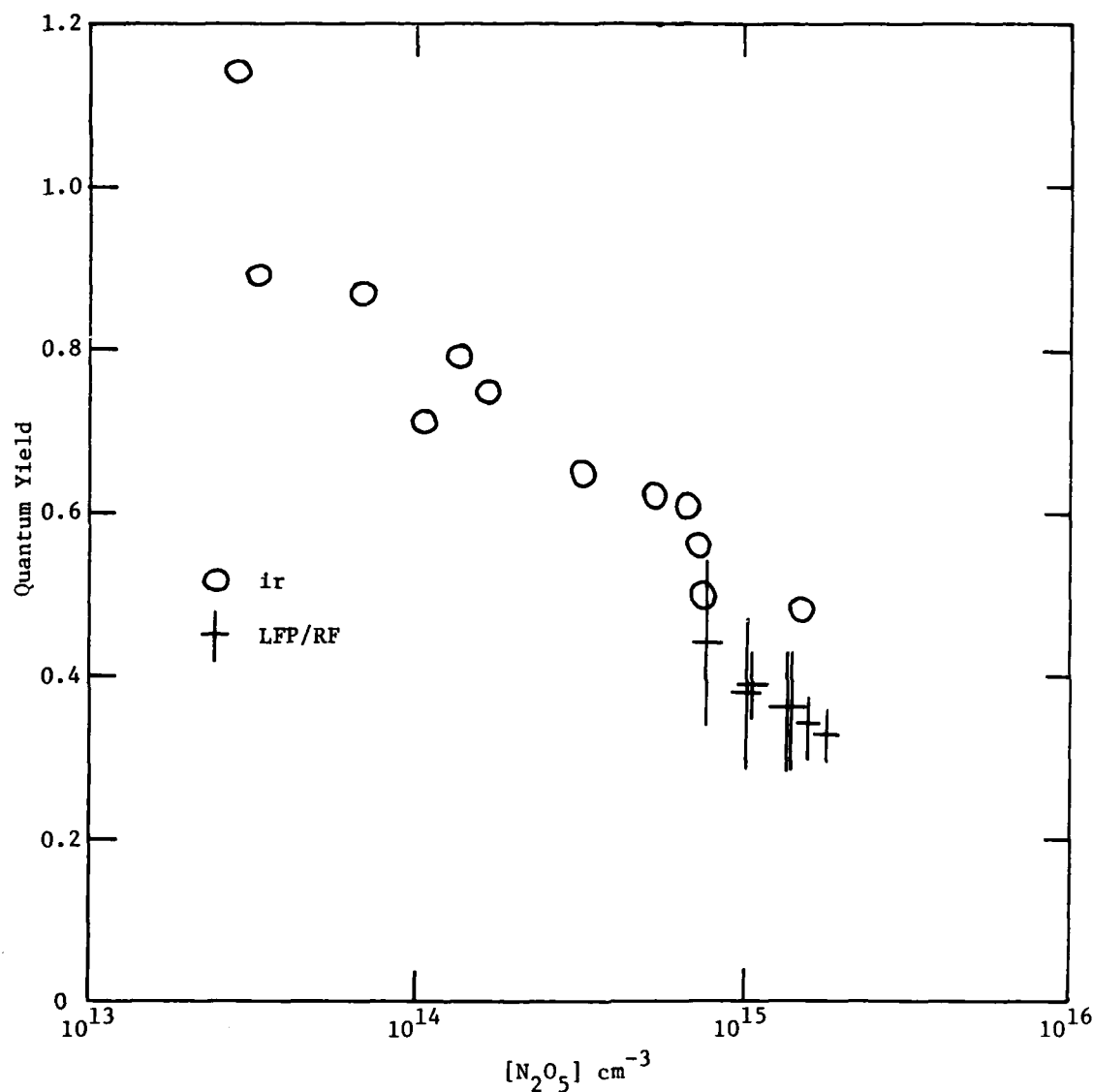


FIGURE 1. Quantum yield dependence on N₂O₅ concentration.

decomposing. Assuming unit quenching efficiency for a collision between electronically excited and ground state N₂O₅, the lifetime is calculated to be $\geq 4 \mu\text{s}$. For N₂O₅ concentrations expected in the stratosphere the quantum yield for dissociation would be essentially one.

Results of experiments designed to observe NO₃ directly in absorption following laser flash photolysis⁶ of N₂O₅ will be presented.

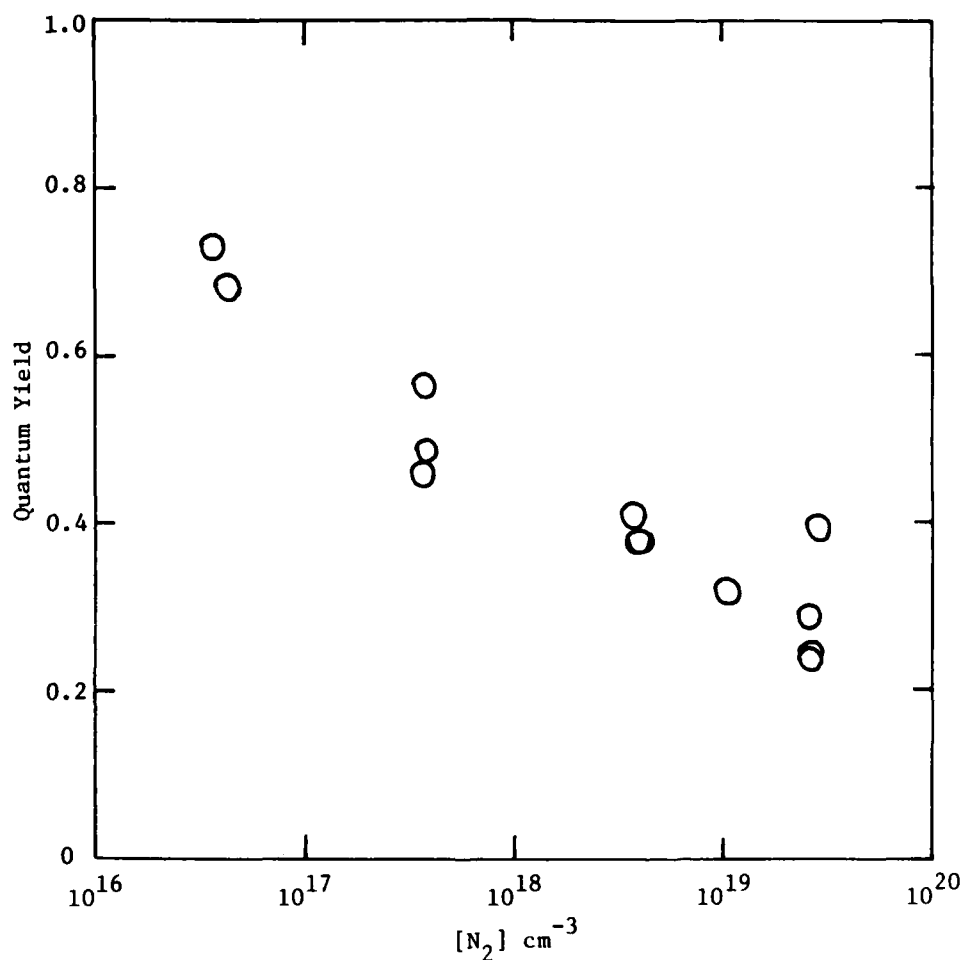


FIGURE 2. Quantum yield dependence on N₂ concentration. [N₂O₅] = 7 × 10¹⁴ cm⁻³.

REFERENCES

1. F. Daniels and E. H. Johnston, J. Am. Chem. Soc., **43**, 72 (1921).
2. H. H. Holmes and F. Daniels, J. Am. Chem. Soc., **56**, 630 (1934).
3. R. Murphy, Ph.D. Thesis, University of California, Los Angeles (University Microfilms, Ann Arbor, 1969).
4. R. A. Graham and H. S. Johnston, J. Phys. Chem., **82**, 254 (1978).
5. P. Connell and H. S. Johnston, Geophys. Res. Lett., **6**, 553 (1979).
6. H. H. Nelson, W. J. Marinelli and H. S. Johnston, Chem. Phys. Lett., **78**, 495 (1981).

ABSTRACT E-3

ClONO₂ Photolysis: Direct Detection of Primary Products

James J. Margitan

Jet Propulsion Laboratory
California Institute of Technology
Pasadena, California 91109

Chlorine nitrate is known to be an important reservoir for odd chlorine in the lower stratosphere, where photolysis of the ClONO₂ is its dominant loss process:



Identification of the primary photolysis products had been attempted in three prior studies, with conflicting results. The channel producing O-atoms has been identified by Smith et al. (1977) using end product analysis of a steady state 302 nm photolysis study and by Adler-Golden and Wiesenfeld (1981) using resonance absorption detection of the atoms in a broadband flash photolysis apparatus. A very low pressure photolysis (VLPP) study using mass spectrometric analysis by Chang et al. (1979), however, determined that Cl + NO₃ constituted the primary channel with an O-atom quantum yield of < 10%.

The photolysis of ClONO₂ has been studied here using 266 nm laser photolysis and atomic resonance fluorescence detection of Cl(119 nm) and O(130 nm). Quantum yields were determined by photolysis of Cl₂ and NO₂. The results of this study indicate that Cl is the dominant photolysis product, with a quantum yield (φ) near unity. The linear dependence of φ(Cl) on power and its independence of residence time, number of flashes and pressure verify

that the chlorine atoms arise from primary photolysis. UV absorption analysis of the ClONO_2 was carried out to ensure that the concentrations of impurities such as Cl_2 , Cl_2O and OClO were inadequate to account for the yield. Some O-atoms were seen, indicating a possible quantum yield of 10%, but the strong, nonlinear power dependence of the O-atom yield suggests that it arises from secondary photolysis, possibly of NO_3 .

The chlorine nitrate sample was obtained from M. J. Molina and L. T. Molina at the University of California, Irvine where it had been synthesized from $\text{Cl}_2\text{O} + \text{N}_2\text{O}_5$. A measured flow of helium was bubbled through the liquid ClONO_2 (maintained in a dry ice bath), passed through a 30 cm absorption cell where the $[\text{ClONO}_2]$ was measured by absorption of 214 nm Zn radiation, and was diluted upon addition to the photolysis cell. The photolysis cell, laser, resonance fluorescence detection and signal processing have been described previously in conjunction with studies of HNO_3 photolysis and the $\text{OH} + \text{HNO}_3$ reaction (Margitan and Watson, 1982).

It is difficult to resolve the discrepancy among the four studies. This study is in excellent agreement with Chang et al. (1979), indicating $\text{Cl} + \text{NO}_3$ as primary products. The other two studies suggest $\text{O} + \text{ClONO}$ as primary products. The Smith et al. (1977) work is the least direct since the primary photolysis step is inferred from end product analysis, but there are no apparent flaws in that technique. The Adler-Golden and Wiesenfeld (1981) work should be direct and unambiguous, but is in total disagreement with the results here. The discrepancy does not seem to be explainable as a wavelength dependence since the O-atoms were observed as a result of 302 nm and broadband ($\lambda > 200$ nm) photolysis, whereas the Cl production was seen in studies with 266 nm and broadband 260-380 nm sources.

The research described in this paper was carried out by the Jet Propulsion Laboratory, California Institute of Technology, under contract with the National Aeronautics and Space Administration.

References

- Adler-Golden, S. M. and J. R. Wiesenfeld, Chem. Phys. Lett. 82, 281 (1981).
Chang, J. S., J. R. Barker, J. E. Davenport and D. M. Golden, Chem. Phys. Lett. 60, 385 (1979).
Margitan, J. J. and R. T. Watson, J. Phys. Chem., to be published (1982).
Smith, W. S., C. C. Chou and F. S. Rowland, Geophys. Res. Lett. 4, 517 (1977).

ABSTRACT E-4

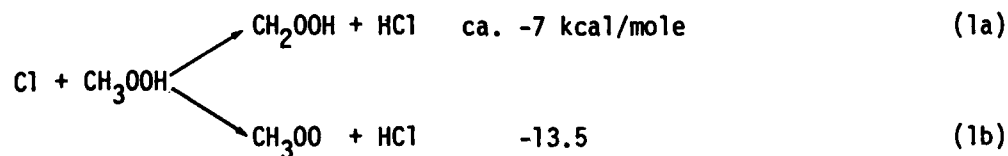
AN FTIR STUDY OF THE Cl-ATOM AND HO-RADICAL REACTIONS OF CH₃OOH

H. Niki, P. D. Maker, C. M. Savage and L. P. Breitenbach

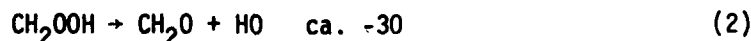
Scientific Research Laboratory, Ford Motor Company, Dearborn, Michigan 48121

Methylhydroperoxide (CH₃OOH) is a potentially important atmospheric constituent formed in the photooxidation of CH₄, i.e., CH₃OO + HOO → CH₃OOH + O₂, and its bimolecular reactions with Cl atom and with HO radical are, therefore, of considerable interest. However, virtually no kinetic and mechanistic studies of these reactions have been made to date, primarily because of numerous experimental difficulties associated with sample-preparation, gas-handling, identification and quantification of the CH₃OOH. In the present long path-FTIR work, these problems have been largely overcome and product studies have been made in the Cl-atom and HO-radical initiated oxidation of CH₃OOH. Both Cl atoms and HO radicals were generated photochemically, from Cl₂ and RONO (R = CH₃ or C₂H₅), respectively.^(1,2)

The major mechanistic features to be addressed are the relative importance of the two possible H-abstraction channels, one involving the CH₃ group and the other the HO group, i.e., reactions 1a and 1b.



and the subsequent unimolecular reaction of the ensuing radical CH₂OOH, reaction 2.



An empirical correlation with related Cl atom abstraction reaction suggests that reaction 1a is fast ($\approx 10^{-10}$ cm³ molecule⁻¹ s⁻¹) and is dominant over reaction 1b.⁽³⁾ However, in our earlier semi-quantitative study of the Cl-CH₃OOH reaction in the presence of NO₂, a substantial yield of CH₃OONO₂ was observed which indicated the significant occurrence of reaction 1b.⁽¹⁾

The present results suggest that reaction 1a accounts for up to 60% of the total reaction and is followed by reaction 2 to give rise to CH₂O and HO. A lower limit for the rate constant ($k_{1a}+k_{1b}$) of 6×10^{-11} cm³ molecule⁻¹ s⁻¹ was obtained from the competitive decay rates of CH₃OOH and C₂H₆. Similarly, the product distribution in the photolysis of C₂H₅ONO-NO-CH₃OOH mixtures in ppm concentration suggests that the HO radical abstracts H atom from the CH₃- and HO-groups at approximately equal rates. Further discussion of these experimental results will be presented at the Conference.

References

- (1) H. Niki, P. D. Maker, C. M. Savage and L. P. Breitenbach, Chem. Phys. Letters, 55, 289 (1978).
- (2) H. Niki, P. D. Maker, C. M. Savage and L. P. Breitenbach, Chem. Phys. Letters, 80, 499 (1981).
- (3) J. V. Michael, D. F. Nava, W. A. Payne and L. J. Stief, Chem. Phys. Letters, 77, 110 (1981).

ABSTRACT E-5

ATMOSPHERIC PHOTODISSOCIATION AND RELATED EXPERIMENTAL PARAMETERS

by

Marcel NICOLET.

The terrestrial photochemistry depends on the variation of the transmission factor of the solar ultraviolet radiation through the mesosphere and stratosphere. Even if the solar flux were accurately determined at the top of the earth's atmosphere, the precision of the various photodissociation rates would always be dependent on the accuracy of the optical depth of molecular oxygen at wavelengths less than 240 nm and of ozone at wavelengths greater than 200 nm.

Several spectral intervals must be known with great accuracy. Lyman-alpha has a particular role in the mesosphere; the bands of the O_2 Schumann-Runge system require special attention particularly at optical depths greater than unity where the precision is not yet sufficient; the Herzberg continuum between 220 and 190 nm is known with poor accuracy. This continuum plays an important role in the atmospheric window at 210 nm where there is a minimum in the ozone absorption. This part of the spectrum, where possible solar activity effects should be taken into account, must be considered particularly in the determination of the photodissociation rates of N_2O , CCl_4 , CF_2Cl_2 and $CFCI_3$ in the upper stratosphere and is responsible for their atmospheric lifetime.

In the spectral range of the Huggins bands, which overlap the end of the Hartley band (production of $O(^1D)$ atoms), the temperature effect must be determined with precision since the photodissociation of many constituents (H_2CO , H_2O_2 , HNO_3 , HNO_4 , etc) depends strongly on the O_3 optical depth.

Finally, the Chappuis bands absorption must be considered with the multiple scattering and albedo effects.

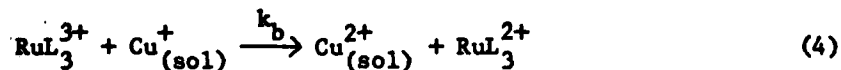
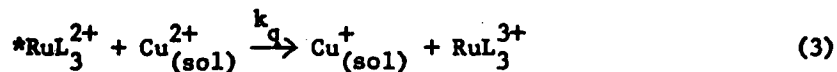
ABSTRACT F-1

Reversible Electron Transfer Reactions of the $\text{RuL}_3^{2+}/\text{Cu(II)}$ System in Various Solvents

B. A. DeGraff*, Pat Morris, Phil Britt, and J. N. Demas, Departments of Chemistry, James Madison University and The University of Virginia.

Excited-state electron transfer reactions have attracted considerable interest due to their potential use in solar energy conversion and as prototype systems to test various models of electron transfer reactions.¹ In this context, because of experimental simplicity and well characterized spectroscopy, the polyimine derivatives of ruthenium(II) have received much attention. For several of the systems studied, there appears to be a good to excellent correlation between the observed kinetics of electron transfer and the predictions of the Marcus model.² However, for systems involving copper(II) as a quencher for excited RuL_3^{2+} complexes, the model works poorly and this has attracted interest as to possible causes.³ To date, all the studies have focused on modifying the structure and environment of the ruthenium complex. We have investigated the $\text{RuL}_3^{2+}/\text{Cu(II)}$ system using different solvents to see what effect the environment of the copper(II) species might have and whether factors other than the electrochemical driving force may be important.

We have studied the reversible electron transfer processes which can be represented as



Where $\text{Cu}_{(\text{sol})}^{2+}$ and $\text{Cu}_{(\text{sol})}^+$ represent a solvated copper (II/I) ion. Using an nsec. lifetime apparatus and conventional flash photolysis, we have obtained values for k_f , k_q , and k_b for a variety of different solvents with copper(II) as the quencher for $L = 2,2'$ bipyridine and 1,10 phenanthroline. Our results are shown in Table 1.

The observed values of k_q and k_b can be compared with the expected values for the diffusion controlled rates taking account of ion pairing in solvents of lower dielectric constants. While there is a reasonable correlation between the electrochemical driving force and the observed rate constants, there are also subtle effects that strongly influence the reaction rates. For example, the reduction potentials of the $\text{Ru}(\text{bpy})_3^{3+}$ and $\text{Ru}(\text{phen})_3^{3+}$ complexes are very comparable in the solvents used. For most of the solvents, the values of k_b are similar for both complexes. Yet, in acetonitrile the k_b 's differ by over 200. Further, in comparing different solvents in which similar driving forces are available, factors of 10 difference between rates are observed.

This paper will examine some of the factors which could be influential in governing the rates of electron transfer and test their applicability to the $\text{RuL}_3^{2+}/\text{Cu}^{2+}$ system in various solvents.

References:

- (1) N. Sutin and C. Creutz, "Advances in Chemistry Series 168, Inorganic and Organometallic Photochemistry," edited by M. Wrighton, 1978.
- (2) C-T. Lin, W. Bottcher, M. Chou, C. Creutz, and N. Sutin, J. Am. Chem. Soc., **98**, 6536 (1976).
- (3) J. E. Baggott and M. J. Pilling, J. Phys. Chem., **84**, 3012, (1980).

Table 1: Rate Constants for the Reversible Electron Transfer Reactions of $\text{RuL}_3^{2+}/\text{Cu(II)}$ System in Various Solvents.

Solvent	τ (nsec)	$k_q \cdot 10^7$ ($\text{M}^{-1} \text{sec}^{-1}$)	$k_b \cdot 10^7$ ($\text{M}^{-1} \text{sec}^{-1}$)	E° (quench) (volts)	E° (back) (volts)
- $\text{Ru}(\text{bpy})_3^{2+}$ -					
Acetone	1.1	22	15	1.60	0.50
Acetonitrile	0.65	94	0.23	2.07	0.37
Dimethyl formamide	0.93	0.43	N.E.T. ^a	0.990	---
Dimethyl sulfoxide	1.0	2.3	N.E.T. ^a	---	---
Methanol	0.83	2.8	263	1.23	0.87
2-propanol	0.75	25	156	1.54	0.56
Water	0.60	6.6 ^b	76 ^b	1.00	1.10
- $\text{Ru}(\text{phen})_3^{2+}$ -					
Acetone	1.3	24	15	1.63	0.50
Acetonitrile	0.46	100	0.0011	2.10	0.41
Dimethyl formamide	---	---	N.E.T. ^a	1.02	---
Dimethyl sulfoxide	---	---	N.E.T. ^a	---	---
Methanol	0.38	2.6	200	1.26	0.89
2-propanol	0.41	42	---	1.57	0.56
Water	0.92	7.5 ^b	133 ^b	1.03	1.10

(a) No net observed electron transfer

(b) 0.104 M HNO_3 and 0.100 M NaNO_3

ABSTRACT F-2

Absolute Rate Constants for the Reactions of $\text{CH}(X^2\Pi)$
with NO , N_2O , NO_2 and N_2 .

S.S. Wagal, Tucker Carrington, S.V. Filseth and C.M. Sadowski

Department of Chemistry, York University, Toronto, Ontario

The reaction of CH with N_2 is the initial step in what is thought to be one of the principle mechanisms for the formation of nitrogen oxides in flames. Reactions of CH with nitrogen oxides may also be important in determining the degree to which it will be possible to reduce emission of these compounds from practical combustion systems.

In order to study these reactions we produced CH radicals by infrared multiple photon dissociation (TEA CO_2 laser, 2J/pulse at 1047 cm^{-1}) of CH_3NH_2 , CH_3CN and $\text{c-C}_3\text{H}_6$. Subsequent removal of CH by reaction with NO , N_2O , NO_2 and N_2 was studied by exciting CH fluorescence in the A-X system (23247.54 cm^{-1} $\text{R}_2(1)$ doublet, $[0,0]$ band) with a 1 cm^{-1} band width tunable dye laser. The fluorescence was collected with an $f/2$ optical system and acquired by gated photon counting methods at rates below 2 MHz. The experimental procedure has been described in detail previously [1].

With each of the three nitrogen oxides CH disappears rapidly in a second order process. The kinetics is studied under pseudo-first order conditions and a weighted least squares fit is used to obtain a first order rate constant for each of several nitrogen oxide partial pressures. These decay constants are corrected for a small contribution due to the reaction of CH with the parent molecule. The remaining decay constant is linearly dependent

upon nitrogen oxide pressure and a weighted least squares analysis of this dependence provides the absolute room-temperature second-order rate constant and its 90% confidence interval as,

$$\begin{aligned}k_{\text{NO}} &= (2.0 \pm 0.3) \times 10^{-10} \text{ cm}^3 \text{ s}^{-1} \\k_{\text{N}_2\text{O}} &= (7.8 \pm 1.4) \times 10^{-11} \\k_{\text{NO}_2} &= (1.7 \pm 0.1) \times 10^{-10} \text{ .}\end{aligned}$$

The rate constant for the NO reaction is in good agreement with that obtained by Butler et al. [2] and with the more recent work [3] of the same group which gives $k_{\text{NO}} = (2.0 \pm 0.2) \times 10^{-10} \text{ cm}^3 \text{ s}^{-1}$. There are no literature values for N_2O or NO_2 .

Several exothermic reaction channels exist for each of these three reactions but this is not the case for the CH reaction with N_2 . While the uncertainties in the thermochemistry for $\text{CH} + \text{N}_2$ are large enough that reaction cannot be absolutely excluded, it seems more likely that the CH disappearance which we observe is due to the formation of a collision stabilized intermediate, HCN_2 . Our measurements were made at pressures up to 75 Torr at room temperature and the psuedo first order pressure dependent decay rates were fit with a simple Lindemann recombination/stabilization model,

$$k_{\text{N}_2} = \frac{P_2 P_3 [\text{N}_2] [\text{M}]}{P_2 + P_3 [\text{M}]}$$

In this expression M corresponds to the sum of N_2 and small ($\leq 10\%$) amounts of Ar present as a diluent, and P_2 and P_3 are the limiting second order (high pressure) and third order (low pressure) rate constants respectively. A weighted least squares fit of this model yields

$$P_2 = (6.3 \pm 1.3) \times 10^{-13} \text{ cm}^3 \text{ s}^{-1} \text{ and}$$

$$P_3 = (2.7 \pm 0.3) \times 10^{-31} \text{ cm}^6 \text{ s}^{-1},$$

at room temperature. The second order rate constants calculated from this fit at 10 Torr, 100 Torr and infinite pressure are $(0.76 \pm 0.05) \times 10^{-13}$, $(3.66 \pm 0.27) \times 10^{-13}$ and $(6.3 \pm 1.3) \times 10^{-13} \text{ cm}^3 \text{ s}^{-1}$ respectively. The result at 100 Torr may be compared with a value of $(9.3 \pm 1.0) \times 10^{-13} \text{ cm}^3 \text{ s}^{-1}$ reported previously [2] and a value of $(3.9 \pm 0.3) \times 10^{-13} \text{ cm}^3 \text{ s}^{-1}$ obtained recently [3].

References

- [1] I. Messing, S.V. Filseth, C.M. Sadowski and Tucker Carrington,
J. Chem. Phys. 74 (1981) 3874.
- [2] J.E. Butler, J.W. Fleming, L.P. Goss and M.C. Lin, Chem. Phys. 56
(1981) 355.
- [3] M.C. Lin, private communication.



ABSTRACT F-3

Radiative and Predissociative Lifetimes of the $V'=0$ Level
of the $A^2\Sigma^+$ State of SH and SD
from Chemical and Spectroscopic Studies

Randall R. Friedl, Wm. H. Brune, and J. G. Anderson

Department of Chemistry and
Center for Earth and Planetary Physics
Harvard University
Cambridge, Massachusetts 02138

Although the $A^2\Sigma$ state of SH is known to be predissociated at all vibrational levels above the ground level ($V' \geq 1$), the $V'=0$ level is thought to be free of predissociative effects.¹ In fact, several recent laser-induced fluorescence studies have successfully used the (0,0) band of the $A^2\Sigma - X^2\Pi$ transition as a diagnostic for SH.²⁻⁴ However, no thorough investigation of predissociation in the $V'=0$ level has yet been conducted. To date, only two, highly contradictory, lifetime measurements have been reported for the $A^2\Sigma$ state; one by Becker and Haaks (550 ns),⁵ and the other by Tsee *et al.* (< 10 ns).³

In order to characterize the $V'=0$ level adequately, we have endeavored to separate the predissociative and radiative parts of the fluorescence lifetime,

$$\frac{1}{\tau_{\text{obs}}} = \frac{1}{\tau_{\text{rad}} + \tau_{\text{pre}}}$$

where τ_{rad} is the radiative lifetime, and τ_{pre} is the predissociative lifetime. If predissociation occurs high in the $V'=0$ rotational manifold, separation of τ_{pre} from τ_{rad} can be achieved by measuring lifetimes at levels above and below the onset of predissociation. The OH radical, the oxygen analog of SH, is an example of this case since predissociation is observed in the $A^2\Sigma$ state beginning at $V'=0$, $N'=23$ for OH, and $V'=0$, $N'=37$ for OD and has been attributed to an interaction between the $4\Sigma^-$ and $2\Sigma^+$ states.^{6,7} OH fluorescence lifetimes have been measured to be approximately 750 ns at low rotational levels, dropping sharply to about 200 ns at $N'=23$. However, if predissociation occurs throughout $V'=0$, then a simple separation is not possible. To achieve separation, one can utilize the fact that the amount of fluorescence obtained for a given radical concentration and experimental apparatus depends explicitly on the product of the inverse of the radiative lifetime (spontaneous emission factor) and the fraction of excited molecules that fluoresce (fluorescent yield). Thus, experimentally determined calibration factors, which relate fluorescent

signal to radical concentration, will reflect the partitioning between radiative and predissociative processes, and values for τ_{rad} and τ_{pre} can be determined by comparison of lifetime measurements to absolute concentration calibrations.

For this investigation, we have coupled a laser-induced fluorescence (LIF) detection system to a fast flow chemical reactor, as is shown in Figure 1. In the reaction zone, which is teflon-coated 2.5 i.d. pyrex tubing, known amounts of SH, SD, and OH were produced by chemical titration. SH and SD were generated by addition of excess $\text{H}_2\text{S}(\text{D}_2\text{S})$ to H or F atoms, while OH was produced by reaction of excess NO_2 with H atoms or excess H_2O with F atoms.

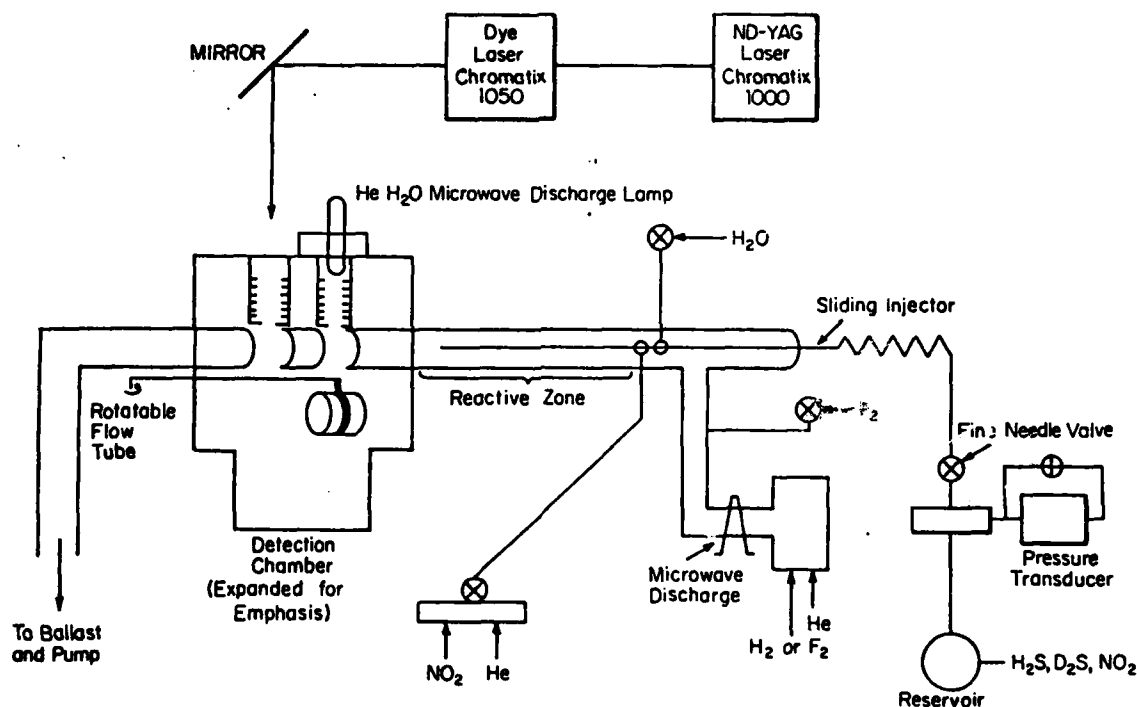


Figure 1.

In the detection chamber, where large scattered light rejection is accomplished because the chamber walls are removed from the detection volume, detection occurred in two gaps in the flow tube; one gap was used for detection of OH with a resonance lamp; the other gap for LIF detection of either SH, SD, or OH. The effect of radical diffusion out of the first gap into the chamber volume on the concentration of radicals reaching the second axis was minimized by the addition of a rotatable flow tube section that could be moved in and out of the first axis. UV laser radiation was produced by coupling a Nd-Yag

laser to a dye laser equipped with Rhodamine 640 dye and a frequency doubling crystal. LIF signal was detected at a right angle to the laser beam with a photomultiplier and a gated boxcar integrator.

With this apparatus, two sets of measurements were performed. First, fluorescence lifetimes for both SH and SD were measured as a function of excited rotational level. For SD, τ_{obs} was measured to be 194 ± 30 ns and did not change as the rotational level was varied from 1 to 10. For SH, the fluorescence essentially followed the temporal behavior of the laser pulse and deconvolution of the fluorescent pulse from the laser pulse resulted in an upper limit for $\tau_{\text{obs}}(\text{SH})$ of 20 ns. Second, calibration factors (C) were determined for SH, SD, and OH from plots of fluorescence signal (S) vs. radical concentration (N), $S = C \times N$. These calibration factors were constant for a given laser flux and a particular choice of laser wavelength. $C(\text{OH})$, which served as a reference (since numerous investigations have already determined that, to within 10 percent, $\tau_{\text{obs}}(\text{OH}) = \tau_{\text{rad}}(\text{OH}) = 750$ ns), was larger than $C(\text{SD})$, which in turn was larger than $C(\text{SH})$. Qualitatively, these calibration results indicate that either the $A^2\Sigma - X^2\Pi$ transition of OH is stronger than those of SH or SD, or that predissociation is significant in the $V'=0$ level of both SH and SD.

Proceeding one step further, an explicit mathematical expression was derived which related C to experimental parameters and radiative and predissociative lifetimes. Combination of lifetime measurements, calibration results, and the derived mathematical expression yielded results which are presented in Table 1, along with the results of other investigations. As will be discussed, it is clear that the transition

Lifetime	Becker and Haaks	Tiee <u>et al.</u>	Becker <u>et al.</u> ⁸	This Work
$\tau_{\text{obs}}(\text{SH})$	550 ± 140	< 10		4 ± 2
$\tau_{\text{obs}}(\text{SD})$	370 ± 70		280 ± 50	194 ± 30
$\tau_{\text{rad}}(\text{SH})$				600 ± 200
$\tau_{\text{pre}}(\text{SH})$				4 ± 2
$\tau_{\text{rad}}(\text{SD})$				600 ± 200
$\tau_{\text{pre}}(\text{SD})$				290 ± 100

Table 1 (all values in nanoseconds)

probability of the $A^2\Sigma - X^2\Pi$ system for SH and SD is comparable to that of OH and predissociation is substantial throughout the $V'=0$ level of SH (SD to a lesser extent). Because of predissociation, the potential of the $A^2\Sigma - X^2\Pi$ system as a sensitive diagnostic for SH is diminished; however, with an appropriate choice of laser system, i.e., low peak power and high average power, SH concentrations as low as 10^8 molecules/cc can be detected.

Reference:

1. D.A. Ramsay, J. Chem. Phys., 20, 1920, 1952.
2. W.G. Hawkins and P.L. Houston, J. Chem. Phys., 73, 297, 1980.
3. J.J. Tise, F.B. Wampler, R.C. Oldenberg and W.W. Rice, Chem. Phys. Lett., 82, 80, 1981.
4. M. Heaven, T.A. Miller and V.E. Bondybey, Chem. Phys. Lett., 84, 1, 1981.
5. K.H. Becker and D. Haaks, J. Photochem., 1, 177, 1972.
6. D.W. Naegeli and H.B. Palmer, J. Mol. Spectr., 23, 44, 1967.
7. K.R. German, J. Chem. Phys., 63, 5252, 1975.
8. K.H. Becker, G. Capelle, D. Haaks and T. Tatarczyk, Ber. Bunsenges Phys. Chem., 78, 1157, 1974.

ABSTRACT F-4

Rotationally Resolved Laser Excitation Spectra of Pb_2 , Sn_2 and Se_2

by

M. C. Heaven, V. E. Bondybey, and Terry A. Miller
Bell Laboratories
Murray Hill, N. J. 07974

ABSTRACT

In traditional studies of metal clusters and other refractory materials, the molecules of interest are usually produced in ovens or furnaces.¹ At the temperatures needed to vaporize sufficient material, the spectra are invariably complex and this often led to difficulties in interpretation. This problem can be partially avoided by use of low temperature matrix techniques. Bondybey and English² have recently used these techniques to study Pb_2 and Bi_2 , and in both cases they found that the previously accepted vibrational constants were in error. However, there are two significant disadvantages to studying species in solid matrices. First, the results are open to the objection that they may be perturbed due to matrix effects. Second, no information concerning the rotational structure of the transition is obtained.

The ideal solution to these problems is to generate low temperature gas phase samples of the species of interest. Several investigators have used supersonic expansions of metal vapors for this purpose.³ More recently, Bondybey and English⁴ have shown that laser vaporization of refractory materials by powerful laser pulses offers an elegant alternative solution, which is extremely simple experimentally.

In the present work, we report new rotationally resolved gas phase spectra for Pb_2 , Sn_2 , and Se_2 . The elemental solids were vaporized by 100 mJ pulses from a YAG laser. The vapor was entrained in a flow of helium which had been precooled to 77K by passage through a coil immersed in liquid N_2 . The resulting mixture was expanded from the vaporization chamber into a small flow cell, where the molecular species were excited by pulses from a tunable dye laser (linewidth $\approx 0.05 \text{ cm}^{-1}$). A total pressure of about 2 Torr was maintained in the flow cell. The concentration of diatomics leaving the vaporization chamber reaches a maximum sometime after the YAG pulse, typically around 100 μs later. Triggering of the dye laser is synchronized with the maximum concentration. Excitation spectra were obtained by pressure scanning the dye laser. Part of the laser beam was

used for the simultaneous recording of a calibration spectrum. In the region $15000 - 20000 \text{ cm}^{-1}$, the $\text{I}_2(\text{B-X})$ spectrum provided the calibration.⁵ Beyond 20000 cm^{-1} the uranium atom spectrum, recorded using the opto-galvanic effect, was used.⁶

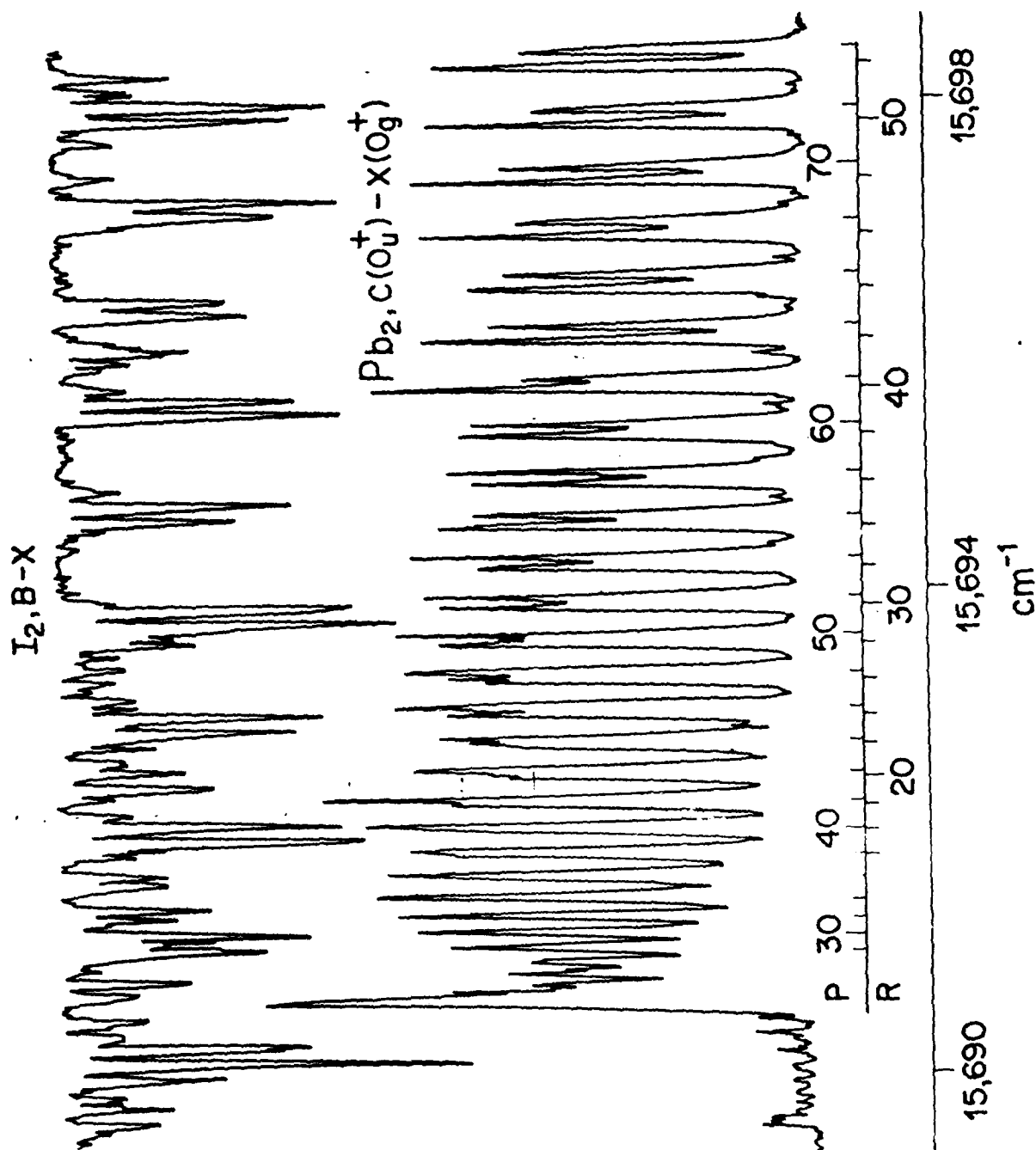
Rotationally resolved spectra for Pb_2 and Sn_2 have not been observed previously. Both elements possess several naturally occurring isotopes of significant abundance. Consequently, it was necessary to use samples of pure ^{208}Pb and ^{116}Sn to obtain tractable spectra. Two electronic transitions were observed for $^{208}\text{Pb}_2$, the $\text{C}(\text{O}_u^+) - \text{X}(\text{O}_g^+)$ and $\text{F}(\text{O}_u^+) - \text{X}(\text{O}_g^+)$ systems. Figure 1 shows an example of a C-X band. The simple rotational structure confirms the assignment of electronic states. Several vibrational bands of both systems have been analyzed, and the results of a global fit to this data will be presented.

The excitation spectrum resulting from vaporization of ^{116}Sn shows two distinct electronic transitions. In this case, the band systems are partially overlapped, producing a dense and complex vibronic structure. Rotational analysis assigns the blue system to a $\text{O}_u^+ - \text{O}_g^+$ transition. Global data analysis is currently in progress.

Excitation spectra of Se_2 reveal a weak new band system underlying the residual hot bands of the well known B-X system. This spectrum has been recorded free from the overlapping B-X bands by detecting only the long lived fluorescence. Vibrational and rotational analysis identifies the upper state as O_u^+ , probably deriving from a $^3\Pi_u$ state. We report spectroscopic constants for this state.

References

1. See, for example, K. Sakurai and H. P. Broida, J. Chem. Phys. 65, 1138 (1976).
W. J. Balfour and R. F. Whitlock, Can. J. Phys. 53, 472 (1975).
2. V. E. Bondybey and J. H. English, J. Chem. Phys. 67, 3405, (1977); J. Chem. Phys. 73, 42 (1980).
3. E.G. W. H. Gerber and E. Schumacher, J. Chem. Phys. 69, 1692 (1978); D. R. Preuss, S. A. Pace, and J. L. Gole, J. Chem. Phys. 71, 3553 (1979).
4. V. E. Bondybey and J. H. English, J. Chem. Phys. 74, 6978 (1981).
5. S. Gerstenkom and P. Luc, "Atlas du Spectre D'Absorption de la Molécule D'Iodide", CNRS, Paris 1978.
6. B. A. Palmer, R. A. Keller, and R. Engleman, "Atlas of Uranium Emission Intensities in a Hollow Cathode Discharge", Los Alamos Scientific Laboratory, LA-8251-MS, 1980.



ABSTRACT F-5

PHOTODISSOCIATION DYNAMICS OF PULSED MOLECULAR BEAMS

Richang Lu, Joshua B. Halpern and William M. Jackson
Department of Chemistry
Howard University
Washington, D.C.

20059

Free jet expansions of seeded molecular beams provides an effective means of cooling the rotational and vibrational degrees of freedom of the seeded gas. Our previous work on photodissociation dynamics in effusive molecular beams have shown that conservation of angular momentum is an extremely strong constraint on the quantum state distribution of fragments, when either the ground or excited state of the parent molecule is linear. In particular, if both states are linear then the sum of the observed rotational angular momenta of the fragments will equal the angular momentum of the parent. Pulsed molecular beams allow one to vary the internal energy distribution of the parent molecules. By examining the effects that this has upon the nascent quantum state distributions of the fragments one can hope to distinguish between angular momentum contributed by bending vibrations of the parent versus that from the original rotational motion of the parent.

We have photolyzed cyanogen, cyanogen chloride and cyanogen bromide in a pulsed molecular beam at 193 nm. CN fragments were probed in the ground state by LIF. For cyanogen, the results show that in a linear to linear transition that all of the angular momentum of the parent is equally shared by the two CN fragments and that there is no orbital angular momentum. There is a complete decoupling of the vibrational and rotational degrees of freedom of the cyanogen. As the cyanogen parent is cooled in the free jet the rotational temperature of the CN fragment cools. The cyanogen absorption at 193 nm is allowed via vibronic interaction in either the ground or excited state. Population of excited bending modes is significant at room temperature in cyanogen. Free jet expansion depopulates these states. A significant decrease of vibrationally excited fragment is observed in the pulsed experiment.

On the other hand the photodissociation dynamics of cyanogen chloride and cyanogen bromide are dominated by the angular momentum contributed to the molecule by excitation of a highly bent excited state. We discuss this in terms of a semi-classical model.

ABSTRACT F-6
BACKGROUND REACTIVITY ESTIMATES FOR
ATMOSPHERIC MODELING STUDIES

By
J. P. Killus

Systems Applications, Inc.
San Rafael, CA 94903

Abstract

Estimates of the photochemical reactivity of "clean air" are necessary for modeling the natural photochemistry of the troposphere and as boundary conditions for urban modeling applications. Ozone in remote areas has been measured in the range of 20-60 ppb, with occasional exceptions due to photochemical destruction or generation (Rutnier, et al., 1980), or from stratospheric intrusion (Singh et al., 1980). Nitrogen oxide data for clean atmospheres ranges from a few ppb to less than a tenth of a ppb (Kelly et al., 1980; Noxon, 1978). Clearly, background concentrations of NO_x are very small when compared with concentrations found in polluted atmospheres. Background NO_x may play a role in the formation of background ozone in the troposphere, however. (Fishman and Crutzea, 1978).

Background hydrocarbon concentrations constitute a problem even at the urban scale. Not only do measured concentrations of background hydrocarbon (and carbon monoxide) constitute a considerable source of reactivity, but there is reason to believe that a considerable amount of background reactivity is due to compounds that are difficult to measure.

For the purposes of this discussion, the term "reactivity" is best defined in a specific chemical sense as the rate at which hydroxyl radicals react with atmospheric gases to form peroxy radicals. These peroxy radicals (HO_2 , CH_3O_2 , CH_3CO_3 , etc.) are responsible for conversion of NO to NO_2 in the photochemical process of smog formation that eventually yields ozone. There are three sources of information concerning the reactivity of background air: (1) measurement of reaction products, principally carbon monoxide (CO), (2) direct measurement of the reactive species, and (3) observation of reactivity effects (NO to NO_2 conversion and ozone formation in smog chambers and power plant plumes).

Background Reactivity of Methane

Methane (CH_4) is usually considered to be an unreactive compound, because its atmospheric reaction rate is two or more orders of magnitude less than reactive hydrocarbons. However, methane does react with hydroxyl (though slowly), and since methane exists throughout the troposphere at appreciable concentrations (1-2 ppm), any discussion of background reactivity begins with this compound.

The reaction rate constant of methane with hydroxyl is $12 \text{ ppm}^{-1}\text{min}^{-1}$ at 298 K at atmospheric pressure (Baulch et al. 1980). When combined with the tropospheric background concentration of 1.6 ppm (Heidt et al. 1980), the hydroxyl conversion reactivity of methane alone is 19.2 min^{-1} , which is equivalent to 0.015 ppmC of a reactive paraffin (e.g., pentane).

Using the accepted oxidation scheme for methane, the reaction products CO and HCHO will assume a photochemical equilibrium of 0.044 ppm and <0.0014 ppm, respectively. The latter figure is an upper limit due to the effects of deposition and photolysis. The calculation of 0.044 ppm CO agrees with measurements of CO in remote areas, (Heidt et al., 1980; Seiler, 1974).

Inference of Reactive Hydrocarbons from CO Observations

The good agreement between the background reactivity of methane and the minimum concentrations of CO observed in remote areas suggests that CO might be used to estimate the reactive hydrocarbon content of background air. Fishman and Crutzen (1978) used a similar procedure in attempting to account for the global tropospheric ozone source and the factor of 4 difference between background CO in the southern and northern hemispheres.

The hydroxyl reactivity associated with the carbon monoxide background at middle latitudes in the northern hemisphere can be calculated from the CO-OH rate constant and background CO. Background CO for the northern hemisphere has been measured at between 0.1 and 0.2 ppm (Heidt et al., 1980; Seiler, 1974; Seiler and Junge, 1970). Over land, especially in the autumn months, the CO concentration appears to be somewhat greater (Jeffries, 1981; private communication, Stevens et al., 1972).

For complex hydrocarbons, some fraction of carbon is directly oxidized to CO₂ rather than CO, because of reduction of the peroxyacyl radical. Taking this process into account, we estimate that the background reactivity of the lower atmosphere is about twice the reactive oxygenates, or six times the reactivity of the carbon monoxide component alone (i.e., about 500 ppm⁻¹min⁻¹).

Direct Measurements of Background RHC

Our picture of the concentration levels and composition of background reactive hydrocarbon derives from several sets of data: Scott Research Laboratories, 1969; Rasmussen, Chatfield, and Holdren, 1977; Altwicker and Dicesare, 1979; and Grosjean, 1980. Two of these data sets include airborne measurements. Using comparisons of RHC measurements aloft with measurements in the planetary boundary layer, we observe that RHC in the free troposphere is very low (~1-10 ppbc), whereas boundary layer concentrations are generally an order of magnitude higher. This observation is in keeping with the conceptual model of Fishman and Crutzen (1978), which uses enhanced photochemical activity in the boundary layer.

There are three possible sources of boundary layer RHC: anthropogenic, geogenic, and biogenic (Mayrsohn and Crabtree, 1976; Altwicker and Dicesare, 1979; Rasmussen and Went, 1965). It is not generally possible to make distinctions among these sources from ambient measurements alone because there is considerable overlap in emitted species, and also because the composition of these sources, especially the biogenic component, is not well characterized.

The minimum NMHC concentrations observed by Rasmussen, Chatfield, and Holdren was 27 µgm/m³ or 38 ppb. Grosjean (1980) reported boundary layer minima NMHC as low as 12 µgm/m³ (17 ppb), while measured concentrations aloft were from 2 to 4 µgm/m³ (3 to 6 ppb), with unreactive ethane as the principal constituent. The Scott Research data base is presumably influenced strongly by urban emissions. The minimum ground measurement of 35

ppb is consistent with the other data sets, however. Airborne monitoring by Scott Research did not exceed 15000 ft. in altitude; however, airborne concentrations were lower than ground values. Minima aloft were as low as 10 to 20 ppb.

On the basis of our examination of these data sets, we suggest that nonmethane hydrocarbon concentrations in the planetary boundary layer (which has a thickness of perhaps 100 to 1000 meters), may be as low as 15 ppbc (0.015 ppmC). However, concentrations as low as this occur only under strong ventilation conditions (e.g., after rainstorms) when the boundary layer air has been mixed with the cleaner air aloft. Concentrations of 30 to 50 ppbc are typically observed, with long range transport of hydrocarbons allowing continental land masses.

Table 1 contains our recommendations for background hydrocarbons for atmospheric modeling within the planetary boundary layer. Our lower limit estimate has a hydroxyl to peroxy conversion reactivity of 128 min^{-1} , which is only twice that of methane and its products. Paraffinic hydrocarbons, the least reactive species, are specified as the only reacting compound. The middle reactivity, or our "best" estimate, has a hydrocarbon concentration of 0.043 ppmC in equilibrium with 0.015 ppm carbonyl compounds. The total hydroxyl to peroxy reactivity is $\sim 400 \text{ min}^{-1}$. This agrees well with our general reactivity estimates based on observed carbon monoxide. The fractional hydrocarbon composition reflects compositions of the previously mentioned rural monitoring studies. The high estimate is an upper limit and probably represents transported contamination; therefore, the high estimate speciation is not in photochemical equilibrium.

TABLE 1. RECOMMENDED BACKGROUND OF REACTIVE HYDROCARBONS

	Carbon Fraction	Concentration	Species*	
Low	0.91	0.03 ppmC	PAR	0.03 ppmC
	0.09	0.003 ppm	CARB	
		0.1 ppm	CO	OH to RO_2 reactivity = 125
Mid	0.61	0.035 ppmC	PAR	0.043 ppmC
	0.083	0.0008 ppm	ARO	(+ 0.015 ppm CARB)
	0.034	0.001 ppm	ETH	
	0.014	0.0004 ppm	OLE	
	0.26	0.015 ppm	CARB	OH to RO_2 reactivity
	0.0005	0.00003 ppm	DCRB	= 387 min^{-1}
		0.2 ppm	CO	
High	0.57	0.1 ppmC	PAR	0.144 ppmC
	0.07	0.002 ppm	ARO	(+ 0.03 ppm CARB)
	0.12	0.01 ppm	ETH	
	0.07	0.006 ppm	OLE	
	0.17	0.03 ppm	CARB	
	0.0005	0.00008 ppm	DCRB	OH to RO_2 reactivity
		0.5 ppm	CO	1153 min^{-1}

Note: All estimates include 0.015 ppmC PAR as surrogate for background methane.

* Speciation is in terms of the Carbon-Bond Mechanism (Killus and Whitten, 1981)

REFERENCES

- Altwick, E., and F. Dicesare (1979), "Relationship between Specific NonMethane Hydrocarbons and Ozone in Urban Air and Their Role in Transportation Control Strategies. DOT/RSPA/DPB-SO/79/25, U.S. Department of Transportation.
- Baulch, D. L., et al. (1980), "Evaluated Kinetic and Photochemical Data for Atmospheric Chemistry," reprint No. 159 from Journal of Physical and Chemical Reference Data, Vol. 9, No. 2, pp. 295-471.
- Fishman, J., and P. Crutzen (1978), "The Origin of ozone in the Troposphere," Nature, Vol. 274, pp. 855-858, 31 August 1978.
- Grosjean, D. (1980), "Measurements in Support of a Photochemical Oxidant Model: Hydrocarbons, Aldehydes, and Ozone Formation in Teflon Tents. Vol. II Appendices. ERT Document P-A029-800
- Heidt, L. E. (1980), "Latitudinal Distributions of CO and CH₄ over the Pacific," Journal of Geophysical Research, Vol. 85, No. C12, 20 December 1980.
- Kelly, T. J., et al. (1980), "Measurements of Oxides of Nitrogen and Nitric Acid in Clean Air," Journal of Geophysical Research, (IBID).
- Killus, J. P., and G. Z. Whitten, (1981a), "A New Carbon-Bond Mechanism of Air Quality Simulation Modeling," SAI No. 81245, Systems Applications, Inc., San Rafael, California.
- Mayrsohn H., and T. H. Crabtree (1976), "Source Reconciliation of Atmospheric Hydrocarbons" Atmospheric Environment, Vol. 10, 1976, p. 137.
- McKay, C., M. Pandow, and R. Wolfgang (1963), "On the Chemistry of Natural Radiocarbon" J. Geophys., Res. 68, pp. 3929-3931.
- Miller et al. (1978), "Ozone Formation Related to Power Plant Emissions" Science, Vol. 202, pp. 1186-1188.
- Noxon, J. F. (1978), "Tropospheric NO_x," J. Geophysical Res., Vol. 83, p. 3051.
- Rasmussen R. A., and F. W. Went (1965), "Volatile Organic Material of Plant Origin in the Atmosphere" Proc. of the N.A.S., Vol. 53, pp. 215-220.
- Rasmussen, R. A., R. B. Chatfield, and M. W. Holdren (1977), "Hydrocarbon Species in Urban Air," Washington State University, Pullman Washington, January 1977.
- Routhier, F., et al. (1980), "Free Troposphere and Boundary Layer Airborne Measurements of Ozone Over the Latitude Range of 58°S to 70°N," Journal of Geophysical Res., Vol. 85, No. C12, 20 December 1980.
- Scott Research Laboratories (1970), "1969 Atmospheric Reaction Studies in the Los Angeles Basin," APRAC Project CABA-7-68 for CRL Inc., and MAPCA (contract No. CPA 70-6), SRL Inc., P.O. Box D-11, Plumsteadville, Pennsylvania 18949. Vol. II. Commerce Ground Data, Vol. III. El Monte Ground Data, Vol. IV. Airborne Data; ESSA Cooperative Data.
- Seiler, W. (1974), "The Cycle of Atmospheric CO," Tellus, XXVI 1974 (1-2), pp. 116-135.
- Seiler, W., and C. Junge (1970), "Carbon Monoxide in the Atmosphere" J. Geophys., Res. 75 2217-2226.
- Stevens, C. M. et al. (1972) "The Isotope Composition of Atmospheric Carbon Monoxide" Meeting on Source, Sinks, and Concentrations of Carbon Monoxide and Methane in the Earth's Environment, St. Petersburg, U.S.A.

ABSTRACT F-7

PHOTODISSOCIATION PROCESSES OF CS_2 AT 1060-1520 Å*

R. L. Day, Masako Sutoh, and L. C. Lee

Department of Electrical and Computer Engineering

San Diego State University

San Diego, California 92182

Recently, CS radicals are found to be abundant in the interstellar medium. This radical is most likely produced by photodissociation of CS_2 . The cross sections for photodissociation of CS_2 into various products are thus needed for modeling the CS abundance in the interstellar medium. The emissions from photofragments of CS_2 could also be used as a new method to measure CS_2 concentrations in the earth atmosphere. CS_2 could have an important role playing in the stratospheric sulfur budget.

Synchrotron radiation produced by the Electron Storage Ring of the University of Wisconsin was used as light source to measure the photoabsorption and photodissociation cross sections of CS_2 at 1060-1520 Å. In the 1060-1200 Å region the absorption is smooth and continuous, except for a strong absorption band ($\sigma_a = 2.1 \times 10^{-16} \text{ cm}^2$) shows at 1117 Å. For wavelengths longer than 1200 Å, the absorption spectrum shows complicated structure of Rydberg states converging to CS_2^+ .

Fluorescences from the photofragments of CS_2 have been observed with an EMI CsTe solar blind (1900-3000 Å) and an EMI 9558QB (1900-8000 Å) photomultiplier tubes (PMT). The fluorescence intensity cross section by calibration against the known cross section¹ of the $\text{CS}(\text{A}^1\Pi \rightarrow \text{X}^1\Sigma^+)$ emission from photodissociation of CS_2 at 1085 and 1239 Å. The measured fluorescence intensity in the 1900-8000 Å region was put into absolute scale by comparing with the $\text{OH}(\text{A}^2\Sigma^+ \rightarrow \text{X}^2\Pi)$ fluorescence from H_2O photodissociation, for which the cross section has been previously measured.²

The correlations of fluorescence cross sections with various photodissociation processes were investigated. The threshold wavelengths for the processes that produce excite species to give emissions in the observed fluorescence wavelength regions are estimated as follows:

$\text{CS}_2 + h\nu \rightarrow \text{CS}(a^{-3}\Sigma^+) + \text{S}(^3\text{P}_2)$	1490 Å
$\quad \quad \quad + \text{CS}(d^3\Delta) + \text{S}(^3\text{P}_2)$	1396
$\quad \quad \quad + \text{CS}(a^3\Pi) + \text{S}(^1\text{D}_2)$	1373
$\quad \quad \quad + \text{CS}(e^3\Sigma^-) + \text{S}(^3\text{P}_2)$	1340
$\quad \quad \quad + \text{CS}(A^1\Pi) + \text{S}(^3\text{P}_2)$	1337
$\quad \quad \quad + \text{CS}(a^{-3}\Sigma^+) + \text{S}(^1\text{D}_2)$	1309
$\quad \quad \quad + \text{CS}(d^3\Delta) + \text{S}(^1\text{D}_2)$	1236
$\quad \quad \quad + \text{CS}(e^3\Sigma^-) + \text{S}(^1\text{D}_2)$	1190
$\quad \quad \quad + \text{CS}(A^1\Pi) + \text{S}(^1\text{D}_2)$	1190
$\quad \quad \quad + \text{CS}(a^3\Pi) + \text{S}(^1\text{S}_0)$	1166
$\quad \quad \quad + \text{CS}(d^3\Delta) + \text{S}(^1\text{S}_0)$	1066

where the dissociation energy of $\text{D}(\text{CS-S}) = 4.463 \text{ eV}^3$ is used.

The fluorescence in the 1900-8000 Å region starts to appear at ~ 1490 Å. The fluorescence is probably composed of the transitions of $\text{S}(^1\text{S}_0 \rightarrow ^3\text{P}_1)$ at 4590 Å and of $\text{CS}(d^3\Delta, a^{-3}\Sigma^+, \text{ and } a^3\Pi \rightarrow X^1\Sigma^+)$ at 3000-4000 Å. The fluorescence in the 1900-3000 Å region starts to appear at 1337 Å. This fluorescence is mainly the $\text{CS}(A^1\Pi \rightarrow X^1\Sigma^+)$ system in the 2400-2800 Å region. There are three excitation bands in the 1090-1120 Å, 1140-1180 Å, and 1210-1330 Å regions that give high UV fluorescence cross sections. Further investigations of the nature of these excite states are interesting.

The quantum yields for the production of fluorescence are determined from the ratios of fluorescence to absorption cross sections. From 1235 to 1490 Å, the apparent quantum yields increase with decreasing wavelengths, the maximum yields at 1235 Å are 13% and 7.5% for the fluorescence in the 1900-8000 Å and 1900-3000 Å regions, respectively. The yields suddenly drop to less than 1% at 1200 Å. The maximum yields for the 1090-1120 Å and 1140-1180 Å bands are 5.5% and 1.7% for the 1900-8000 Å fluorescence, and 3.3% and 0.8% for the 1900-3000 Å fluorescence, respectively.

- 1) L. C. Lee and D. L. Judge, J. Chem. Phys. 63, 2782 (1975)
- 2) L. C. Lee, J. Chem. Phys. 72, 4334 (1980)
- 3) H. Okabe, J. Chem. Phys. 56, 4381 (1972)

* This work is based upon the materials supported by NASA under contract no. NASW-3270 and NSF under grant no. ATM-8205849. The synchrotron radiation facility of the University of Wisconsin is supported by NSF under grant no. DMR-77-21888.

ABSTRACT F-8

MULTIPHOTON EXCITATION OF DIETHYL ETHER

L. Butler, R. J. Buss, R. Brudzynski and Y. T. Lee

Materials and Molecular Research Division
Lawrence Berkeley Laboratory and
Department of Chemistry, University of California
Berkeley, California 94720 USA

ABSTRACT

Infrared multiphoton excitation of molecules isolated in a beam has been shown to be a useful tool for studying the dynamics of unimolecular reactions. Most reactions studied by this method have involved simple bond ruptures, isomerization and multicenter elimination of a diatomic molecule. Several studies on larger molecules, ethyl vinyl ether, for example reveal complex mechanisms in which six centered eliminations compete with simple bond ruptures and release an unusually large fraction of available energy as translation.

Pyrolysis studies of diethyl ether¹ have shown two decomposition routes to be dominant: the simple rupture of a C-O bond and the formation of ethanol and ethylene through a four centered cyclic transition state. There has been disagreement concerning the relative rates of these channels.

Using a crossed molecular beam-laser apparatus we have obtained angular and velocity distributions of the products from decomposition of diethyl ether excited by multiphoton absorption from a TEA CO₂ laser. The products were identified by comparing the velocity spectra obtained at various masses and using kinematic relations as well as energy and momentum conservation to distinguish dynamically distinct channels. The time of

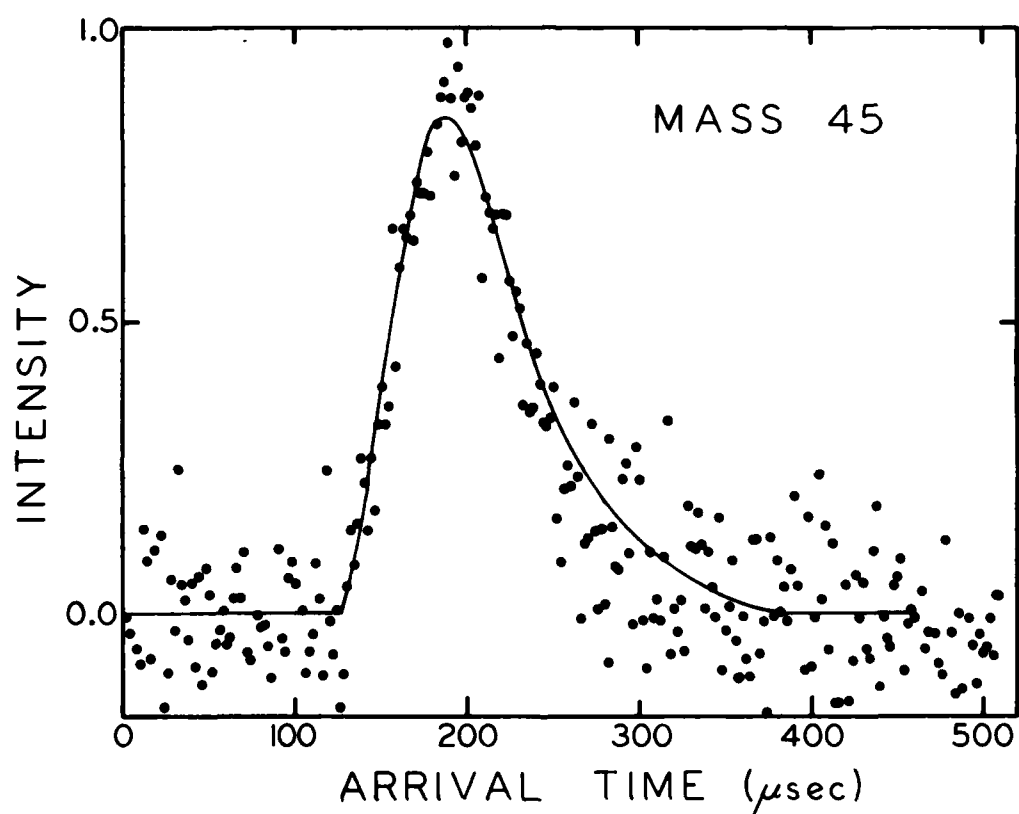
flight spectrum of mass 45, from the simple bond rupture yielding $C_2H_5 + C_2H_5O$ is shown in Fig. 1. The much faster mass 31 signal, shown in Fig. 2 is identified as arising from the four centered reaction $C_2H_4 + C_2H_5OH$.

The experimentally determined product translational energy distributions for both channels show that the four centered reaction results in a large energy release to translation (average ~40%) while the simple bond rupture exhibits very low product translation. The branching ratio for the channels at different laser fluence and the dependence of yield on fluence will be discussed in connection with the barrier heights for the two channels.

This work was supported by the Office of Naval Research under Contract No. N00014-75-C-0671.

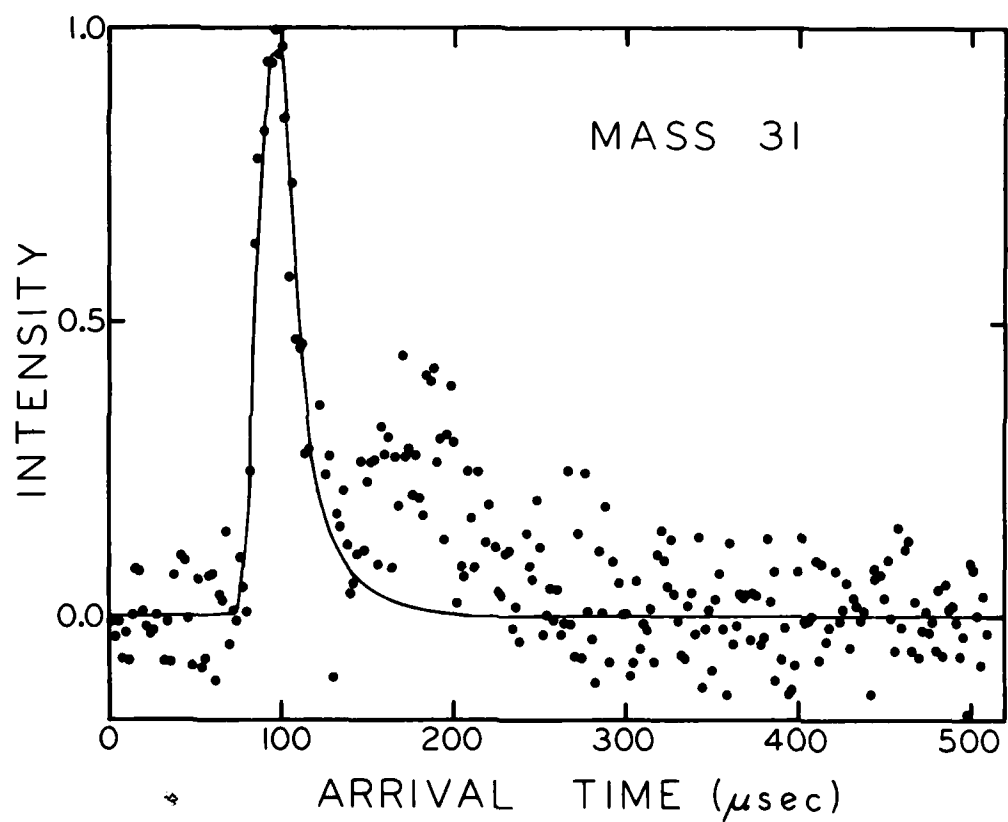
References

1. K. J. Laidler and D. J. McKenney, Proc. Roy. Soc. 278A, (1964) 517.
I. Seres and P. Huhn, Magy. Kem. Foly. 81(3) (1975) 120.



XBL 824-9130

Fig. 1. Time of flight spectrum of product measured at $m/e = 45$, which corresponds to the formation of $C_2H_5 + C_2H_5O$ products.



XBL 824-9133

Fig. 2. Time of flight spectrum of product measured at $m/e = 31$, which corresponds to the formation of $\text{C}_2\text{H}_4 + \text{C}_2\text{H}_5\text{OH}$ products.

ABSTRACT F-9

STATISTICAL LIMIT QUENCHING OF S_1 PYRIMIDINE*

by

Gary Loge

University of California
Los Alamos National Laboratory
P. O. Box 1663
Los Alamos, NM 87545

ABSTRACT

An excited state molecule that undergoes a conversion or crossing from a bound potential state to higher vibrational levels of a lower lying bound potential state exhibits one of three different behaviors.^{1,2} Large molecule behavior exhibits exponential decay with the statistical limiting rate constant $k_{nr} = \frac{2\pi}{h} \rho V^2$, which is not influenced by collisions and occurs in molecules that have a large density of states in the lower electronic state at the same energy as the initial state. Another type of behavior is the intermediate case, which shows biexponential decay with one exponential rate constant showing a strong pressure dependence. Small molecule behavior is the other limiting type of behavior; the initial state interacts with only a few lower state levels and undergoes irreversible crossing only during collisions.

A Stern-Volmer plot of the inverse of the fluorescence intensity vs pressure shows a linear dependence for small molecule type of behavior. However, recent experimental evidence has shown that at higher pressures (>10-100 torr) non-linear Stern-Volmer plots can be observed.^{3,4,5} This behavior has been previously predicted for S_1 - T_1 crossing of glyoxal ($C_2H_2O_2$),

*Work performed under the auspices of US DOE.

but no analytical solution was given.⁶ To allow a better comparison between the theory and experimental observations, a kinetic model is presented that approximates the coupling between the two states as a collisionless equilibrium in which collisions cause irreversible crossing to the lower state. This model has been previously applied to intermediate case molecules where correspondence to the exact quantum treatment was shown.⁷ The analytical expression for the inverse of the fluorescence yield is derived from this kinetic model for small molecule behavior and is found to be the same as for intermediate case molecule behavior, but non-linear pressure dependence is seen only at higher pressures for small molecule behavior. This model fits the previous small molecule data on SO₂ and glyoxal collision-induced crossing.^{3,4}

The validity of the kinetic model is further confirmed by the S₁-T₁ collision-induced crossing in pyrimidine, which shows small molecule behavior in the lowest vibrational level.⁸ Linear Stern-Volmer plots are obtained for added gas pressure below one torr as shown in Fig. 1. The slope of the plots for different added gases are nearly the same, which is consistent with the fact that the S₁ state of pyrimidine is weakly coupled to the T₁ state so the equilibrium rate between the two states is slow, allowing any collision partner to cause irreversible crossing. The pressure dependence becomes non-linear at higher pressure as the statistical limiting crossing rate is reached, and above 300 torr the limiting value is reached independent of the added gas used, see Fig. 2. O₂ and NO used as added gases show slightly different values for the limiting rate of S₁-T₁ pyrimidine crossing, presumably because of an increase in S₁-T₁ coupling under the influence of O₂ and NO. Comparison with previously obtained time dependent decay of S₁ pyrimidine⁸ allows the density of states ρ and the coupling strength V to be obtained.

REFERENCES

1. P. Avouris, W. M. Gelbart, and M. A. El-Sayed, *Chem. Rev.*, 77, 793 (1977).
2. A. Tramer and R. Voltz, in Excited States, Vol. 4, p. 281-394, Academic Press, Inc. 1979.
3. S. J. Strickler and R. N. Rudolph, *J. Amer. Chem. Soc.* 100, 3326 (1978).
4. G. W. Loge, Ph.D Thesis, Indiana University, 1979.
5. J. J. Tiee and F. B. Wampler, manuscript in preparation.
6. K. F. Freed, *Chem. Phys. Lett.* 37, 47 (1976).
7. F. Lahmani, A. Tramer, and C. Tric, *J. Chem. Phys.* 60, 4431 (1974).
8. K. G. Spears and M. El-Manguch, *Chem. Phys.* 24, 65 (1971).

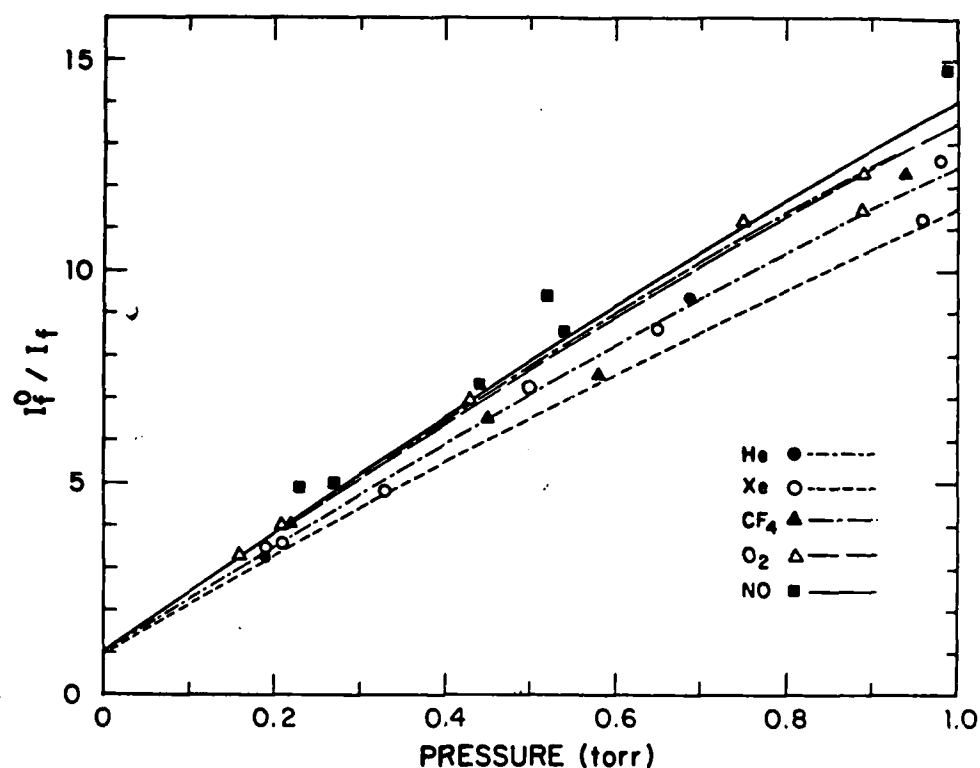


Figure 1. The S_1 pyrimidine quenching data below one torr is shown along with the non-linear least squares fit of the kinetic model to the data at all pressures (see Figure 2).

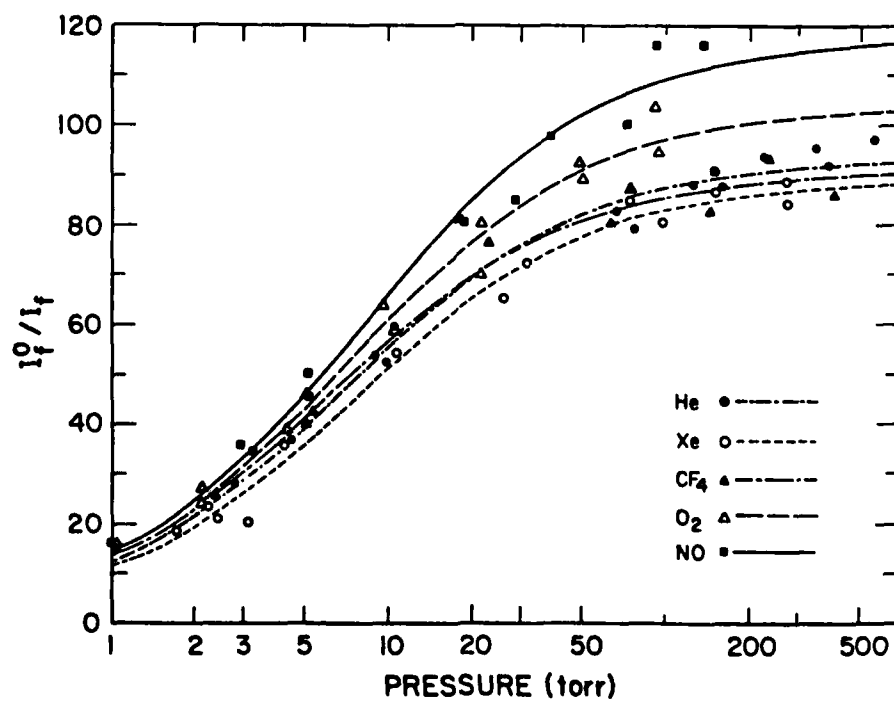


Figure 2. The S_1 pyrimidine quenching data above one torr is shown along with the non-linear least squares fit for each added gas.

ABSTRACT F-10

Vacuum Ultraviolet Photolysis of H_2O and NO_2

J. B. Nee and J. G. Anderson

Department of Chemistry and
Center for Earth and Planetary Physics
Harvard University
Cambridge, Massachusetts 02138

Vacuum ultraviolet (VUV) photolysis of the polyatomic molecules H_2O and NO_2 have been the subject of extensive investigation. The absolute cross sections of $\text{OH}(\text{A}^2\Sigma^+)$ from H_2O have been measured by Lee¹ and Vinogradov *et al.*² There are also numerous studies devoted to understanding the abnormal $\text{A}^2\Sigma^+$ state rotational distribution exhibited by the OH produced in photolysis.

VUV photolysis of NO_2 generates NO in electronically excited states also, and the fluorescence spectrum consists of emissions mainly from λ and β bands, as shown first by Welge.³ Lenzi and Okabe⁴ suggested that higher excited states, including $\text{C}^2\Pi$, $\text{D}^2\Sigma^+$, $\text{B}'^2\Delta$, among others, might also be produced and they measured the total fluorescence yield by detecting the emissions in the wavelength range of 1900 - 6000 Å. Their values are low compared to more recent measurements done by Lee *et al.*⁵ and Vinogradov *et al.*⁶ However, there are no measurements of quantum yields of specific electronic states of NO.

We have carried out the photolysis of H_2O and NO_2 in a 3-inch flow tube at wavelengths 1216, 1236, and 1302 Å from hydrogen, krypton, and oxygen atomic resonance lamps. Quantum yields of $\text{OH}(\text{A}^2\Sigma^+)$ and $\text{NO}(\text{B}^2\Pi)$ were measured absolutely, but only an upper limit was obtained for the $\text{NO}(\text{A}^2\Sigma^+)$ state. The H_2O experiment was calibrated against Rayleigh scattering of argon at 3188 Å for which the cross section is known. Helium sealed inside the lamps was the source of the 3188 Å

emission. The cross sections obtained for $\text{OH}(\text{A}^2\Sigma^+)$ from H_2O were then used to calibrate the NO_2 experiment. The absolute flux of VUV emissions were measured with an EMR two-inch photodiode (Model 543-P). The concentrations of H_2O and NO_2 were measured using the method of long path optical absorption. Detection of the $\text{OH}(\text{A}^2\Sigma^+)$ state and $\text{NO}(\text{B}^2\Pi)$ state were made with interference filters centered at the (0,0) band of $\text{OH}(\text{A}^2\Sigma^+ - \text{X}^2\Pi)$ and the (0,9) band of $\text{NO}(\text{B}^2\Pi - \text{X}^2\Pi)$ transition. Accurate measurement on the quantum yield of $\text{NO}(\text{A}^2\Sigma^+)$ state was impossible to obtain because of the complexity of the fluorescence spectrum below 2500, as shown in Figure 1. Results of our measurements on $\text{OH}(\text{A}^2\Sigma^+)$ and $\text{NO}(\text{B}^2\Pi)$ as given in Table 1. The quantum yield of $\text{NO}(\text{A}^2\Sigma^+)$ was found to be less than 2 percent.

The beta band emissions were found to be dependent on the pressure, and correction of this variation has been made to get the true quantum yields shown in Table 1. Based on previous studies of Young and Sharpless⁷ and by Campbell and Mason,⁸ we conclude that the pressure-dependent behavior for beta bands is related to the quartet state $\text{b}^4\Sigma^-$, which is also produced in NO_2 photolysis. The $\text{b}^4\Sigma^-$ state has a potential energy curve crossing with the $\text{B}^2\Pi$ state at ground vibrational level⁹ and collisions can aid the transition between these two states. Production of the $\text{b}^4\Sigma^-$ state is allowed energetically and does not violate the correlation rule. A six-step model which included photolysis, radiation, quenching, and collision-induced crossing between the $\text{b}^4\Sigma^-$ and $\text{B}^2\Pi$ states was used to interpret the pressure data. Results of the treatment summarized in Figure 2 will be discussed.

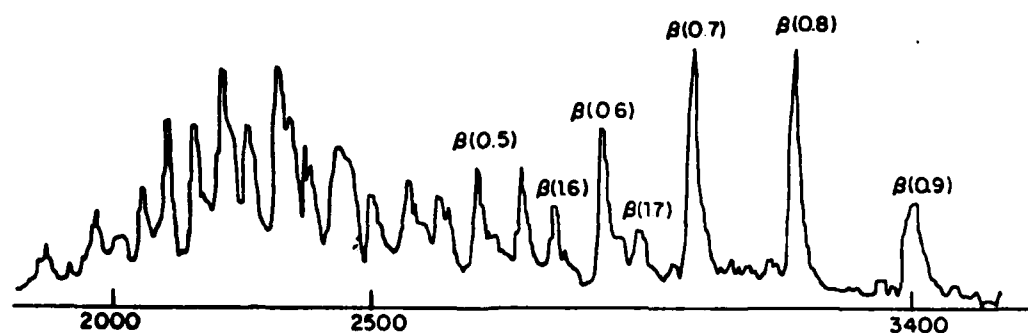


Figure 1. NO fluorescence following photolysis of NO_2 at 1216 \AA . The spectrum is uncorrected for the efficiency of the spectrometer.

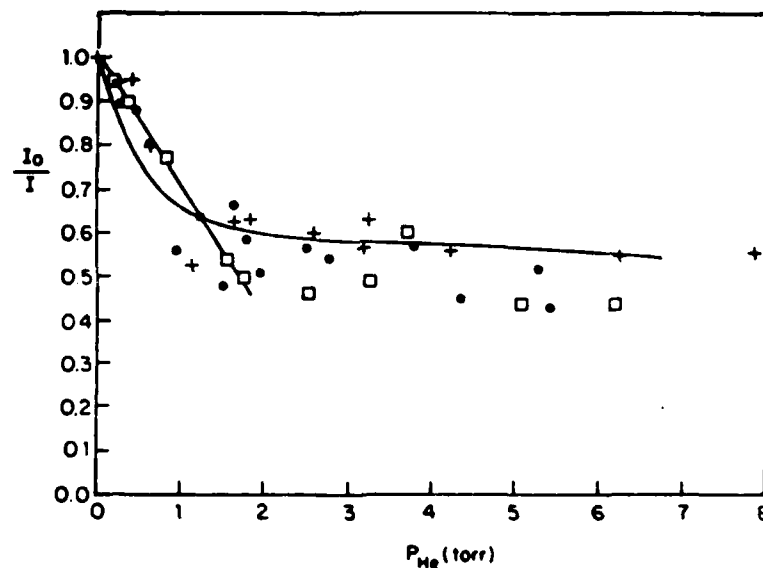


Figure 2. Dependence of the beta band fluorescence on the pressure of helium. I_0 was obtained from fitting the data below 1.5 torr to a straight line. The curve is the result of the theoretical study. "•, ◻, +" are data from different runs of the experiment, all obtained from photolyzing NO at 1216 \AA .

Wavelengths (\AA)	1216	1236	1302
$\text{OH}(\text{A}^2\Sigma^+)$ [$\pm 36\%$]	9.3%	7.5%	9.9%
$\text{NO}(\text{B}^2\Pi)$ [$\pm 41\%$]	2.8%	2.7%	1.3%

Table 1. Quantum yields of $\text{OH}(\text{A}^2\Sigma^+)$ and $\text{NO}(\text{B}^2\Pi)$

References:

1. L.C. Lee, J. Chem. Phys., 72, 4334, 1978.
2. I.P. Vinogradov and F.I. Vilesov, Opt. Spectros., 40, 32, 1976.
3. K. Welge, J. Chem. Phys., 45, 1113, 1966.
4. M. Lenzi and H. Koabe, Ber. Bunsenges, Phys. Chem., 72, 168, 1968.
5. L.C. Lee, to be published, 1982.
6. I.P. Vinogradov and F.I. Vilesov, Russion J. of Phys. Chem., 51, 1176, 1977.
7. R.A. Young and R.L. Sharpless, Dis. Faraday Soc., 33, 228, 1962.
8. I.M. Campbell and R.S. Mason, J. Photochem., 8, 321, 1978.
9. I.M. Campbell and R.S. Mason, J. Photochem., 8, 375, 1978.

ABSTRACT F-11

The Reaction of OH with CO. The Pressure Dependence of the Rate Constant.

G. Paraskevopoulos and R.S. Irwin

Division of Chemistry, National Research Council of Canada
Ottawa, Ontario, Canada, K1A 0R9

Absolute rate constants for the reaction $\text{OH} + \text{CO} + \text{M}$ have been determined in the gas phase, at room temperature and in the pressure range 20-700 torr of various third bodies M ($\text{M} = \text{He}, \text{N}_2, \text{CF}_4, \text{and SF}_6$).

The measurements were made by using the flash photolysis-resonance absorption technique. Hydroxyl radicals were generated by flash photolysis of low pressures of H_2O vapor in the vacuum U.V. ($\lambda > 165 \text{ nm}$). The OH concentration was monitored in absorption by time resolved attenuation of the OH resonance radiation at 308.15 nm, $\text{OH} (\text{A}^2\Sigma^+ \rightarrow \text{X}^2\Pi)$. Repeated flashing and signal averaging were used to improve the signal-to-noise ratio.

The bimolecular rate constant was found to depend on the nature and pressure of the third body M. It increased with increasing pressure of M from $\sim 8.6 \times 10^{10} \text{ cm}^3 \text{ mol}^{-1} \text{ s}^{-1}$ at 20 torr of all three bodies to $\sim 2.1 \times 10^{11} \text{ cm}^3 \text{ mol}^{-1} \text{ s}^{-1}$ at 700 torr of SF_6 . The efficiency of the gases as third bodies were: $\text{SF}_6 > \text{CF}_4 > \text{N}_2$. Helium was completely inefficient. A mechanism consistent with the results will be discussed.

Careful purification of the reactants showed that the pressure dependence of the rate constant is not due to an O_2 impurity. The possible effect of O_2 on the rate measurements will be discussed.

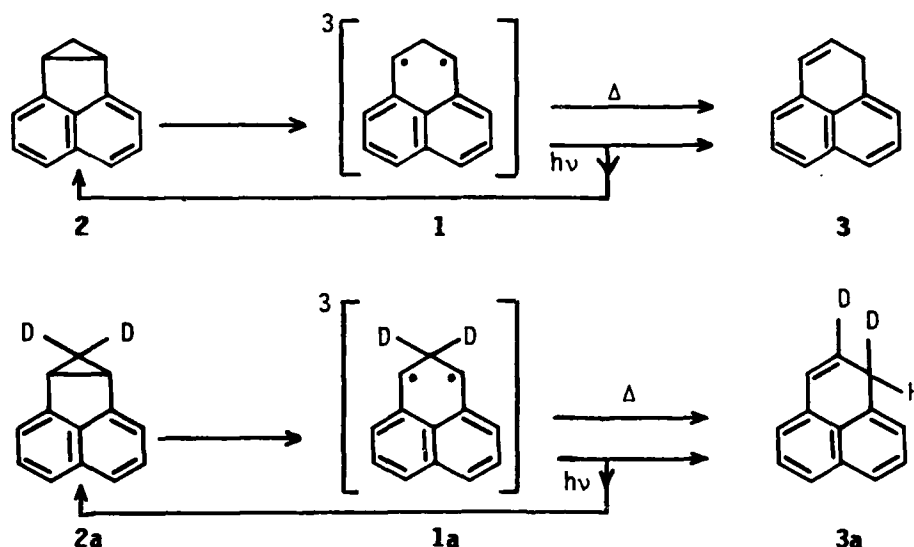
ABSTRACT F-12

LOW-TEMPERATURE CHEMISTRY OF A 1,3-BIRADICAL, by John H. Penn, Detlef Döhnert, and Josef Michl, Department of Chemistry, University of Utah, Salt Lake City, Utah 84112, USA

ABSTRACT

During our previous studies on potential photochemical intermediates, we observed the 1,8-perinaphthadiyl biradical **1** at temperatures less than 100 K during the photolysis of the dihydrocycloprop[*a*]acenaphthylene **2** and characterized it by its optical and esr spectra and by the kinetics of its thermal transformation to **3**.¹ Curie law analysis of the esr signal intensity shows this species to be a ground state triplet.²

We have now obtained the infrared spectra of **1** and its dideuterated analog **1a** in argon and cyclohexane matrices. The biradical **1** is converted thermally to phenalene, **3**, and photochemically to a mixture of **2** and **3**; biradical **1a** behaves similarly.



A comparison of the thermal kinetics of the 1,2-shift in **1** and **1a** isolated in a cyclohexane matrix revealed an unusual inverse primary deuterium kinetic isotope effect. The Arrhenius parameters for **1** and **1a** have been determined by monitoring the disappearance of the esr signal intensity over the temperature range 110-138 K (Figure 1): $E_a(\text{H}) = 5.1 \pm 0.5$ kcal/mole, $\log A(\text{H}) = 5.2 \pm 1.0$ (s^{-1}), $E_a(\text{D}) = 7.2 \pm 0.7$ kcal/mole, $\log A(\text{D}) = 8.6 \pm 1.0$ (s^{-1}). These results compare well with the values determined previously for **1** in a 1-pentanol glass:¹ $E_a(\text{H}) = 4.5 \pm 0.6$ kcal/mole, $\log A(\text{H}) = 4.5 \pm 1.0$ s^{-1} . Note that k_{H} is greater than k_{D} at temperatures less than -134 K while k_{H} is less than k_{D} at higher temperatures. This interesting result arises from a large difference in the frequency factors for this rearrangement: $A(\text{D})/3000 A(\text{H})$. To provide confirmation for this strange result, the decay rates of **1** and **1a** were also measured by infrared spectroscopy at a few temperatures and are also shown in Figure 1.

A possible explanation for these unusual kinetic results will be proposed.

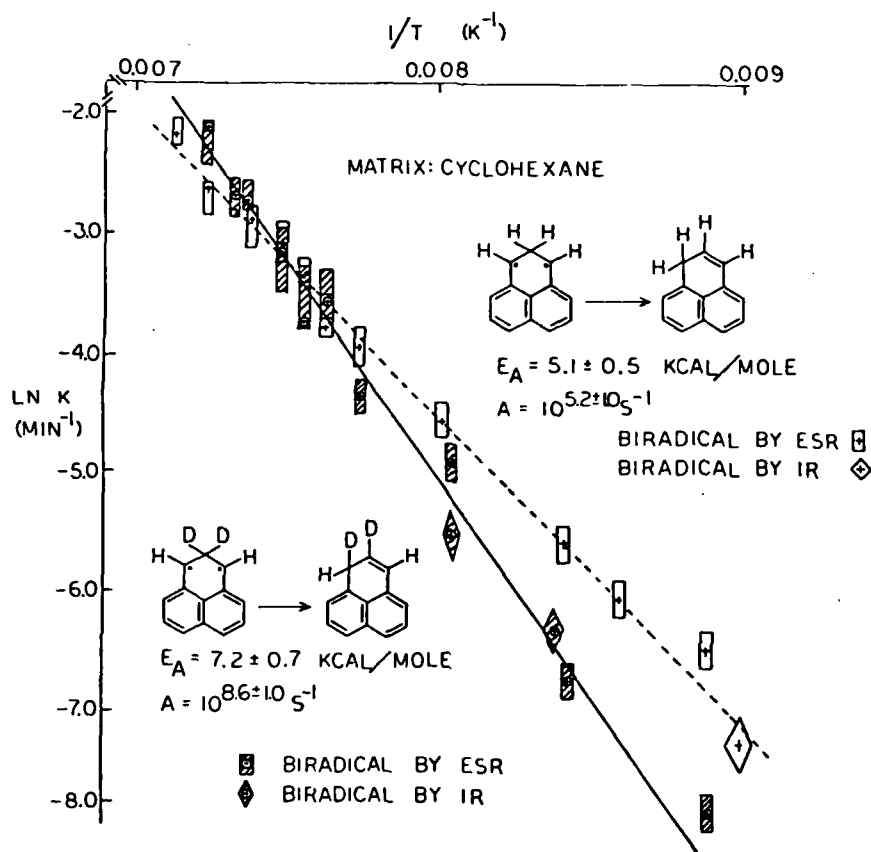


Figure 1. Arrhenius plot for the thermal isomerization of perinaphthadiyl.

References

1. J.-F. Muller, D. Muller, H.J. Dewey, and J. Michl, J. Am. Chem. Soc. **100**, 1629 (1978).
2. M. Gisin, E. Rommel, J. Wirz, M.N. Burnett, and R.M. Pagni, J. Am. Chem. Soc. **101**, 2216 (1979).

Acknowledgement

This work was supported by NSF grant CHE 78-27094, by a NIH National Research Service Award (1 F32 EY055113-01) to John H. Penn and by a NATO Scholarship to Detlef Döhnert.

ABSTRACT F-13

THE REACTION OF HOT H ATOMS WITH CO₂^{*}

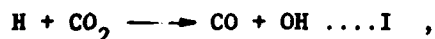
by

C. R. Quick, Jr. and J. J. Tiee

University of California
Los Alamos National Laboratory
P. O. Box 1663
Los Alamos, NM 87545

ABSTRACT

The uv photolysis of simple hydrogen bearing molecules such as HCl, HBr, HI, and H₂S produces H atoms that are translationally "hot" (up to a few eV excess kinetic energy) in comparison with their thermal environment.^{1,2} These hot atoms lose their excess energy in elastic and inelastic energy transfer collisions with surrounding molecules and/or are consumed by chemical reaction with a suitable molecular species. Recent investigations of the collision dynamics of hot H atoms have focused on the infrared emission produced by a translational to vibrational (T-V) energy transfer process^{3,4} between hot H atoms and simple target molecules such as HCl, HBr, CO₂, and N₂O. In this report, we are concerned with *reactive* collisions involving hot H atoms. In many cases, the energy of collision is sufficiently high so as to open up new reaction channels, which do not occur appreciably at room temperature. A case in point is the reaction



which is approximately 25 kcal/mol (1.08 eV) endothermic and occurs at such a slow rate at room temperature⁵ ($\sim 11 \text{ s}^{-1} \text{ torr}^{-1}$) as to become almost unobservable.

*Work performed under the auspices of the US DOE.

The experimental approach taken here consists of using laser-induced fluorescence detection of OH to monitor the reaction of simple oxygen bearing molecules with hot H atoms produced by excimer laser photolysis of hydrogen halides and H₂S. In initial experiments with HBr:CO₂ mixtures irradiated with an ArF laser at 193 nm (~2.6 eV H-atoms) we have detected fast production of OH radicals. The production of OH radicals in reaction I occurs within the first few collisions and is strongly affected by the presence of inert buffer gas, as expected for a hot atom reaction. Several aspects of hot atom reactions (such as reaction I) are currently under investigation and will be reported. Some of these aspects include: the internal energy distribution within the OH reaction product, the effect due to an increase (or decrease) in the initial collision energy, and reactions using deuterated atom sources.

References

1. C. Vermeil, Israel J. Chem. 8, 147 (1970).
2. G. A. Oldershaw in "Gas Kinetics and Energy Transfer," Vol. 2, pp. 96-122 (1977).
3. C. R. Quick, Jr., R. E. Weston, Jr. and G. W. Flynn, Chem. Phys. Lett. 83, 16 (1981).
4. F. Magnotta, D. J. Nesbitt and S. R. Leone, Chem. Phys. Lett. 83, 21 (1981).
5. D. C. Baulch, D. D. Drysdale, J. Duxbury, and S. Grant, in "Evaluated Kinetic Data for High Temperature Reactions," Vol. 3, pp. 251.

ABSTRACT F-14

QUENCHING OF $\text{CF}_2(^1\text{B}_1)$ AND $\text{CF}_2(^3\text{B}_1)$ EMISSION IN THE REACTION OF OZONE WITH TETRAFLUOROETHENE

S. TOBY, F. S. TOBY

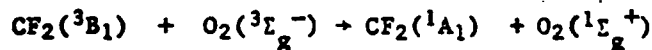
Department of Chemistry, Rutgers University, Box 939, Piscataway, NJ 08854

Singlet and Triplet CF_2 Emission

In 1975 Toby *et al* (1) observed a strong chemiluminescence in the gas-phase reaction between ozone and tetrafluoroethene at room temperature and assigned it to $\text{CF}_2(^1\text{B}_1 \rightarrow ^1\text{A}_1)$. A weaker emission in the visible region was also seen but was not identified. The kinetics of the $\text{O}_3 + \text{C}_2\text{F}_4$ reaction were studied (2) but no completely satisfactory explanation was given for the source of the large amount of energy required for emission at wavelengths as short as 245 nm.

The first direct evidence for the formation of triplet CF_2 was obtained by Koda (3) who reacted oxygen atoms with C_2F_4 and observed a UV band due to $\text{CF}_2(^1\text{B}_1 \rightarrow ^1\text{A}_1)$. He also obtained a visible emission (which had been seen by Toby *et al* (1) but not identified) and assigned it to the long-sought triplet $\text{CF}_2(^3\text{B}_1 \rightarrow ^1\text{A}_1)$. Koda estimated the triplet energy as 57 kcal mole⁻¹, considerably higher than the theoretical estimate of 47 kcal mole⁻¹ (4). And he postulated that the excited singlet arose from triplet-triplet annihilation: $2\text{CF}_2(^3\text{B}_1) \rightarrow \text{CF}_2(^1\text{B}_1) + \text{CF}_2(^1\text{A}_1)$ ($\Delta H^\circ = -7$ kcal mole⁻¹) which explained the source of the highly energetic singlet emission. In a subsequent paper Koda (5) investigated the quenching characteristics of $\text{CF}_2(^3\text{B}_1)$ and estimated the lifetime as ~ 1 sec.

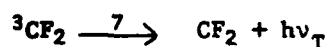
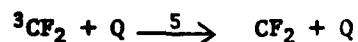
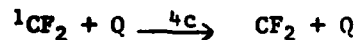
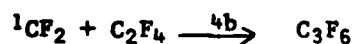
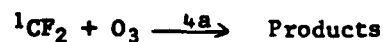
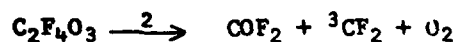
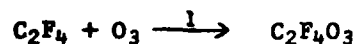
Additional evidence was obtained by both Koda (3) and Toby and Toby (6) in the presence of oxygen. In both cases singlet oxygen emission was seen, presumably from the reaction



which is spin-allowed and 20 kcal/mole exothermic.

Quenching of Singlet and Triplet CF₂

We have carried out experiments in which O₃ was reacted with C₂F₄ in the presence of a quenching gas Q to determine the reactivity of excited singlet difluoromethylene (¹CF₂) and triplet difluoromethylene (³CF₂) with respect to the quencher. The mechanism may be written:



Assuming steady states in the concentrations of C₂F₄O₃, ³CF₂ and ¹CF₂ yields

$$I_S = \frac{k_3 k_6}{k_4 [X] + k_6} \left[\frac{A - k_5 [Q] - k_7}{4k_3} \right]^2$$

and

$$I_T = k_7 (A - k_5 [Q] - k_7) / 4k_3$$

where I_S and I_T are the singlet and triplet emission intensities,

$$A = [(k_5 [Q] + k_7)^2 + 8k_1 k_3 [\text{C}_2\text{F}_4] [\text{O}_3]]^{1/2}, \text{ and } k_4 [X] = k_{4a} [\text{O}_3] + k_{4b} [\text{C}_2\text{F}_4] + k_{4c} [\text{Q}].$$

These expressions may be simplified, depending on the experimental conditions and tested by plotting $1/I_S$ and $1/I_T$ versus the pressure of the quencher. Examples of such quenching plots are shown and the results will be discussed for several different quenchers.

References

- 1) Sheinson, R., Toby, F.S., Toby, S. 1975, J. Am. Chem. Soc., 97, 6593.
- 2) Toby, F.S., Toby, S. 1976, J. Phys. Chem., 80, 2313.
- 3) Koda, S. 1978, Chem. Phys. Lett., 55, 353.
- 4) Staemmler, V. 1974, Theoret. Chim. Acta, 35, 309.
- 5) Koda, S. 1979, J. Phys. Chem., 83, 2065.
- 6) Toby, S., Toby, F.S. 1980, J. Phys. Chem., 84, 206.

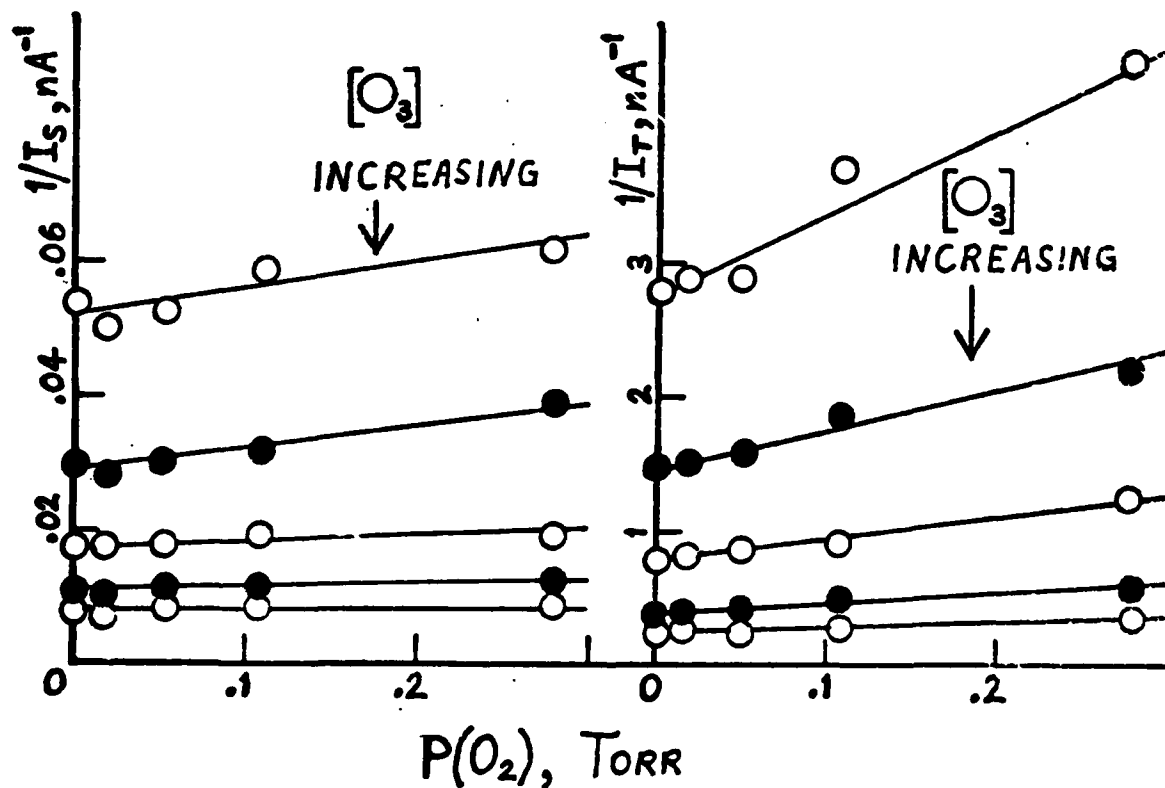


Figure 1. Plots of reciprocal singlet and reciprocal triplet emission versus pressure of added oxygen at 24°C.

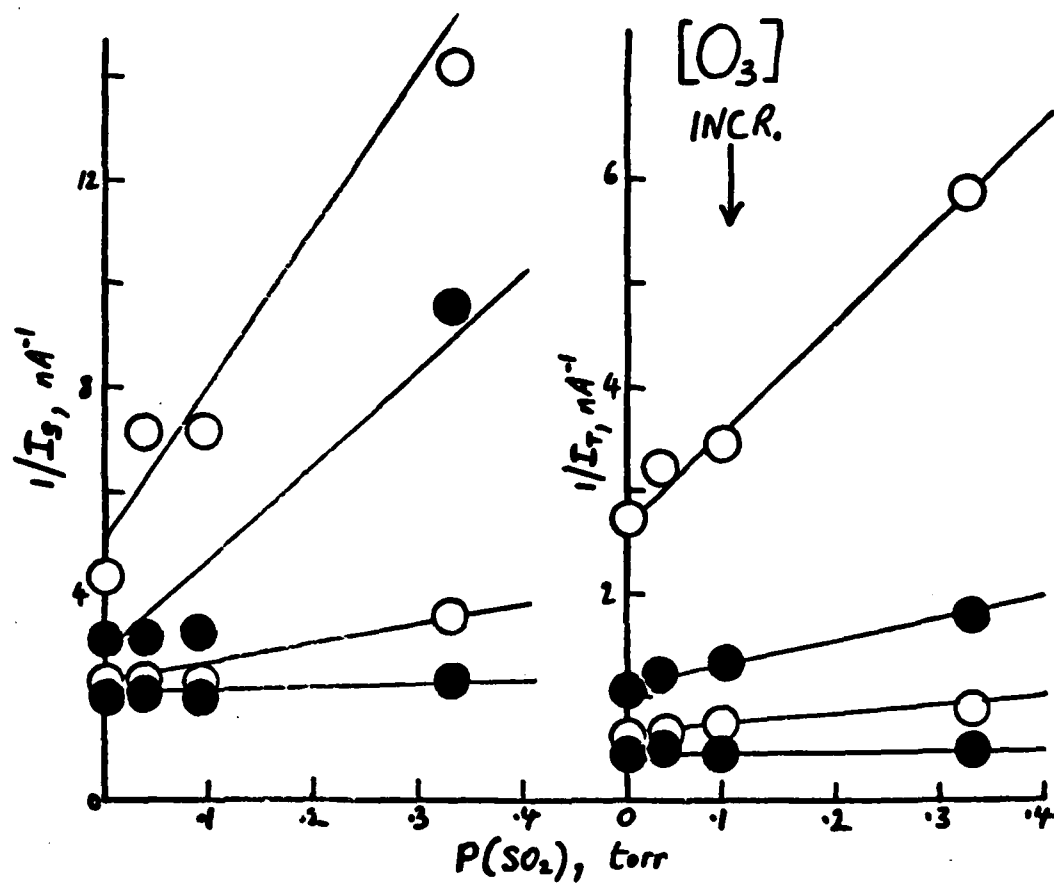


Figure 2. Plots of reciprocal singlet and reciprocal triplet emission versus pressure of added sulfur dioxide at 20°C:

ABSTRACT F-15

THE REACTION OF METHYL RADICALS WITH OXYGEN AT LOW PRESSURES

K. D. Bayes and E. A. Schultz, Dept of Chemistry & Biochemistry,
University of California, Los Angeles, CA 90024

and

M. J. Pilling, M. Macpherson and M. Smith, Physical Chemistry
Laboratory, Oxford University, Oxford OX1 3QZ, U. K.

The rates of reaction of methyl radicals with molecular oxygen have been measured for a variety of pressures and third bodies. The observed pressure dependence of the rate constant is not consistent with a simple three body recombination in its low pressure limit. A mechanism is proposed that can explain the observed behavior and the findings of others [1-3].

The methyl radicals were formed in low concentrations ($\sim 10^{11}$ molec/cm³) by photolyzing nitromethane with a defocused ArF laser at 193 nm. The methyl radical concentration was followed as a function of time with a photoionization mass spectrometer. A krypton resonance lamp was used as the ionizing radiation.

In the absence of oxygen, the methyl radicals decayed with rates of about 15 s^{-1} . Most of this decay rate was due to loss by pumping out of the cell. When molecular oxygen was added, the decay rates increased. Using the measured decay rates with the known partial pressures of oxygen gave the desired rate constants. Small corrections were necessary to account for the differing third body efficiencies between oxygen and the inert bath gases, helium, argon and nitrogen. These corrections were done using the data with nitrogen as the bath gas and assuming that oxygen and nitrogen had the same third body efficiency.

The new measurements using helium as the bath gas are in reasonable agreement with the values reported by Washida and Bayes [1]. Since these new measurements are more direct and avoid the complications in the oxygen atom-ethylene system [4-6], they should be more reliable. This general agreement between old and new measurements supports the rate constant for the reaction of oxygen atoms with methyl radicals reported in reference 1.

Similar measurements using argon as the bath gas show a strong curvature in the plot of k vs. pressure, as can be seen in Figure 1. As the total pressure approaches zero, the rate constant also approaches zero. Such low pressure curvature is not expected for a simple three body recombination well below its high pressure limit [7,8]. A similar effect is probably present in the helium data, but it is less prominent. Measurements in nitrogen show a pressure dependence similar to that observed in argon.

We propose a mechanism to explain this behavior based on two parallel three body recombinations. At higher pressures the normal three body recombination along the ground state ($^3A'$) surface results in the formation of methylperoxy radicals. This process reaches its high pressure limit only at pressures above one atmosphere. At low pressures a second reaction channel becomes evident. This involves a collision along the quartet surface ($^4A'$), followed by a spin-forbidden collision-induced cross over to the electronically excited $^2A'$ state of the

methylperoxy radical. Since the $^2A'$ state can only dissociate by a spin-forbidden process, its lifetime is long enough for it to be collisionally stabilized at total pressures of a few torr. This mechanism is compatible with the present findings and with those of previous workers.

This work has been supported by a grant from the National Science Foundation and by a NATO Travel Grant.

- [1] N. Washida and K. D. Bayes, *Int. J. Chem. Kinet.* **8**, 777 (1976).
- [2] A. C. Baldwin and D. M. Golden, *Chem. Phys. Lett.* **55**, 350 (1978).
- [3] O. Klais, P. C. Anderson, A. H. Laufer and M. J. Kurylo, *Chem. Phys. Lett.* **66**, 598 (1979).
- [4] A. Luntz and K. Kleihermans, *J. Phys. Chem.* **85**, 1966 (1981).
- [5] H. E. Hunziker, H. Kueppe and H. R. Wendt, *J. Photochem.* **17**, 377 (1981).
- [6] G. Inoue and H. Akimoto, *J. Chem. Phys.* **74**, 425 (1981).
- [7] N. Basco, D. G. L. James and F. C. James, *Int. J. Chem. Kinetics* **4**, 129 (1972).
- [8] A. H. Laufer and A. M. Bass, *Int. J. Chem. Kinetics*, **7**, 639 (1975).

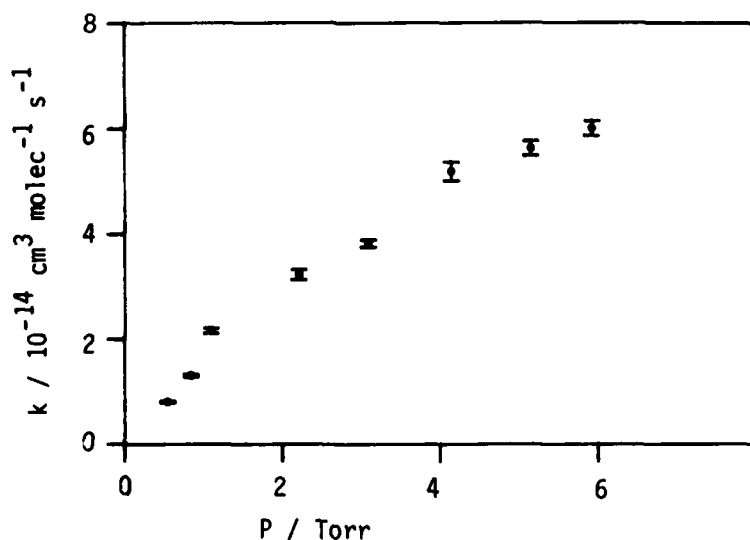


Figure 1. The apparent rate constants for the reaction of methyl radicals with oxygen in argon at room temperature. The error bars give one standard deviation.

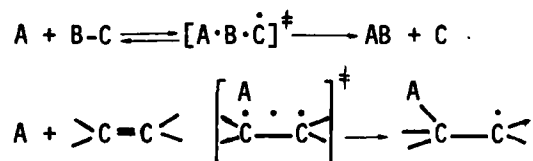
ABSTRACT -1

"THE TRANSITION STATE MODEL FOR BIMOLECULAR REACTIONS. LOOSE AND TIGHT COMPLEXES."

by

SIDNEY W. BENSON
Professor of Chemistry and
Scientific Co-Director
Hydrocarbon Research Institute
University of Southern California
Los Angeles, California 90007

Typical radical-molecule reactions, either for metathesis or for association (addition to pi bonds) have predominantly fallen into the classification of tight transition-state pathways.



Both reaction types proceed through 3-center, 3-electron complexes in which bond distances and frequencies are very close to those for regular molecules. This has been true for those cases in which intrinsic activation energies E_{int} are above 1.5-2.0 kcal/mole. There are now a number of cases in which E_{int} is essentially zero and we find characteristics of the loose transition state.

Until recently loose transition states were reserved to describe radical recombinations and followed the Gorin model, or the "restricted free rotor" variant of the Gorin model. Here the rate determining

interaction occurs at a distance about 3 times the final bond length where the radical-radical coupling is of the order of RT and angular orientation seemed to be constrained only by non-bonded van der Waals' repulsion. It now appears that radical disproportionation, a metathesis with zero activation energy fits an intermediate description, one in which bond distances are like those in normal metathesis but the bending force constants are essentially zero, bending being constrained as in the Gorin model only by non-bonded repulsions.*

We shall review some recent calculations and data in each of these categories.

*P. Hadju, M. Vaisman and S. W. Benson, unpublished work

ABSTRACT G-2

Rates and Product Channels of the Reactions of

HO_2 with O- and H-Atoms at 298 K

U. C. Sridharan, L. X. Qiu, and F. Kaufman
Department of Chemistry, University of Pittsburgh,
Pittsburgh, PA 15260

In spite of much experimental work over the past 20 years, major uncertainties persist, regarding the rate constants of the two title reactions, $\text{O} + \text{HO}_2 \xrightarrow{1} \text{OH} + \text{O}_2$ and $\text{H} + \text{HO}_2 \xrightarrow{2a, 2b, 2c} \text{OH} + \text{OH}, \text{H}_2\text{O} + \text{O}, \text{H}_2 + \text{O}_2$, and, especially, the relative importance of the three product channels of reaction (2). Because of the difficulty of bringing together known, initial concentrations of two reactive species and of measuring their rate of reaction, much of the published work has been indirect and has had to rely on modeling of complicated reaction systems. Whereas published rate data on reaction (1) are of recent vintage¹⁻⁴ and are in moderate agreement, $k_1 = 3.1$ to $7.0 \times 10^{-11} \text{ cm}^3 \text{ s}^{-1}$, those on reaction (2)⁵⁻¹² cover a wider range, $k_2 \sim 3$ to 12×10^{-11} , and differ drastically in their estimates of the relative importance of the three product channels, e.g. $k_{2c}/k_2 \sim 0.17$ to 0.62 and $k_{2b}/k_2 \sim 0.02$ to 0.52 . The reactions are of great interest both as important steps in atmospheric ozone photochemistry and as examples of elementary atom-radical reactions whose detailed dynamics are poorly understood.

The discharge-flow apparatus used in this study was described earlier.¹³ Its flow tube (110 cm long, 2.54 cm i.d.) is fitted with a movable, coaxial double injector tube. At its downstream end, back-to-back laser-induced fluorescence and vacuum u.v. resonance fluorescence detection ports, 6 cm apart, allow sensitive atom and radical concentration measurements, i.e. $[\text{OH}]$ at $\sim 10^8 \text{ cm}^{-3}$, $[\text{O}]$ and $[\text{H}]$ at $\sim 10^9 \text{ cm}^{-3}$, and $[\text{HO}_2]$ by conversion to $[\text{OH}]$ with excess NO. All flow tube surfaces were coated with Teflon or fluorocarbon wax to inhibit surface recombination, i.e. k_w of O, H, and HO_2 was 2 to 4 s^{-1} and k_w of OH was 8 s^{-1} .

HO_2 was generated within the double injector by the reaction $\text{F} + \text{H}_2\text{O}_2 \rightarrow \text{HF} + \text{HO}_2$ as described earlier.¹³ O- or H-atoms were generated by microwave discharges of traces of O_2 or H_2 in He, the carrier gas used in all experiments. Typical total pressure of ~ 3 torr, average flow velocities of $\sim 1200 \text{ cm s}^{-1}$, $[\text{HO}_2]$ of $\sim (2 \text{ to } 19) \times 10^{11} \text{ cm}^{-3}$, and initial $[\text{H}]$ or $[\text{O}]$ of $(4 \text{ to } 5) \times 10^{10} \text{ cm}^{-3}$ were used in kinetic experiments, i.e. $[\text{HO}_2]$ was in 5 to 40 fold excess over

[H] or [O] whose pseudo-first-order decays were monitored as function of the HO₂ injector position. These decay constants were plotted vs. [HO₂] and least squares fitted to provide the desired second-order rate constants, k_1 and k_2 . Small corrections were applied for axial diffusion, $k_w^{HO_2}$, and for the injector surface effect in the pseudo-first-order decay plots and for k_w^{OH} , the OH + OH and OH + NO reactions after the HO₂ to OH conversion by excess NO 5 cm upstream of the LIF port.

Five sets of experiments for O + HO₂, consisting of 26 [O] decays at different [HO₂], gave $k_1 = (5.4 \pm 0.3) \times 10^{-11} \text{ cm}^3 \text{ s}^{-1}$, and six sets of experiments for H + HO₂, consisting of 33 [H] decays gave $k_2 = (7.4 \pm 0.3) \times 10^{-11} \text{ cm}^3 \text{ s}^{-1}$, where the uncertainty limits represent a single standard deviation of the mean. Including reasonable estimates of other experimental uncertainties, $k_1 = (5.4 \pm 0.9) \times 10^{-11}$ and $k_2 = (7.4 \pm 1.2) \times 10^{-11} \text{ cm}^3 \text{ s}^{-1}$.

For reaction (1), there is only a single product channel. This was confirmed experimentally by analysis of the rise and decay of product [OH] with increasing injector distance. For (2), the product channel distribution was measured in separate experiments by adding small, measured [HO₂] of (1 to 6) $\times 10^{11} \text{ cm}^{-3}$ to a large excess [H] of $\sim 5 \times 10^{13} \text{ cm}^{-3}$ and measuring the products OH and O. The HO₂ injector was placed 5 cm upstream of the LIF port in order to minimize correction factors for post-conversion reactions such as OH + O \rightarrow O₂ + H.

The OH yield of reaction (2) was measured in 34 experiments, and, in 28 of these, the O-atom yield was measured simultaneously. The fractional yield of OH of channel (2a) was found to be surprisingly large, 0.87 ± 0.04 , and that of (2b) was small, 0.04 ± 0.015 . The "dark" channel (2c), could only be estimated by difference, 0.09 ± 0.04 , since neither H₂ nor O₂ can be monitored in our experiments. All product yields were corrected for surface and gas phase reactions, and calibrated absolutely by H + NO₂ (for OH) and N + NO titrations (for O). The corresponding rate constants, k_{2a} , k_{2b} , and k_{2c} are therefore 6.4, 0.3, and $0.7 \times 10^{-11} \text{ cm}^3 \text{ s}^{-1}$, respectively, at 298 K.

Our value for k_1 , $(5.4 \pm 0.9) \times 10^{-11} \text{ cm}^3 \text{ s}^{-1}$, is in good agreement with a recent measurement by Keyser,⁴ $(6.1 \pm 0.6) \times 10^{-11}$, who used similar techniques, and with Lii, et al.,³ $(7 \pm 2) \times 10^{-11}$, who calculated best-fit values of k_1 in a ten-step model of the decay of [HO₂] following pulse radiolysis at 1.6 atm total pressure. It is in poorer agreement with results of Burrows, et al.,¹ $(3.1 \pm 1.0) \times 10^{-11}$, and Hack, et al.,² $(3.3 \pm 1.0) \times 10^{-11}$, that are based on erroneous values of other rate constants, particularly that for OH + H₂O₂. For k_2 , $(7.4 \pm 1.2) \times 10^{-11} \text{ cm}^3 \text{ s}^{-1}$, three recent studies have reported (6.0 ± 1.7) ,¹⁰

(4.6 ± 1.0) ,¹¹ and $(5.0 \pm 1.3) \times 10^{-11}$,¹² but they are based mainly on steady-state $[\text{HO}_2]$ measurements and are thus dependent on other rate data. They also suffer from large, irreproducible surface effects.

Only one recent study¹⁰ has reported branching ratios for (2a), (2b), and (2c), i.e. 0.69, 0.02, and 0.29. These are in fair agreement with our results except for the factor of three overestimate of the "dark" channel ratio. Earlier, much less direct measurements have ranged far and wide, as indicated above. Thus, Dodonov, et al.⁶ reported only 0.05 for the (2a) ratio for which we find 0.87, and they ascribed 0.52 to (2b) for which we report 0.04. Westenberg and deHaas⁷ reported 0.27 for (2a), 0.11 for (2b), and 0.62 for (2c) compared to our 0.87, 0.04, and 0.09.

Reaction (1) is a major link in the HO_x catalyzed destruction of O_3 in the upper stratosphere and mesosphere. Reaction (2c) is an important HO_x radical sink in the mesosphere. Its smaller rate constant, reported here, seems to be consistent with mesospheric O_3 modeling calculations.¹⁴ A thorough, theoretical interpretation of the rates of these and other HO_2 radical-radical reactions must await studies of their temperature dependences. For $\text{O} + \text{HO}_2$, Keyser⁴ has reported a weak, negative dependence, $\exp(200/T)$ which suggests the formation of a bound intermediate. The large value of k_2 and the strong dominance of the $\text{OH} + \text{OH}$ product channel suggest the formation of a bound, energetic $\text{H}_2\text{O}_2^\ddagger$ intermediate. Whether $\text{H}_2 + \text{O}_2$ originate by H_2 elimination from this $\text{H}_2\text{O}_2^\ddagger$ or by simple H-abstraction is an interesting subject for ab initio quantum theoretical calculations.

ACKNOWLEDGMENT. This work was supported by NASA under Grant NGR 39 011 161.

REFERENCES

1. J. P. Burrows, G. W. Harris, and B. A. Thrush, *Nature*, **267**, 233 (1977).
J. P. Burrows, D. I. Cliff, G. W. Harris, B. A. Thrush, and J. P. T. Wilkinson, *Proc. Roy. Soc.*, **A368**, 463 (1979).
2. W. Hack, A. W. Preuss, F. Temps, and H. Gg. Wagner, *Ber. Bunsenges. Phys. Chem.*, **83**, 1275 (1979).
3. R.-R. Lii, M. C. Sauer, Jr., and S. Gordon, *J. Phys. Chem.*, **84**, 817 (1980).
4. L. F. Keyser, *J. Phys. Chem.*, in press.
5. M. A. A. Clyne and B. A. Thrush, *Proc. Roy. Soc.*, **A275**, 559 (1963).
6. A. F. Dodonov, G. K. Lavrovskaya, and V. L. Tal'roze, *Kinetika i Kataliz*, **10**, 701 (1969).
7. A. A. Westenberg and N. deHaas, *J. Phys. Chem.*, **76**, 1586 (1972).

8. D. L. Baulch, D. D. Drysdale, D. G. Horne, and A. C. Lloyd, *Evaluated Kinetic Data for High Temperature Reactions*, Vol. 1, Butterworths, London (1972).
9. F. Kaufman, in *Atmospheres of Earth and the Planets*, B. M. McCormac (ed.), Reidel Publishing Company, Dordrecht-Holland, 1975, p. 219.
10. W. Hack, H. Gg. Wagner, and K. Hoyer mann, *Ber. Bunsenges. Phys. Chem.*, 82, 713 (1978).
11. W. Hack, A. W. Preuss, H. Gg. Wagner, and K. Hoyer mann, *Ber. Bunsenges. Phys. Chem.*, 83, 212 (1979).
12. B. A. Thrush and J. P. T. Wilkinson, *Chem. Phys. Letts.*, 84, 17 (1981).
13. U. C. Sridharan, L. X. Qiu, and F. Kaufman, *J. Phys. Chem.*, 85, 3361 (1981).
14. M. Allen, Y. L. Yung, and J. W. Waters, *J. Geophys. Res.*, 86, 3617 (1981).

ABSTRACT G-3

CO₂ LASER PHOTOLYSIS OF C₆F₅X COMPOUNDS - A USEFUL SOURCE OF FREE RADICALS FOR CHEMICAL KINETIC STUDIES

Irene R. Slagle and David Gutman

Department of Chemistry
Illinois Institute of Technology
Chicago, Illinois 60616

We are currently using compounds containing the hexafluorophenyl group (C₆F₅-) to produce polyatomic free radicals under conditions which are suitable for quantitative studies of their reactions. Reactions have been studied either under pseudo first-order conditions or under second-order conditions, the latter being possible due to the ability to directly determine the initial free-radical concentrations following the photolysis process. Details of the use of these free-radical precursors and of the chemical kinetic studies which have been performed to date will be presented.

C₆F₅X Compounds

Compounds containing the aromatic C₆F₅ group all absorb radiation near 10 μ due to an in-plane ring deformation vibrational mode (ν_{13} in C₆F₆).¹ The spectrum of the "parent compound", C₆F₆, is shown in Figure I. Due to the presence of a large number of heavy atoms, these molecules have a high density of vibrational states even under ambient conditions. The large absorption coefficient at laser wavelengths and virtual continuum of available vibrational states ($>200/\text{cm}^{-1}$) assures efficient up-pumping even at modest laser fluences.^{2,3}

In Figure II the density of states of C₆F₆ is compared to those of C₃H₅Br and SF₆ at ambient temperature and after the absorption of from 1-3 photons of radiation at 1000 cm^{-1} . SF₆ is another molecule which dissociates to a significant extent at mild fluences and its density of vibrational states at 300K is only 0.01/ cm^{-1} .

In our experiments light from a Lumonics 103-2 CO₂ TEA laser is mildly concentrated with a 5m focal length concave mirror. The long beam waist is concentric with and located along the axis of a 35 cm-long, 0.95 cm I.D. tubular Pyrex reactor. Gas flowing through the reactor is irradiated with almost uniform intensity along the reactor's length at a repetition rate of 0.5 Hz. Laser fluences up to 3.5 J/cm² are used.⁴

Direct photolysis yields are 5-15% decomposition/pulse at the highest fluences. Surprisingly, the extent of decomposition is not a strong function of the bond strength of the bond which is broken in the C_6F_5X compound. Typical photolyses which have produced free radicals for kinetic studies are listed below:

REACTION	ΔH (Kcal/mole)
$C_6F_5C_2H_5 \xrightarrow{h\nu} C_6F_5 + C_2H_5$	~ 113
$C_6F_5OCH_3 \xrightarrow{h\nu} C_6F_5O + CH_3$	~ 67
$C_6F_5Cl \xrightarrow{h\nu} C_6F_5 + Cl$	92

The first reaction is typical of those used to produce free radicals by C-C bond cleavage at the ring. The second reaction, which involves the formation of a phenoxy radical, provides a lower energy route for producing polyatomic free radicals, and the final reaction has been used as a source of chlorine atoms for producing polyatomic free radicals via rapid secondary reactions. The radicals C_2H_5 , CH_3CO , and $C_6H_5CH_2$ have been produced by the Cl-atom reactions with C_2H_6 , CH_3CHO , and $C_6H_5CH_3$ respectively. The free radicals, whether produced directly or indirectly, are all generated homogeneously in the tubular reactor.

Kinetics of Polyatomic Free Radicals

The chemical kinetics following laser photolysis is monitored in real time using photoionization mass spectrometry (PIMS). Gas is continuously sampled from a 0.044 cm-diameter hole in the side of the reactor. The emerging gas is formed into a beam by a conical skimmer as it enters the vacuum chamber containing the PIMS. As the gas traverses the ion source, a portion is photoionized and mass selected by a quadrupole mass filter. In separate experiments, temporal ion signal profiles of reactants and possible products are recorded with a multichannel scalar from a period just before each laser pulse to about 50 msec following the pulse.⁵

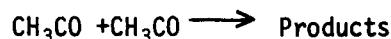
Reactions First-Order in Radical Concentration

Several reactions of polyatomic free radicals with NO_2 have been studied in detail at ambient temperature under pseudo first-order conditions. These studies have yielded not only the rate constants but also the mechanisms of the reactions studied. All have been found to proceed by O-atom transfer from NO_2 to the organic radical. The reactions are rapid and proceed with essentially no activation energy. The rate constants measured at $300 \pm 2K$ are listed below.

<u>REACTION</u>	<u>k (cm³ molecule⁻¹ sec⁻¹)</u>
$\text{CH}_3 + \text{NO}_2 \rightarrow \text{CH}_3\text{O} + \text{NO}$	2.5×10^{-11}
$\text{C}_3\text{H}_5 + \text{NO}_2 \rightarrow \text{C}_3\text{H}_5\text{O} + \text{NO}$	3.9×10^{-11}
$\text{C}_2\text{H}_5 + \text{NO}_2 \rightarrow \text{C}_2\text{H}_5\text{O} + \text{NO}$	4.2×10^{-11}
$\text{CF}_2\text{Cl} + \text{NO}_2 \rightarrow \text{CF}_2\text{ClO} + \text{NO}$	9.6×10^{-12}
$\text{CH}_3\text{CO} + \text{NO}_2 \rightarrow \text{CH}_3\text{CO} + \text{NO}$	2.5×10^{-11}

Reactions Second-Order in Radical Concentration

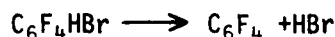
Due to the significant decomposition of the free radical precursors during each laser pulse and the ability to directly monitor the loss of precursor concentration following photolysis, it is possible to directly measure the initial free-radical concentrations after photolysis. This knowledge makes it possible to quantitatively study second-order processes, particularly recombination reactions. We have now studied the reaction,



and have measured the rate constant at 300K which is 4.2×10^{-11} cm molecule⁻¹sec⁻¹. The potential of the procedure to study free radical recombination reactions will be discussed as well as complications which arise caused by secondary photolysis processes.

Production of Unusual Intermediates

Other six-membered ring compounds containing a large number of fluorine atoms also absorb radiation in the 9-11 μ spectral region. Interesting intermediates can be produced by their photolyses. For example, we have attempted to produce tetrafluorobenzene from the photolysis of C₆F₄HBr:

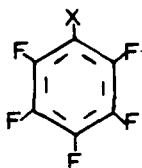


Details of these experiments will also be presented.

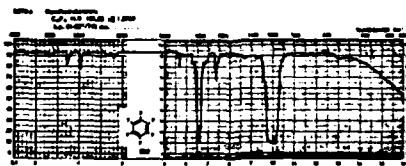
1. G. Herzberg, "Molecular Spectra and Molecular Structure II. Infrared and Raman Spectra of Polyatomic Molecules", D. van Nostrand, New York, 1945, p. 118.
2. D.M. Golden, M.J. Rossi, A.C. Baldwin, and J.R. Barker, Acc. Chem. Res. 1981, 14, 56-62.
3. Aa. Sudbø, P.A. Schulz, E.R. Grant, Y.R. Shen, and Y.T. Lee, J. Chem. Phys. 1979, 70, 912-929.
4. I.R. Slagle, F. Yamada, and D. Gutman, J. Am. Chem. Soc. 1981, 103, 149-153.

FIGURE I

COMPOUNDS CONTAINING C₆F₅ GROUP AS
FREE RADICAL SOURCES I



9-11 μ strong absorption
In-plane ring deformation
[E_{1g} (ν_{13}) in C₆F₆]



C₆F₆
Absorption
Spectrum

FIGURE II

DENSITY OF VIBRATIONAL STATES AT AMBIENT TEMPERATURE
AND AFTER ABSORPTION OF 1-5 1000 cm⁻¹ PHOTONS

	<u>CH₂CHCH₂Br</u>	<u>SF₆</u>	<u>C₆F₆</u>
VIBRATIONAL ENERGY (300K)	700 cm ⁻¹	800 cm ⁻¹	1720 cm ⁻¹

DENSITY OF VIB.
STATES (No./cm⁻¹)

1. 300K	0.05	0.01	2.5x10 ²
2. +1000 cm ⁻¹	0.45	1.6	1.0x10 ⁴
3. +2000 cm ⁻¹	8.1	18.	2.2x10 ⁵
4. +5000 cm ⁻¹	9.2x10 ²	3.7x10 ³	2.9x10 ⁸

Calculated by K. Christoffel, IIT

ABSTRACT G-4

A LASER-PHOTOLYSIS/RESONANCE FLUORESCENCE STUDY OF THE RATE OF THE REACTIONS OF OH WITH HNO_3 , PH_3 , $\text{C}_2\text{H}_4\text{O}$, C_6H_6 and NAPHTHALENE *)

K. Lorenz and R. Zellner

Institut für Physikalische Chemie, Universität Göttingen
3400 Göttingen, F.R.G.

As part of an extended series of kinetic investigations of reactions of OH with natural and anthropogenic atmospheric trace constituents we have recently studied the title reactions using a newly designed laser photolysis/resonance fluorescence (LPRF) system (Fig. 1).

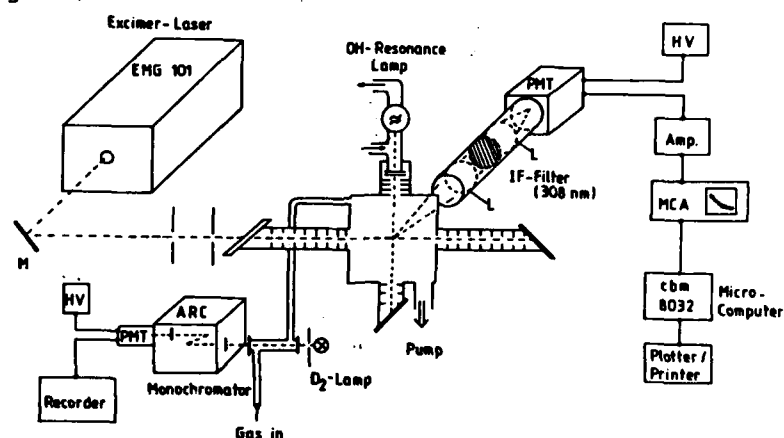
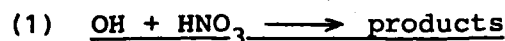


Fig. 1: Laser flash photolysis/resonance fluorescence (LPRF) experiment

An excimer laser is used as a monochromatic photolysis light source. Due to the availability of various UV laser lines, the photolytic precursor of OH (HNO_3 , HNO_2 , H_2O_2 , $\text{O}_3/\text{H}_2\text{O}$) can be chosen as to avoid as much as possible unwanted photolysis or photoexcitation of the reagent. For most of the experiments described below HNO_3 has been used as OH precursor at wavelength 193 nm (ArF) and 248 nm (KrF). In the latter case an absorption cross section of $2 \times 10^{-20} \text{ cm}^2$ is sufficient for the generation of OH with a typical laser energy of 50 - 100 mJ/puls and without submitting undue high concentrations of the precursor ($\text{PHNO}_3 \leq 100 \text{ mTorr}$). The detection of OH is by time resolved resonance fluorescence in the $A^2\Sigma^+ - X^2\Pi - (0,0)$ band, using a conventional microwave discharge source and photoelectric detection coupled to signal averaging equipment.

*) submitted to: XV Inf. Conference on Photochemistry, Stanford, USA, 1982.

*) work supported by BMFT and "Umweltbundesamt".



This reaction has been studied in the range $T = 250 - 435$ K and over a tenfold variation of HNO₃ concentration (determined by in-situ absorption measurements). The result

$$k_1 = (1.5 \pm 0.4) 10^{-14} \exp(622/T) \text{ cm}^3/\text{molecule s}$$

is in good agreement with the larger rate constant at 298K and the negative dependence recently reported by Wine et al. [1]. In an attempt to further identify the cause of this unusual T-dependence, we have also carried out measurements at higher pressures (using a resonance absorption arrangement). It is found that over the pressure range 10 Torr - 1 atm at 298 K k_1 increases by about a factor of 2, indicating that reaction (1) is probably not a direct H-atom abstraction reaction, but presumably occurs via intermediate complex formation. Confirmatory studies of the p dependence at lower temperatures should be very useful.



The rate constant for this reaction, which to our knowledge has never been measured before, is found to show little dependence on temperature. Over the range 248 - 438 K we deduce

$$k_2 = (2.7 \pm 0.6) 10^{-11} \exp(-155/T) \text{ cm}^3/\text{molecule s}$$

which corresponds to $1.6 \times 10^{-11} \text{ cm}^3/\text{molecule s}$ at 298 K. The magnitude of the rate constant as well as thermochemistry suggest that the reaction proceeds by H atom abstraction. The low activation energy then is qualitatively consistent with a $(35 \pm 2) \text{ kcal/mol}$ exothermicity for this process.



This reaction has been studied at total pressures between 10 - 20 Torr (Ar) and over the temperature region 297 - 435 K. k_3 is found to be

$$k_3 = (1.1 \pm 0.4) 10^{-11} \exp(-1460/T) \text{ cm}^3/\text{molecule s}$$

corresponding to $(8.0 \pm 1.6) 10^{-14} \text{ cm}^3/\text{molecule s}$ at 298 K. Hence the rate coefficient for this reaction is - as expected - considerably lower than the one for OH with ethylene or with larger epoxides [2]. Although an investigation of the primary products of this reaction has not yet been performed, one may expect H-atom abstraction to dominate. Unfortunately, there appears to be no value available in the literature for the heat of formation of the cyclic C₂H₃O radical and hence the C-H bond strength in ethylene oxide. The relatively low activation energy, however, suggests that simultaneous isomerization of cyclic C₂H₃O to linear vinyl-oxi (CH₂CHO) may occur, prompted by the high ring strain energy of C₂H₄O (27 kcal/mol). This is supported by a recent

study of the $F + C_2H_4O$ reaction, where CH_2CHO in high yield in detected by laser induced fluorescence [3]. Experiments to directly identify the products of reaction (3) are in progress in this laboratory.

(4) $OH + C_6H_6 \longrightarrow$ products

The reaction between OH and benzene has been studied between 245 - 520 K and at pressures ranging from 2 - 100 Torr of Ar (at 298 K). k_4 is found to strongly increase with pressure up to 25 Torr ($k_4 = 0.5 \times 10^{-12}$, 0.85×10^{-12} and $(1.1 \pm 0.1) \times 10^{-12}$ $cm^3/molecule\ s$ at 2, 10 and 25 Torr of Ar), but to be essentially pressure independent at still higher pressures. This is in good agreement with previous observations [4,5]. The temperature variation of k_4 was studied at $p > 30$ Torr (Ar) and is found to show the general trend of a complex T dependence resulting from the transition from OH-addition to equilibration of the addition channel to H-atom abstraction [4,5]. Slight differences compared to previous investigations are, however, noted, which we attribute to the generally shorter time scale of our experiment.

(5) $OH +$ naphthalene \longrightarrow products

This reaction has been studied between 337 and 525 K. Over this range the rate coefficient is decreasing from $(2.5 \pm 0.7) \times 10^{-11}$ $cm^3/molecule\ s$ at 337 K to $(2.6 \pm 0.8) \times 10^{-12}$ $cm^3/molecule\ s$ at 525 K. The decrease of k with temperature, however, is relatively weak up to 470 K and stronger at still higher temperatures. It is concluded from this observation that we are observing a transition from an OH addition process (having a negative T dependence and absolute rate constants more than an order of magnitude larger than OH + benzene) to a temperature region where the addition reaction is equilibrating. Unfortunately, we have not yet been able to observe the onset of an abstraction reaction. Studies at still higher temperature are presently carried out.

1. P.H. Wine, A.R. Ravishankara, N.M. Kreutter, R.C. Shah, J.M. Nicovich, R.L. Thompson, D.J. Wuebbles, J. Geophys. Res 86, 1105 (1981).
2. R. Atkinson, K.R. Damall, A.C. Lloyd, A.M. Winer, J.N. Pitts, Jr., Adv. Photochemistry 11, 375 (1979).
3. G. Inoue, H. Akimoto, J. Chem. Phys. 74, 425 (1981).
4. R.A. Perry, R. Atkinson, J.N. Pitts, J. Phys. Chem. 81, 296 (1977), 81, 1607 (1977).
5. F.P. Tully, A.R. Ravishankara, R.L. Thompson, J.M. Nicovich, R.C. Shah, N.M. Kreutter, P.H. Wine, J. Phys. Chem. 85, (1981)

ABSTRACT G-5

VINYLDENE RADICALS: LONG MAY THEY LIVE

A. H. Laufer

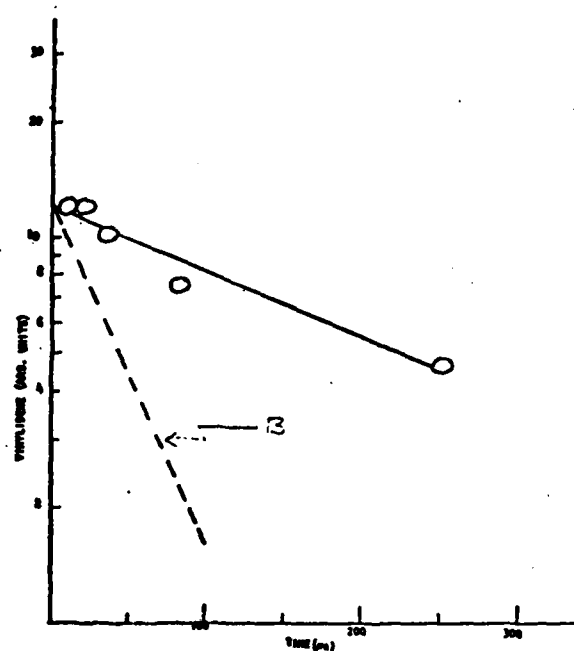
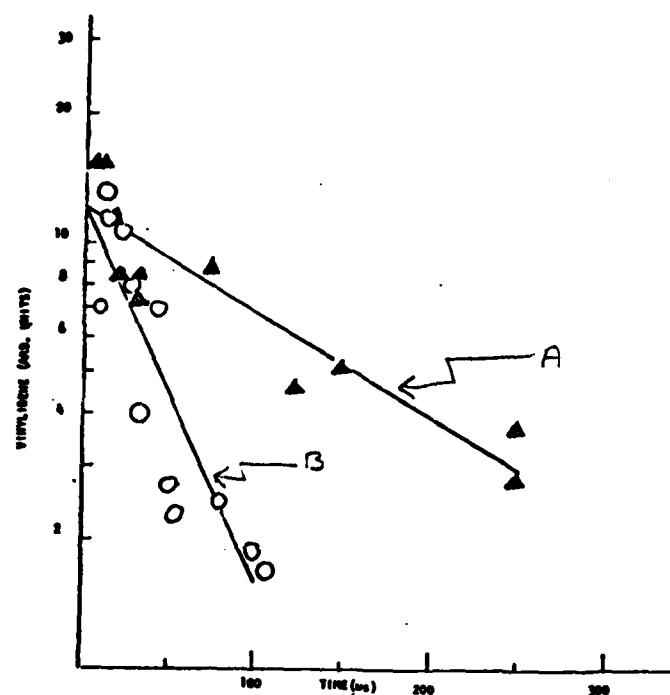
Chemical Kinetics Division
Center for Chemical Physics
National Bureau of Standards
Washington, DC 20234

The vinylidene radical ($\text{H}_2\text{C} = \text{C}$), which has been proposed as an intermediate in both the photolysis of C_2H_2 ¹ and the combination of triplet CH_2 radicals², has a relatively long lifetime in that it is observed spectroscopically, at 137 nm, for several hundred microseconds. The metastable nature of the transition is suggestive of a triplet state which is not connected to the singlet ground state manifold. The lifetime of the excited triplet has not been determined, either experimentally or theoretically. In this work we provide the first rate measurements for its removal.

The vinylidene radical was produced by the vacuum ultraviolet flash photolysis of C_2H_2 in the presence of He and its decay was monitored spectroscopically, in absorption, at 137 nm. The decay rate, shown in the accompanying figures, may be expressed as a rate constant for removal by helium. The value for removal of the protonated vinylidene species is equal to $1.3 \pm 0.3 \times 10^{-14} \text{ cm}^3 \text{ molec}^{-1} \text{ s}^{-1}$. Comparable data for the totally deuterated species yields a rate constant of $2.4 \pm 0.4 \times 10^{-15} \text{ cm}^3 \text{ molec}^{-1} \text{ s}^{-1}$.

The rate constants and isotope effect will be discussed with respect to the transition responsible for the absorption and the various loss mechanisms for the triplet vinylidene carrier.

1. A. H. Laufer, J. Chem. Phys., 73, 49 (1980).
2. A. H. Laufer, J. Chem. Phys., 76 945 (1982).



VINYLDENE AS A FUNCTION OF TIME

▲ $150 \mu C_2H_2 + 15 \text{ Torr He}$ (A)

○ $150 \mu C_2H_2 + 50 \text{ Torr He}$ (B)

----- Line from B

○ $-150 \mu C_2D_2 + 50 \text{ Torr He}$

ABSTRACT H-1

NON-THERMAL BIMOLECULAR REACTIONS by J. Wolfrum, MPI Fuer Stroemungsforschung, Goettingen and Institut fuer Physikalische Chemie der Universitaet Heidelberg, Goettingen, W. Germany.

Thermal Arrhenius parameters of bimolecular reactions contain no simple informations how the various degrees of freedom of the reacting molecules and in the "activated complex" contribute to the overcoming of the potential energy barrier of the reaction. Information of reactivity as a function of specific excitation of the reactants can give important insights into the microscopic chemical dynamics and can also be used to drive reactions more selectively than by thermal heating. The paper gives an overview on the effects of selective translational, rotational, vibrational, and electronic excitation on the reactivity in simple elementary gas-phase reactions. Experimental results obtained with crossed molecular beams and by laser stimulation and detection are compared with results obtained by ab initio theoretical calculations and simulation of the reaction dynamics by classical and quantum methods.

ABSTRACT H-2

CHEMILUMINESCENCE OF PH_3 , AsH_3 and SbH_3 WITH OZONE

Donald H. Stedman and Mark E. Fraser

Department of Chemistry
The University of Michigan
Ann Arbor, Michigan 48109

Chemiluminescence spectra are reported from the reaction of arsine, phosphine, and stibine with ozone at reduced pressure. Spectra from the reaction of arsine with oxygen free ozone and from oxygen atoms are also presented. Discrete band systems attributed to AsO and SbO are observed in the arsine, stibine systems. A strong apparent continuum in the visible is observed with phosphine and arsine. The species responsible for the visible continua are unknown but we suggest that they may be PO_2 and AsO_2 .

At low pressures in a flow system both the visible (Vis) and discrete/ultraviolet (UV) chemiluminescent emission from the $\text{AsH}_3/\text{O}_3/\text{O}_2$ system increased to a maximum well downstream of the injection port. This induction period, the subsequent decay, peak and total intensities were found to be dependent on $[\text{O}_3]$, $[\text{O}_2]$, and pressure. A numerical kinetic model was constructed which reproduces several of the observed phenomena including decreasing UV/Vis ratio, decreasing UV and Vis intensities and increasing induction periods as $[\text{O}_2]$ is increased. The model features a slow initiation reaction of arsine with ozone and a subsequent branched chain reaction involving the odd hydrogen radicals OH and HO_2 .

Chemiluminescence from Group V compounds has a long history. The oldest artificial chemiluminescing system, that of phosphorus vapor with moist air, was first observed by Brandt in 1669. Robert Boyle¹ was the first to perform a scientific investigation of the phenomenon. He recognized, among other things, the need for air. Subsequent investigators¹ observed the need for traces of water, the production of ozone by the reaction, as well as upper and lower bounds of oxygen pressure necessary to sustain the chemiluminescence. The emission is characterized by discrete band emission in the 220-270 nm range and a broad intense apparent continuum in the visible containing superimposed fine structure in the green. In 1926, Emeléus² observed similar UV and visible emission from phosphine burning in air and oxygen. The spectral similarities between these two phenomena have led investigators to regard them as arising from the same emitting species.

Figure 1 shows a spectrum of the newly discovered PH_3/O_3 chemiluminescence, compared to the continuous emission from P_4 in dry air given by VanZee and Khan.⁷ Apparently the same (unknown) light emitter is involved.

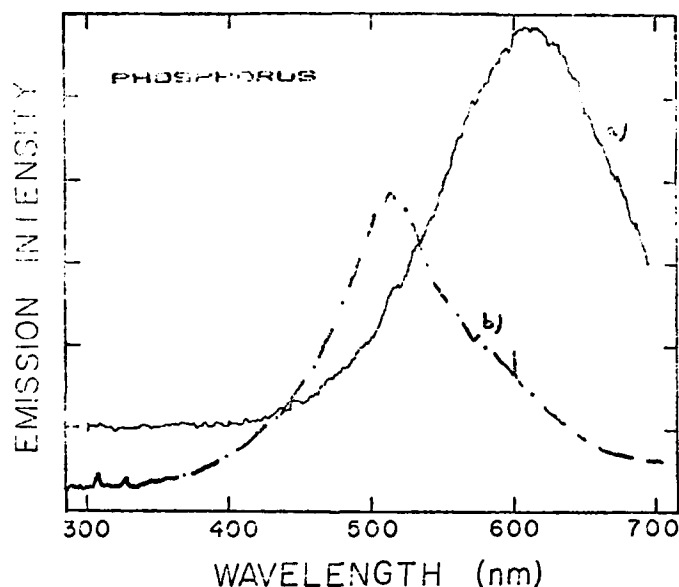


Figure 1. a) $\text{PH}_3 + \text{O}_3/\text{O}_2$ Spectrum. Uncorrected photoelectric spectrum obtained from the chemiluminescence generated by mixing 29.5 ml min^{-1} of 8.2% PH_3 in N_2 with 600 cc/min of 2.2% O_3 in O_2 at a total pressure of 2 Torr. b) The dotted curve is the spectrum of phosphorus emission in dry air redrawn from ref. 7.

A number of possibilities for the nature of the emitter have included P_2O_5 , HOPO , $(\text{PO}^*)_2$ excimer and PO_2 .³⁻⁸ Arsenic and antimony emission from flames of the element, and from hydride chemiluminescence have been observed by other investigators,⁹⁻¹⁷ but our recent study is also the first to report the AsO band emission¹⁸ shown in Figure 2 under several different conditions. At the high pressures used by Fujiwara et al.¹⁷ we expect these bands to be quenched. Figure 3 shows our observed spectrum from SbH_3 and O_3 .

A study of the kinetics of the AsH_3/O_3 system show that the chemiluminescence is characterized by an induction period followed by a rapid buildup to a peak intensity and subsequent decay.

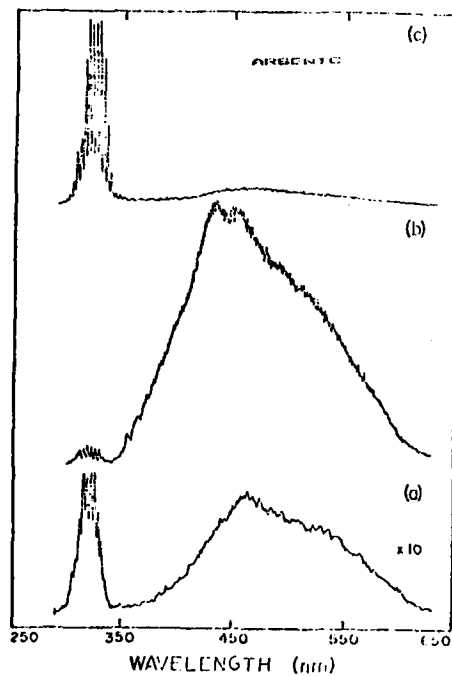


Figure 2. a) $\text{AsH}_3 + \text{O}_3/\text{O}_2$ Spectrum. An uncorrected photoelectric spectrum obtained from the chemiluminescence generated by mixing 14.2 ml min^{-1} of 6.8% AsH_3 in N_2 with 500 ml min^{-1} of 3.1% O_3 in O_2 at a total pressure of 1.9 Torr. b) $\text{AsH}_3 + \text{O}_3/\text{N}_2$ Spectrum. Uncorrected photoelectric spectrum obtained from the chemiluminescence generated by mixing 6.7 ml min^{-1} of 6.8% AsH_3 in N_2 with 620 ml min^{-1} of 2.63% O_3 in N_2 at a total pressure of 2 Torr. c) $\text{AsH}_3 + \text{O}/\text{O}_2$. Uncorrected photoelectric spectrum obtained from the chemiluminescence generated by mixing 9.2 ml min^{-1} of 6.8% AsH_3 in N_2 with 650 ml min^{-1} at discharged oxygen of a total pressure of 2 Torr. The scale of relative response in (a) is a factor of ten greater than that in (b) or (c).

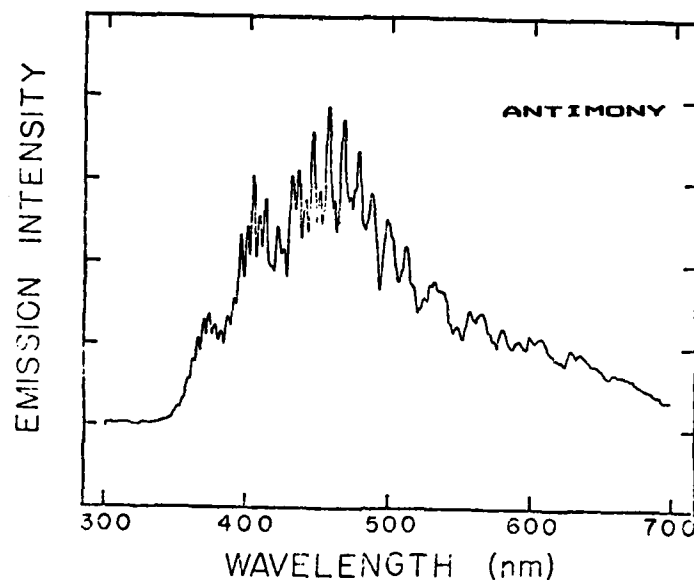
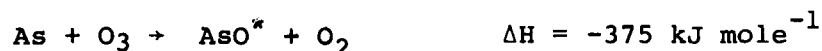


Figure 3. $\text{SbH}_3 + \text{O}_3/\text{O}_2$. Uncorrected photoelectric spectrum obtained from the chemiluminescence generated by mixing 28.3 ml min^{-1} of 8.4% SbH_3 in N_2 with 500 ml min^{-1} of 3.1% O_3 in O_2 at a total pressure of 2 Torr.

A chemical kinetics computer model was constructed to attempt to understand the mechanism of this process. We postulate that the continuum is excited AsO₂ formed by



and that the AsO emission arises from



where As atoms are formed by



The fact that the similar reaction is very exothermic for SbO, but endothermic for PO may help to explain the predominance of SbO band emission and the lack of observed PO emission. Other features of the model include the participation of odd hydrogen radical chains which partially succeed in reproducing the observed induction period, but still seem to be inadequate in the low O₂ system. Many features of the model appear to be correct, but the lack of several critical rate constants presently hinders further progress.

1. E. N. Harvey, A History of Luminescence (American Philosophical Society, Philadelphia, 1957).
2. H. J. Emeléus, J. Chem. Soc., 1925, 127, 1362.
3. T. E. Thorpe and A. E. Tulton, J. Chem. Soc. Trans., 1890, 57, 545; 1891, 59, 1019.
4. P. N. Ghosh and G. N. Ball, Z. Phys., 1931, 71, 362.
5. H. Cordes and W. Witschel, Z. Phys. Chem. (Frankfurt am Main) 1965, 46, 35.
6. P. B. Davies and B. A. Thrush, Proc. R. Soc. London Ser. A, 1968, 302, 245.
7. R. J. VanZee and A. U. Khan, J. Chem. Phys., 1976, 65, 1764.
8. T. A. Cool, Methods of Exp. Phys., 1979, 15, 95.
9. H. J. Emeléus, J. Chem. Soc., 1927, 132, 783; 1929, 134, 1846; 1934, 139, 974.
10. J. Joubert, Compt. Rend. 1874, 78, 1853.
11. A Comprehensive Treatise on Inorganic and Theoretical Chemistry, Volume IX, J. W. Mellor Ed., Longmans, Green and Co., NY, 1957.
12. L. Bloch, Compt. Rend., 1909, 149, 775.

13. E. Soubeiran, Ann. Chim. Phys., 1830, 43, 407.
14. J.B.A. Dumas, Ann. Chim. Phys. 1826, 33, 355.
15. J. L. Gay Lussac and L. J. Thenard or Ann. Chim. Phys., 1810, 73, 229.
16. K. Fujiwara, J. N. Bower, J. D. Bradshaw, J. D. Winefordner,
Anal. Chim. Acta, 1979, 109, 229.
17. K. Fujiwara, Y. Watanabe, K. Fuwa, J.D. Winefordner, Anal. Chem.,
1982, 54, 125.
18. M. E. Fraser, D. H. Stedman, M. S. Henderson, Anal. Chem.

ABSTRACT H-3

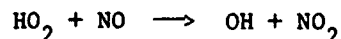
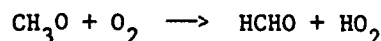
EFFECT OF RING STRAIN ON GAS PHASE OH RADICAL REACTION RATE CONSTANTS WITH BI- AND TRI-CYCLOALKANES AT 299 ± 2 K

Roger Atkinson, Sara M. Aschmann and W. P. L. Carter, Statewide Air Pollution Research Center, University of California, Riverside, CA 92521

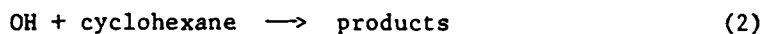
The hydroxyl radical is an important reactive intermediate in combustion processes and in atmospheric chemistry. Hence rate constants for the reaction of OH radicals with organics are both of fundamental chemical kinetic interest as well as being required for computer modeling studies of these systems. While a data base is available for the reaction of OH radicals with many classes of organics, the effect of ring strain on the OH radical reaction rate constants in cyclic and polycyclic organics has received little attention to date [1].

In order to investigate the effect of ring strain and of the structure of polycyclic alkanes on OH radical abstraction reactions, rate constants have been determined at 299 ± 2 K for the reaction of OH radicals with the series of bi- and tri-cyclic alkanes shown in Table 1.

The experimental technique was as described previously [2]. OH radicals were generated by the photolysis, at wavelengths $\lambda \geq 290$ nm, of methyl nitrite (CH_3ONO) in air at part-per-million ($1 \text{ ppm} = 2.37 \times 10^{13} \text{ molecule cm}^{-3}$ at 299 K and 735 torr total pressure) concentrations:



Irradiations of $\text{CH}_3\text{ONO}/\text{NO}/\text{cyclohexane}/\text{polycyclic alkanes}/\text{air}$ mixtures were carried out at 299 ± 2 K in an ~75-liter FEP Teflon cylindrical reaction bag surrounded by 24 GE F15T8-BL 15-watt blacklights. The reactant hydrocarbons were quantitatively monitored prior to and during the irradiations by gas chromatography with flame ionization detection. Under the experimental conditions employed, cyclohexane (the reference organic) and the polycyclic alkanes reacted essentially solely with the OH radical:



and hence

$$\ln \left\{ \frac{[\text{alkane}]_{t_0}}{[\text{alkane}]_t} \right\} = \frac{k_1}{k_2} \ln \left\{ \frac{[\text{cyclohexane}]_{t_0}}{[\text{cyclohexane}]_t} \right\} \quad (I)$$

where k_1 and k_2 are the rate constants for reactions (1) and (2), respectively, $[\text{alkane}]_{t_0}$ and $[\text{cyclohexane}]_{t_0}$ are the concentrations of the bi- and tri-cyclic alkanes and of cyclohexane, respectively, at time t_0 , and $[\text{alkane}]_t$ and $[\text{cyclohexane}]_t$ are the corresponding concentrations at time t .

A typical plot of equation (I) is shown in Figure 1, and the rate constants k_1 (using a literature value for k_2 of $7.57 \times 10^{-12} \text{ cm}^3 \text{ molecule}^{-1} \text{ sec}^{-1}$ [2]) obtained are given in Table 1.

Table 1. Rate constants k_1 for the gas phase reaction of OH radicals with a series of bi- and tri-cyclic alkanes.

Alkane	Ring Strain (kcal mole ⁻¹)	$10^{12} \times k_1 (\text{cm}^3 \text{ molecule}^{-1} \text{ sec}^{-1})^a$
Bicyclo[2.2.1]heptane	16.1	5.53 ± 0.15
Bicyclo[2.2.2]octane	9.6	14.8 ± 1.0
Bicyclo[3.3.0]octane	11.1	11.1 ± 0.6
<i>cis</i> -Bicyclo[4.3.0]nonane	7.9	17.3 ± 1.2
<i>trans</i> -Bicyclo[4.3.0]nonane	6.9	17.8 ± 1.3
<i>cis</i> -Bicyclo[4.4.0]decane	2.9	20.1 ± 1.4
<i>trans</i> -Bicyclo[4.4.0]decane	-0.3	20.6 ± 1.2
Tricyclo[5.2.1.0 ^{2,6}]decane	22.8	11.4 ± 0.4
Tricyclo[3.3.1.1 ^{3,7}]decane	4.2 - 6.6	23.2 ± 2.1

^a) At $299 \pm 2 \text{ K}$, error limits are two standard deviations.

In order to obtain a quantitative assessment of the effect of ring strain on the OH radical rate constants, it is necessary to estimate the rate constants for the unstrained structures. This has been carried out using the approach originally proposed by Greiner [3] which has been recently extended in these laboratories [4]. From these calculated and experimental rate constants, the effect of ring strain can be assessed. Figure 2 shows a plot of $\ln(k_{\text{exp}}/k_{\text{calc}})$ against the overall ring strain energy for the bi- and tri-cyclic alkanes studied here, and for cyclobutane, cyclopentane and cyclohexane. The data in Figure 2 indicates that ring strain effects are indeed substantial, and a quantitative knowledge of such effects are necessary before *a priori* predictive techniques can be used to accurately estimate OH radical rate constants and hence atmospheric lifetimes of organics with respect to OH radical reactions.

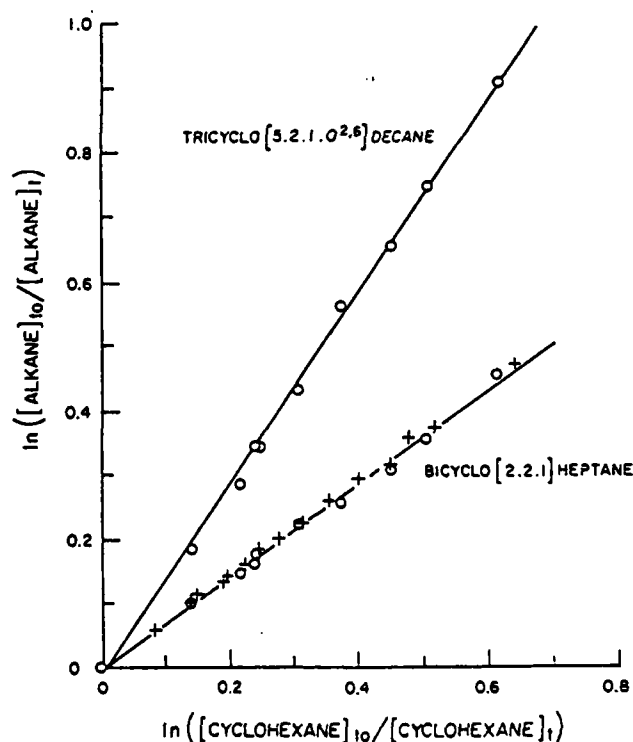


Figure 1. Plot of equation (I) for bicyclo[2.2.1]heptane and tricyclo[5.2.1^{2,6}]decane. The two sets of symbols for bicyclo[2.2.1]heptane are for two independent gas chromatographic analyses.

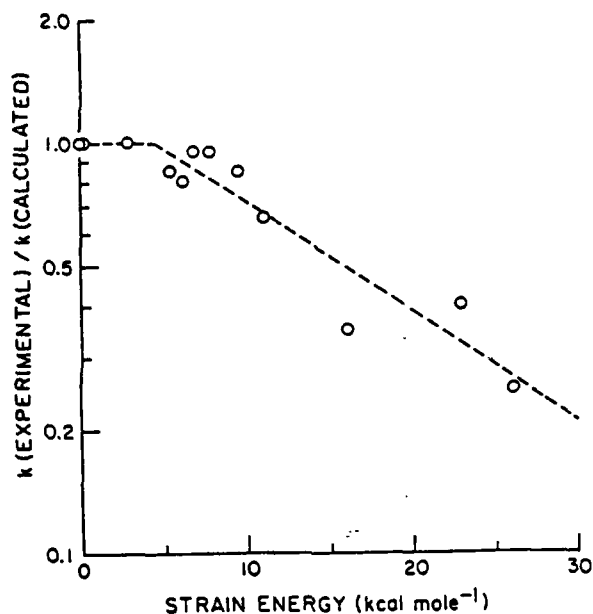


Figure 2. Plot of $\log(k_{\text{exp}}/k_{\text{calc}})$ against the overall ring strain energy for the cycloalkanes for which OH radical rate constant data are available.

References

1. R. Atkinson, K. R. Darnall, A. C. Lloyd, A. M. Winer and J. N. Pitts, Jr., *Adv. Photochem.*, **11**, 375 (1979).
2. R. Atkinson, S. M. Aschmann, A. M. Winer and J. N. Pitts, Jr., *Int. J. Chem. Kinet.*, in press (1982).
3. N. R. Greiner, *J. Chem. Phys.*, **53**, 1070 (1970).
4. R. Atkinson, S. M. Aschmann, W. P. L. Carter, A. M. Winer and J. N. Pitts, Jr., *Int. J. Chem. Kinet.*, in press (1982).

Acknowledgments

This work was supported by U. S. Air Force Contract No. F08635-80-C-0086 and by U. S. Environmental Protection Agency Grant No. CR804247-01.

ABSTRACT H-4

ARRHENIUS PARAMETERS FOR THE GAS PHASE REACTIONS OF C_2 WITH SELECTED OLEFINS OVER THE TEMPERATURE RANGE 300-650 K

H. Helvajian*, H. H. Nelson*, L. Pasternack and J. R. McDonald

Chemistry Division, Naval Research Laboratory, Washington, D.C. 20375

Introduction:

The C_2 radical has been observed in flames under fuel rich conditions of incipient soot formation¹ at concentrations near 10^{15} cm⁻³; it must, therefore, be considered as an important flame reactant species. Previous studies show that C_2 does not react ($<10^{-15}$ cm³ molecule⁻¹ s⁻¹) with O₂ or alkanes at room temperature and undergoes addition reactions with alkenes, alkynes and allenes²⁻⁴. These reactions likely convert the olefins to larger carbon-rich species. Understanding the reactions of C_2 radicals at higher temperatures is therefore important in elucidating its role in combustion chemistry.

In the present study, we report the Arrhenius parameters for the gas phase reactions of C_2 with selected olefins over a temperature range between 300 and 650K. These results not only allow insight into the dynamics of C_2 reactions with the unsaturated hydrocarbons, but they also supplement the body of data on similar reaction systems (C_2O , O(³P), O₃ with olefins).

Experiment:

The experimental set-up is described in detail elsewhere.^{2,5} Briefly, C_2 is produced by multiphoton UV photolysis of benzene at 249 nm using a mildly focused KrF laser. The removal of C_2 is monitored via laser induced fluorescence using a Nd-YAG pumped dye laser which is frequency upconverted and tuned to the C_2 , $A^1\Pi_u(0,0,0) \leftarrow X^1\Sigma_g^+(0,0,0)$ resonance transition at 405 nm. The resulting fluorescence from the $A^1\Pi_u(0,0,0) \rightarrow X^1\Sigma_g^+(0,0,2)$ transition at 485 nm is collected at right angles to the counter propagating lasers and filtered using a combination of dielectric and glass filters. The signal is averaged by a boxcar integrator, digitized and stored by a Nicolet 1180 computer for linear least squares analysis.

*NRC/NRL Resident Research Associate

The reaction cell, contained in a commercial convection oven (temperature stability $\pm 1\text{K}$), consists of a 5 cm stainless steel cross with baffled side arms through which the lasers propagate. Calibrated flows of benzene, reactant and buffer gas are combined and pass through the cell in a slow-flow. The experiments are performed using pseudo-first-order conditions with the C_2 disappearance fit by a single exponential over 4-5 observed lifetimes.

Discussion:

The Arrhenius parameters derived from the kinetic measurements of C_2 reactions with the alkenes and alkynes are presented in Table 1. One can see that within each class of reactant, the activation energies decrease dramatically with increasing alkyl substitution and become negative for multiple alkyl substituents on the olefinic backbone. Similar trends have been observed in reactions of C_2O , $\text{O}(^3\text{P})$ and O_2 with the olefins.⁶⁻⁸ The decrease in activation energy has been associated with a decrease in the ionization potential of the olefin, while the negative activation energy has been attributed to the location of the surface crossing (between the reactant approach surface and the product surface) and the velocity of the collision complex at the crossing point.⁹

In our experiments, one method of accessing other product channels is by collisional quenching of the reaction complex. Such a process would be reflected by a pressure dependence of the reaction rate. Using N_2 , CH_4 and SF_6 as buffer gases, with total pressures of up to 100 Torr, we see no pressure dependence in the reaction rate for any of the reactants listed. These results indicate that either the energized transition complex lasts for a time short compared to the collision frequency or that under our experimental conditions, we are in a high pressure limit where the number of collisions channel the complex to "favored" products.

We also monitored the interaction of C_2 with O_2 , CH_4 and butane, at elevated temperatures. We are able to place the following upper reaction rate limits O_2 , $k \leq 2 \times 10^{-16}$ at 520K, CH_4 , $k \leq 5 \times 10^{-16}$ at 600K and butane, $k \leq 2 \times 10^{-16}$ at 607K. This extends results measured at room temperature.

In comparing reactions of C_2O , O_2 and our results in C_2 , differences in activation energy are observed for reactions with cis-2-butene and isobutene. For C_2 and C_2O , reactions with isobutene (Table 1) have substantially lower activation energies compared to reactions with cis-2-butene, while in O_2 reactions, the opposite trend is observed. It seems that the

location of the two methyl groups has an effect on the reaction path followed by C_2 and C_2O and the one followed by O_3 . Studies of O_3 -alkene reactions show initial intermediates to be ozonides¹⁰ while studies on C_2O and C_2 predict cyclopropane ring structures.¹¹⁻¹²

In conclusion, C_2 -olefin reactions show trends characteristic of reactions via an electrophilic pathway. Reaction rates show no pressure dependence and over the temperature range studied, no pronounced deviations are seen from Arrhenius behavior. Steric influences on the reaction rate along with possible differences in reaction with ethylene and acetylene will be discussed.

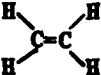
References:

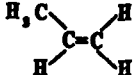
1. A. G. Gaydon, *The Spectroscopy of Flames*, 2nd Ed. (Wiley Sons, New York, 1974).
2. H. H. Nelson, L. Pasternack, J. R. Eyler and J. R. McDonald, *Chem. Phys.* 60, 231 (1981).
3. H. Reisler, M. S. Mangir and C. Wittig, *Chem. Phys.* 47, 49 (1980).
4. M. L. Lesiecki, K. W. Hicks, A. Orenstein and W. A. Guillory, *Chem. Phys. Letters* 71, 72 (1980).
5. V. M. Donnelly and L. Pasternack, *Chem. Phys.* 39, 427 (1979).
6. D. G. Williamson and K. D. Bayes, *J. Am. Chem. Soc.*, 90, 1957 (1968).
7. R. J. Cvetanovic, *Adv. Photochem.* 1, 115 (1963).
8. R. E. Huie and J. T. Herron, *Int. J. Chem. Kinet.*, Symp. No. 1, 165 (1975).
9. J. Connor, A. Van Roodselaar, R. W. Flair and O. P. Strausz, *J. Am. Chem. Soc.* 93, 560 (1971).
10. J. T. Herron and R. E. Huie, *Int. J. Chem. Kinet.*, Vol. X, 1019 (1978).
11. R. T. Mullen and A. P. Wolf, *J. Am. Chem. Soc.*, 84, 3712 (1962).
12. P. S. Skell, J. J. Havel and M. J. McGlinchey, *Accounts Chem. Res.* 6, 97 (1972).

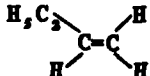
Table 1

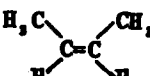
Reactant	Structure	Reactant Pressure (Torr)	A($\pm 1\sigma$) (10^{-18} cm ² molecule ⁻¹ s ⁻¹) (cal/mole)	E($\pm 1\sigma$)
----------	-----------	--------------------------	--	--------------------

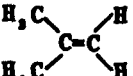
I Alkenes

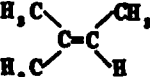
Ethylene		0-50	17.1 \pm 5.2	6511 \pm 333
----------	---	------	----------------	----------------

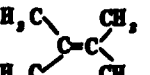
Propene		0-6.25	1.04 \pm 0.06	315 \pm 41
---------	---	--------	-----------------	--------------

1-butene		0-7	1.22 \pm 0.05	276 \pm 33
----------	---	-----	-----------------	--------------

<i>cis</i> -2-butene		0-1	2.10 \pm 0.10	-400 \pm 37
----------------------	--	-----	-----------------	---------------

<i>iso</i> -butene		0-0.08	4.20 \pm 0.17	-1509 \pm 30
--------------------	---	--------	-----------------	----------------

2-methyl-2-butene		0-0.1	5.57 \pm 0.45	-2014 \pm 67
-------------------	---	-------	-----------------	----------------

2,3 dimethyl-2-butene		0-0.08	21.0 \pm 1.8	-1822 \pm 65
-----------------------	---	--------	----------------	----------------

II. Alkynes

acetylene	H-C \equiv C-H	0-30	90.9 \pm 26.7	8077 \pm 320
-----------	------------------	------	-----------------	----------------

methyl acetylene	H ₃ C-C \equiv C-H	0-1	4.93 \pm 0.46	241 \pm 70
------------------	---------------------------------	-----	-----------------	--------------

2-hexyne	H ₃ C-C \equiv C-CH ₃	0-0.07	10.8 \pm 0.08	-1381 \pm 49
----------	---	--------	-----------------	----------------

ABSTRACT H-5

Abstraction vs. Exchange in the Reaction of D + HCl*

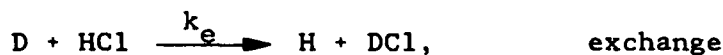
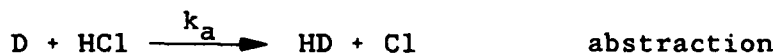
John C. Miller and Robert J. Gordon

Department of Chemistry

University of Illinois at Chicago

Chicago, Illinois 60680

The reaction of deuterium atoms with hydrogen chloride,



has been the subject of a controversy for many years, with various experimental and theoretical determinations of the branching ratio, k_a/k_e , differing by as much as four orders of magnitude.^{1,2} Recently³ we confirmed that surface effects in flow tube measurements of the H+HCl reaction had produced erroneous values of the rate constant. By using the flash photolysis - resonance fluorescence (FP-RF) method, we were able to obtain accurate values of the temperature dependent rate constant which satisfied detailed balance. It is likely that isotopic scrambling on surfaces may also have been responsible for previous inconsistencies in measurements of k_a and k_e .

In the present study we employed a variation of the real time FP-RF method. A gas mixture consisting of typically 7% D₂, 0.3% SF₆, and 1% HCl diluted with Ar was flowed slowly through a cubical monel cell. The experiment was carried out at room temperature, at total pressures ranging from 20 to 50 Torr.

A mildly focussed CO₂ TEA laser was used to dissociate < 1% of the SF₆ molecules. The resulting F atoms reacted very rapidly with D₂, producing deuterium atoms. Microwave powered atomic resonance lamps were used to excite selectively H, D, and Cl atoms in the reaction cell. A solar-blind photomultiplier tube, mounted perpendicular to the plane of the laser beam and resonance lamps, was used to monitor the atomic fluorescence in real time. To distinguish between D and H atoms, an H(D) atom filter, produced by an auxilliary microwave discharge, was inserted between the D(H) lamp and the cell.

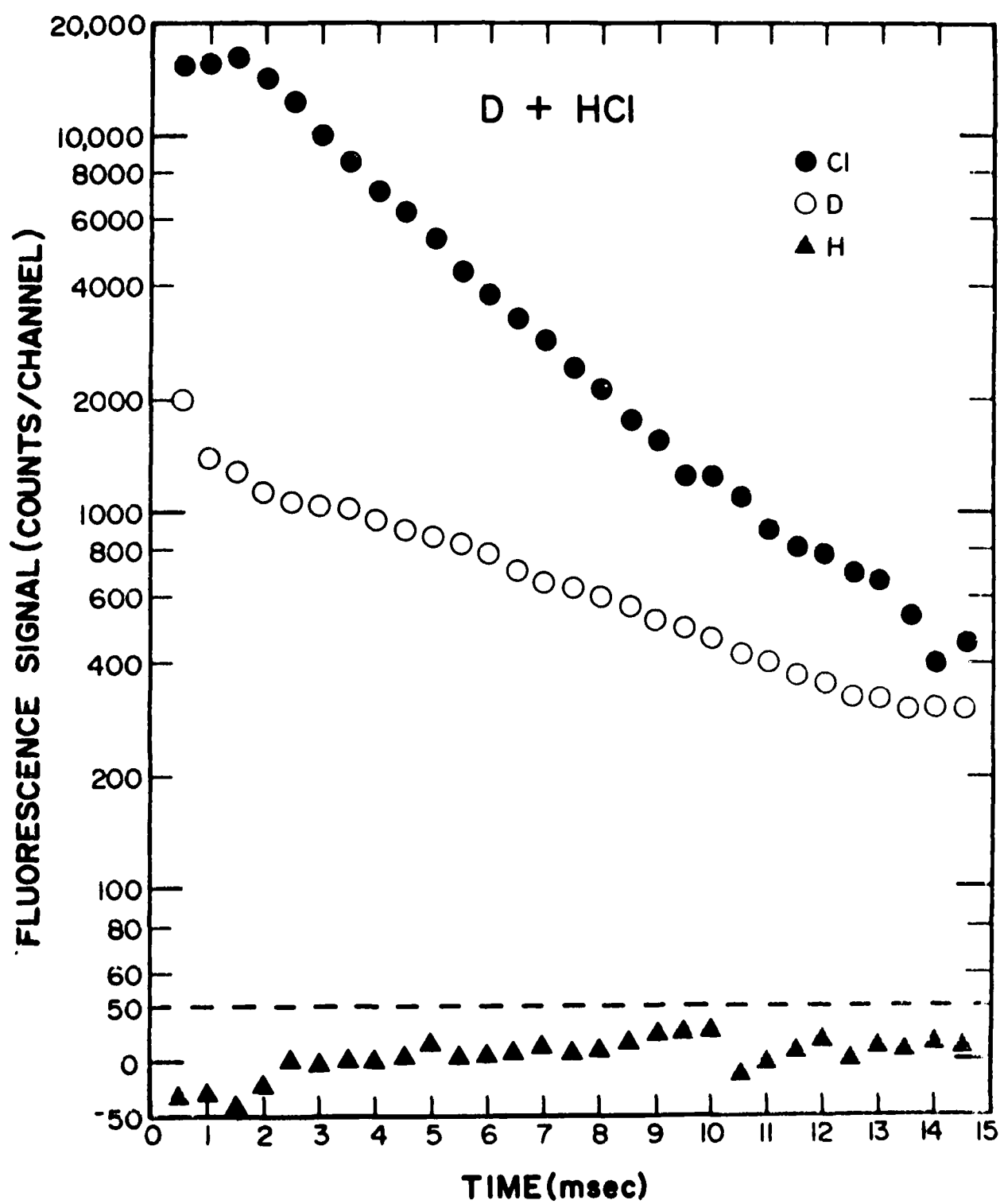
Typical time-resolved fluorescence signals generated with the three resonance lamps are shown in the accompanying figure. The D and Cl signals were found to decay exponentially, whereas no H atom signal was observed above the background. Calibrations were carried out to determine the sensitivity of the H atom detector. Gas mixtures consisting of SF₆, D₂, and variable amounts of H₂ in Ar were irradiated with the CO₂ laser. Hydrogen atom concentrations as low as 0.2% of the D concentration were clearly detectable with the H atom resonance lamp and the D filter. From these and other data we obtain an upper bound for k_e/k_a of 0.002 at 325 K. Since the molecular beam experiment of McDonald and Herschbach⁴ showed that the steric factor for exchange is large, we conclude from our study that the barrier for exchange must be much larger than that for abstraction. Our results disagree strongly with the photochemical studies of Wood⁵ and Klein *et al.*,^{6,7} and are consistent with the measurements of Endo and Class⁸ and of Kneba and Wolfrum⁹. Our finding

also supports the large exchange barrier predicted by several ab initio calculations.¹⁰⁻¹²

References

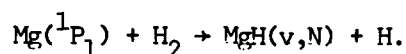
*Support by the Department of Energy is gratefully acknowledged.

1. R. E. Weston, Jr., J. Phys. Chem. 83, 61 (1979).
2. D. L. Thompson, H. H. Suzukawa, Jr., and L. M. Raff, J. Chem. Phys. 62, 4727 (1975).
3. J. C. Miller and R. J. Gordon, J. Chem. Phys. 75, 5305, (1981).
4. J. D. McDonald and D. R. Herschbach, J. Chem. Phys. 62, 4740 (1975).
5. G. O. Wood, J. Chem. Phys. 56, 1723 (1972).
6. A. E. DeVries and F. S. Klein, J. Chem. Phys. 41, 3428 (1964).
7. F. S. Klein and I. Veltman, J. Chem. Soc., Faraday Trans. II 74, 17 (1978).
8. H. Endo and G. P. Glass, Chem. Phys. Lett. 44, 180 (1976).
9. J. Wolfrum, Ber. Bunsenges. Phys. Chem. 81, 114 (1977).
10. P. Botschwina and W. Meyer, Chem. Phys. 20, 43 (1977).
11. T. H. Dunning, Jr., J. Chem. Phys. 66, 2752 (1977).
12. A. F. Voter and W. A. Goddard III, J. Chem. Phys. 75, 3638 (1981).



ABSTRACT I-1

THEORETICAL AND EXPERIMENTAL STUDIES OF THE REACTION:



W.H. Breckenridge, N. Adams, and H. Umemoto,

Department of Chemistry
University of Utah,
Salt Lake City, Utah 84112 U.S.A.

and

K.D. Jordan and R.P. Blickensderfer

Department of Chemistry
University of Pittsburgh
Pittsburgh, Penn. 15260, U.S.A.

The reaction $\text{Mg}(^1\text{P}_1) + \text{H}_2 \rightarrow \text{MgH}(\text{v},\text{N}) + \text{H}$ is being investigated theoretically and experimentally as a prototype system for the reactions of electronically excited Group IIa and IIb atoms with the hydrogen molecule. Experimentally, the initial $\text{MgH}(\text{v},\text{N})$ quantum-state distribution is being determined via a laser "pump-and-probe" technique whereby $\text{Mg}(^1\text{P}_1)$ is created with a short laser pulse and product $\text{MgH}(\text{v},\text{N})$ is detected by laser-induced fluorescence at time delays of a few nanoseconds. Theoretically, accurate ab initio calculations of the relevant excited and ground-state MgH_2 surfaces are being conducted with a view towards understanding the dynamics of this interesting reaction. Of particular importance is the fact that the attractive $\text{MgH}_2(^1\text{B}_2)$ entrance-channel surface crosses the "ground-state" $\text{MgH}_2(^1\text{A}_1)$ surface at a wide range of nuclear geometries in C_{2v} symmetry. A possible mechanism for the efficient production of highly rotationally excited MgH will be discussed in light of the theoretical calculations.

ABSTRACT I-2

Recent Applications of Flash Photolysis Resonance Fluorescence to Stratospheric Chemical Kinetics

Michael J. Kurylo

Chemical Kinetics Division
Center for Chemical Physics
National Bureau of Standards
Washington, DC 20234

Since its initial appearance (some 15 years ago) as a new optical technique for the investigation of gas phase reactions, flash photolysis resonance fluorescence (FPRF) has been applied to more than 100 different chemical reaction systems. Its sensitivity and specificity for detection of atomic and radical transients, coupled with its versatility with respect to the operational ranges of pressure and temperature, have marked it as one of several techniques of choice for studying homogeneous stratospheric kinetics. However, these features do not come cheaply (i.e. certain operational sacrifices must be made). Foremost among these are the limitations associated with photolytic (flash lamp or laser) production of the transient species of interest. Quite frequently, the atom or free radical cannot be produced in the total absence of other transients (atoms or radicals or even excited molecular species). More often than not, the appearance of such photofragments has a marked effect on closeness to pseudo first order kinetic behavior of the species of interest. The frequently used diagnostic of varying the photoflash (or laser) intensity and thence the radical concentration may not necessarily generate unequivocal

information about such complications. It is important, therefore, to be able to perform suitable functional analyses of the transient decay curves over various time regimes. Such examination, coupled with computer simulation of the complex reaction system, allows one to evaluate the validity of the kinetic behavior assumed and thus of the data reduction employed.

The results of our very recent reinvestigation of the $\text{OH} + \text{H}_2\text{O}_2$ reaction system will be discussed in light of the complexities (and consequent erroneous interpretations) associated with some earlier studies. Our experiments utilized the flash photolytic ($\lambda > 165 \text{ nm}$) production of OH radicals from water vapor - hydrogen peroxide mixtures. The H_2O_2 concentration entering the reaction cell was monitored optically at 213.9 nm and its stability during transit through the pyrex reaction chamber was repeatedly verified. The purely exponential behavior of the pseudo first order OH decay was observed for more than one decadic decrease in its concentration in agreement with model calculations of our reaction conditions. The results of this study (together with three other most recent investigations) yield a recommended Arrhenius expression for atmospheric modeling purposes between $245 \text{ K} \leq T \leq 460 \text{ K}$.

$$k = (2.80 \pm 0.26) \times 10^{-12} \exp[-(159 \pm 29)/T] \text{ cm}^3 \text{ molec}^{-1} \text{ s}^{-1}$$

Our results support the conclusions reached by these workers regarding the effects of this rate constant value on atmospheric HO_x profiles and H_2O_2 losses as well as on other laboratory studies of HO_2 kinetics.

ABSTRACT I-3

KINETICS OF HYDROXYL RADICAL REACTIONS WITH ALKANES

Larry G. Anderson and Robert D. Stephens
Environmental Science Department
General Motors Research Laboratories
Warren, Michigan 48090

Hydrocarbons play a very important role in atmospheric chemistry. Hydrocarbons are involved in the chain-carrying reactions which oxidize NO to NO₂ in the atmosphere, as described by Demerjian et al. [1]. The participation of hydrocarbons in these chain-carrying reactions is initiated by the OH radical attack upon the hydrocarbons. Calvert [2] has calculated the relative rate of hydroxyl radical reactions with the hydrocarbons measured in the Los Angeles atmosphere. It was found that about 33% of the OH radicals reacting in chain-carrying steps react with alkanes, 35% with alkenes, 20% with aromatics, and 12% with CO. Clearly each of these classes of compounds plays a very significant role in the conversion of NO to NO₂ in the urban atmosphere.

Atkinson et al. [3] have reviewed the kinetics data available for the gas phase reactions of hydroxyl radicals with organic compounds. This review showed that the only temperature dependent studies of OH-alkane kinetics were due to the early work of Greiner in 1970 [4], except for methane and n-butane. Atkinson et al. [3] concluded that there was a need to more accurately determine the rate constants for the OH reactions with alkanes, preferably as a function of temperature. This work is intended to fulfill this need for further study. The series of alkanes included in this study are methane, ethane, propane, n-butane, isobutane and neopentane. The hydroxyl radical kinetics with these alkanes were studied over the temperature range from about 240 to 370 K.

The discharge flow-resonance fluorescence technique was used in this study. The system used in the current study is similar to that described previously [5]. In the current system an aluminum flow tube is used with eight fixed reactant injection ports at 5 cm intervals corresponding to reaction distances between 10 and 45 cm. The walls of the flow tube were coated with a halocarbon wax (series 15-00, Halocarbon Products Corp., Hackensack, New Jersey). This wall treatment resulted in an OH wall loss rate which typically measured less than 10 s⁻¹.

Table I show a comparison of our preliminary room temperature rate data with that reported previously for the direct measurements of the OH + alkane kinetics. In general, there is good agreement between our room temperature measurements and those reported previously. Our data does tend to be on the lower side of the range of rate constants reported previously.

Figure 1 shows the preliminary results of the temperature dependence of the rate constants for the OH reactions with four of the six alkanes included in the study: ethane, propane, n-butane and isobutane. The results of this study will be discussed further.

TABLE I. Comparison of room temperature results for the kinetics of OH reactions with alkanes.

Alkane	k, cm ³ molecule ⁻¹ s ⁻¹	Method	Reference
Ethane	2.50 x 10 ⁻¹³	DF-RF	This work
	2.83 x 10 ⁻¹³	FP-KS	Greiner (70)
	2.64 ± 0.17 x 10 ⁻¹³	FP-RA	Overend et al. (75)
	2.90 ± 0.60 x 10 ⁻¹³	DF-LMR	Howard & Evenson (76)
Propane	0.93 x 10 ⁻¹²	DF-RF	This work
	1.20 x 10 ⁻¹²	FP-KS	Greiner (70)
	0.83 ± 0.17 x 10 ⁻¹²	DF-ESR	Bradley et al. (73)
	2.02 ± 0.10 x 10 ⁻¹²	FP-RA	Overend et al. (75)
n-Butane	2.14 x 10 ⁻¹²	DF-RF	This work
	2.57 x 10 ⁻¹²	FP-KS	Greiner (70)
	4.1 x 10 ⁻¹²	DF-MS	Morris & Niki (71)
	2.35 ± 0.35 x 10 ⁻¹²	FP-RF	Stuhl (73)
	2.72 ± 0.27 x 10 ⁻¹²	FP-RF	Perry et al. (76)
	2.67 ± 0.22 x 10 ⁻¹²	FP-RA	Paraskevopoulos & Nip (80)
i-Butane	1.60 x 10 ⁻¹²	DF-RF	This work
	2.46 x 10 ⁻¹²	FP-KS	Greiner (70)

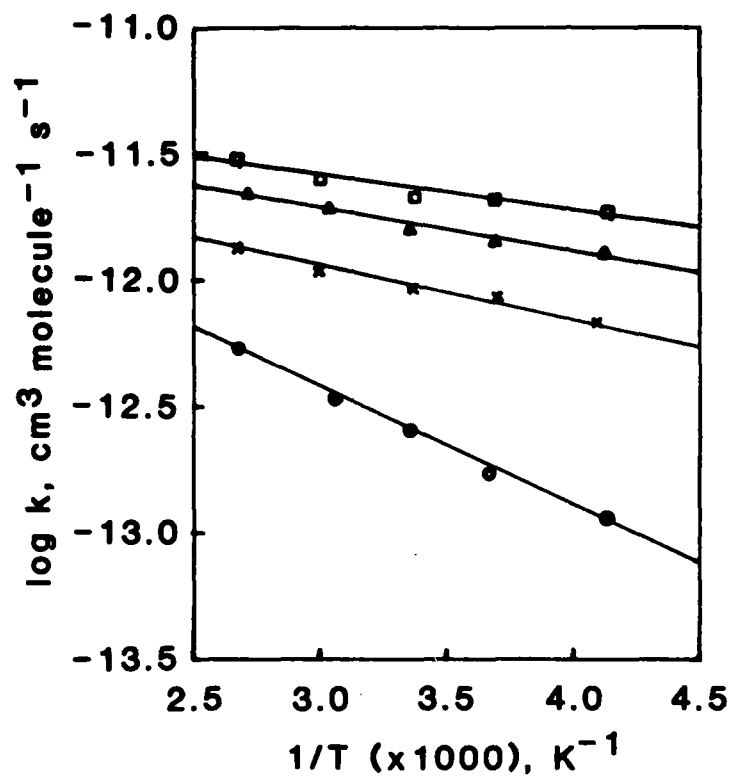


Figure 1. Arrhenius plots for the OH-alkane kinetics for ●-ethane; ×-propane; ■-n-butane; and ▲-isobutane.

REFERENCES

- [1] K. L. Demerjian, J. A. Kerr and J. G. Calvert, *Adv. Environ. Sci. Technol.* **4**, 1-262 (1974).
- [2] J. G. Calvert, *Environ. Sci. Technol.* **10**, 256-262 (1976).
- [3] R. Atkinson, K. R. Darnall, A. C. Lloyd, A. M. Winer and J. N. Pitts, *Adv. Photochem.* **11**, 375-488 (1979).
- [4] N. R. Greiner, *J. Chem. Phys.*, **53**, 1070-1076 (1970).
- [5] L. G. Anderson, *J. Phys. Chem.*, **84**, 2152-2155 (1980).

ABSTRACT I-4

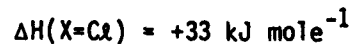
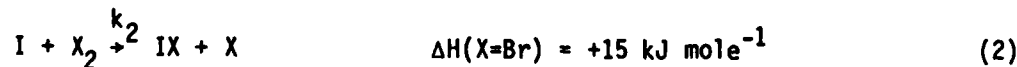
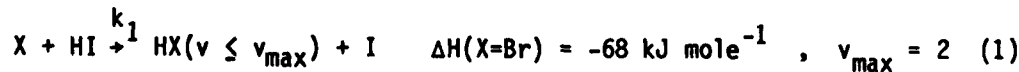
Laser Initiated Chain Reactions of Br₂ and Cl₂ with HI

David A. Dolson^a and Stephen R. Leone^b

Joint Institute for Laboratory Astrophysics
National Bureau of Standards and University of Colorado and
Department of Chemistry, University of Colorado
Boulder, Colorado 80309

Pulsed laser initiation coupled with time-resolved infrared fluorescence detection of vibrationally excited products has recently been introduced as a powerful tool in the measurement of specific rate processes occurring within complex chemical chain reaction systems.¹⁻³ The application of this technique in several investigations has proven its tremendous versatility to extract detailed rate coefficients for many different chain propagation reactions and vibrational deactivation processes. The strengths of the laser-initiated realtime method are embodied in the ability to generate, with short pulse tunable laser photolysis, specific radical populations, varying over several orders of magnitude in number density, and to follow the reaction kinetics by state specific detection of molecular vibrational chemiluminescence.

Two key problems concerning chemical chain reactions are considered in the recent work to be discussed here: the treatment of (1) multiple vibrational state production in the various propagation steps and (2) vibrational deactivation of multiple vibrational levels with differing rates. The success of our analysis is predicated on the detection of single levels in emission, which greatly simplifies the extraction of correct rate information. This treatment is applied to a comprehensive study⁴ of two multiple state systems that propagate by the reactions



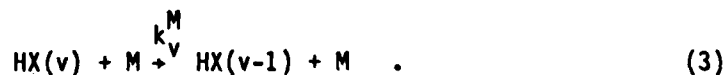
^a)NRC-NBS Postdoctoral Fellow.

^b)Staff Member, Quantum Physics Division, National Bureau of Standards.

where $X = \text{Br}, \text{Cl}$ ($1 \text{ kJ} = 0.239 \text{ kcal}$). These systems are both characterized by a relatively slow endothermic propagation step that regenerates the more reactive X atoms. Reaction (1) has been extensively studied, yielding values for k_1 ^{5,6} and product vibrational state distributions.⁷ In contrast, reaction (2) has not been investigated previously due to the small rate coefficients, which can be anticipated from their endothermicities. The application of a complete multiple vibrational state kinetic analysis to the state-selected realtime observations has enabled us to obtain both propagation reaction rate coefficients and also the vibrational deactivation rate coefficients for $\text{HBr}(v=2)$ and $\text{HCl}(v=3,4)$ by HI .⁴

In a typical experiment the purified reagents (X_2, HI) are mixed in a slow argon buffer gas flow (linear velocity = $0.2\text{--}1.0 \text{ m s}^{-1}$) in a pyrex reaction cell coated with a halocarbon wax. Ultraviolet photolysis pulses (355 nm, 2-75 mJ, 5 ns, 0.5-10 Hz) from a frequency-tripled Nd:YAG laser generate small concentrations, typically $\leq 10^{14} \text{ atom cm}^{-3}$, of X ($2P_{3/2}$) atoms from Br_2 or Cl_2 . Fractional dissociation of the parent diatomic is not allowed to exceed 5×10^{-3} so that pseudo first-order reaction conditions are maintained. Infrared fluorescence from the $\text{HX}(v)$ products of reaction (1) is observed with a 1 MHz response time InSb (77 K) photovoltaic detector. Appropriate dielectric interference filters and "cold" gas filter cells are used to state-select the realtime infrared emission. The detector output is amplified ($1\text{--}5 \times 10^5$), digitized (minimum 10 ns/channel), and summed in a signal averaging computer for 50-2000 laser pulses. The digitized data are saved in a computer file, and a hard copy plot of intensity versus time is also generated for kinetic analyses. A complete mathematical analysis has been derived to account for the multiple vibrational state production and cascade deactivation in these chain systems. Detection of individual levels in emission affords a tremendous simplification of the analysis, and is the method of choice here. It can be shown that detection of several states at once yields either incorrect results or signals that cannot be successfully deconvoluted.

A single state observation of IR chemiluminescence from $\text{HBr}(v=2)$ is shown in Fig. 1. The rapid rise is due to the production of $\text{HBr}(v=2)$ in reaction (1), in which nearly all of the Br atoms are initially exchanged for the less reactive I atoms. Following this initial "burst" of intensity the production of $\text{HBr}(v=2)$ falls to a lower level set by the steady-state Br atom concentration and the deactivation rate of $\text{HBr}(v=2)$. Consequently the fluorescence intensity decays with a characteristic time constant, $\tau_{v=2}^{\text{decay}}$, determined primarily by process (3) with $M = \text{HI}$.



State-selected emission enables us to extract k_1 and $k_{v=2}^{\text{HI}}$, respectively, from the rise and decay times, while k_2 is determined from the ratio I_{ss}/I_0 (see Fig. 1). The results of this chain investigation are summarized in the table below in which the rate coefficients are given in units of $\text{cm}^3 \text{ molecule}^{-1} \text{ s}^{-1}$.

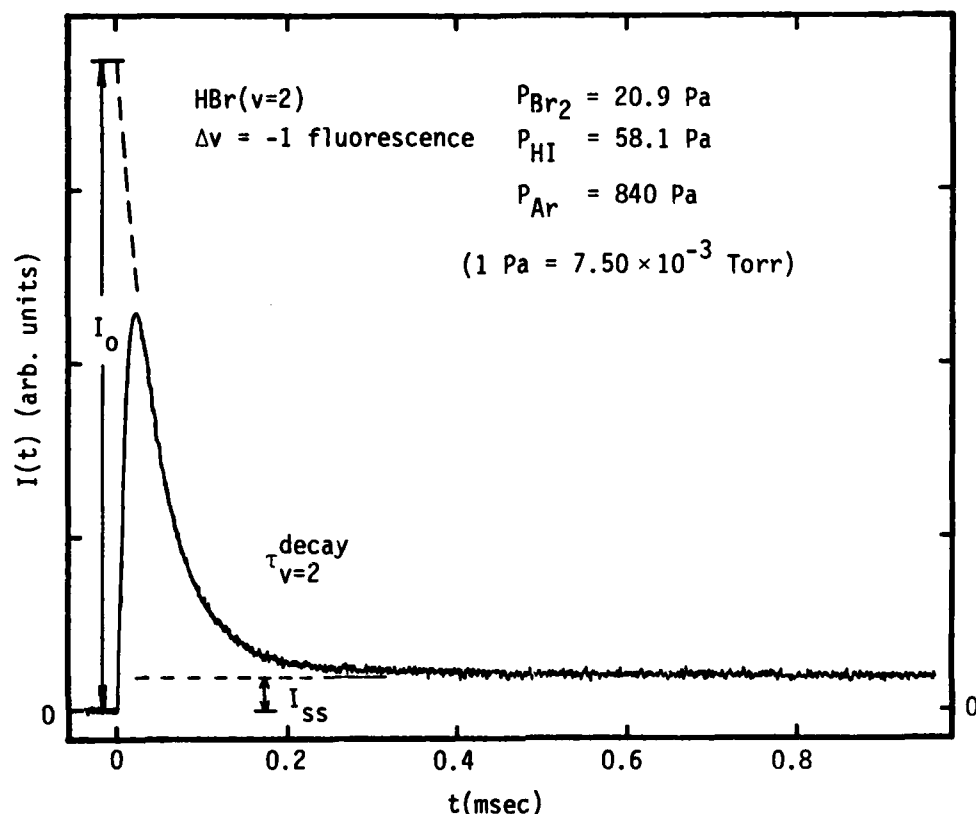


Fig. 1. Infrared fluorescence from $\text{HBr}(v=2)$ produced by reaction (1).

	k_1	k_2	$k_{v=2}^{\text{HI}}$	$k_{v=3}^{\text{HI}}$	$k_{v=4}^{\text{HI}}$
X=Br	$8.9(\pm 1.3) \times 10^{-11}$	$3.0(\pm 1.3) \times 10^{-13}$	$1.7(\pm 0.2) \times 10^{-12}$	---	---
X=Cl	$1.4(\pm 0.3) \times 10^{-10}$	$(8 \times 10^{-17})^*$	---	$7.0(\pm 2.4) \times 10^{-13}$	$3.2(\pm 0.7) \times 10^{-12}$

*Preliminary result from $\text{HCl}(v=1)$ observations.

Our measurements for k_1 are in good agreement with literature values.^{5,6} While no previously reported k_2 values exist for comparison, detailed balancing predicts $k_2(\text{X=Br}) = 2.1 \times 10^{-13}$ and $k_2(\text{X=Cl}) = 6.9 \times 10^{-17}$ based upon the reverse reaction rate coefficients.⁸ Both k_2 values extracted from the chain reaction are in good agreement with the detailed balancing predictions. It

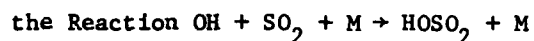
is interesting to note that the chain behavior was not detected in a previous investigation of the Br + HI reaction.⁶ Highly endothermic chain propagation reactions may be important in other kinetic studies as well and could influence the proper determination of rate coefficients in many systems. The vibrational deactivation rate coefficients obtained here for HCl($v=3,4$) and that reported for HCl($v=1$) deactivation by HI^{9,10} roughly fit a v^n dependence with $n=2$. Such behavior has also been reported for other systems.¹¹ These results confirm the necessity for state selected observations and illustrate the potential power of multiple state kinetic analyses in extracting detailed rate coefficients for reactive systems that generate products in many vibrational levels.

References

1. D. J. Nesbitt and S. R. Leone, J. Chem. Phys. 72, 1722 (1980).
2. D. J. Nesbitt and S. R. Leone, J. Chem. Phys. 75, 4949 (1981).
3. D. J. Nesbitt, Thesis, University of Colorado (1981).
4. D. A. Dolson and S. R. Leone, J. Chem. Phys. (to be submitted).
5. C.-C. Mei and C. B. Moore, J. Chem. Phys. 67, 3936 (1977); and references therein.
6. K. Bergmann, S. R. Leone and C. B. Moore, J. Chem. Phys. 63, 4161 (1975).
7. D. H. Maylotte, J. C. Polanyi and K. B. Woodall, J. Chem. Phys. 57, 1547 (1972).
8. M. A. A. Clyne and H. W. Cruse, J. Chem. Soc. Far. Trans. II 68, 1377 (1972).
9. H.-L. Chen, J. C. Stephenson and C. B. Moore, Chem. Phys. Lett. 2, 593 (1968).
10. H.-L. Chen and C. B. Moore, J. Chem. Phys. 54, 4080 (1971).
11. I. M. W. Smith and D. J. Wrigley, Chem. Phys. 63, 321 (1981); and references therein.

ABSTRACT I-5

Temperature Dependence of the Rate Constants for



Ming-Taun Leu

Molecular Physics and Chemistry Section
Jet Propulsion Laboratory, California Institute of Technology
Pasadena, California 91109

I. Introduction

The reaction of the hydroxyl radical with SO_2 ,



is one of the important OH reactions in atmospheric chemistry because it is one of the key reactions for sulfuric acid and aerosol formation, and it is an important path for SO_2 depletion in the atmospheres of Earth and possibly Venus.

Recently this reaction has been the subject of several reviews in the literature (1-3). The rate constant k_1 has been studied in the low pressure region by the discharge flow technique and in the fall-off region between second and third-order kinetics by the flash photolysis system. Unfortunately these experimental data are inconsistent with each other. In this work we report k_1 for $\text{M} = \text{He}, \text{Ar}, \text{N}_2, \text{O}_2, \text{SO}_2$, and CO_2 over the temperature range of 261 to 414K and at the low pressure region of 1 to 10^{-4} torr by the discharge flow technique using resonance fluorescence detection.

II. Experimental Method

The apparatus and techniques were the same as those described in detail previously (4,5). Briefly, the 2.50 cm inside diameter Pyrex flow tube had a fixed OH radical source, fixed detectors and a movable SO₂ injector. Hydroxyl radical at concentrations less than 5×10^{11} molecule cm⁻³ was generated by the reaction of nitrogen dioxide with atomic hydrogen which was produced in a microwave discharge of a dilute mixture of molecular hydrogen in helium. Resonance fluorescence at 306.4 nm was used to follow the decay of hydroxyl radical in the presence of a large excess of sulfur dioxide. Flow rates of all gases used were measured by calibrated mass flowmeters. Total pressure was measured by a calibrated MKS Baratron pressure meter. The temperature of the flow tube was controlled by a Haake circulator with thermostatted fluids flowing through the jacket and measured by a chromel-constantan thermocouple in the middle of the jacket. In addition, a quadrupole mass spectrometer located downstream of the resonance fluorescence cell was used to identify the possible reaction product, HOSO₂.

All of the gases used for this research were supplied by either Union Carbide Corporation or Matheson Gas Products, including helium (99.999%), argon (99.999%), nitrogen (99.999%), oxygen (99.95%), nitrogen dioxide (99.5%), hydrogen (99.999%), carbon dioxide (99.99%), and sulfur dioxide (99.98%). Nitrogen dioxide was treated by oxygen overnight to remove nitric oxide and purified by vacuum distillation. Sulfur dioxide was further purified by vacuum distillation and stored in a 20 liter Pyrex cell in the dark.

III. Results

The results are summarized in the following table.

<u>T(K)</u>	<u>M</u>	<u>k_1 (cm⁶/s)</u>	<u>Number of Experiments</u>
261-414	He	$(7.91 \pm 0.24) \times 10^{-32} \left(\frac{T}{298}\right)^{-2.85 \pm 0.21}$	108
298	Ar	$(1.09 \pm 0.09) \times 10^{-31}$	20
298	N ₂	$(2.54 \pm 0.33) \times 10^{-31}$	18
298	O ₂	$(2.46 \pm 0.32) \times 10^{-31}$	14
298	CO ₂	$(1.20 \pm 0.17) \times 10^{-30}$	21
261-414	SO ₂	$(1.15 \pm 0.09) \times 10^{-30} \left(\frac{T}{298}\right)^{-2.78 \pm 0.39}$	53

The uncertainty represents the first standard deviation of k_1 . Comparison with previous measurements will be discussed in the Conference.

References

- (1) J. G. Calvert, F. Su, J. W. Bottenheim, and O. P. Strauss, *Atmos. Environ.* 12, 197 (1978).
- (2) S. W. Benson, *Chem. Rev.* 78, 23 (1978).
- (3) R. Zeller, *Ber. Bunsenges. Phys. Chem.* 82, 1172 (1978).
- (4) M. T. Leu, *J. Chem. Phys.* 70, 1662 (1979).
- (5) M. T. Leu and R. H. Smith, *J. Phys. Chem.* 85, 2570 (1981).

ABSTRACT I-6

LIFETIMES OF ACETALDEHYDE ($^3A''$) AND ITS DEUTERATED ANALOGUES IN THE VAPOR PHASE

Merlyn D. Schuh, Mark P. Thomas, T. John Trout and Warren F. Beck

Department of Chemistry, Davidson College, Davidson, North Carolina 28036

The effect of deuterium substitution on the decay rates of aromatic hydrocarbons are generally considered to be well understood, and the decrease in rate of radiationless decay is usually attributed to a decrease in Franck-Condon factors associated with C-H stretching modes. In contrast, the effects of deuterium substitution in carbonyl-containing compounds are not as well understood and are still being investigated.

Deuterium substitution lengthens the triplet state lifetimes of most alkyl carbonyls by less than three-fold, but formaldehyde shows an exceptional increase of $\gg 40$. The asymmetry and intermediate structure of acetaldehyde make it a good structural link between the symmetric molecules formaldehyde and acetone, which have served as a model aldehyde and a model ketone, respectively, in previous studies. In view of the lack of information about the photophysics of deuterated acetaldehydes, we have begun studies to determine the effect of deuterium substitution on S_1 and T_1 states of these compounds, and report the triplet state lifetimes here.

In our experiments a filtered, low intensity flash (flash energy of 10 J/pulse) is used to produce S_1 -state acetaldehyde molecules. A fraction of these molecules pass to the T_1 state and phosphorescence. The phosphorescence passes through a 1/4m grating spectrometer and is detected by a photomultiplier with S-20 response. 1000 signals are averaged and processed by a digital, data-processing oscilloscope. All phosphorescence signals have been found to be exponential over the usable range of intensities, which is typically 1.5-2.0 decades.



Reciprocal lifetimes were found to increase linearly with acetaldehyde pressure over the pressure range 1.0-12.0 Torr in accordance with equation 1.

$$\tau^{-1} = \tau_o^{-1} + k_{sq}(A) \quad (1)$$

The results are given in the table below.

<u>Molecule</u>	<u>$\tau_o^{-1}(s^{-1})$</u>	<u>$k_{sq} \text{ (Torr}^{-1}s^{-1}\text{)}$</u>
CH ₃ CHO	27,000 ± 2000	950 ± 90
CD ₃ CHO	27,000 ± 2000	900 ± 90
CH ₃ CDO	5,100 ± 400	280 ± 30
CD ₃ CDO	3,500 ± 300	280 ± 30

To our knowledge, this is the second largest deuterium effect reported for the triplet state lifetime of alkyl aldehydes. Arguments will be presented to show that photodissociation does not depopulate the triplet state significantly and that the observed deuterium effect is due to a change in the rate of inter-system crossing. From Table 1 it seems clear that the aldehyde C-H modes exercise more control than the methyl C-H modes in dissipating electronic energy through both unimolecular and bimolecular processes.

Our results will be discussed and compared to the results on the effects of deuterium substitution in aromatic aldehydes, other alkyl aldehydes and ketones.

We acknowledge financial support from Research Corporation, the Petroleum Research Fund and the National Science Foundation for this research.

ABSTRACT J-1

PICOSECOND INTERMEDIATES OF CHEMICAL REACTIONS

P. M. Rentzepis, Bell Laboratories, Murray Hill, New Jersey 07974

Progress in the technology of picosecond spectroscopy in the past few years has made possible the generation of well characterized pulses emitted by synchronously pumped tunable dye lasers. In addition, the development of sensitive emission and absorption detection methods, and the advent of picosecond Raman and CARS spectroscopy, make possible the direct observation of picosecond transient spectra and lifetimes which allow complete determination of mechanisms through identification of transient states, radicals, and ions which evolve during the course of a chemical or biological reaction.

ABSTRACT J-2

Fluorescence Quenching of Aromatic Liquids at Energies Above and Below the Photoionization Threshold

Frederick P. Schwarz and Michael Mautner

Chemical Thermodynamics Division

Center for Chemical Physics

National Bureau of Standards

Washington, D.C. 20234

Recently, the S_1 fluorescence yield of liquid benzene excited in the photoionization region (7.1 to 10.5 eV) was determined as a function of excitation energy and of electron scavenger concentration (1). The fluorescence in this region is assumed to result from charge recombination between the benzene cation and its correlated electron to directly regenerate the S_1 state (2). It was observed that the recombination yield and the recombination quenching constants increase from 6.52 eV (1900 Å) to 8.9 eV (1400 Å) and level off from 8.9 eV to 10.8 eV (1150 Å) (1). Below 1750 Å, the quenching constants of the electron scavengers, CCl_3H , CH_3Cl , and C_2H_5Cl are proportional to their reaction rate constants with quasi-free electrons. From the reaction rate constants, a lifetime of the quenched entity in the photoionization region is calculated and found to be typical of ion-pair recombination lifetimes. This investigation is presently extended to the alkylbenzene derivatives of toluene, ethylbenzene, isopropylbenzene, n-propylbenzene, decylbenzene, indane, p-xylene, o-xylene, mesitylene and to 1-methylnaphthalene with chloroform as the electron scavenger to elucidate in more detail the ionization mechanism in aromatic liquids.

Below the photoionization threshold, the chloroform quenching constants of the S_1 fluorescence, q_1 , are shown in Table 1 and range from $0.6 \pm 0.1 \text{ M}^{-1}$ for benzene to $19 \pm 1 \text{ M}^{-1}$ for p-xylene. The transient quenching term, k_t , of Einstein-Smoluchowski equation (3) is

$$q_1/\tau = k_t = 4\pi N p^2 R^2 D (\pi D \tau)^{1/2} \quad (1)$$

where N is 6.02×10^{20} molecules/millimole, p is the probability that a reaction would take place within encounter radius R , D is the sum of the diffusion coefficients of the aromatic and the chloroform, and τ is the lifetime of the excited state. The transient quenching term yield quenching probabilities near unity when the quenching encounter radii are equal to the sum of the molecular radii for o-xylene, p-xylene, and mesitylene as shown in Table 1. The quenching probabilities are close to 0.5 for the mono alkyl benzenes and ~ 0.2 for benzene indicating that the transient quenching is enhanced by alkyl substituents on the aromatic ring. The methylnaphthalene fluorescence is exclusively from the excimer with a chloroform quenching constant of $6.6 \pm 0.7 \text{ M}^{-1}$. Near the ionization threshold, the fluorescence excitation spectra decrease to a minimum value as a result of two competitive effects; the forbiddenness of the $S_3 + S_1$ transition at this energy and a small contribution from the ion-pair recombination fluorescence. The minimum fluorescence yield relative to the S_1 fluorescence yield ranges from 0.28 ± 0.02 for benzene to 0.68 ± 0.05 for decylbenzene near the photoionization threshold.

Above the photoionization threshold and up to 10.8 eV (1150 Å), the S_1 fluorescence is generated from recombination of the aromatic cation-electron pairs and increases to a maximum fluorescence yield ranging from 0.9 ± 0.1 (ethylbenzene) to 0.6 ± 0.1 (isopropylbenzene) near 8.55 eV (1450 Å) relative to the S_1 fluorescence yield. If the recombination fluorescence is corrected for the known quenching of the S_1 state by chloroform, an additional

quenching of the ion-pair formation or the ion-pair is observed in the photoionization region (2). The chloroform quenching constants of the recombination range from $3.0 \pm 0.2 \text{ M}^{-1}$ for mesitylene to $1.7 \pm 0.2 \text{ M}^{-1}$ for indane as shown in Table 1. All the quenching constants increase with excitation energy similarly to the recombination fluorescence and extrapolate to zero at the estimated ionization potential of the liquid except for benzene. For benzene, quenching of a charge transfer state below the estimated IP must be taken into account in the extrapolation. From the transient term of the Einstein-Smoluchowski diffusion equation, quenching encounter radii of 47 Å are calculated for benzene, toluene, o-xylene, mesitylene, n-propylbenzene, isopropylbenzene, of 41 Å for p-xylene, and of 63 Å for decylbenzene. The large encounter radii are the same as the average ion-pair separation distances of ion-pairs formed exclusively in the radiolysis of aromatic liquids (4). Because of the large encounter radii and the energy dependence of the quenching constant, it is unlikely that the quenching of the charge recombination is due to the formation of a charge transfer complex between the excited state of the aromatic and the chloroform. The chloroform quenches the ion-pair and the chloroform quenching constant dependence on energy may be considered as a relative photoionization efficiency versus energy curve. The lack of charge recombination quenching in methylnaphthalene is believed to result from the affinity of the methylnaphthalene for the electron which competes effectively with the scavenging of the electron by the chloroform.

REFERENCES

- (1) F.P. Schwarz, and M. Mautner, Chem. Phys. Lett., 85, 239 (1982).
- (2) C. Fuchs, F. Heisel and R. Voltz, J. Phys. Chem., 76, 3867 (1972).
- (3) J. Birks, Photophysics of Aromatic Molecules, (Wiley-Interscience, New York, 1970).
- (4) S.G. Lias and P. Ausloos, Ion-Molecule Reactions, Their Role in Radiation Chemistry (American Chemical Society, Washington, D.C. (1975).
- (5) F.D. Rossini, K.S. Pitzer, R.L. Arnett, R.M. Braun, G.C. Pimental, ed, Selected Values of Physical and Thermodynamic Properties of Hydrocarbons and Related Compounds (American Petroleum Institute Research Project 44, Carnegie Press, Pittsburgh, 1953).
- (6) P.K. Ludwig and C.D. Amata, J. Chem. Phys. 40, 333 (1968).
- (7) A.O. Allen and R.A. Holroyd, J. Phys. Chem. 78, 796 (1974).

Table 1

	CCl ₃ H Quenching		Estimated ^c		CCl ₃ H		CCl ₃ H Quenching		CCl ₃ H Transient ^f	
	Constant of the		Encounter		Transient Quenching		Constant of the Charge		Quenching of the	
	S ₁ state	(M ⁻¹)	Radii	(Å)	of S ₁ fluorescence	P	above 9.0 eV	Recombination	Charge Recombination	Encounter Radii for p = 1
				(Å)	pr(Å)		(M ⁻¹)			(Å)
benzene ^a	0.6 ± 0.1		5.2		1.2	0.23	2.9 ± 0.1			47
toluene	4.0 ± 0.3		5.7		2.8	0.49	2.4 ± 0.2			47
o-xylene	16 ± 1		6.0		6.1	1.0	2.9 ± 0.3			47
p-xylene	19 ± 1		6.0		6.3	1.0	2.3 ± 0.2			41
mesitylene	13 ± 1		6.2		5.5	0.89	3.0 ± 0.2			47
n-propylbenzene	6.5 ± 0.5		7.7		4.0	0.52	2.1 ± 0.2			47
isopropylbenzene	6.0 ± 0.7		6.4		4.8	0.75	2.0 ± 0.2			47
decylbenzene	1.3 ± 0.2		12.0 ^d		2.6	0.22	2.0 ± 0.2			63
indane	8.4 ± .4		6.0			0.44				
1-methylnaphthalene ^b	6.6 ± 0.6						1.7 ± 0.2			
							0			

a) Reference 1.

b) 1-Methylnaphthalene fluorescence is from the excimer.

c) Encounter radii estimated from the sum of the radius of CCl₃H (1.7 Å) and molecular model radius of the aromatic.

d) Smaller radius of decylbenzene is with the side chain folded over the ring.

e) From equation 1 where D is twice the self diffusion coefficient (4) and τ is lifetime of ~ 30 × 10⁻⁹ of the S₁ state (5).f) Same as e except the lifetime of the quenched entity is from a ratio of the quenching constant to an estimated CCl₃H reaction rate constant with quasi-free electrons of 10¹² M⁻¹ sec⁻¹ (6).

ABSTRACT J-3

NON-LINEAR PHOTOREDUCTION OF YTTERBIUM(III) AND SAMARIUM(III)

Terence Donohue
Laser Physics Branch
Naval Research Laboratory
Washington, DC 20375

Introduction

The increasing use of lasers in gas phase photochemical studies has resulted in the discovery of new types of processes involving multiphoton absorption (and dissociation) using both infrared¹ and ultraviolet² sources. It would be almost surprising if similar effects were not observed in liquid phase experiments, and, indeed, several reports have appeared on non-linear effects in solution, including sequential absorption of a second photon by an excited state³ and simultaneous two-photon absorption through a virtual intermediate state.⁴ We report here the profound photochemical changes that can occur when employing a powerful rare-gas halide (RGH) excimer laser in photoredox studies of simple lanthanide (Ln) halide salts. These reactions are among the most endothermic photochemical processes ever reported.

Earlier studies had shown that Eu(III) could be photoreduced (E_0 of -0.35 eV) using either low-power continuous (CW) sources (lamps, etc.)⁵ or more powerful pulsed laser sources (RGH or nitrogen),⁶ and as would be expected, the quantum yields for photoreduction at a given wavelength were independent of the type of source employed, for instance, similar quantum yields were measured using a low-pressure Hg lamp at 254 nm and a KrF RGH laser at 248 nm. Photoreduction here occurs in a charge-transfer (CT) band, which is generally broad and featureless, thus small changes in photolysis wavelength would not be expected to produce any appreciably different results. Another interesting feature of the photochemistry of a number of lanthanides and actinides is that the reduced product can be photooxidized in its f-d bands, which generally overlap the CT band(s) of the oxidized state. When the rates of photoreduction and photooxidation become equal, a dynamic equilibrium results at the photostationary state. When we attempted more endothermic photoreductions, such as that of U(IV) (E_0 of -0.63 eV), pulsed laser (thus higher peak power) sources gave higher photoreduction quantum yields than CW lamp or laser sources.⁷ In pushing these thermodynamic limits further, we have found that photoreduction of Yb(III) and Sm(III) (E_0 's of -1.15 and -1.55 eV, respectively) is possible only with sufficiently high power sources,⁸ as we report here.

It is also possible to favor the relatively unstable reduced state by selective complexation. Recent studies have shown that the most suitable ligands are the (poly)macrocyclic polyethers, including the crown ethers and cryptands. 18-crown-6, 21-crown-7 and 2.2.2 cryptand bind Eu(II) more strongly than Eu(III), thus stabilizing the reduced



species.⁶ Similarly, 18-crown-6 stabilizes U(III)⁷ and we have found similar results for Sm(II).⁸ Thus use of a high peak-power photolysis source combined with the influence of stabilizing ligands allows the photochemical preparation and study of oxidation states not previously attainable.

Experimental

The output of the excimer laser (Lumonics model TE-861) was masked to both fill the photolysis cell uniformly and to remove the weaker fringes from the beam profile so that most of the beam energy was in an area of 0.18 cm². The laser was operated on KrF (248 nm), with a pulse length of 10 nsec, and at a repetition rate of 10 hz in most experiments. The average power, thus the peak power per pulse, was varied by both adjusting the operating voltage (from 20 to 42 kV) or by the insertion of neutral density filters. The average power into the cell was determined using a power meter (Scientech 362) and peak powers calculated using the known repetition rate and pulse length.

Samples were prepared from Ln(III) chlorides, dissolved in methanol, and thoroughly degassed with Ar to remove atmospheric oxygen. Reagent concentrations were adjusted such that virtually all of the photolysis light was absorbed in the 1 cm path length, and were in the range of 0.01 to 0.1 M in Ln(III), with a slight stoichiometric excess of particular macrocyclic ligands added in certain experiments. Concentrations were determined spectrophotometrically, using previously calibrated spectra or literature values for molar extinction coefficients. Quantum yields were calculated assuming linear absorption of the photolytic light by the sample.

Results and Discussion

Our earlier attempts at the photoreduction of Yb(III) and Sm(III) involved the use of low-pressure mercury lamps at 254 nm, but no effects were ever observed. However, when a pulsed RGH laser operating at about the same wavelength was used, immediate and dramatic changes were seen, where in the case of Sm, deep purple Sm(II) was observed. This species is quite unstable of course, and had a lifetime of only about 1 sec in methanol, precluding further study. However, when the macrocyclic ether 18-crown-6 was added to a SmCl₃ solution, the resulting SmCl₂(18-crown-6) complex lived for several hours, adequate for spectrophotometric studies. The reduced state of Yb also displayed a lifetime of several hours, but addition of several crown ethers or cryptands did not prolong its lifetime significantly.

The power dependence of quantum yields for photoreduction of both Yb(III) and Sm(III)(18-crown-6) were similar in shape and decidedly non-linear (see Fig. 1), with the most striking feature being the crossing over of the curve from positive to negative quantum yields as the power is reduced. In other words, at high peak-power levels, (net) photoreduction is occurring, while photolysis using low peak-powers results in net photooxidation. This remarkable observation clearly explains why

continuous sources, such as mercury lamps, were ineffective at reducing these species. The average, thus peak powers of these types of sources are just too low to cause photoreduction. It is interesting to compare this result with the photoreduction of UCl_4 . For this ion, low-power lamps were observed to cause small amounts of photoreduction to U(III) , but using a high peak-power RGH laser increased the quantum yields for photoreduction significantly.

There are two possible non-linear photochemical processes that can most readily account for these results. Most likely is that single-photon excitation into the CT band of the reagent species is not effective at photoreduction (except to a limited extent in U(IV)), but absorption of another photon by the excited species lifts the ion to an even more excited state from which (photo)reduction can then occur.

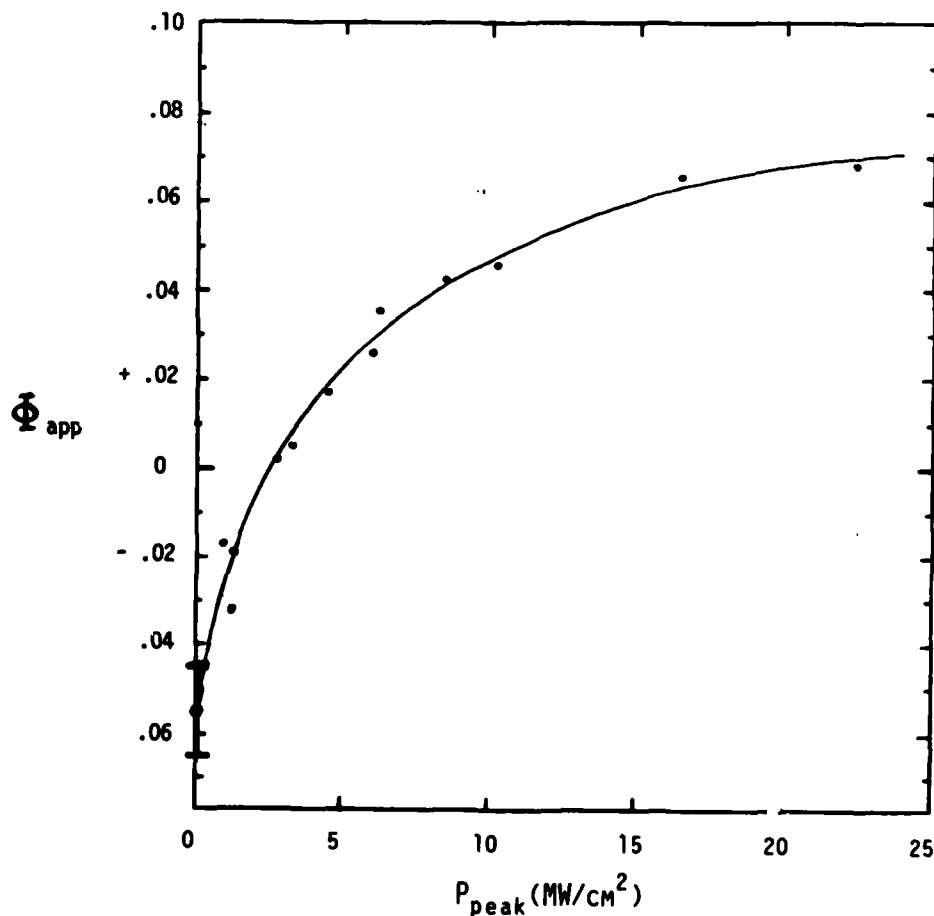


Figure 1. Apparent quantum yields for photoreduction of SmCl_3 (18-crown-6) in methanol as a function of power density. The data was obtained with a KrF laser (248 nm), except for the lowest point, which was derived using a low-pressure Hg lamp (254 nm). A smooth curve is drawn through the points for clarity.

This mechanism is similar to one proposed earlier³ and is reasonable, since the excited state lifetime is expected to be on the order of tens of nsecs,⁵ comparable to or longer than the laser pulse length. In all cases, the reduced species, being relatively unstable, can be photo-oxidized in its f-d bands. Thus a photostationary state can be created, one in which the ratio of concentrations of the reduced and oxidized states is power dependent, since the cross section for two photon photo-reduction would be dependent on the square of the peak power. This shifting of the photostationary state with changes in peak power was actually observed in an experiment using Yb. It is also possible that a "hyper-excited" state is not involved, but the non-linear effect is caused by progressive saturation of first the f-d transition (corresponding to photooxidation), then of the CT transition. These two theories can be tested by a careful measurement of the photoreduction power dependence at very low reduced state conversions. The first theory predicts a square dependence on power whereas if the second applies, then a linear power dependence would be observed. In either case, however, a high peak-power photolysis source is necessary to produce significant amounts of photoreduced species. Application of these types of processes may allow increasingly more endothermic photochemical studies in the future.

References

1. D. King, in "Advances in Chemical Physics," ed. K. Lawley (Wiley-Interscience, New York, 1981).
2. L. Pasternack and J.R. McDonald, Chem. Phys. 43, 173 (1979).
3. K.M. Cunningham and J.F. Endicott, J.C.S. Chem. Comm., 1024 (1974); R. Sriram, J.F. Endicott and S.C. Pyke, J. Am. Chem. Soc. 99, 4824 (1977).
4. A.V. Egunov and V.V. Korobkin, Khim. Vys. Energ. 1, 202 (1967); H. Zipin and S. Speiser, Chem. Phys. Lett. 31, 102 (1975).
5. Y. Haas, G. Stein and M. Tomkiewicz, J. Phys. Chem. 74, 2558 (1970); Y. Haas, G. Stein and R. Tenne, Isr. J. Chem. 10, 529 (1972).
6. T. Donohue, in "The Rare Earths in Modern Science and Technology: Vol. 2," ed. G.J. McCarthy, J.J. Rhyne and H.B. Silber (Plenum, New York, 1980), p. 105.
7. T. Donohue, in "Chemical and Biochemical Applications of Lasers, Vol. V," ed. C.B. Moore (Academic, New York, 1980), p. 239.
8. T. Donohue, in "The Rare Earths in Modern Science and Technology: Vol. 3," ed. G.J. McCarthy et. al. (Plenum, New York, 1982), p. 223; in "Photochemical Conversion and Storage of Solar Energy," ed. J.S. Connolly (Academic, New York, 1981), p. 463.

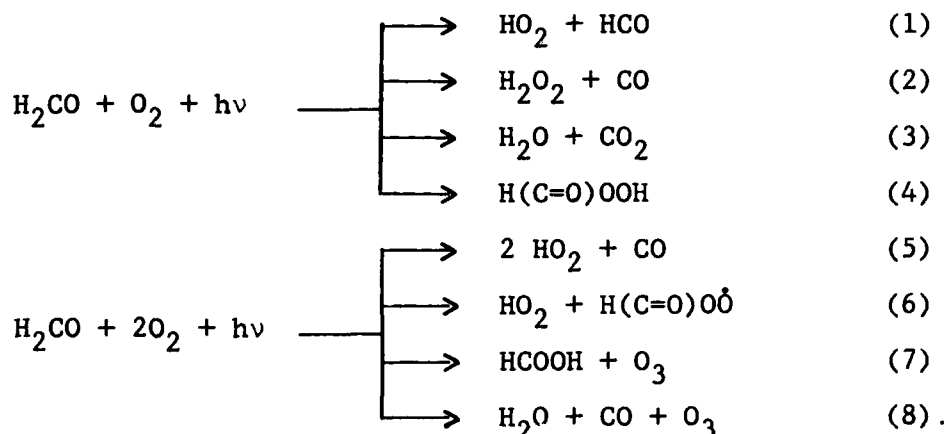
ABSTRACT J-4

"PHOTOCHEMICAL GENERATION OF $(\text{HO}_2)_2$ AND $\text{H}(\text{C}=\text{O})\text{OO}$ FROM FORMALDEHYDE AND GLYOXAL IN AN O_2 MATRIX"*

Tai-Ly Tso, Michael Diem and Edward K.C. Lee

Department of Chemistry
University of California
Irvine, California 92717

In the uv photolysis of the $\text{O}_2:\text{H}_2\text{CO}$ sample at 12-13K, most of the photooxidation products result from the secondary reactions of the primary photodissociation products, H atom and HCO radical. From the stoichiometry of H_2CO photooxidation, several sets of products can be envisioned, and most of them are observed.



In the uv photolysis of the $\text{O}_2:\text{H}_2\text{C}_2\text{O}_2$ sample at 12-13K, most of the photooxidation products result from the secondary reactions of the primary photodissociation products, two HCO radicals. The most predominant products are HO_2 , $(\text{HO}_2)_2$ and CO. Other products are present in very minor amounts, unlike in the photooxidation of H_2CO where reactions of H atoms are important.

*This research has been supported by the National Science Foundation grant CHE-79-25451.

HCO was not trapped directly but it was trapped as $\text{H}(\text{C}=\text{O})\text{OO}\cdot$ under our experimental condition. Formylperoxy radical is characterized by the $\text{C}=\text{O}$ group absorption at 1790 cm^{-1} . We observe satellite absorptions near the IR absorption peaks of HO_2 monomer at 3411 cm^{-1} (ν_1 , HO stretch), 1391.6 cm^{-1} (ν_2 , HOO bend) and 1101.3 cm^{-1} (ν_3 , OO stretch). The satellite absorptions observed in the $\text{O}_2:\text{H}_2\text{C}_2\text{O}_2$ sample are shown in Figure 1. We assign the satellite absorptions at 3323 cm^{-1} , 1416 cm^{-1} and 1108 cm^{-1} to a hydrogen-bonded dimer of HO_2 .¹ When the photolyzed sample is warmed up to 25-30K (compare c to b in Figure 1), the $(\text{HO}_2)_2$ peaks disappear and the H_2O_2 peaks appear. This thermal dissociation behavior at low temperature is analogous to the gas phase self-reaction of two HO_2 radicals. Two distinct models of the long-lived intermediate have been postulated recently, an open-chain (HOOOOH) with an internal hydrogen bond and a cyclic (head-to-tail dimer) with two hydrogen bonds. We favor the latter possibility.

The above results illustrate the successful trapping of the oxidation intermediates at low temperature, their thermal decomposition behavior and their spectroscopic characterization. Furthermore, the characterization of the molecular complexes as the caged partners provides the information on the reactant-product mass balance.

Dilute matrix samples of formaldehyde and glyoxal were prepared by pulse-depositing the gaseous mixture of O_2 and the carbonyls ($\text{M}/\text{R} = 1000\text{-}2000$) onto a cold CsI sample window maintained at 12-13K by a closed cycle refrigerator. A broad band-pass of 290-400 nm was used. Product distributions at various photolysis times and those resulting from post-photolysis warm-up were measured with a Fourier transform infrared spectrometer at a resolution of $0.2\text{-}0.3\text{ cm}^{-1}$.

-
1. M. Diem, T.-L. Tso, and E.K.C. Lee, J. Chem. Phys., to be published.

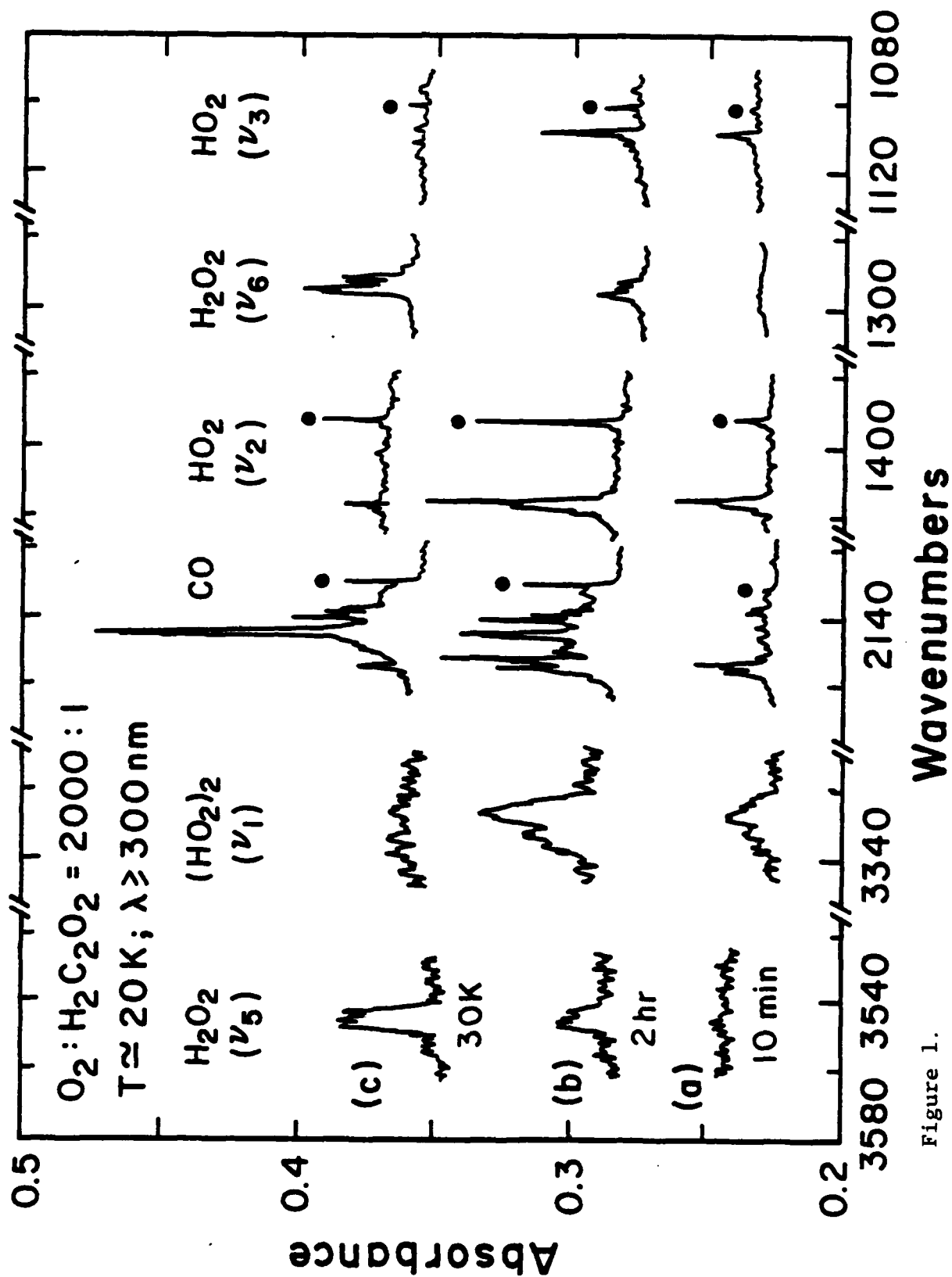
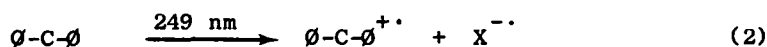
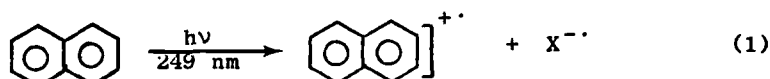


Figure 1.

ABSTRACT J-5

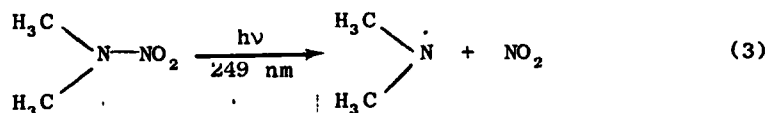
PHOTOIONIZATION VERSUS BOND HOMOLYSIS IN POLYATOMIC MOLECULES IN CONDENSED PHASE. Michel J. Rossi, Department of Chemical Kinetics SRI International, Menlo Park, CA 94025.

It has been discovered recently in transient absorption spectroscopic studies that aromatic and hydroaromatic molecules undergo photoionization in polar solution upon 249 nm irradiation according to the following scheme:

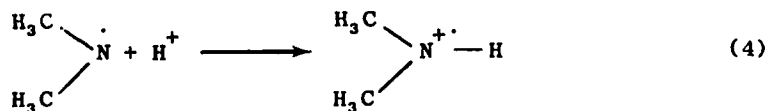


This process has been found to be monophotonic and results in the corresponding radical cations which decay extremely fast in a bimolecular reaction ($k^2 = 8 \times 10^{10} \text{ M}^{-1} \text{ s}^{-1}$). The nature of the negative species $\text{X}^{\cdot-}$ could not be established in the course of our studies.

On the other hand, N,N-dimethylnitramine and other polynitroamines do not yield the corresponding radical cations when subjected to the same irradiation conditions as in (1) and (2), but result in N-NO_2 bond homolysis according to (3):



The transient absorption spectrum of $\begin{array}{c} \text{H}_3\text{C} \\ \diagdown \\ \text{N}^{\cdot} \\ \diagup \\ \text{H}_3\text{C} \end{array}$ was recorded, and in acidic solution, the corresponding transient absorption spectrum of N,N-dimethyl aminium radical was obtained (4):



The former group of molecules is characterized by "low" gas-phase ionization potentials (IP) and "high" bond dissociation energies (BDE), whereas the latter is characterized by a high IP and a low BDE.

We report results on the 249 nm irradiation of nitrogen-containing polyatomic molecules with low IP and high BDE in order to achieve a direct comparison with transient absorption spectra of the nitramines. We discuss two representative molecules, namely, triethylamine (TEA) and N,N-dimethylaniline (DMA), whose radical cations have been observed upon 249 nm irradiation. For DMA, a very broad transient absorption covering the whole visible spectrum is also observed. Possible interpretations will be given. Finally, a group of molecules with low IP and low BDE (tetramethylhydrazine and 1,1-dimethylhydrazine) is investigated with respect to photoionization and/or bond homolysis.

The relaxation of electronically excited polyatomic molecules in condensed phase is discussed in terms of the competition between photoionization and bond homolysis pathways.

ABSTRACT K-1

LARGE MOLECULE INTERMOLECULAR ENERGY TRANSFER IN THE ELECTRONIC GROUND STATE: NEW TECHNIQUES FOR NON-REACTIVE SYSTEMS. John R. Barker, Department of Chemical Kinetics, SRI International, Menlo Park, CA 94025

Traditionally, energy transfer involving large molecules has been investigated in unimolecular reaction studies.¹ Recently, progress has been made in applying new techniques to non-reactive systems to obtain detailed information about energy transfer. These new techniques can be described in terms of (1) preparation of ensembles of excited molecules and (2) detection of the energy transfer process.

Nonequilibrium ensembles of highly vibrationally excited molecules (HVEMs) in the electronic ground state can be prepared by chemical activation, photoactivation, and by infrared multiple-photon absorption (MPA). Since chemical reactions are usually accompanied by numerous complications that can obscure details of energy transfer, photoactivation and MPA are desirable, if not accompanied by reaction. Photoactivation requires "clean" photophysics (low yields of intersystem crossing and fluorescence). Azulene has been an excellent subject for energy transfer studies,²⁻⁶ because its first two excited singlet states undergo rapid internal conversion to high vibrational levels of the electronic ground state, and it has very low quantum yields for fluorescence and intersystem crossing. Infrared MPA is a more generally applicable technique^{7,8} because many molecules absorb infrared light from a CO₂ laser. A drawback of MPA, however, is that the population distribution of HVEMs that results from it are very broad. A special category of methods of preparing HVEMs is photoactivation, followed by an exothermic isomerization reaction (i.e., cycloheptatriene \rightarrow toluene).⁹

Once the ensembles of HVEMs have been prepared, the energy transfer process must be detected. A direct technique for accomplishing this is to monitor infrared fluorescence (IRF) from the excited molecules.^{2-4,10} It is not necessary to have detailed spectroscopic information to predict the unresolved IRF band intensity dependence on E_{vib} , the vibrational energy in the molecules. Experiments performed using azulene excited to several different values of E_{vib} gave IRF intensities in good agreement with the theoretical

prediction.³ Incorporation of this prediction into master equation simulations of the experiments provides a means for interpretation of experimental data on energy transfer. A related method for monitoring the internal energy of the HVEMs is uv-absorption spectrometry,⁹ when the spectrum has a known dependence on E_{vib} .

Whereas IRF or uv-absorption due to the HVEMs is useful for monitoring total deactivation of the HVEMs, the time-dependent thermal-lensing (TDTL) technique¹¹ can be used to isolate V-T/R energy transfer. The unified theory¹² of the TDTL technique makes it possible to account properly for acoustic effects, diffusion, thermal conductivity, and the V-T/R energy transfer rate. For suitable systems, this is a good approach for studying energy transfer.

In experiments utilizing photoactivation of azulene vapor, we have addressed several important questions about energy transfer involving large molecules:

- (1) Are the average energies transferred per collision ($\langle \Delta E_d \rangle$) from nonreactive molecules similar to those observed in unimolecular reaction studies?
- (2) Does $\langle \Delta E_d \rangle$ depend on the level of excitation (E_{vib})?
- (3) Is the deactivation process primarily V-V or V-T/R energy transfer?

The first two questions were addressed by investigating the total deactivation of excited azulene as monitored with IRF from the C-H stretch modes.^{2,3,6} The azulene excitation energy was varied by about a factor of two: $\sim 17,000 \text{ cm}^{-1}$ to $30,000 \text{ cm}^{-1}$, and $\langle \Delta E_d \rangle$ was measured for a number of collider gases: unexcited azulene, He, Ne, Ar, Kr, Xe, H_2 , D_2 , N_2 , O_2 , CO, CO_2 , CH_4 , C_4H_{10} , SF_6 , etc. In nearly all cases, $\langle \Delta E_d \rangle$ depends strongly on E_{vib} , and its magnitude is comparable to that measured in unimolecular reactions studies.

To determine whether V-T/R or V-V energy transfer dominates in deactivation of excited azulene, TDTL experiments were used to isolate the V-T/R

process. The results were not clear-cut, but they suggested that V-V energy transfer may dominate in deactivation of excited azulene by unexcited azulene.⁵

In another series of experiments,⁴ excited azulene was deactivated by CO₂, and IRF from the asymmetric stretch of CO₂ was observed. Each excited azulene had enough energy (30644 cm⁻¹) to excite twelve CO₂ molecules to the (001) state (2349 cm⁻¹), but the total yield of CO₂(001) was only ~ 1.5 ± 0.5%. This result indicates that V-T/R energy transfer may dominate in this system, but we have not yet studied other states of the produce CO₂. Deactivation of CO₂(001) by azulene was also measured, and it required ~ 105 collisions. Further experiments are underway to observe other vibrational states of CO₂ and studies with deuterated azulene are planned to determine whether the near-resonance between the C-D stretch frequencies and CO₂(001) will enhance the V-V process.

In addition to the photoactivation experiments using azulene, the more generally applicable technique of IR-MPA is being applied to energy transfer involving several fluorinated compounds. Multiphoton decomposition (MPD) of these molecules is observed, as well as IRF from specific vibrational modes. The experiments are currently underway, and it is planned to combine the data (MPA, MPD, and IRF) in the context of a computer model to describe all of these processes in a unified manner. In this way, we can establish the population distributions of HVEMs following the laser pulse, and then study their energy transfer properties, bimolecular reactions, etc. Current progress in these experiments will be described.

References:

1. D. C. Tardy and B. S. Rabinovitch, Chem. Rev., 77, 369 (1977); M. Quack and J. Troe, Gas Kinetics and Energy Transfer, Spec. Periodical Reports 2, 175 (1977).
2. G. P. Smith and J. R. Barker, Chem. Phys. Lett., 78, 253 (1981).
3. M. J. Rossi and J. R. Barker, Chem. Phys. Lett., 85, 21 (1982).

4. J. R. Barker, M. J. Rossi, and J. R. Pladzewicz, Chem. Phys. Lett., submitted.
5. P. L. Trevor, T. Rothem, and J. R. Barker, Chem. Phys., in press.
6. M. J. Rossi, J. R. Pladzewicz, and J. R. Barker, manuscript in preparation.
7. P. A. Schultz, A. S. Subdo, D. J. Krajnovich, H. S. Kwok, Y. R. Shen, and Y. T. Lee, Ann. Rev. Phys. Chem., 30, 379 (1979).
8. For example, see A. C. Baldwin and H. van den Bergh, J. Chem. Phys., 74, 1012 (1981).
9. H. Hippler, J. Troe, and H. J. Wendelkin, Chem. Phys. Lett., 84, 257 (1981).
10. J. F. Durana and J. D. McDonald, J. Chem. Phys., 64, 2518 (1976).
11. F. R. Grabner, D. R. Siebert, and G. W. Flynn, Chem. Phys. Lett., 17, 189 (1972); D. R. Siebert, F. R. Grabner, and G. W. Flynn, J. Chem. Phys., 60, 1564 (1974).
12. J. R. Barker and T. Rothem, Chem. Phys., in press.

ABSTRACT K-2

VIBRATIONAL ENERGY RELAXATION IN SMALL MOLECULES

Ian W.M. Smith,
Department of Physical Chemistry,
University Chemical Laboratories,
Lensfield Road, Cambridge CB2 1EP, England.

Collisions in which vibrational energy is transferred are crucial to our understanding of a number of phenomena : for example, (a) any state-to-state description of the process of thermal activation, (b) the operation of molecular gas lasers, and (c) the degradation of selective excitation in attempts to promote chemical reactions by absorption of laser radiation. Nevertheless, the eruption of research on vibrational relaxation which took place about 10 years ago has now largely subsided. This is not because all the important questions have been answered, but rather because the (relatively) easy problems have been solved.

In this brief review, an attempt will be made to summarise progress - and to draw attention to our continuing ignorance - under three headings :

1) Rates and Mechanisms for the Vibrational Relaxation of Diatomic Molecules in High Vibrational Levels.

This section will include a rapid survey of recent research on energy transfer processes involving HF, HCl and NO by techniques such as direct, high overtone, optical pumping, steady-state and time-resolved vibrational chemiluminescence and observation by laser-induced fluorescence following electronic excitation and spontaneous fluorescence.

2) Intermode Vibrational-Vibrational Energy Transfer in Small Polyatomic Molecules. This process will be discussed in terms of recent results on the relaxation of HCN(OO1) and HCN(OO2) obtained in our laboratory, using an optical parametric oscillator to excite HCN to selected excited levels.

3) Relaxation in the presence of Strong or Medium-strength Attractive Forces. Rate constants for the vibrational relaxation of one radical by another will be surveyed. These show clearly that in the presence of 'chemical bond' forces collision complexes can form in which all modes are strongly coupled and energy transfer is facile. This is to be contrasted with the case where the collision energy is much greater than any attractive part of the intermolecular potential, the collisions are direct, and energy transfer is improbable. Some discussion will be presented of our present state-of-knowledge regarding the intermediate case where moderate attraction, such as a hydrogen-bond, exists between the collision partners.

ABSTRACT K-3

Vibrational Excitation of Molecules
by Collisions with "Hot" Hydrogen Atoms

R. E. Weston, Jr. , C. R. Quick, Jr., S. D. Ghosh,

Department of Chemistry, Brookhaven National Laboratory, Upton, NY 11973

G. W. Flynn, J. Chu,

Department of Chemistry, Columbia University, New York, NY 10027

and T. H. McGee

York College of the City University of New York, Jamaica, NY 11415

The collisional relaxation of vibrationally excited molecules, i.e. the conversion of vibrational to translational and rotational energy (V-T,R) is a widely studied phenomenon. Although the inverse process (T-V) is related by microscopic reversibility, it has been much less investigated. An obvious reason for this is that a typical vibrational energy quantum of 1000 cm^{-1} corresponds to thermal energy at a temperature of 900K. At such temperatures, chemical reactions are likely to obscure the kinetics of the energy transfer process. Crossed molecular beam experiments eliminate some of these problems, but have difficulties of their own. Nevertheless, since T-V processes may be important pathways in the thermalization of "hot" atoms, and in atmospheric chemistry, they deserve further study.

We have developed a new technique for the study of "hot" atom processes, based on a time-honored technique in which the photolysis of hydrogen halides or other small hydrides with photons having energy

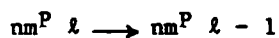
in excess of the bond dissociation energy produces "hot" hydrogen atoms. This has been done in the past with continuous radiation sources, but excimer lasers now make it possible to form the H atoms in a 10-nsec pulse, and to follow subsequent processes in real time.^{1,2} Photolysis of HCl, H₂S, or HBr with an ArF laser at 193 nm produces H atoms with translational energies of 44.6, 55, and 60.7 kcal/mole, respectively.

Vibrational excitation of polyatomic molecules by these H atoms has been monitored by measuring time-resolved IR emission through an interference filter with suitable solid-state detectors (InSb, Cu:Ge, HgCdTe).

Most of our work so far has concentrated on CO₂ as the "target" molecule, because of the high intensity of emission for transitions involving the antisymmetric stretching mode, ν_3 . This makes it possible to work at pressures of <0.1 torr of HX and CO₂. Even at these low pressures, the IR emission typically shows an initial rise that is limited by instrument response (≈ 2 μ sec). We attribute this to direct T-V excitation. A slowly-rising component is probably dominated by V-V energy transfer between CO₂ and vibrationally excited substrate molecules, HX[†]. Then there is a slow decay in emission intensity, due to vibrational relaxation of CO₂ by the inert buffer gas present at a relatively high pressure. Decay rate constants are in good agreement with those measured by Yardley and Moore.³

Added inert gas reduces the intensity of the fast-rising fluorescence component, as would be expected if thermalization of the H atoms is occurring. The relative efficiencies for He, Ne, Ar, Kr, and Xe agree qualitatively with the predicted hard-sphere collision rates.

Wavelength-resolved emission from CO₂ has been obtained by using a circular variable filter (CVF) with a band pass of ~30 cm⁻¹, FWHM. The emission spectrum resembles the absorption spectrum of room temperature CO₂ shifted ~40 cm⁻¹ to the red. This indicates that most of the emission involves "hot-band" transitions of the type



The absence of observable rotational broadening indicates that rotational excitation is relatively slight.

This method is being extended to other molecules, such as CH₃F, in order to determine the relative excitation of different modes of vibration. It should also be possible to observe chemical reactions of hot H atoms, such as



by using laser-induced fluorescence as a probe for reaction products.

Acknowledgment

This work was supported by the Office of Basic Energy Sciences, U.S. Department of Energy, and in part by an Industrial Research Participation grant from the National Science Foundation.

References

1. C. R. Quick, Jr., R. E. Weston, Jr., and G. W. Flynn, Chem. Phys. Lett. 83, 15 (1981).
2. F. Magnotta, D. J. Nesbitt, and S. R. Leone, Chem. Phys. Lett. 83, 21 (1981).
3. J. T. Yardley and C. B. Moore, J. Chem. Phys. 46, 4491 (1967).

ABSTRACT K-4

Abstract for the 15th Informal Photochemistry Conference-June 1982

VIBRATIONAL REDISTRIBUTION IN S_1 p-DIFLUOROBENZENE

R.A. Coveleskie, D.A. Dolson, S.C. Munchak and C.S. Parmenter

Department of Chemistry
Indiana University
Bloomington, Indiana 47405

Chemical timing has been used to monitor the collision-free picosecond time evolution of vibrational states near $\epsilon_{\text{vib}} = 2200\text{cm}^{-1}$ within S_1 p-difluorobenzene (pDFB). These data have been combined with data from high resolution $S_1 \leftarrow S_0$ absorption spectroscopy and collision-free fluorescence spectroscopy to yield a rather detailed view of vibrational redistribution (IVR) in a region of S_1 pDFB where the vibrational state density is about 80 per cm^{-1} . The results can be summarized briefly. IVR from a level initially pumped ($3'5'30'$ with $\epsilon_{\text{vib}} = 2189\text{ cm}^{-1}$) into the neighboring S_1 field occurs with an initial level lifetime of about 35 psec. This time scale is seen both in high resolution absorption line widths (as measured by T.M. Dunn, University of Michigan) and the fluorescence timing experiments. The actual kinetics of initial state decay fit to within experimental error those predicted by the intermediate case of radiationless transition theory. The collision-free fluorescence spectra at long times support these kinetics by sustaining emission structure from the initially pumped vibrational level even though the S_1 emitting molecules have lived an average of 6600 psec. The theory and the

fluorescence spectra require that the surrounding field into which IVR occurs be at least in order of magnitude more dense than the calculated level density. In all probability, this density is supplied by the rotational levels using Coriolis vibration-rotation coupling.

The crucial role of vibration-rotation coupling in pDFB IVR is emphasized in studies of the IVR threshold as initial excitation climbs the S_1 manifold. Chemical timing experiments place that threshold near $\epsilon_{\text{vib}} \approx 1490 \text{ cm}^{-1}$ where the density of vibronic states alone is less than 5 levels per cm^{-1} .

ABSTRACT K-5

INELASTIC AND REACTIVE SCATTERING OF METASTABLE RARE GAS ATOMS

K.M. Johnson, R. Pease and J.P. Simons

Chemistry Department, The University, Nottingham NG7 2RD, U.K.

The application of the rotor accelerated molecular beam technique to studies of metastable atomic reactions continues to provide insight into their molecular dynamics^{1,2} In particular, the technique provides a direct method for determining excitation functions and the translational energy dependence of product branching ratios and rotational alignment.

Reactions of $\text{Xe}(^3\text{P}_{2,0})$ and $\text{Kr}(^3\text{P}_{2,0})$ with halogens and halide donors follow dynamics which for the most part, closely parallel those of the neighbouring alkali metal atoms^{1,3} Unlike the alkali metals, however, the electronic excitation in the metastable rare gases also offers competition from competing channels leading to inelastic scattering and electronic energy transfer^{3,4} For example, rare gas halides (or excited halogen atoms) are the principal products of collisions of Xe, Kr or $\text{Ar}(^3\text{P}_{2,0})$ with Br_2 but in the case of $\text{Kr}(^3\text{P}_{2,0})$, electronically excited $\text{Br}_2(\text{D})$ is also a major product with a branching ratio $\Gamma(\text{Br}_2) \approx 25\%$ at thermal collision energy³ Increasing the collision energy in the range (10-70) kJmol^{-1} raises the relative branching ratio $\Gamma(\text{KrBr}^*)/\Gamma(\text{Br}_2(\text{D}))$ by $\sim 30\%$. The $\text{KrBr}(\text{B})$ is rotationally aligned but far less than the $\text{XeBr}(\text{B})$ produced from $\text{Xe}(^3\text{P}_{2,0})$ ⁴ and it carries much less vibrational excitation⁴ These observations can all be accommodated by a simple model which includes the possibility of electron transfer in either sense between the collision partners, and transfer onto alternative ionic potential surfaces leading either to atom or to energy transfer. The model also explains the 'special' behaviour in the Kr/Br_2 system compared with Xe and Ar as well as the relative branching ratios for the other halogens. Indeed it provides a rationale for the branching behaviour in many excited rare gas - molecular systems,

in particular the relative probabilities of electronic energy transfer to reactive scattering.

A crossed beam study of the molecular dynamics of electronic energy transfer in the system $\text{Ar}(^3\text{P}_{2,0}) + \text{N}_2$ has been initiated. Previous experiments in discharge flow systems have shown preferential population of one of the Λ -doublet components in the $\text{N}_2(\text{C})$ indicating a preference for rotational alignment of the $\text{N}_2(\text{C})$ perpendicular to the collision plane⁵. As expected, we have found that the $\text{N}_2(\text{C} \rightarrow \text{B})$ fluorescence is strongly polarised parallel to the relative velocity of the collision partners. However, the polarisation (and alignment) decrease with increasing collision energy in the range $E_{\text{t}} \leq 50 \text{ kJ mol}^{-1}$. This behaviour should be matched by corresponding changes in the $\text{N}_2(\text{C} \rightarrow \text{B})$ fluorescence spectrum. Supersonic beam-gas experiments currently in progress, show that polarisations can still be recorded, and, following the procedure of Prisant, Rettner and Zare⁶, converted into product alignment coefficients. The signal intensities promise to be sufficient to allow recording of the rotationally resolved fluorescence at super-thermal collision energies.

We are grateful to SERC for their support.

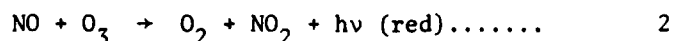
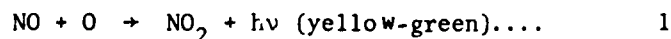
- (1) R.J. Hennessy, Y. Ono & J.P. Simons, *Mol.Phys.*, **43**, 181 (1981)
- (2) R.J. Hennessy and J.P. Simons, *Mol.Phys.*, **44**, 1027 (1981)
- (3) D.W. Setser, T.D. Dreiling, H.C. Brashears, Jr. and J.H. Kolts, *Faraday Diss. Chem. Soc.*, **67**, 255 (1979)
- (4) R.J. Hennessy and J.P. Simons, *Chem.Phys.Lett.*, **75**, 43 (1980)
- (5) J. Derouard, T. Nguyen & N. Sadeghi, *J.Chem.Phys.*, **72**, 6698 (1980)
- (6) M.G. Prisant, C.T. Rettner and R.N. Zare, *J.Chem.Phys.*, in press.

ABSTRACT K-6

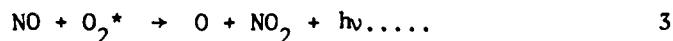
Orange Chemiluminescence From NO_2

R.D. Kenner and E.A. Ogryzlo
Department of Chemistry
University of British Columbia
Vancouver, B.C. Canada V6T 1Y6

Two reactions of nitric oxide which yield emission from electronically excited NO_2 have been well characterized:



A third such reaction of nitric oxide was postulated by Harteck and Reeves (1) to explain a surface catalyzed emission from NO_2 :



The spectrum of the emission was not determined and therefore Thrush (2) suggested that it could be due to reaction 1.

We have carried out a spectroscopic and kinetic study of this chemiluminescent reaction in a fast flow system. Electronically excited oxygen was produced by the recombination of oxygen atoms on a nickel surface. When nitric oxide is introduced into the stream an orange glow is observed with a short wavelength cut off near 500 nm (compared with 400 nm for reaction 1 and 600 nm for reaction 2). Such a spectrum shows that the simple reaction between ground state ozone molecules and nitric oxide (reaction 2) is not the source of the emission.

Nevertheless, our kinetic data indicates that reaction 3 is also not the source of the emission. A determination of the orange emission intensity as a function of [NO], [O₂], [O], [O₂(A³Σ_u⁺)], [He] and [Ar] reveals a complex rate law that not only shows a first order dependence on [NO] and [O₂(A³Σ_u⁺)] but also on [O₂]. Such an O₂ dependence is not consistent with direct excitation of NO₂ in reaction 3. The only process consistent with both our kinetic and spectroscopic data is:



where O₂^{*} is electronically excited oxygen (O₂(A and A')), and O₃^{*} is some unidentified excited state of ozone with at least 9 kcal of vibrational or electronic excitation.

References

1. P. Hartick and R.R. Reeves, Discuss. Faraday Soc., 37, 82 (1964).
2. B.A. Thrush, Discuss. Faraday Soc., 37, (1964).

This work was supported by the Air Force Office of Scientific Research, Air Force Systems Command, U.S.A.F. under Grant No. AFOSR-79-0088.

ABSTRACT L-1

Laboratory Studies of Hydrogen-Oxygen, Radical-Radical Reactions
with Combined Laser Magnetic Resonance, Resonance Fluorescence
and Atomic Absorption Detection

Wm. H. Brune, J. J. Schwab, and J. G. Anderson

Department of Chemistry and
Center for Earth and Planetary Physics
Harvard University
Cambridge, Massachusetts 02138

The hydrogen-oxygen, atom-small radical reaction system is difficult to study in the laboratory because of the rapid interconversion of HO_x species. Study of any single reaction requires the ability to monitor simultaneously, with sufficient sensitivity, the key radical reactants, products, and contaminants, and to specify completely the chemical sources forming the reactants. We have combined the detection techniques of laser magnetic resonance (LMR), resonance fluorescence and absorption, and photofragment fluorescence with a fast flow system to undertake studies of the reactions:



We have sufficient sensitivity to detect the primary and secondary reactants of atomic oxygen and the hydrogen-containing radicals and to measure absolutely the sum of $[H]$, $[OH]$, $[HO_2]$, $[H_2O_2]$, and $[H_2O]$ to test for hydrogen continuity. Further, we use a computer calculation to determine the best method for studying a particular reaction, and, for reactions schemes in which some interference is inevitable, to measure the error introduced into the rate constant. For this paper, we will discuss briefly the experiment apparatus, insights of the computer studies for reaction (1) $OH + HO_2 \rightarrow H_2O + O_2$, and, finally, preliminary results of the $O + OH \rightarrow H + O_2$ reaction.

The apparatus is shown in Figure 1. The fast flow and gas handling systems are similar to those discussed by several other experimenters¹,

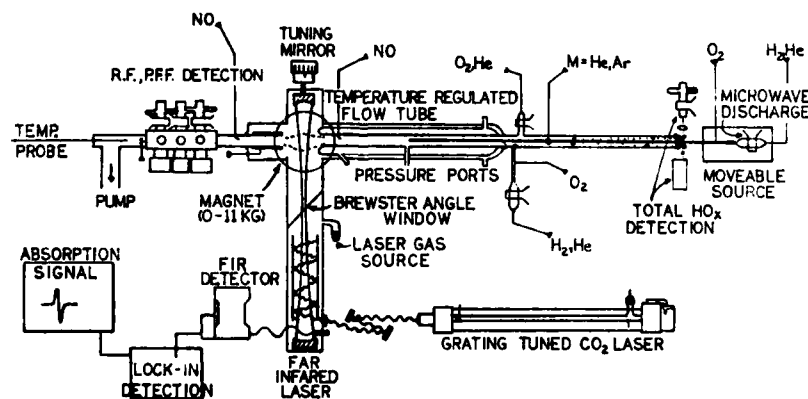


Figure 1

but the unique feature is the multiple detection systems. Four detection ports include an LMR axis for detection of OH (sensitivity of $\lesssim 10^8 \text{ cm}^{-3}$) and HO_2 ($\sim 3 \times 10^8 \text{ cm}^{-3}$), and three axes grouped together on a stainless steel manifold which may be used interchangeably for:

- (a) resonance fluorescence detection of H atoms ($5 \times 10^7 \text{ cm}^{-3}$), O ($\sim 10^8 \text{ cm}^{-3}$), and OH ($2 \times 10^8 \text{ cm}^{-3}$);

(b) absorption detection (2.5 cm path) for O and H; and

(c) photofragment fluorescence of H_2O ($\sim 2 \times 10^{10} \text{ cm}^{-3}$)
and H_2O_2 ($\sim 1 \times 10^{11} \text{ cm}^{-3}$).

Cross calibration of the various axes and detection techniques is possible by a variety of chemical titrations and absorption measurements. For instance, total reactive H is measured by addition of excess O atoms which rapidly convert both HO_2 and OH to H.

The difficulties of the HO_x radical-radical kinetics and the need for detection of many species is exemplified by reaction (1) $\text{OH} + \text{HO}_2 \rightarrow \text{H}_2\text{O} + \text{O}_2$. Recent experiments have demonstrated the necessity of sensitive O and H atom detection along with the detection of OH and $\text{HO}_2^{2,3}$, as well as the usefulness of computer modelling for assessment of possible interference from contaminants. From our computer studies of this reaction, we have found that:

- (a) Since the interfering reactants (predominantly O and H atoms) have comparable rate constants to reaction (1) and are produced in the OH and HO_2 chemical sources, curvature is not a good indication of these side reactions.
- (b) Lowering the concentration of the excess reactant, either HO_2 or OH, does not eliminate the problems of disproportionation of that reactant since only the ratio of disproportionation to reaction (1) rates is important.
- (c) For psuedo first order experiments with HO_2 in excess over OH, all contaminants act to reduce the inferred reaction rate constant for this reaction; for OH in

excess, all secondary reactants act to increase the inferred rate constant.

Thus, rate constants obtained with HO_2 in excess and OH in excess act as lower and upper bounds to the actual rate constant.

The first reaction we are studying with our system is $\text{O} + \text{OH} \rightarrow \text{H} + \text{O}_2$. Our preliminary rate constant is in rough agreement with the Lewis and Watson value⁴ ($3.1 \times 10^{-11} \text{ cm}^3 \text{ molecule}^{-1} \text{ s}^{-1}$), although our technique is substantially different. We monitor the decay of OH in the presence of excess O and the formation of the H atom product as well. Small impurities in the radical sources, primarily the O atom source, reform OH from H, causing quite clear curvature in the second decade of OH decay. In this case, the rate constant may be obtained from the OH decay over the first decade with only a small error due to OH regeneration because the interfering reactant, H, is a product of the reaction and does not come from either chemical source.

References:

1. U.C. Sridharan, B. Reimann and F. Kaufman, J. Chem. Phys., **73**, 1286 (1980); and many others.
2. U.C. Sridharan, L.X. Qiu and F. Kaufman, J. Phys. Chem., **85**, 3361 (1981).
3. Leon F. Keyser, J. Phys. Chem., **85**, 3667 (1981).
4. R.S. Lewis and R.T. Watson, J. Phys. Chem., **84**, 3495 (1980).

ABSTRACT L-2

The UV Spectrum of SiF, SiCl and CCl

H. Bredohl, I. Dubois, Y. Houbrechts and F. Melen

Institut d'Astrophysique
Université de LIEGE
B 4200 COINTE-UGREE
BELGIUM

1. Nineteen Rydberg states of SiF have been observed between 35000 and 56000 cm^{-1} under high resolution. Rotational analysis have yielded molecular constants for these states which have been arranged into eight Rydberg series : $ns\sigma$, $np\sigma$, $np\pi$, $nd\sigma$, $nd\pi$, $nd\delta$, nfn and $nf\delta$. These identifications allow us to determine a precise value of the first ionization potential of SiF
$$\text{I.P} = (7.29 \pm 0.02) \text{ eV}$$
2. Similar experiments have been done on SiCl, in emission as well as in absorption. Five Rydberg states have been observed. Four of them have been analysed and attributed to the following configurations : $4s\sigma$ ($B^2\Sigma^+$), $4p\pi$ ($C^2\Pi_r$), $4p\sigma$ ($D^2\Sigma^+$) and $5s\sigma$ ($F^2\Sigma^+$). The fifth one, which is the E state reported by Oldershaw and Robinson (J. Mol. Spectrosc. **38**, 306, 1971) under low resolution is heavily predissociated. In spite of a good deal of research, no discrete absorption has been observed above 47000 cm^{-1} . This leads to the conclusion that, above this limit, all the electronic states of SiCl are completely predissociated.
3. The situation is worst for CCl since, for this radical, no discrete absorption has been observed, except the known $^2\Delta$ state at 36000 cm^{-1} . In the region between 53000 and 57000 cm^{-1} , we have observed several broad bands. Some of them show a separation of about 140 cm^{-1} , corresponding to the spin-orbit coupling constant of the 2 ground state. The $\Delta G(\frac{1}{2})$ value of the ground state (2860 cm^{-1}) also appears in the spectrum. These diffuse bands could therefore be due to predissociated states of CCl.

ABSTRACT L-3

Multiphoton Ionization of the Trifluoromethyl Radical, CF_3

Michael T. Duignan,* Jeffrey W. Hudgens and Jeffrey R. Wyatt

Chemistry Division, Naval Research Laboratory
Washington, D.C. 20375

*NRC/NRL Research Associate

The technique of mass selective resonance enhanced multiphoton ionization (REMPI) has been successfully applied to the study of gas phase trifluoromethyl radicals. As in the case of the methyl radical, also recently investigated through REMPI, [1] CF_3 apparently does not fluoresce and all electronic absorptions are in the far or vacuum UV. We show that REMPI may be especially suited for detection and spectroscopic investigation of free radicals.

CF_3 radicals were generated by thermal pyrolysis of CF_3I in a resistively heated tantalum oven at $\sim 1000^\circ\text{C}$. A composite REMPI spectrum in the 415-490 nm region is presented in Figure 1. A series of thirteen multiplets sharply degrading to the red is immediately apparent. Features correlate well with those observed in single-photon VUV absorption [2] at $1/3\text{rd}$ the indicated wavelength. Several bands farthest toward the blue have not previously been attributed to CF_3 . The red edges of each multiplet are separated by an average spacing of 820 cm^{-1} in three-photons. The observed transition is almost certainly associated with promotion of the lone electron to a molecular Rydberg orbital (possibly $3p$). The 820 cm^{-1} spacing is then interpreted as ν_2' , the umbrella mode of the upper state. Extensive excitation of this mode is explained by the large conformational change (pyramidal \rightarrow planar) associated with the transition. The ionization potential of the CF_3 radical has been put at 9.25 eV by the photoionization technique [3]. We conclude that in the 415-490 nm region, $m/z\ 69$ (CF_3^+) ion current results from four-photon ionization via a three-photon resonant state of the trifluoromethyl radical.

Infrared multiphoton dissociation (IRMPD) of several substrates (CF_3I , CF_3Br , $(\text{CF}_3)_2\text{CO}$) was also employed for collisionless production of CF_3 .

Trifluoromethyl radicals from CF_3Br and hexafluoroacetone showed no resonance structure in their MPI spectra. CF_3 from IRMPD of CF_3I showed broader resonances and evidence of hot band formation, complicating the already congested REMPI spectrum of CF_3 . These results have been interpreted as evidence that parent molecules were pumped by the CO_2 laser to levels well above threshold before dissociation. Smaller fluences yielded insufficient radical concentrations. Excessive internal energy in daughter species is then seen as a fundamental limitation for collisionless IRMPD production of radicals suitable for spectroscopic investigation.

References

1. T. G. DiGiuseppe, J. W. Hudgens and M. C. Lin, J. Phys. Chem., 86, 36 (1982)
2. N. Basco and F. G. M. Hathorn, Chem. Phys. Lett., 8, 291 (1971)
3. C. Lifshitz and W. A. Chupka, J. Chem. Phys. 47, 3439 (1967)

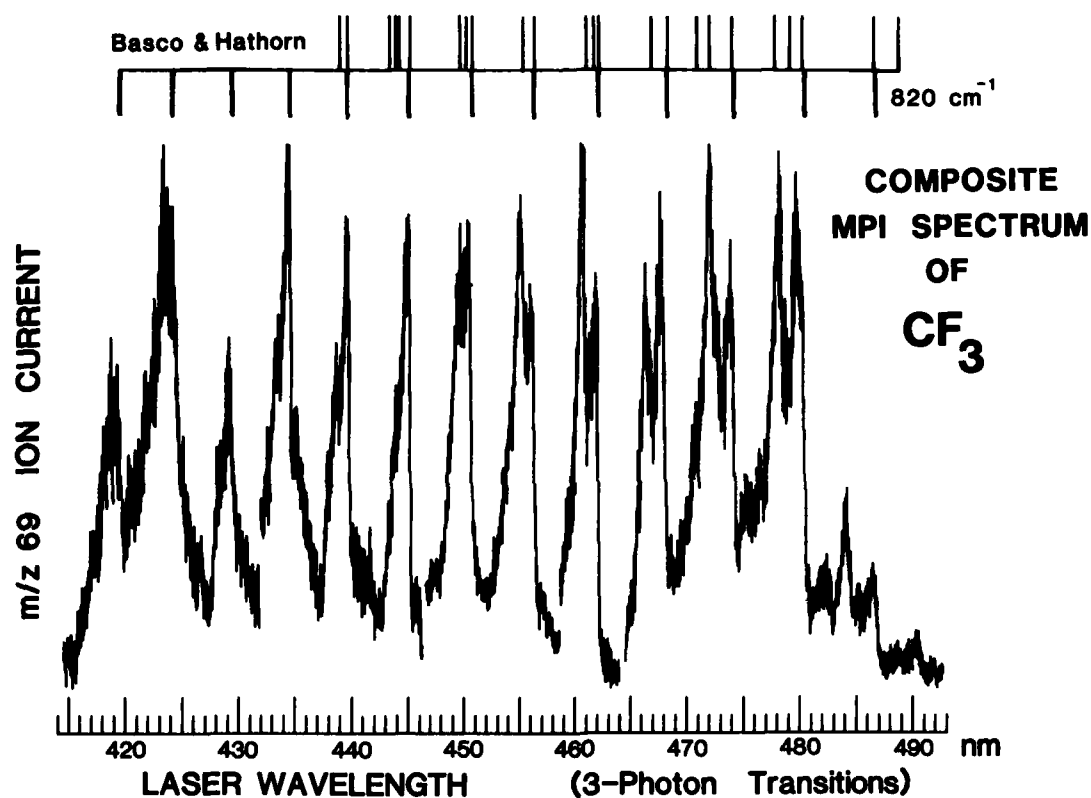


Figure 1. Composite REMPI spectrum of CF_3 . Five scans, using four different laser dyes were used and spectra are not normalized to laser power. Uppermost lines denote band heads observed in single-photon VUV absorption [2] at 1/3rd indiwavelength. The next lower lines mark a three-photon spacing of of 820 cm^{-1} .

ABSTRACT L-4

INTENSITY EFFECTS IN INFRARED MULTIPHOTON ABSORPTION AND DECOMPOSITION

by

D.K. Evans and Robert D. McAlpine

Physical Chemistry Branch
Chalk River Nuclear Laboratories
Chalk River, Ontario K0J 1J0

Infrared multiphoton absorption (MPA) and decomposition (MPD) have been widely studied during the last few years. For large molecules such as SF_6 an understanding of MPA and MPD has developed. Excitation of the molecule goes through three regimes: resonance, quasi-continuum and dissociative. Theory predicts that MPD will occur by the lowest thermodynamically available channel and the probability of decomposition will be nearly independent of laser intensity and depend only on laser fluence.

For smaller molecules, where the onset of the quasi-continuum is higher (~ 10 photons), one may see effects of laser intensity on decomposition probability or channel ratio. We have studied several small molecules, including monomethylamine, methyl alcohol and fluoroform, using a 2-60 ns pulse length CO_2 laser. With this laser, we are able to vary the pulse intensity while keeping the fluence constant. When we have irradiated small molecules, we have observed a dependence on laser pulse intensity for both MPA and MPD.

For monomethylamine, the MPA shows a dependence on laser intensity which is reflected in the decomposition yields

(molecules/pulse/kPa). At low pressure (0.667 kPa) there is a change in slope for average number of photons absorbed plotted against laser fluence at about 2 J/cm^2 for a 6 ns pulse but this does not occur until about 14 J/cm^2 for a 40 ns pulse.

A dependence on intensity is also seen in the relative decomposition yields of H_2 at 20 J/cm^2 and summarized in Table 1.

Table 1

Relative Laser Intensity	0.14	0.7	1
Pulse Length FWHM (ns)	40	9	6
Relative H_2 Yield (0.667 kPa)	0.19	0.64	1
Relative H_2 Yield (0.267 kPa)	0.035	0.45	1

There is a strong dependence on gas pressure for both MPA and MPD even at the very low number of collisions during the laser pulse (less than 4-5 for the longest pulse and highest pressure).

Methyl alcohol MPD depends on laser pulse intensity and pressure very strongly. MPD appears to follow one of two channels. Either H_2 and CO are products or the C-O bond is broken. The ratio of these channels as well as the probability of decomposition are sensitive to both pressure and laser pulse intensity. Experiments have covered an order of magnitude change in intensity at 80 J/cm^2 and pressures 0.267-1.33 kPa

(corresponding to $\sim 0.1 - 4$ collisions during the laser pulse).

CDF_3 has shown what appears to be an intensity dependence in MPA as well as a pressure dependence. Data using 2 ns and 6 ns FWHM pulses and various pressures up to 1.3 kPa show this effect.

It is possible to interpret these results in terms of the existing understanding of MPA and MPD by recognizing the relatively large number of photons which must be absorbed by these molecules to reach a quasi-continuum. Resonance must be maintained and slight mismatches can be overcome by mechanisms such as power broadening or by collisions which remove the small mismatch between photon energy and the molecular transition.

ABSTRACT L-5

GAS PHASE REACTIONS OF THE VINOXY RADICAL WITH NO AND O₂

H. H. Nelson and D. Gutman¹

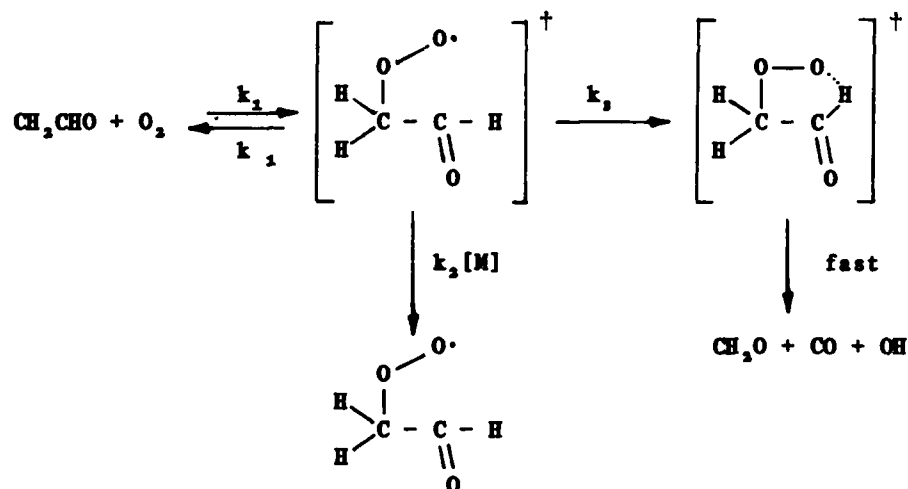
Chemistry Division, Naval Research Laboratory, Washington D.C. 20375

Alkoxy radicals, which are formed during the course of the gas phase oxidation of hydrocarbons, are important intermediates in combustion processes and photochemical smog. There have been few direct studies of alkoxy radical reactions due to the lack of a method for monitoring them in typical laboratory kinetic systems. Recently, however, Inoue, Akimoto and Okudu [2] have observed laser-induced fluorescence (LIF) spectra of the methoxy (CH₃O), ethoxy (CH₃CH₂O), and vinoxy (CH₂CHO) radicals. This has made possible several direct studies of reactions of methoxy and ethoxy [3].

We have used the technique of LIF to study the kinetics of the reactions of the vinoxy radical with O₂ and NO as a function of temperature and pressure. Vinoxy radicals are produced by 193 nm (ArF excimer laser) photolysis of vinyl methyl ether. Fluorescence is excited by a flash-lamp pumped dye laser operating at 337 nm which counterpropagates through a 5 cm stainless steel cross with 30 cm glass sidearms which serves as a reaction cell. The cell is enclosed in a convection oven for temperature control. Fluorescence, monitored at right angles to the laser beams, is isolated by glass filters and detected by a PMT. The resulting signal is averaged by a boxcar integrator and digitized and stored in a minicomputer. Vinoxy decays are observed by varying the time delay between the photolysis and probe laser pulses thus tracing out a pseudo-first-order decay curve. Gases used in the experiments are mixed and flowed through the cell at total flow rates of 0.5 l/min.

We have measured the second-order rate constants for the reactions of vinoxy radicals with O₂ and NO for a range of total pressures at four temperatures with both N₂ and SF₆ as the buffer gas. The data at room temperature with N₂ buffer gas, which are the most complete, are plotted in Figure 1. The vinoxy + NO reaction rate exhibits the fall-off behavior expected

for a three-body reaction but the vinoxy + O₂ rate constants approach a limiting second-order rate constant at low total pressure. We interpret these results as indicating an additional, pressure independent channel open to the vinoxy-O₂ adduct which is unavailable in the NO reaction.



We have probed the products of the vinoxy + O₂ reaction in two ways in order to test the postulated mechanism. In the kinetics apparatus, we use LIF detection at 306.5 nm to follow the build up and subsequent decay of the OH radical. OH is observed in the reaction of vinoxy + O₂ but not vinoxy + NO or N₂. In a separate investigation, we used a flow reactor coupled to a photoionization mass spectrometer [4] to observe other products of the vinoxy + O₂ reaction. The vinoxy radicals were produced by H atom abstraction from ethylene oxide using Cl atoms formed in the IR multiphoton dissociation of C₂F₄Cl. In the presence of O₂, a signal at m/e=30 was observed which we attribute to CH₂O production.

In summary, we have measured the kinetics of the three body reactions of the vinoxy radical (C₂H₃O) with O₂ and NO as a function of temperature and total pressure in the fall off region of both reactions. Based on the pressure dependence data and our observation of OH and CH₂O as products of the vinoxy + O₂ reaction, we postulate the existence of a pressure independent rearrangement and subsequent fragmentation of the vinoxy-O₂ adduct which is closed to the NO adduct.

REFERENCES

1. On sabbatical from the Department of Chemistry, Illinois Institute of Technology, Chicago, IL 60616
2. G. Inoue, H. Akimote, and M. Okuda, J. Chem. Phys. **72** ,1769 (1980)
G. Inoue and H. Akimote, ibid **74** ,425 (1980)
G. Inoue, Okuda, and H. Akimoto, ibid **75** ,2060 (1981)
3. N. Sanders, J. E. Butler, L. R. Pasternack, and J. R. McDonald, Chem. Phys. **48** , 203 (1980)
D. Gutman, N. Sanders, and J. E. Butler, J. Phys. Chem. **86** , 66 (1982).
4. I. R. Slagle, F. Yamada, and D. Gutman, J. Am. Chem. Soc **102** , 149 (1981)

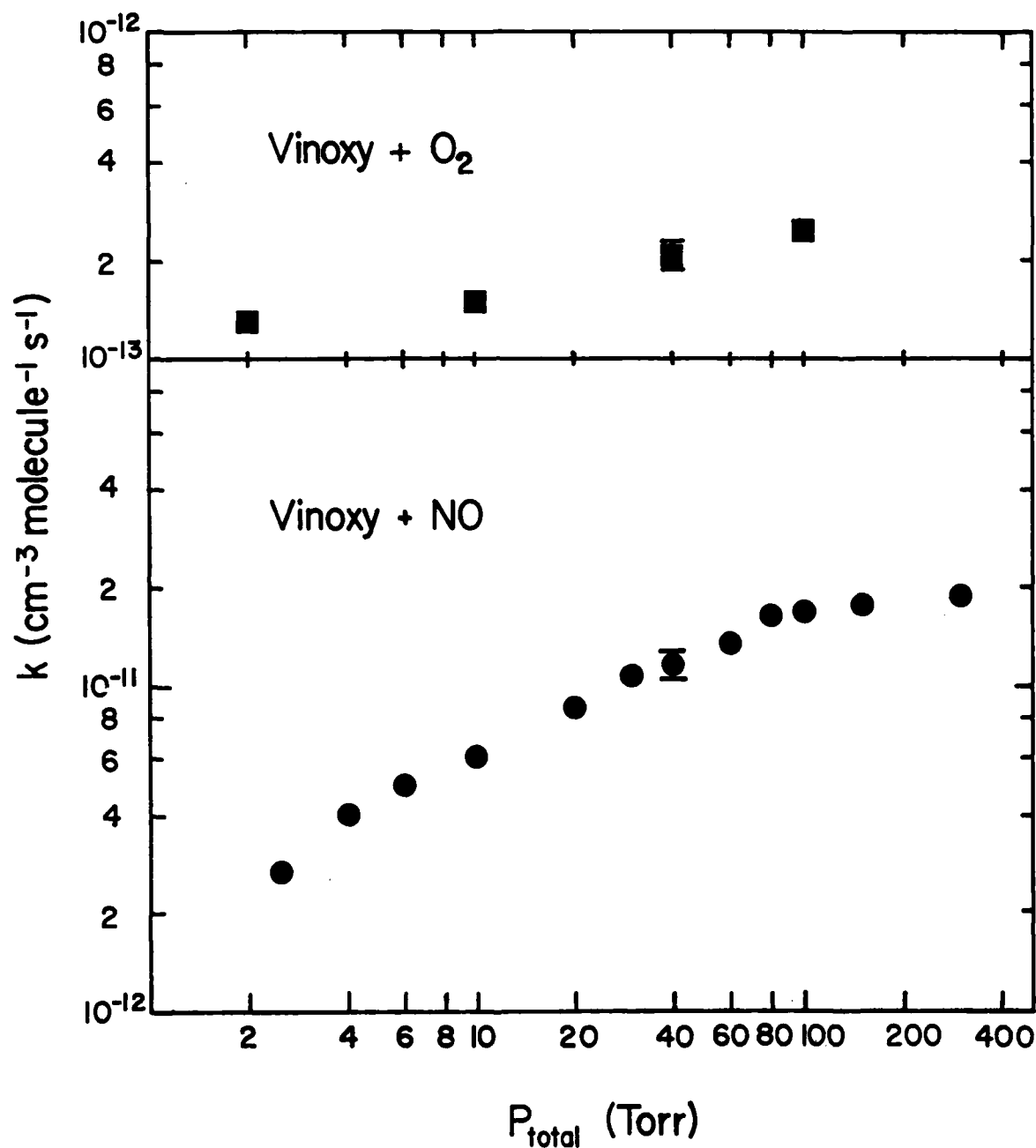


Figure 1. Second order rate constants as a function of total pressure ($M = \text{N}_2$) for the reactions of the vinoxy radical with O_2 (upper panel) and NO (lower panel) at 292K.

ABSTRACT L-6

Time-Resolved Resonance Raman Investigation of Photostimulated Electron Transfer from and to Trans-Stilbene

W. Hub, S. Schneider*, F. Doerr
Institut für Physikalische und Theoretische Chemie,
Technische Universität München, D8046 Garching

F. T. Simpson, F. Oxman, F. D. Lewis
Department of Chemistry, Northwestern University,
Evanston, Ill 60201

Abstract

Time-resolved resonance Raman (TR^3 -) spectroscopy is used to establish the formation and monitor the decay of trans-stilbene radical ions upon pulsed laser photolysis of solutions of trans-stilbene and different electron donors and acceptors, respectively. Kinetic schemes are discussed for various cases.

Quenching of singlet stilbene by tertiary amines, including ethyldiisopropylamine, results in moderately efficient formation of stilbene-amine adducts and reduced stilbene; whereas, quenching by Dabco (1,4-diazabicyclo [2.2.2] octane) is not chemically productive [1].

Our TR^3 investigation provide the first experimental evidence for the formation of the stilbene radical anion via photostimulated electron transfer. The difference spectra shown in figure 1 for singlet stilbene and ethyldiisopropylamine at various delay times between photolysis and probing pulse demonstrate the absence of persistent Raman active species. The frequencies and relative intensities of the prominent peaks correlate well with those previously reported for the radical anion of trans-stilbene [2,3]. Despite the lack of product formation, the same difference Raman spectrum is recorded with Dabco.

The time dependence of the stilbene anion radical signal intensity obeys a second order law with both amines (fig. 2).

*On leave at: IBM Research Laboratory, 5600 Cottle Rd., San Jose, Ca. 95193

In the presence of fumaronitrile, excited singlet trans-stilbene acts as electron donor thereby producing the trans-stilbene cation radical, whose resonance Raman spectrum is dominated by two bands at 1605 and 1281 cm^{-1} , respectively. In order to proof the above assignment, trans-stilbene was photolysed in the presence of 9-cyanoanthracene. The TR^3 -spectrum of the trans-stilbene cation radical produced hereby agrees with that recorded in the presence of fumaronitrile (fig. 3). Furthermore, the resonance Raman excitation spectrum (fig. 4) matches the transient optical absorption spectrum derived from flash photolysis experiments /4/.

- /1/ F. D. Lewis, T.-I. Ho, F. T. Simpson, J. Org. Chem. 46 (1981) 1077
- /2/ C. Takahashi, S. Maeda, Chem. Phys. Letters 28 (1974) 22
- /3/ L. R. Dosser, F. B. Pallix, G. H. Atkinson, H. C. Wang, G. Levin, M. Swarc, Chem. Phys. Letters 62 (1979) 555
- /4/ L. T. Spada, Ch. S. Foote, J. Amer. Chem. Soc. 102 (1980) 391

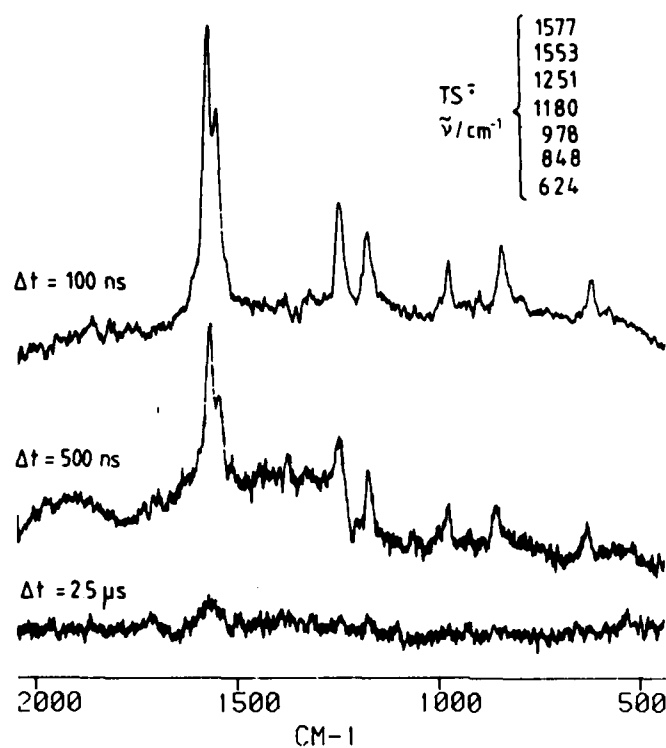


Figure 1: Resonance Raman spectra of trans-stilbene anion radical at various delay times.

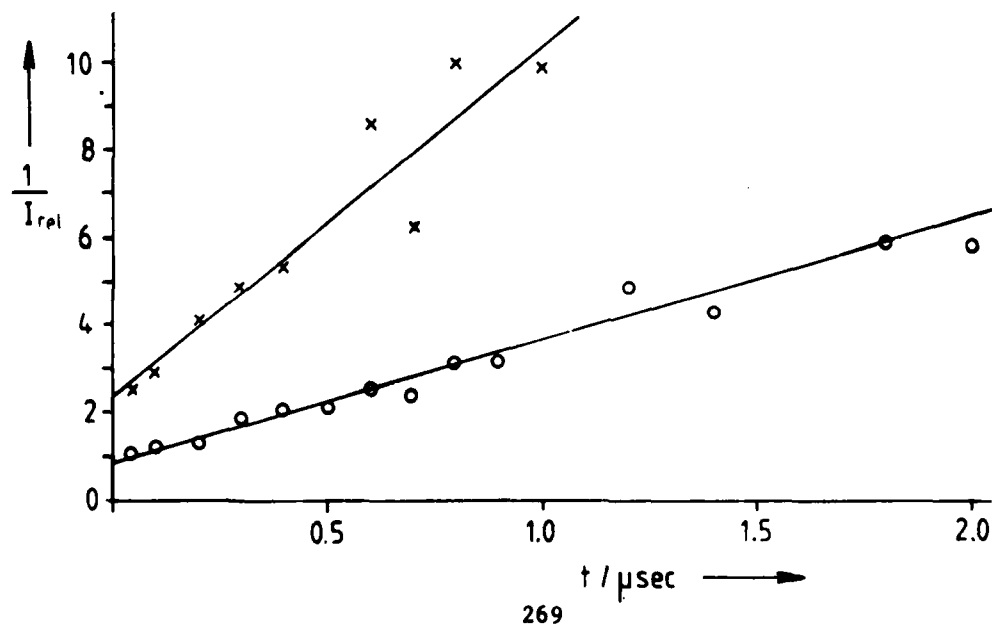
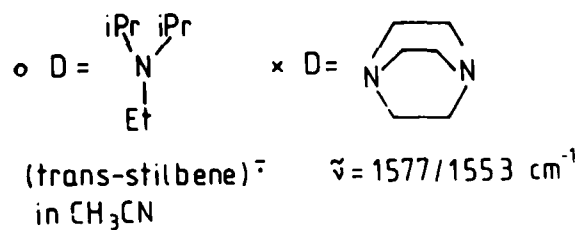


Figure 2: Time dependence of disappearance of trans-stilbene anion radical formed by different amines.

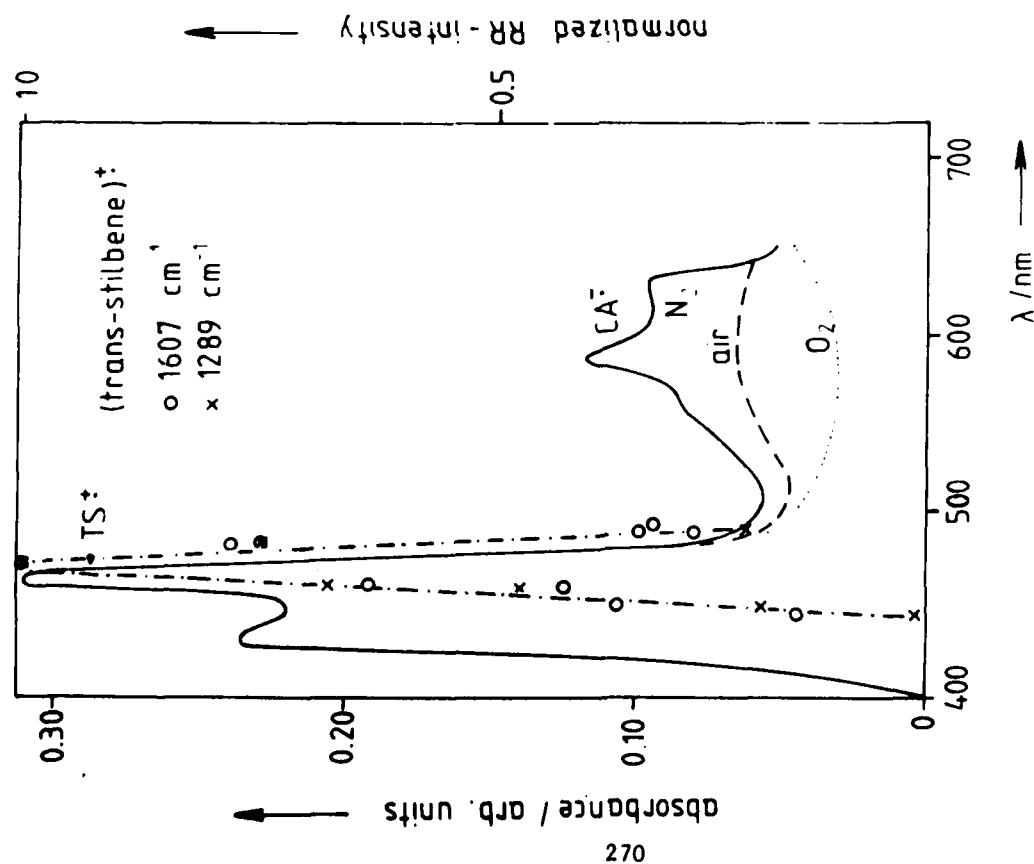


Figure 4: Resonance Raman excitation spectrum derived from the 2 major bands in comparison to the UV-absorption spectrum of trans-stilbene radical cation.

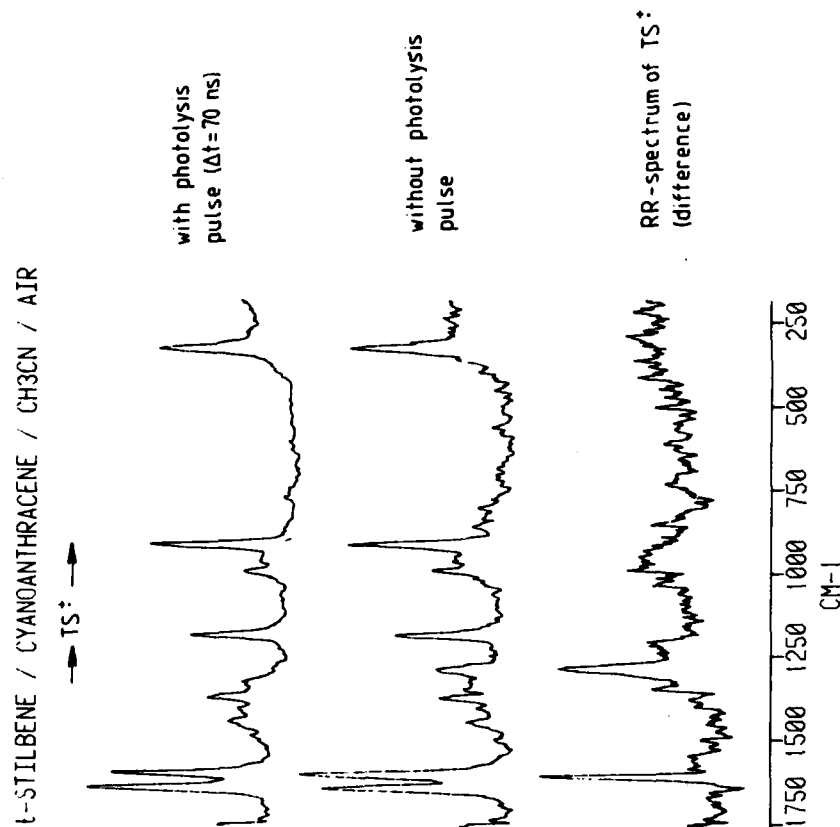


Figure 3: Resonance Raman spectrum of trans-stilbene radical cation.

ABSTRACT L-7

Comparison of the $O(^3P)$ + trimethylene sulfide reaction
with photolysis of trimethylene sulfoxide

D.L. Singleton
Division of Chemistry
National Research Council of Canada
Ottawa, Ontario, Canada K1A 0R9

Following the initial identification of an addition route in the reaction of oxygen atoms with methyl sulfide^{1,2} and with thiols,² quantitative information on the reaction channels was obtained.³ As an example, the $O+CH_3SCH_3$ reaction proceeds by attack at the sulfur atom to form CH_3SO and CH_3 , and although the reaction could be visualized as involving an excited dimethyl sulfoxide intermediate, stabilization of the sulfoxide was insignificant (<5% of the reaction, if it occurs at all) even at 1200 Torr.³

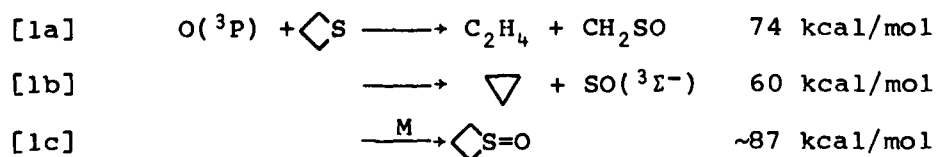
In the direct and mercury sensitized photolysis of trimethylene sulfoxide, a biradical intermediate has been postulated, formed by breaking a C-S bond.⁴ The reaction of $O(^3P)$ with trimethylene sulfide could generate the same biradical if the reaction proceeds by breaking a C-S bond as in $O+CH_3SCH_3$. The biradical would be formed with less excitation energy than in the photolysis experiments, and with spin multiplicity restrictions similar to those for mercury sensitized decomposition of trimethylene sulfoxide. These considerations led to the study of the O + tetramethylene sulfide reaction.

In the present work, oxygen atoms were generated by mercury photosensitized decomposition of N_2O at 254 nm in a cylindrical quartz cell at 25°C, as described in Reference 3.

After irradiation, the reaction mixture was divided into two fractions by distillation at -175°C , and each fraction was analyzed by gas chromatography. The products volatile at -175°C were N_2 and C_2H_4 ; the remainder were cyclopropane ($\text{c-C}_3\text{H}_6$) and propylene (C_3H_6). The amount of N_2 is a direct measure of the number of oxygen atoms formed, and the rates of formation of products relative to the rate of formation of N_2 , $\Gamma/\Gamma_{\text{N}_2}$, give the yields per oxygen atom.

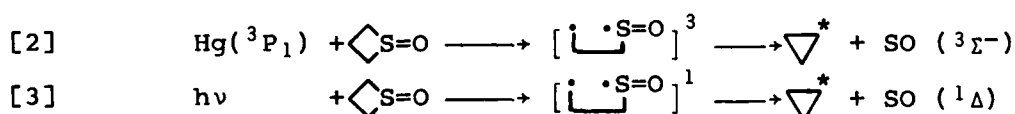
The ratio $\Gamma_{\text{C}_2\text{H}_4}/\Gamma_{\text{N}_2}$ and $\Gamma_{\text{c-C}_3\text{H}_6}/\Gamma_{\text{N}_2}$ are independent of the yield of N_2 (or irradiation time) as seen in Figure 1a, indicating that C_2H_4 and $\text{c-C}_3\text{H}_6$ are primary reaction products. Together they account for 90% of the oxygen atoms generated. A very small amount of propylene is formed, but in contrast, $\Gamma_{\text{C}_3\text{H}_6}/\Gamma_{\text{N}_2}$ increases with irradiation time, and at least some of it is probably formed in a secondary reaction. There is no significant pressure dependence in $\Gamma_{\text{C}_2\text{H}_4}/\Gamma_{\text{N}_2}$, but $\Gamma_{\text{c-C}_3\text{H}_6}/\Gamma_{\text{N}_2}$ appears to increase slightly at lower pressures, as seen in Figure 1b, in which the $\Gamma/\Gamma_{\text{N}_2}$ values have been corrected for very small contributions from mercury photosensitized decomposition of trimethylene sulfide.⁵

The reaction channels can be described as



where the $-\Delta H^\circ_{\text{rxn}}$ (25°) values are indicated for products in their ground states. To conserve electron spin, the major reaction channel 1a would produce CH_2SO in a triplet state, which may be just accessible by analogy with the triplet levels at ~ 74 kcal/mol for the isoelectronic SO_2 molecule. Reaction 1c, if it occurs, contributes less than 10% at these pressures.

The relative yields of the products $\text{C}_2\text{H}_4/\text{c-C}_3\text{H}_6/\text{C}_3\text{H}_6$ are: for reaction 1, 1/0.3/ ~ 0.004 ; for $\text{Hg}(^3\text{P}_1) + \text{Cyclo-S=O}$, 1/8/1 (Ref. 4); for $h\nu(254 \text{ nm}) + \text{Cyclo-S=O}$, 1/2/0.5 (Ref. 4). At lower wavelengths the relative yield of C_3H_6 increases. The photolysis studies were interpreted in terms of a biradical intermediate.



The excited cyclopropane, ∇^* , can rearrange to C_3H_6 ($E_{\text{act}} = 65.5$ kcal/mol) or be deactivated by collisions. Reaction 1 probably involves a biradical similar to that in reaction 2. The absence of any significant yield of C_3H_6 from excited $\text{c-C}_3\text{H}_6$ in reaction 1b could be ascribed to the smaller available excitation energy of ~ 60 kcal/mol in reaction 1b, compared with 86 kcal/mol in reaction 2 and in reaction 3 at 254 nm.

References

1. J.H. Lee, R.B. Timmons, and L.J. Stief, *J. Chem. Phys.*, **64**, 300 (1976).
2. I.R. Slagle, R.E. Graham, and D. Gutman, *Int. J. Chem. Kinet.*, **8**, 451 (1976).
3. R.J. Cvetanovic, D.L. Singleton, and R.S. Irwin, *J. Am. Chem. Soc.*, **103**, 3530 (1981).
4. F.H. Dorer and K.E. Salomon, *J. Phys. Chem.*, **84**, 3024 (1980).
5. H.A. Wiebe and J. Heicklen, *J. Am. Chem. Soc.*, **92**, 7031 (1970).

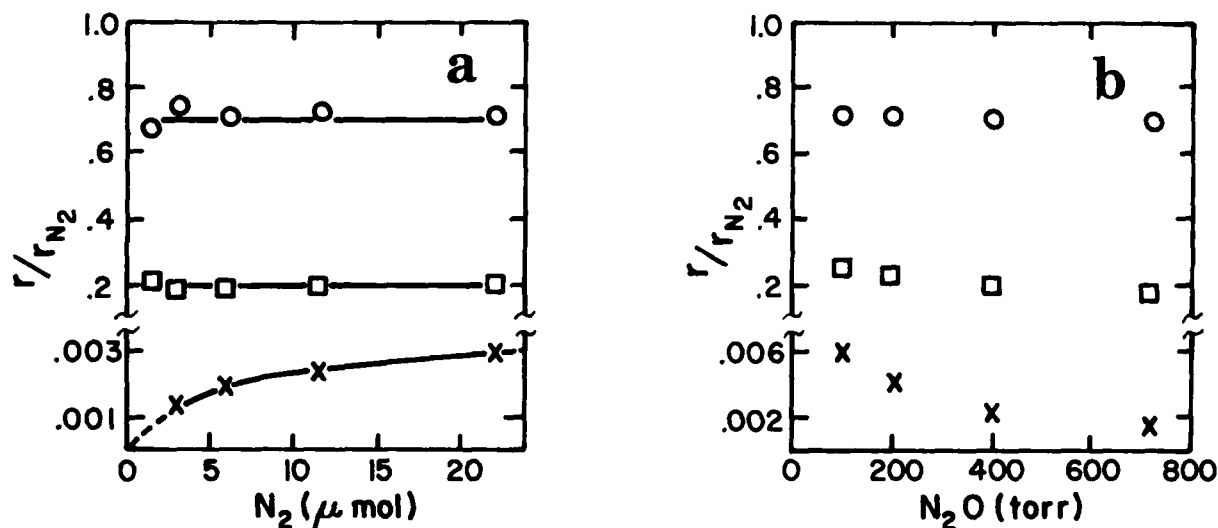


Figure 1. Rates of product formation relative to rate of N_2 formation, r/r_{N_2} , as a function of N_2 yield (Figure 1a, $N_2O=717$ Torr, $\angle S = 13$ Torr) and as a function of N_2O pressure (Figure 1b, $\angle S = 6$ Torr, N_2 yield = 6 μ mol). \circ C_2H_4 ; \square $c-C_3H_6$; \times C_3H_6

ABSTRACT L-8

PHOTODISSOCIATION PROCESSES OF SO_2 AT 1060-1330 \AA^*

Masako Sutoh, R. L. Day, and L. C. Lee

Department of Electrical and Computer Engineering

San Diego State University

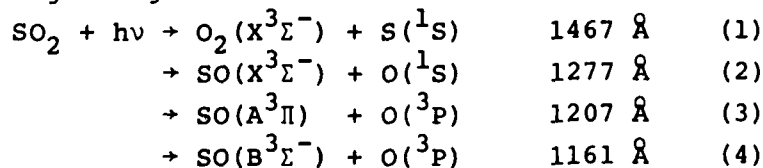
San Diego, California 92182

It is known that SO_2 is abundant in the interstellar medium and in the atmospheres of earth, Venus and Jupiter's Satellite (Io). Its photodissociation processes are important for understanding its role playing in the interstellar and atmospheric photochemistry. Emissions from the photofragments can also be used as a new technique to measure SO_2 concentrations in earth atmosphere.

The photoabsorption cross sections of SO_2 were measured in the 1060-1330 \AA region using synchrotron radiation as light source. More vibrational bands are observed in this measurement than the earlier data.¹ These vibrational bands are the Rydberg states converging to the SO_2^+ electronic states² of similar vibrational frequencies.

The fluorescence from photofragments of SO_2 were measured by two photomultiplier tubes (PMT) sensitive in the 1900-8000 \AA and 3000-8000 \AA regions. The fluorescence cross sections were determined by calibrating the fluorescence intensities against the $\text{OH}(A^2\Sigma^+ \rightarrow X^2\Pi)$ fluorescence from photodissociation of H_2O , for which the cross section is known.³ The photodissociation cross sections were measured at pressure less than 5 mtorr. Pressure dependence of emission intensity was measured to investigate the quenching effect of excited photofragments by SO_2 .

The threshold wavelengths for the photodissociation processes that possibly produce the fluorescence in the currently observed wavelength regions are estimated as follows:



where the dissociation energy $D_0(\text{SO}-\text{O})$ of 5.52 eV is used for the calculation. This dissociation energy is larger than the value given by Warneck et al,⁴ but is smaller than that by Okabe.⁵ Using Okabe's data, we calculate the ratios of the SO_2^* fluorescence rates

to the SO_2 absorption for the various absorption bands in the 2200-2300 Å region, and find that the dissociation starts at wavelengths larger than 2245 Å (5.52 eV) instead of 2200 ± 10 Å originally suggested by Okabe.⁵ The energy thresholds for (1) - (4) processes calculated for this dissociation energy are consistent with the current observations that the $\text{S}(^1\text{S} \rightarrow ^3\text{P})$ (4589 Å) and $\text{O}(^1\text{S} \rightarrow ^1\text{D})$ (5577 Å), $\text{SO}(\text{A}^3\Pi \rightarrow \text{X}^3\Sigma^-)$ (2400-4000 Å), $\text{SO}(\text{B}^3\Sigma^- \rightarrow \text{X}^3\Sigma^-)$ (3060-4000 Å) emissions appear at 1300, 1200, and 1160 Å, respectively.

In the 1200-1300 Å region, the cross sections measured by both PMT are the same. The apparent quantum yields are less than 0.5%. The fluorescence produced in this excitation wavelength region is most likely from the $\text{O}(^1\text{S} \rightarrow ^1\text{D})$ and $\text{S}(^1\text{S} \rightarrow ^3\text{P})$ transitions. These excited metastables are subject to fast quenching by SO_2 . Thus, although the apparent quantum yields are small, their true yields may be large.

In the 1200-1150 Å region, the cross sections for the fluorescence in the 1900-8000 Å region increases with decreasing excitation photon wavelengths. This indicates the occurrence of process (3). The quantum yield of visible emission increases suddenly around 1160 Å, which corresponds to the threshold wavelength of process (4).

For wavelengths shorter than 1140 Å, the fluorescence cross sections measured by both PMT show complex band structures similar to absorption cross section. The quantum yields are almost constant, which are 9% for the 1900-8000 Å region and 4% for the 3000-8000 Å region.

REFERENCES

- 1) D. Golomb, K. Watanabe, and F. F. Marmo, J. Chem. Phys. 36, 958 (1962).
- 2) J. H. D. Eland and C. J. Danby, Int. J. Mass Spectr. Ion Phys. 1, 111 (1968).
- 3) L. C. Lee, J. Chem. Phys. 72, 4334 (1980).
- 4) P. Warneck, F. F. Marmo, and J. O. Sullivan, J. Chem. Phys. 40, 1132 (1964).
- 5) H. Okabe, J. Amer. Chem. Soc. 93, 7094 (1971)

* This material is based upon work supported by NASA under contract no. NASW-3270 and by NSF under grant no. ATM-8205849. The synchrotron radiation facility at the University of Wisconsin is supported by NSF under grant no. DMR-77-21888.

ABSTRACT L-9

MULTIPHOTON LASER-INDUCED FLUORESCENCE STUDIES OF ATOMIC AND SIMPLE MOLECULAR SPECIES

by

J. J. Tice, M. J. Ferris, G. Loge, and F. B. Wampler
University of California
Los Alamos National Laboratory
P. O. Box 1663
Los Alamos, NM 87545

ABSTRACT

The recent availability of spectrally intense and continuously tunable lasers in the visible - uv region has opened up the possibility of time-resolved detection and studies of high-lying states of simple species via a multiphoton excitation and fluorescence scheme. For example, by exciting a two-photon allowed transition, an upper electronic state in the vacuum uv can be reached. The subsequent time-resolved fluorescence spectrum reveals useful spectroscopic and dynamic information concerning the excited state. Some recent works have demonstrated this scheme in the studies of atoms (O, N, Cl, H, and D)¹⁻³ and molecules (NO in the $A^2\Sigma^+$ state and CO in the $A^1\Pi$ state).⁴⁻⁶ In this paper we present the investigation of I atoms, CO molecules, and HS and DS radicals. The fragments are generated through photolysis of various molecular precursors by an excimer or a CO₂ laser and are probed in real-time via the two-photon laser-induced fluorescence (LIF) using a tunable dye laser.

The experimental apparatus is rather conventional, much like what was described previously.⁷ Briefly, the photodissociation laser is a modified Tachisto excimer laser operated either at 193 nm or 248 nm, or a Lumonics CO₂ laser. A Nd:YAG laser pumped dye laser system (tunable from 220 to 700 nm) is used as the two-photon LIF probe. All lasers are aligned to overlap spatially within the observation zone. The fluorescence signals are monitored at right angle to the laser beams with a detection system that consists of a 1/4-M monochromator, band-pass filters, signal collecting optics, and a PMT (RCA C31034 or C70128). The LIF signals are processed using boxcar averagers and a chart recorder for spectral scanning and transient digitizer and a mini-computer for temporal studies and signal averaging.

Figure 1 shows one example of the two-photon excitation and fluorescence scheme for the I atom. Both the $5^2P_{3/2}^{\circ}$ and $5^2P_{1/2}^{\circ}$ states of the I atoms are produced by the laser photolysis of CH₃I and CF₃I. Two-photon resonances to the $2^{\circ}D_{5/2}$ and $4^{\circ}D_{7/2}$ states and the $2^{\circ}D_{3/2}$ state near 150 nm are used for exciting the $2^{\circ}P_{3/2}^{\circ}$ and $2^{\circ}P_{1/2}^{\circ}$ levels, respectively. Fluorescence signals in the visible and near ir are observed from the two-photon excited states and states in their near proximity to some inter-

mediate opposite parity states. Figure 2 depicts such an excitation and fluorescence spectra. The excited state fluorescence lifetime, energy transfer and quenching rates, and relative two-photon transition probabilities are studied and will be reported. Furthermore, the $I(^2P_{3/2} \text{ and } ^2P_{1/2})$ branching ratio of the uv photodissociation of these molecular precursors will be discussed.

Investigations of the two-photon excitation of HS and DS species are also carried out to complement the recent single-photon LIF studies of HS⁸⁻¹⁰ and DS.¹¹ Figure 3 shows the two-photon excitation spectra of the ($A^2\Sigma^+ - X^2\Pi$) transition of HS and DS. Laser photolysis of ~50 mTorr of H₂S and D₂S is used to generate the species of interest. The allowed P, Q, R, O, and S branches are observed and identified over the 650-nm region. Their relative transition strengths are estimated and are compared to simple theories.

The $B^1\Sigma^+$ state of the CO molecule in the region of 115 nm is being excited from the ground $X^1\Sigma^+$ state via two-photon excitation. Figure 4 displays an excitation spectrum at 2 Torr of CO pressure. Time-resolved emission from both vibronic transitions of the $B^1\Sigma^+ \rightarrow A^1\Pi$ (450 to 700 nm) and the $b^3\Sigma^+ \rightarrow a^3\Pi$ (280 to 370 nm) are observed and resolved, with the triplet manifold becoming more prominent at higher CO concentrations. Experiments using both linearly and circularly polarized laser sources are also implemented to provide additional information concerning the symmetry of the excited intermediate states. Ionization measurements are made to explain the laser power dependence of the LIF signal through suspected competing channels such as multiphoton ionization and third harmonic generation.

REFERENCES

1. W. K. Bischel, B. E. Perry, and D. R. Crosley, Chem. Phys. Lett. **82**, 85 (1981).
2. J. Boker, R. R. Freeman, J. C. White, and R. H. Storz, paper Th58-1, Conference on Lasers and Electro-Optics (CLEO), (June 1981).
3. T. A. Miller, M. Heaven, J. White, J. Boker, and R. R. Freeman, paper FC3, Am. Phys. Soc. Meeting Dec. 1981.
4. R. G. Bray, R. M. Hochstrasser, and J. E. Wessel, Chem. Phys. Lett. **27**, 167 (1974).
5. R. A. Bernheim, C. Kittrell, and D. K. Veirs, Chem. Phys. Lett. **51**, 325 (1977).
6. S. V. Filseth, R. Wallenstein, and H. Zacharias, Optics Comm. **23**, 231 (1977).
7. J. J. Tiee, F. B. Wampler, and W. W. Rice, Chem. Phys. Lett. **65**, 425 (1979).
8. W. A. Hawkins and P. L. Houston, J. Chem. Phys. **73**, 297 (1980).
9. J. J. Tiee, F. B. Wampler, R. C. Oldenborg, and W. W. Rice, Chem. Phys. Lett. **82**, 80 (1981).
10. M. Heaven, T. A. Miller, and V. E. Bondybey, Chem. Phys. Lett. **84**, 1 (1981).
11. J. J. Tiee, M. J. Ferris, and F. B. Wampler, paper in preparation.

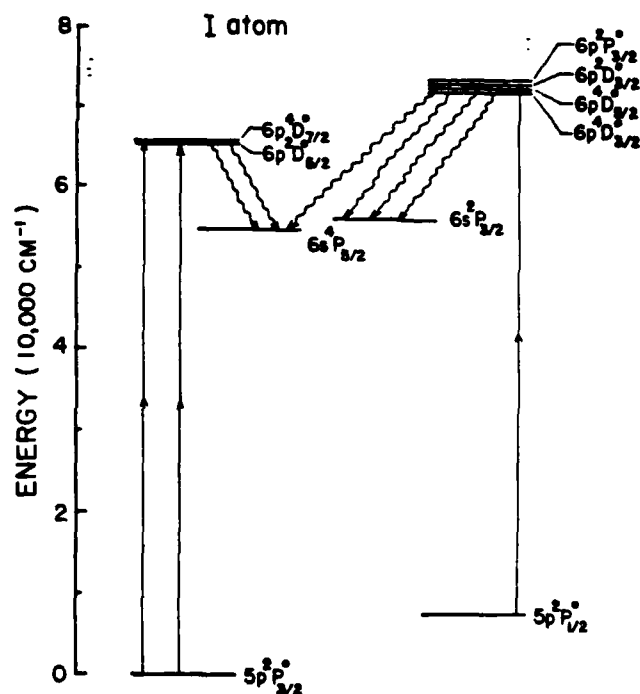


Figure 1

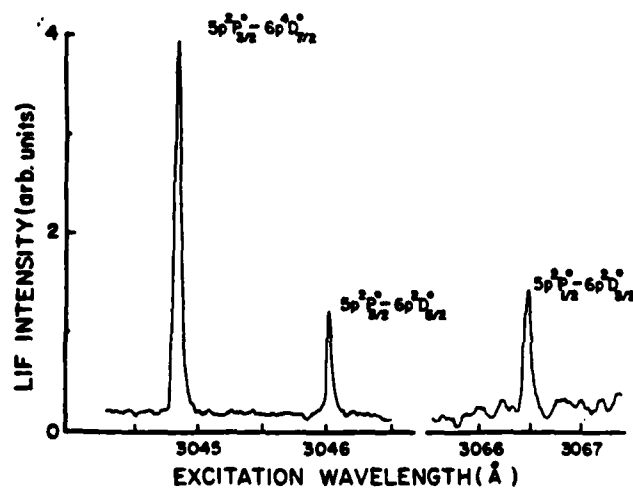


Figure 2a

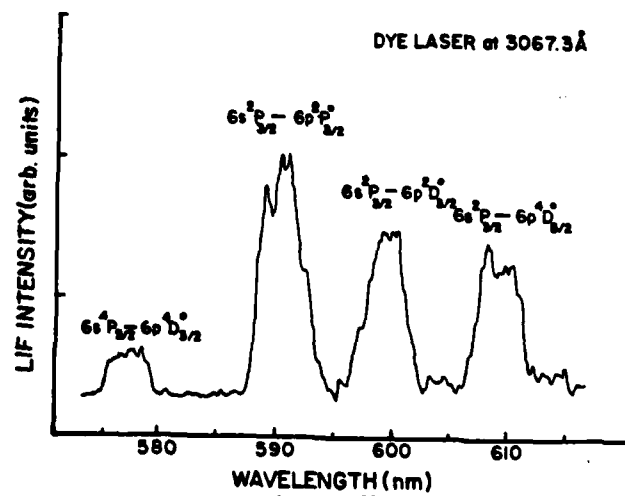


Figure 2b

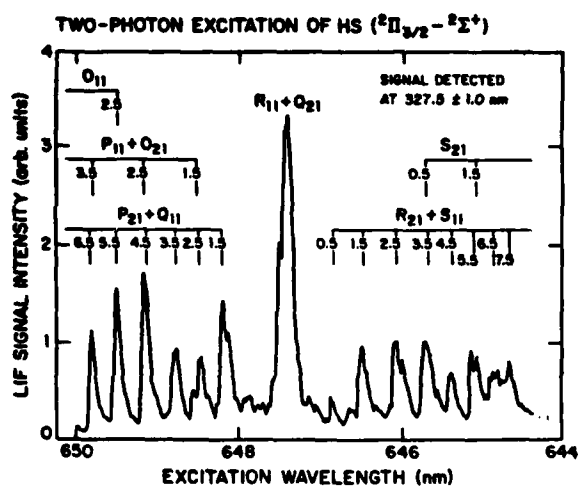


Figure 3a

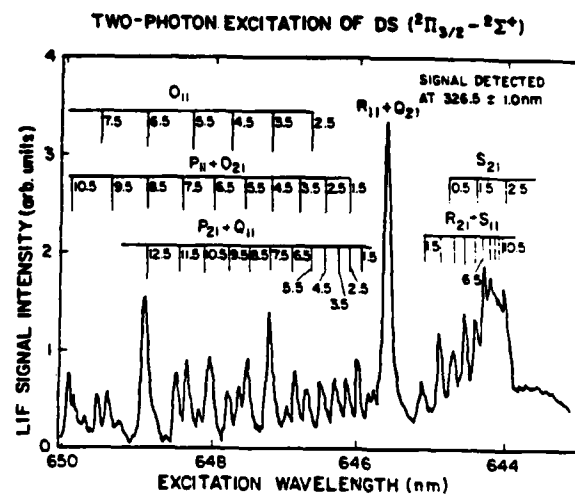


Figure 3b

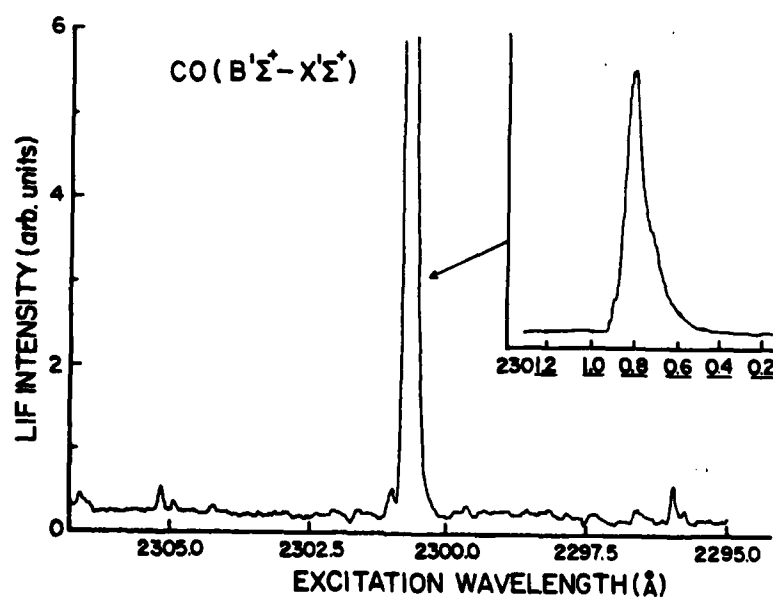


Figure 4

ABSTRACT L-10

Formation of Radiative Exciplex in the Quenching of Excited Uranyl Ion (UO_2^{2+*}) by Organic Molecule

Kunihiro Tokumura

Radiation Laboratory
University of Notre Dame
Notre Dame, Indiana 46556

In the physical (chemical) quenching of the lowest excited uranyl ion (UO_2^{2+*}) by benzene (ethanol), weak absorption and emission spectra were detected after the decay of the spectra due to UO_2^{2+*} . They were ascribed to the exciplex $[\text{UO}_2^{\delta-2+} \cdots \text{Q}^{\delta+}]^*$, with weak charge transfer interaction.

Introduction

For the effective physical quenching of UO_2^{2+*} by benzene (Bz), the intermediacy of the exciplex (excited state π complex), $(\text{UO}_2^{\delta-2+} \cdots \text{Bz}^{\delta+})^*$, was firstly proposed by Matsushima et al. [1]. For the chemical quenching of UO_2^{2+*} , while, they assumed [1] the exciplex intermediate formed through the charge transfer interaction of the n-electron of oxygen atom in ethanol. It was also assumed that the transfer of α -hydrogen of ethanol to UO_2^{2+} moiety in the exciplex results in the formation of U(V) species and ethanol radical (primary photo-products). Hitherto, however, no direct evidences have been reported for such exciplexes. A transient absorption (emission) technique was employed to detect them in this study.

Results and Discussion

In the UO_2^{2+} quenching by benzene ($1.1 \times 10^{-1} \text{ M}$) in CH_3CN at room temperature, the disparity in the decay rates of transient absorption and emission is clearly seen from the decay traces of Fig. 1. Also shown in Fig. 1 is the emission spectrum, remaining after the decay of the absorption, which is different from the well-structured spectrum of UO_2^{2+} . The formation of a radiative excited species was distinctly confirmed by the detection of its transient absorption (emission) with $\tau \sim 890 \text{ ns}$ at -40°C , remaining after the decay ($\tau \sim 35 \text{ ns}$) of the absorption (emission) of UO_2^{2+} . The double exponential decay traces are shown in Fig. 2, and the absorption and emission spectra of the long-lived species ($\tau \sim 890 \text{ ns}$) are shown, together with those of UO_2^{2+} , in Fig. 3. It was found that the initial concentration of the long-lived species increases with increasing benzene concentration. While no absorptions indicating the ground state interaction between UO_2^{2+} and benzene were

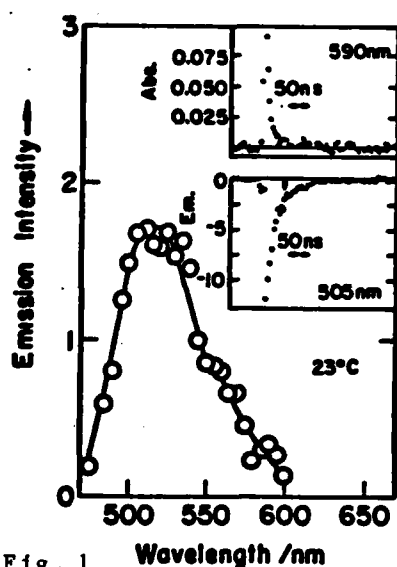


Fig. 1

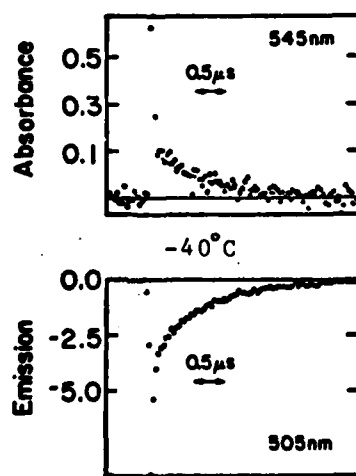


Fig. 2

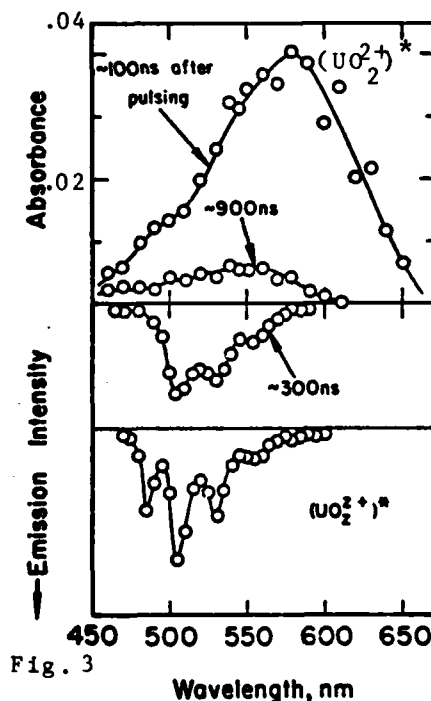


Fig. 3

detected at -40°C . These facts strongly suggest the formation of the long-lived excited species through the interaction between UO_2^{2+} and benzene. The excimer formation may be ruled out by no detection of such a long-lived excited species in the absence of benzene as a quencher. Then, it is reasonable to

identify the excited species as the exciplex, $(\text{UO}_2^{2+} \cdots \text{Bz})^*$. The emission spectra of the long-lived species in the UO_2^{2+} quenching by benzene and ethanol are not identical, as shown in Fig. 4. The fact strongly supports the formation of the exciplex, $(\text{UO}_2^{2+} \cdots \text{Q})^*$, in the quenching of UO_2^{2+} .

For the singlet exciplex between organic molecules, vibrationally unstructured emission spectrum usually appears on the red of the emission even at low temperature. The behavior of the emission spectrum of $(\text{UO}_2^{2+} \cdots \text{Q})^*$ at -40°C is very different from that mentioned above: 1) There still remains UO_2^{2+} -derived vibrational structure, which is less pronounced in comparison with that of UO_2^{2+} emission. 2) Small shift (820 cm^{-1}) occurs for 0-0 bands of the spectra of UO_2^{2+} and $(\text{UO}_2^{2+} \cdots \text{Q})^*$. These facts seem to imply the weak charge transfer interaction in the exciplex.

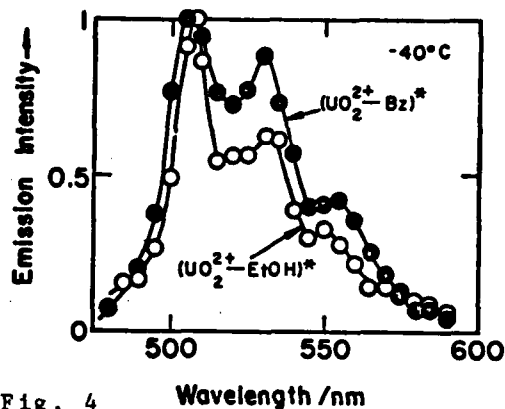


Fig. 4

Reference

- 1) R. Matsushima, J. Am. Chem. Soc., 94 (1972) 6010.

ABSTRACT L-11

ENHANCEMENT OF SMOG BY THE PRESENCE OF CHLORINE

By

G. Z. Whitten

Systems Applications, Inc.
San Rafael, CA 94903

Abstract

An evidently unique air pollution problem exists in the southeast Las Vegas Valley near the community of Henderson, Nevada. Air pollution problems have been identified in this area for over 30 years; however, it has only recently been discovered that on many winter mornings ozone exceeds the National Air Quality Standard of 0.12 ppm. Normal urban smog tends to be associated with ozone exceedances during summer and fall afternoons. However, in many areas of the country, it is not unusual for winter meteorological conditions to contribute to the low mixing depths and stable air that, in turn, produce high concentrations of primary pollutants. Thus, winter exceedances of CO and SO₂ standards are common. Winter exceedances of the secondary pollutant O₃, however, particularly in the morning, are rare indeed. Urban O₃ is typically produced by the proper combination of ultraviolet light, reactive hydrocarbons, and nitrogen oxides. The winter combination of cool temperatures, short days, late sunrises, and low solar angles cannot normally produce urban smog by 1000 to 1100 hours without extremely high levels of reactive hydrocarbons. Recent hydrocarbon samples of the early morning Henderson air, however, indicate typical (< 0.5 ppmC) rather than extremely high (> 10 ppmC) levels of reactive hydrocarbons.

One significant feature of the Henderson area is the presence of molecular chlorine that is released from a large titanium production facility. It is currently estimated that chlorine is released at a rate of about 250 pounds per hour from equipment that has been in operation for nearly 40 years. Recent ambient levels of Cl₂ in Henderson are approximately 0.1 to 0.2 ppm, with peak chloride levels as high as 0.7 ppm as chlorine. This initial modeling study involved the development of an atmospheric photochemical model that included the chemistry of chlorine; the study addressed whether low levels of sunlight combined with cool temperatures and normal urban hydrocarbon and nitrogen oxide precursor levels can produce morning urban smog in the presence of the chlorine levels described. This model was also used to determine the implications of controlling chlorine, hydrocarbons, or nitrogen oxide emissions.

This presentation describes the model that was developed to study the chlorine enhancement of urban smog and how this model was adapted for use in the Henderson area.

The Catalytic Action of Chlorine

Molecular chlorine acts as a powerful accelerator of the smog formation process because of its enhancement of free radical oxidation of hydrocarbons. Typically smog formation is driven by the oxidation of hydrocarbons by the hydroxyl radical, for example [in the Carbon Bond Mechanism (or CBM)]:



The resultant peroxy radical then oxidizes nitric oxide to nitrogen dioxide:



which photolyzes to form ozone:



The methoxy radical ($\text{MeO}\cdot$) reacts further:



The resultant hydroxyl radical may then oxidize more hydrocarbon to continue the process.

Because the lifetime of the hydroxyl radical in the atmosphere is short (< 1 sec), the generation of hydroxyl radicals is usually the limiting step in smog formation. In the presence of chlorine, however, another sequence occurs.



The generation of hydroxyl radicals in smog involves the photolysis of carbonyl hydrocarbons. At typical hydrocarbon and chlorine levels ($\text{RHC} \approx 0.4 \text{ ppmC}$, $\text{Cl}_2 = 0.1 \text{ ppm as chloride}$), chlorine may produce radicals at a rate that is two orders of magnitude greater than carbonyl photolysis. At these concentration levels, hydrocarbon oxidation may be as much as 800 times faster than without chlorine.

Model Results and Discussion

A simple trajectory model used in this study was built into the OZIPM computer code. This code was originally developed to test possible refinements to the EPA-EKMA; therefore, all of the original benefits associated

with the EPA-EKMA approach were available for this study. As a result, the computer code could be operated in the single trajectory mode or in the isopleth mode. In the single trajectory mode, information on the simulated diurnal behavior of all species utilized in the chemical mechanism can be obtained. The isopleth mode demonstrates graphically how simulated peak ozone concentrations respond to changes in the hydrocarbon and nitrogen oxide emission rates.

Because this study was preliminary, the purpose of the trajectory model runs was to try to bracket the actual situation. Rather than model it precisely. Close attention to detailed emissions and dispersion effects was beyond the scope of the present study.

The actual trajectory model results are presented in table 1 which shows that the model performed normally without chlorine present rather low levels of O_3 and PAN were generated by 1000 hours. After that time, the rate and timing of the inversion height movement became much more important relative to the chemistry; however, effects after 1000 to 1200 hours were not of concern in this study.

When chlorine was present in the model, both ozone and PAN increased substantially by 1000 hours. However, as more chlorine was added, the chemistry accelerated significantly so that the ozone showed sharper peaks at earlier times during the morning.

At the highest chlorine levels studied (0.5 ppm initial Cl_2), very high concentrations of peroxyacyl nitrate (PAN) (> 100 ppb) were generated. In fact, virtually all of the NO_x available showed up as PAN. In the 0.5 ppm Cl_2 simulation, by 0815 the PAN was up to 134 ppb (shown in table 1) and the NO_x was down to nearly 30 ppb. It should be noted that both aldehydes and PAN in the Carbon-Bond Mechanism represent the total concentration of all such compounds (i.e., PAN would be all peroxyacylnitrates). Therefore, comparisons of model predictions with observations should take into account that the CBM values should always be equal to, or greater than, observations; only specific aldehydes and PAN (i.e., peroxyacetylnitrate) would be observed.

Our base case emissions estimates indicate concentrations of 10 ppb to 43 ppb of PAN (with ozone from 0.14 to 0.22 ppm) for the chlorine concentration ranges of 0.02 to 0.2 ppm. Peak observed peroxyacetylnitrate concentration was 21 ppb, with ozone of 0.12 ppm. Considering the range of uncertainties in levels of emission and meteorological characteristics, the trajectory analysis seems to be a reasonable approximation.

TABLE 1. TRAJECTORY MODEL RESULTS

<u>Initial Cl₂</u> <u>(ppm)</u>	<u>HC Emissions</u> <u>Relative</u> <u>to Base Case</u>	<u>NO_x Emissions</u> <u>Relative</u> <u>to Base Case</u>	<u>O₃</u> <u>at</u> <u>1000</u> <u>Hours</u> <u>(ppm)</u>	<u>O₃</u> <u>Maximum</u> <u>1-hour</u> <u>Average</u> <u>(ppm)</u>	<u>O₃</u> <u>Time of</u> <u>Maximum</u>	<u>PAN</u> <u>(ppb)</u>
0	1	1	0.05	0.03	1000+	1
0.01	1	1	0.1	0.09	1000+	4
0.02	1	1	0.13	0.14	1045	10
	2	1	0.21	0.21	1030	17
	0.3	1	0.06	0.07	1100	4
	1	2	0.09	0.12	1230	5
	1	0.3	0.11	0.12	0915	9
0.05	1	1	0.18	0.18	0930	22
0.1	1	1	0.18	0.22	0900	43
	0.3	1	0.13	0.14	0900	44
	1	0.3	0.11	0.08	0845	22
0.2	1	1	0.13	0.21	0830	72
0.5	1	1	0.06	0.14	0815	134
	0.3	1	0.01	0.05	0745	146
	1	0.3	0.02	0.03	0815	56

ABSTRACT L-12

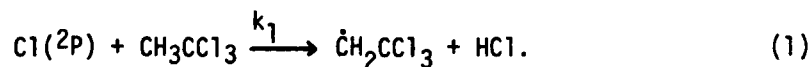
KINETICS OF $\text{Cl}(^2\text{P})$ REACTIONS WITH SEVERAL CHLORO-SUBSTITUTED ETHANES

P. H. Wine, D. H. Semmes, and A. R. Ravishankara

Molecular Sciences Group, Engineering Experiment Station,
Georgia Institute of Technology, Atlanta, Georgia 30332

Reactions involving abstraction of a hydrogen atom by ground state atomic chlorine, $\text{Cl}(^2\text{P})$, have been studied extensively by kineticists for many years. Early work,¹ involving the application of end product analysis techniques to the determination of relative rate coefficients for reactions with hydrogen, alkanes, and chlorinated alkanes, was motivated by the desire to test the ability of various theories to predict the rates of a series of related reactions.^{1,2} In recent years, the controversy concerning the extent of chlorine catalyzed destruction of stratospheric ozone³ has led to renewed interest in reactions which convert $\text{Cl}(^2\text{P})$ into the relatively stable reservoir species HCl . Modern "direct" kinetic techniques have been applied in numerous investigations of $\text{Cl}(^2\text{P})$ reactions with hydrogen-containing atmospheric constituents such as H_2 , CH_4 , HO_2 , H_2O_2 , and H_2CO . However, because stratospheric concentrations of chloroalkanes are low, their reactions with $\text{Cl}(^2\text{P})$ have received little attention. Two studies of $\text{Cl}(^2\text{P})$ reactions with chloromethanes have been reported,^{4,5} but no direct data exists for reactions of $\text{Cl}(^2\text{P})$ with any of the chloro-substituted ethanes.

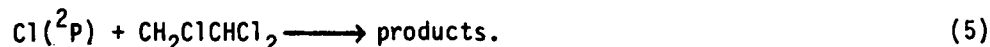
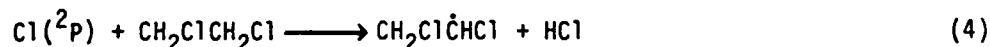
Atmospheric CH_3CCl_3 concentration profiles are employed as a "tracer" for OH. In deriving OH concentrations from CH_3CCl_3 measurement data, it is assumed that at altitudes where photolysis is unimportant (i.e. below ~ 20 km), reaction with OH is the only significant CH_3CCl_3 sink. At 220 K, a temperature typical of the upper troposphere and lower stratosphere, the reaction of CH_3CCl_3 with OH is quite slow - $k \sim 1.4 \times 10^{-15} \text{ cm}^3 \text{ molecule}^{-1} \text{ s}^{-1}$.^{6,7} Since the reaction of $\text{Cl}(^2\text{P})$ with ethane is very fast ($k \sim 5 \times 10^{-11} \text{ cm}^3 \text{ molecule}^{-1} \text{ s}^{-1}$ at 220 K) and $[\text{OH}] \sim 10^3 [\text{Cl}]$ at the tropopause, it has been suggested⁸ that reaction (1) could be an important CH_3CCl_3 sink. Hence we undertook to measure k_1 as a function of temperature:



The experimental apparatus was nearly identical to one employed previously in our laboratory to study the reaction of $\text{Cl}(^2\text{P})$ with CH_4 .⁹ $\text{Cl}(^2\text{P})$ was produced by 355 nm laser photolysis of Cl_2 ; its (pseudo-first order) rate of disappearance in the presence of varying amounts of CH_3CCl_3 was measured using time resolved resonance fluorescence detection. All experiments were carried out in the presence of 100 Torr of argon buffer gas, thus insuring that a thermal distribution of $\text{Cl}(^2\text{P})$ spin orbit states was maintained throughout the progress of the reaction.⁹ A sample of unstabilized CH_3CCl_3 was obtained from Dow Chemical. Gas chromatographic analysis showed the overall purity of the sample to be 99.88 mole %. Major impurities were $\text{CHCl} = \text{CHCl}$ (.061 mole %), $\text{CHCl}_2\text{CHCl}_2$ (.050 mole %), and CH_3CHCl_2 (0.13 mole %). The sample was further purified by vacuum distillation with only the middle fraction used in the experiments.

Reaction (1) was found to be much slower than expected. Furthermore, as more and more of the sample was withdrawn from the storage vessel for use in experiments, the measured rate coefficient continually decreased. Clearly, a significant fraction of the $\text{Cl}(^2\text{P})$ removal which was observed was due to a reactive impurity (probably $\text{CHCl} = \text{CHCl}$) whose mole fraction decreased as the sample was used up. Measurements using the final remaining aliquot of sample gave the following values for $k_1(T) + 2\sigma$ (in units of $10^{-14} \text{ cm}^3 \text{ molecule}^{-1} \text{ s}^{-1}$): 2.40 at 259 K, 3.68 at 298 K, and 7.64 at 356 K; these values represent upper limits for k_1 . Attempts to obtain a CH_3CCl_3 sample of higher purity were not undertaken because an experimental problem, absorption of resonance lamp radiation by CH_3CCl_3 , prevented extension of our measurements to higher CH_3CCl_3 concentration levels. It is clear even from the upper limits we report that reaction (1) is of no importance in atmospheric chemistry.

The reactivity trend observed in $\text{Cl}(^2\text{P})$ reactions with CH_3CH_3 and CH_3CCl_3 is qualitatively the same as is observed in OH reactions with these compounds, i.e. CH_3CH_3 is more reactive than CH_3CCl_3 . However, the reactivity difference is much larger in the case of $\text{Cl}(^2\text{P})$ reactions than in the case of OH reactions. At 298 K, $\text{Cl}(^2\text{P})$ reacts with CH_3CH_3 at least 1300 times faster than with CH_3CCl_3 , whereas the comparable OH reaction rate constants differ by a factor of 24. To better understand this unexpected result, we decided to extend our measurements to cover a series of reactions which "bridge the gap" between reaction (1) and the reaction of $\text{Cl}(^2\text{P})$ with CH_3CH_3 . The following reactions were investigated:



$\text{CH}_3\text{CH}_2\text{Cl}$ was obtained from Matheson gas products and had a stated purity of 99.7%; it was degassed repeatedly at 77 K before use. $\text{CH}_2\text{ClCH}_2\text{Cl}$ was Fisher reagent grade (no stabilizers added) and had an overall purity of ~99%. Special samples of unstabilized CH_3CHCl_2 and $\text{CH}_2\text{ClCHCl}_2$ were obtained from Dow Chemical. The overall purities of these samples, as determined by gas chromatographic analysis, were 99.75 mole % and 99.20 mole %, respectively. The major impurities in the CH_3CHCl_2 sample were $\text{CH}_3\text{CH}_2\text{Cl}$ (0.15 mole %), $\text{CHCl}=\text{CHCl}$ (0.07 mole %) and CH_2CCl_3 (0.015 mole %) while the major impurities in the $\text{CH}_2\text{ClCHCl}_2$ sample were $\text{CH}_2\text{ClCCl}_3$ (0.48 mole %) and $\text{CH}_2\text{ClCH}_2\text{Cl}$ (0.32 mole %). All liquid samples were purified by vacuum distillation with only the middle fraction used in experiments.

Reactions (2) - (5) were studied over the temperature range 257 - 426 K. Pseudo-first order conditions were employed in all experiments with the chloroethane in large excess over $\text{Cl}(^2\text{P})$. Kinetic complications resulting from regeneration of $\text{Cl}(^2\text{P})$ by fast secondary reactions were observed under some experimental conditions. However, it was always possible to isolate the desired reaction for study by either reducing the Cl_2 concentration or adding O_2 to the reaction mixture to scavenge intermediate free radicals.

The results are adequately described by the following Arrhenius expressions (units are $\text{cm}^3 \text{ molecule}^{-1} \text{ s}^{-1}$):

$$k_2 = (2.34 \pm 0.42) \times 10^{-11} \exp[-(310 \pm 56)/T]$$

$$k_3 = (8.19 \pm 1.84) \times 10^{-12} \exp[-(554 \pm 71)/T]$$

$$k_4 = (2.21 \pm 0.51) \times 10^{-11} \exp[-(793 \pm 73)/T]$$

$$k_5 = (4.88 \pm 1.41) \times 10^{-12} \exp[-(786 \pm 88)/T].$$

The errors in the above expressions are 2σ and represent precision only. At the lowest temperatures investigated, the observed dependence of the $\text{Cl}(^2\text{P})$ temporal profiles on $[\text{Cl}_2]$ suggests that the only secondary reactions which influenced the $\text{Cl}(^2\text{P})$ temporal profile were



where $\dot{\text{R}}$ represents the radical products of reactions (2) - (5). Rate coefficients for reactions (6) were estimated by modelling the observed non-exponential decays and found to lie in the range $(5-12) \times 10^{-14} \text{ cm}^3 \text{ molecule}^{-1} \text{ s}^{-1}$ ($T = 258 \pm 1 \text{ K}$).

Substitution of Cl for H in ethane and chloroethanes dramatically reduces the "abstractability" of remaining H atoms. At 298 K the rate constants per H atom for reaction of $\text{Cl}(^2\text{P})$ with ethane and the mono-, di-, and tri-chloroethanes are as follows (units are $10^{-12} \text{ cm}^3 \text{ molecule}^{-1} \text{ s}^{-1}$): CH_3CH_3 : 9.50¹⁰; $\text{CH}_3\text{CH}_2\text{Cl}$: 1.65; CH_3CHCl_2 : 0.319; $\text{CH}_2\text{ClCH}_2\text{Cl}$: 0.386; $\text{CH}_2\text{ClCHCl}_2$: 0.116; CH_3CCl_3 : <0.0123. Both A factors and activation energies are affected by Cl substitution, but the increase in E_{act} with increasing Cl substitution is the dominant factor controlling the observed decrease in reactivity. The activation energy for reaction (1) is found to be much larger than that for reaction (5). A similar result is obtained for OH reactions with CH_3CCl_3 and $\text{CH}_2\text{ClCHCl}_2$.⁶ These results suggest that substitution of Cl at the α position substantially increases the dissociation energy of β C-H bonds. On the other hand, both kinetic¹⁰ and thermodynamic¹¹ measurements demonstrate that substitution of Cl for H in methane decreases the dissociation energy of remaining C-H bonds. Some end product analysis data is available which suggests that Cl substitution also reduces the dissociation energy of α C-H bonds in chloroethanes. For example, photolysis of Cl_2 in the presence of $\text{CHD}_2\text{CD}_2\text{Cl}$ gives exclusively $\text{CHD}_2\text{C}^*\text{DCl}_2$ as a photo-product.¹² The lower activation energy and lower A factor we obtain for reaction (3) as compared with reaction (4) is consistent with the hypothesis that reaction at the α position is dominant. Direct measurements of kinetic isotope effects and product distributions are needed to unequivocally confirm this hypothesis.

Acknowledgements

We would like to thank D. Gerard and S. Collier of Dow Chemical for supplying us with analyzed samples of unstabilized CH_3CCl_3 , CH_3CHCl_2 , and $\text{CH}_2\text{ClCHCl}_2$. This work was supported in part by The National Aeronautics and Space Administration through a sub-contract from the Jet Propulsion Laboratory and in part by The National Science Foundation.

REFERENCES

1. G. C. Fettis and J. H. Knox, Prog. React. Kinet. 2, 1(1964), and references therein.
2. H. S. Johnston and P. Goldfinger, J. Chem. Phys. 37, 700(1962).
3. F. S. Rowland and M. J. Molina, Rev. Geophys. Space Phys. 13, 1(1975).
4. R. G. Manning and M. J. Kurylo, J. Phys. Chem. 81, 291(1977).
5. M. A. A. Clyne and R. F. Walker, J. Chem. Soc. Far. Trans. I 69, 1547(1973).
6. K. M. Jeong and F. Kaufman, Geophys. Res. Lett. 6, 757(1979).
7. M. J. Kurylo, P. C. Anderson, and O. Klais, Geophys. Res. Lett. 6, 760(1979).
8. P. J. Crutzen, private communication.
9. A. R. Ravishankara and P. H. Wine, J. Chem. Phys. 72, 25(1980).
10. "Chemical Kinetic and Photochemical Data for Use in Stratospheric Modelling," Evaluation No. 4, NASA panel for data evaluation, JPL publication 81-3, 1981.
11. S. Furuyama, D. M. Golden, and S. W. Benson, J. Amer. Chem. Soc. 91, 7564(1969).
12. D. C. McKean and B. W. Laurie, J. Mol. Struct. 27, 317(1975).

ABSTRACT L-13

UNKNOWN RADICAL SOURCES IN ENVIRONMENTAL CHAMBERS

William P. L. Carter, Roger Atkinson, Arthur M. Winer and James N. Pitts, Jr., Statewide Air Pollution Research Center, University of California, Riverside, CA 92521

An important aspect of the development of reliable computer models for the formation of photochemical smog is their validation against environmental chamber data. Although at the present time, detailed mechanisms of the NO_x -air photooxidations of certain alkanes, alkenes and aromatics are qualitatively or semi-quantitatively accurate, all such recent computer models have invoked the presence of uncharacterized sources of radicals in order to match computer-predicted time-concentration profiles with the data from environmental chamber experiments. In order to investigate this problem, a series of NO_x -air irradiations have been carried out in four different environmental chambers (ranging in volume from ~100 to 40,000 liters) at varying temperatures, humidities, pressures and reaction conditions. Trace levels (~10 ppb) of hydrocarbons (usually propane and propene) were included in the reaction mixtures to monitor hydroxyl (OH) radical levels from their relative rates of disappearance.

The validity of this hydrocarbon tracer technique in monitoring OH levels has been demonstrated by control experiments which showed that (1) essentially the same OH radical levels were obtained for experiments carried out under similar conditions but with differing sets of organic tracers; (2) the rate of NO oxidation in runs with high levels of added CO were consistent with OH radical levels monitored using the organic tracer technique; and (3) the addition of benzaldehyde, a known radical inhibitor, to tracer- NO_x -mixtures during irradiations suppressed the rates of consumption of the tracers by the expected amount, to within the experimental uncertainties.

Data from our tracer- NO_x -air experiments have shown conclusively that a continuous, NO_2 -dependent OH radical source exists during environmental chamber irradiations, with the OH radical levels after the first 30-60 minutes of irradiation being at least one order of magnitude higher than predicted by model calculations which do not include a continuous radical input flux. The radical fluxes required to account for these observed

radical levels were found to be proportional to light intensity, depended on the chamber employed and increased with increasing temperature, relative humidity, and NO_2 concentrations.

The dependence of OH radical levels (normalized for differences in light intensity) on the chamber employed and on chamber history, for a constant set of initial reactant concentrations, is shown in Table 1. It is evident that the radical source depends to some extent on the chamber material and on chamber conditioning; though the dependence is inconsistent with it being a "dirty chamber" effect. It is also interesting to note that the OH radical levels vary more from chamber to chamber of the same volume than they do with the size of the chamber, and that they do not decrease significantly in the Teflon chambers as the size is increased from ~6,400 l to ~40,000 l. This suggests -- but does not prove -- that although there clearly is a heterogeneous component to this effect which is influenced by the nature of the surface, there may also be a homogeneous, non-surface-dependent component to this radical source which may operate in the open atmosphere.

Table 1. Dependence of OH Radical Levels Observed in Comparable^a NO_x -Air Irradiations on Chamber Employed.

Chamber	Approx. Volume (l)	NO_2 Photolysis Rate k_1 (min^{-1})	[OH] (10^6 cm^{-3})	[OH]/ k_1 (normalized) ^b
Evacuatable (standard condition)	5,800	0.49	2.5 ± 0.2	(1.0)
Evacuatable (pumped and baked)	5,800	0.49	5.2	2.1
Small Teflon Bag #4	100	0.27	4.4 ± 0.7	3.2 ± 0.5
Small Teflon Bag #5	100	0.27	1.4	1.0
Indoor Teflon	6,400	0.45	0.65 ± 0.15	0.3 ± 0.1
Outdoor Teflon (new)	40,000	0.3 ± 0.05	0.6 ± 0.3	0.4 ± 0.2
Outdoor Teflon (used)	40,000	0.3 ± 0.05	1.0 ± 0.3	0.6 ± 0.2

^aInitial [NO] \approx 0.4 ppm; [NO₂] \approx 0.1 ppm RH < 10%, T = 303-308 K.

^bNormalized to ratio observed in the standard evacuatable chamber runs.

The radical input rates increase linearly with increasing NO_2 levels, but apparently do not depend on the amount of NO present. The linear dependence of the radical source on NO_2 levels was demonstrated by experiments with varying initial NO_2 levels, and also in experiments in which NO_2 was injected into the middle of the irradiation. This linear dependence on NO_2 concentration was also demonstrated by runs in which NO was converted to NO_2 by the injection of O_3 , where it was found that the addition of NO_2 caused no measurable change in the OH radical concentrations observed, despite the fact that reaction of OH radicals with NO_2 is the only significant radical sink in NO_x -air systems (after HONO reaches a photostationary state). Furthermore, in benzaldehyde- NO_x irradiations, addition of NO_2 actually caused the OH radical levels to increase.

It is interesting to note that the increase in the apparent radical input rate upon the addition (or formation) of NO_2 occurred within the 15 minute time resolution of our radical-monitoring gas chromatographic technique. The rapidity of this response of the radical input to changes in $[\text{NO}_2]$ provides further support to the idea (mentioned above) that the radical source cannot be exclusively heterogeneous.

The mechanism of this NO_2 -dependent radical source remains unknown, although the results of our experiments, reported here and elsewhere [1], allow a large number of possibilities to be ruled out. The proportionality of the radical source to light intensity means that off-gasing or heterogeneous formation of a photoreactive radical precursor cannot be the rate determining step. The fact that it does not depend on $[\text{NO}]$ rules out its being due to HONO formation from the $\text{NO} + \text{NO}_2 + \text{H}_2\text{O}$ reaction. There does not appear to be any significant excess conversion of NO to NO_2 associated with the radical source, suggesting that it is probably not due to initial formation of HO_2 or peroxy radicals, which ultimately give rise to OH radicals after reacting with NO .

Results of experiments where the spectral distribution of the photolizing light was varied rule out its being due to species such as oxygenates, O_3 , and peroxides, which photolyze at significantly shorter wavelengths than do HONO or NO_2 . In addition, as discussed in the subsequent presentation, it can be shown that HONO is also not the immediate radical precursor. Possible mechanisms for this unknown radical source, which may

represent a significant and previously unsuspected process which occurs in the atmosphere, continue to be investigated in our laboratories.

References

1. W. P. L. Carter, R. Atkinson, A. M. Winer and J. N. Pitts, Jr., Int. J. Chem. Kinet., in press (1982).

Acknowledgments

This work was supported primarily by California Air Resources Board Contract No. A1-030-32.

ABSTRACT L-14

THE KINETICS OF ALKYL RADICALS REACTING WITH OZONE

R. Paltenghi, E. A. Ogryzlo*, and Kyle D. Bayes†

Department of Chemistry, University of California, Irvine, California

*Department of Chemistry, University of British Columbia, Vancouver, B.C.

†Department of Chemistry and Biochemistry, University of California, Los Angeles, California

The rate constants for the reactions of methyl, ethyl, 1-propyl, 2-propyl, and t-butyl radicals with ozone have been measured with a photo-ionization mass spectrometer. The alkyl radicals were generated in the presence of ozone by photodissociating radical precursor molecules at 1933Å with an ArF excimer laser. The concentration of radicals was kept sufficiently low to avoid radical-radical reactions and to insure pseudo-first order conditions. The ozone concentration was measured by absorption at 2537Å. The absolute rate constant was then determined from the first-order decay rate plotted as a function of the ozone concentration.

The alkyl radical - ozone rate constants were studied at 2 Torr and 298K. The bimolecular rate constants are tabulated below.

Radical	$k/10^{-12} \text{ cm}^3 \text{ molec}^{-1} \text{ sec}^{-1}$
CH ₃	2.53 ± 0.23
C ₂ H ₅	23.2 ± 3.6
1-C ₃ H ₇	24.4 ± 4.8
2-C ₃ H ₇	46.5 ± 5.3
t-C ₄ H ₉	54.5 ± 4.8

The CH₃ + O₃ reaction rate constant has been measured over the temperature range 243-384K. The Arrhenius plot is quite flat and gives a small activation energy of about ½ kcal/mole [1].

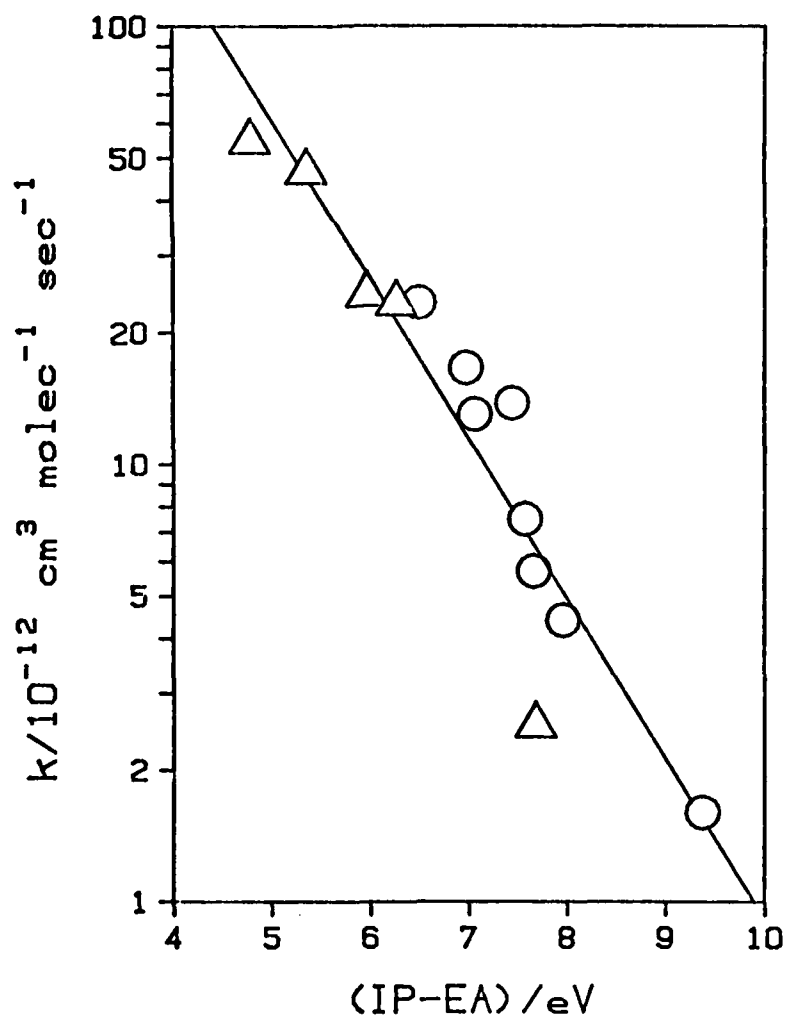
The rate constants are observed to increase monotonically with decreasing ionization potential of the radical. An approximately linear correlation is obtained when Log k is plotted against the ionization potential of the radical (IP) minus the electron affinity (EA) of O₃ [2]. A similar result has been observed for the high pressure limit recombination reactions of alkyl radicals with O₂ [3]. Figure 1 shows a plot of Log k versus IP - EA for the R + O₃ reactions (Δ) and the R + O₂ reactions (○). The observed trend is interpreted to indicate the influence of charge transfer from the radical to the ozone molecule.

The rate constants will be compared to theoretical predictions of the harpoon model [4] which describes electron transfer in terms of the interaction between ionic and covalent potential curves. In addition, a modification of the Adiabatic Channel Model [5] for application to bimolecular reactions will be discussed with respect to the R + O₃ reactions.

References

1. E.A.Ogryzlo, R.Paltenghi, and K.D.Bayes, *Int.J.Chem.Kinet.*, **13**,667(1981).
2. R.Paltenghi, E.A.Ogryzlo, and K.D.Bayes, *15th International Symposium on Free Radicals*, Ingonish Beach, Nova Scotia, Canada, 1981.
3. K.D.Bayes, T.M.Lenhardt, C.E.McDade, and R.P.Ruiz, *14th International Symposium on Free Radicals*, Ed, Y.Morino, I.Tanaka, E.Hirota, K.Obi, and S.Saito, Yamada Science Foundation, Japan, 1979.
4. J.L.Magee, *J.Chem.Phys.*, **8**,687(1940).
5. M.Quack and J.Troe, *Ber.Bunsenges.Phys.Chem.*, **81**,329(1977).

Figure 1.



ABSTRACT M-1

THE PHOTOPHYSICS OF UNIMOLECULAR REACTION:

PRODUCT V,R,T ENERGY DISPOSAL

H. Reisler and C. Wittig

Departments of E.E., Physics, and Chemistry

University of Southern California

Los Angeles, CA 90007, USA

It is now well established that the collisionless IR multiple photon excitation and dissociation (MPE and MPD) of molecules results in unimolecular reactions in which the vibrations behave "statistically." However, there exists no simple theory which describes the disposition of parent internal excitation into product degrees of freedom, and therefore, "joint" nascent distributions into all product degrees of freedom need to be monitored in order to determine the extent of parent excitation achieved via IR MPE. In addition, although it is now widely appreciated that the amount of parent vibrational excitation can be controlled with the laser intensity, no systematic studies are available which determine this dependence, and the levels of product excitation that can be achieved via IR MPE.

We have studied the nascent CN electronic, vibrational, rotational, and translational (E,V,R,T) state distributions following the simple bond fission unimolecular reaction



Excitation under collision free conditions is provided by IR MPE using the focused output from a CO₂ TEA laser, and therefore reaction occurs from a range of energies, E^\ddagger , centered at some value which is determined by the laser intensity. Nascent reaction products are detected by laser induced fluorescence (LIF), and by exciting the $\Delta v=0, -1$, and -2 sequences of the $B^2\Sigma + X^2\Sigma$ system, rotational distributions can be determined for $v''=0, 1$, and 2 with no interference. Product translational energies are estimated by monitoring LIF intensities as a function of the delay between the onsets of the CO₂ and dye laser pulses. We find that product V,R,T excitations can be described by temperatures, albeit different ones, and that modified statistical theories are required to explain the observed distributions. Our results can be reconciled with a statistically based model, in which the CN vibration acts as a thermometer of parent excitation, and where nuclear motions, including vibrations as well as motions not influenced by potential energy, are in equilibrium at the transition state.

As the laser intensity is varied between 3 and 150 J cm^{-2} , large changes in product V,R excitations are observed, which result from changes in the level of excitation of the parent molecule. The ultimate level of excitation achieved by the IR laser pumping depends both on the fluence and on the peak intensity of the laser. The majority of the molecules dissociate from vibrational levels where the net laser pumping rate is equal to the unimolecular dissociation rate.

At fluences 3-20 J cm⁻², the CN(X) rotational temperature increases monotonically from 500 to 1200K with increasing fluence, and its appearance time becomes shorter. At fluences 30-150 J cm⁻², the rotational and vibrational temperatures do not increase further and are T_R=1200K and T_V=2400K. The observed "saturation" in product excitation is interpreted as a pulse shape effect, since at high fluences most of the molecules that dissociate do so during the early, rise portion of the CO₂ laser pulse, and the sample is depleted before the CO₂ laser pulse reaches its peak intensity. The experimental observations are simulated by a computer model, which has been extended to include the laser pulse shape effects. Our results, which show that the slow rise of the CO₂ laser pulse imposes a limitation on the level of excitation in the parent molecule, explain the low internal excitations observed in many IR MPD products, as compared with those achieved via uv and visible laser dissociation.

We will summarize all of the results which have appeared in the literature to date, and compare them to estimates based on the model discussed above. Also, recent experimental results of laser excited unimolecular reactions of species of the form RNO will be presented and discussed in the context of the above.

ABSTRACT M-2

SUPERFLUORESCENCE FROM CHEMICALLY PUMPED IODINE MOLECULES

F. J. Comes, K.-H. Stephan-Rossbach

Institut für Physikalische und Theoretische Chemie,
Frankfurt am Main, Germany

Superfluorescence in the visible has been observed to occur in the photolysis of CF_3I and $n\text{-C}_3\text{F}_7\text{I}$ at 266 nm. The photolysis products $\text{I}(^2\text{P}_{3/2})$ and $\text{I}^*(^2\text{P}_{1/2})$ recombine in the presence of the parent molecules forming $\text{I}_2^*(\text{B}^3\Pi)$. The stabilization is shown to proceed via two mechanisms: the radical mechanism and the energy transfer mechanism. Most of the observed Laser emission is from the vibrational state $v' = 55$, which indicates that the molecules have lost a minimum of 221 cm^{-1} of their internal energy. This energy loss is interpreted as the equivalent of a van der Waals bond which has been formed in the collisional stabilization of the diatomics.

ABSTRACT M-3

SURFACE PHOTOCHEMISTRY: THE PHOTOPHYSICS OF PYRENE ADSORBED ON SILICA GEL, ALUMINA AND CaF_2 .

Richard K. Bauer, Paul de Mayo,
William R. Ware and Kam C. Wu

Photochemistry Unit
Department of Chemistry
The University of Western Ontario
London, Ontario, Canada N6A 5B7

The occurrence of inter- and intramolecular motion or aromatic hydrocarbons on dry silica gel has been demonstrated.¹ Evidence includes (a) the observation of dimerisation of acenaphthylene in static and agitated systems to give cis and trans isomers; (b) the quenching and sensitization of the dimerisation of acenaphthylene (c) the dimerisation of cyanophenanthrene (d) the quenching of pyrene emission by 2-halonaphthalenes, with a linear plot of τ_0/τ versus halonaphthalene concentration (e) the equilibration of adsorbed pyrene as regards preferred sites, from a study of the emission decay characteristic, as also those of anthracene and cyanophenanthrene (f) the direct, (static) observation of pyrene diffusion by observation of translation movements of its emission (g) a direct, kinetic, demonstration of intergranular movement of adsorbed acenaphthylene and pyrene between grain of silica gel of different sizes and (h) the demonstration, by the fluorescence quenching of pyrene, of the intergranular motion of 2-bromonaphthalene. These studies provide the first qualitative data for diffusion rates on silica gel, that from (b) and (d) being in agreement, and reveal the possibilities for photochemical and photophysical studies in the adsorbed state.

In this paper a detailed study of the emission, excitation spectra and fluorescence decay of pyrene adsorbed on silica gel, porous Vycor, alumina and calcium fluoride is reported. Monomer emission and a longer wavelength broad band emission (neither decaying with single exponentials) was observed on silica. The excitation spectrum of the broad band emitter was red-shifted in comparison with the absorption responsible for the monomer emission. These, and other, results are interpreted as indicating the existence of bimolecular ground state pyrene association.

The effect of coadsorbates (glycerol, n-decanol) was examined: at high coverage the monomer emission approaches a single exponential and the long wavelength emission deconvolutes with a double exponential with a negative preexponential term indicating true excimer formation. Adamantanol did not have this effect.

The picture that emerges from these results can be summarized as follows. The distribution of pyrene molecules on the surfaces in question is not random: there appear to be preferred sites. The result is an inhomogeneous distribution which yields a multicomponent decay. Strong evidence exists for the formation of a very weakly bound ground state bimolecular association product, particularly on silica gel, and the data suggest associating this phenomenon with particular sites at which an interaction stabilizes this bimolecular association. The data also indicate that this phenomenon may be related to some peculiarity of the hydrogen-bonding interaction with the

π -system of the aromatic hydrocarbon. It is suggested that the static and highly asymmetric interaction may cause pyrene to behave in a different manner than in hydroxylic solvents where the interactions are rapidly averaged and, on the time scale of the lifetime of pyrene, the interactions are symmetric over the whole of the π -system.

If the silanol groups are blocked by a long chain alcohol and polyalcohol, the pyrene molecules appear forced to be adsorbed in areas of weaker interactions where the tendency to form the bimolecular ground state arrangement is diminished. The mobility during the lifetime also appears to be greatly enhanced and dynamic excimer formation is then possible.

1. R.K. Bauer, R. Bornstein, P. deMayo, K. Okada, M. Rafalska, W.R. Ware and K.C. Wu. Journ. Am. Chem. Soc. In press.

ABSTRACT M-4

Anomalies in IR Multiphoton Excitation of Cl_2CS : Theoretical Insight

D. M. Brenner

Department of Chemistry, Brookhaven National Laboratory

Upton, New York 11973

M. W. Spencer and J. I. Steinfeld

Department of Chemistry, M.I.T.

Cambridge, Mass. 02138

The photophysics of IR multiphoton excitation (IRMPE) of the ladder has been investigated in thiophosgene, Cl_2CS . Theory predicts¹ that absorption in this region is a coherent phenomenon in which detunings from the laser frequency due to anharmonicity are compensated by power broadening and rotational energy. The time evolution of the populations of the pumped mode-ladder is given by a set of optical Bloch equations.² When the dephasing time of the laser is short ($< 10^{-9}$ s) as is typical of most CO_2 lasers, steady state populations in the ladder are achieved rapidly and can be measured directly by IR-visible double resonance. Under these conditions, however, distinctions between a coherent and an incoherent interaction cannot be determined.

Populations of the ladder have been determined for a number of conditions: effusive and supersonic beams; higher pressures (1-300 mTorr); mixed gases. The following observations have been made:

1. Under both effusive and supersonic beam conditions, a nearly homogeneous bleaching of all rotational states is observed (Figure 1). The extent of pumping depends on rotational temperature, i.e., Boltzmann populations of rotational states.
2. Under collision-free conditions, depletion of the ground state is efficient and has a CO_2 laser-frequency dependence uncorrelated with the low energy IR absorption spectrum (see Figure 2). This implies that the oscillator strength is not derived primarily from the $0 \rightarrow 1$ transition.
3. Depletion of the ground state shows no obvious threshold-fluence effects and has a $I^{1-1.5}$ dependence at low fluence, even though depletion is due to a multiphoton process. These characteristics are probably the consequence of resonantly enhanced absorption.

4. At higher pressures (5-300 mTorr) of pure Cl_2CS , the depletion depends inversely on pressure. This quenching behavior has an unusually large cross section. In the presence of other gases, similar behavior is observed (Figure 3) and correlates with polarizability and dipole moment.
5. Hot bands of the $2\nu_4$ ladder are not populated under collision-free conditions when $\omega_{\text{CO}_2} = 944 \text{ cm}^{-1}$ -- only when collisional perturbations are present. This is explained either by the fact that $2\nu_4$ is not the pumped mode (see Figure 2) or the ladder is strongly coupled to the quasicontinuum as suggested by model calculations.

Insight into these somewhat surprising results is obtained from solution of the optical Bloch equations for an N-level system. The experimental results are to a large extent attributed to the very high density of rotational states ($> 1000 \text{ states/cm}^{-1}$) in Cl_2CS . These states provide a large number of ladders by which molecules are moved efficiently and irreversibly from the ground state to the quasicontinuum. Increases in laser detunings or reduction of the overall oscillator strength have the same attenuating effect as the observed pressure studies on the ground state depletion.

Because of the relatively high density of rovibronic states at energies $> 4000 \text{ cm}^{-1}$, we have postulated that collision-induced perturbation of rovibronic levels leading to vibrational dephasing may be the underlying explanation for our observations (see 4 above). This mechanism can be related to the theory of radiationless transitions but occurs in the same electronic state and is collision-induced. In the theory of IRMPE¹, it would lead to enhanced anharmonic interaction with background states which is approximated by Fermi's Golden Rule and related inversely to the rate of absorption.

Thus it is postulated that long range collisions induce vibrational mixing in which essentially infrared inactive background states become mixed with the pumped mode. This causes oscillator strength to be spread over a larger number of states, only a fraction of which are then able to interact at the given laser frequency because of detunings. The overall effect is to reduce the oscillator strength for the multiphoton

transition. These energy-mixing collisions are akin to a T_1 -relaxation mechanism which has the net affect of decreasing the probability of absorption.

1. H. W. Galbraith and J. R. Ackerhalt in Laser-Induced Chemical Processes, edited by J. I. Steinfeld (New York: Plenum, 1981), pp. 1-44.
2. J. Stone, E. Thiele, and M. F. Goodman, *J. Chem. Phys.* 59, 2909 (1973).

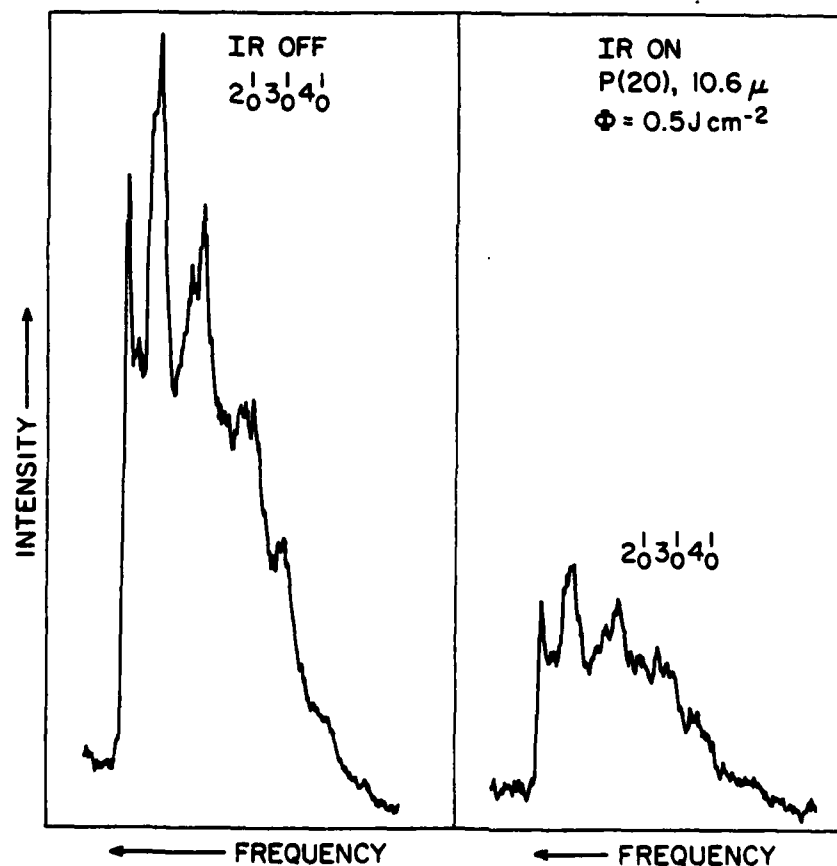


Figure 1. Laser excitation spectrum of the $2_0^1 3_0^1 4_0^1$ band at 300°K showing the effect of IR laser pumping on populations of the vibrationless level (000000). The fluence ϕ is 500 mJ cm⁻²; the IR frequency, 944 cm⁻¹.

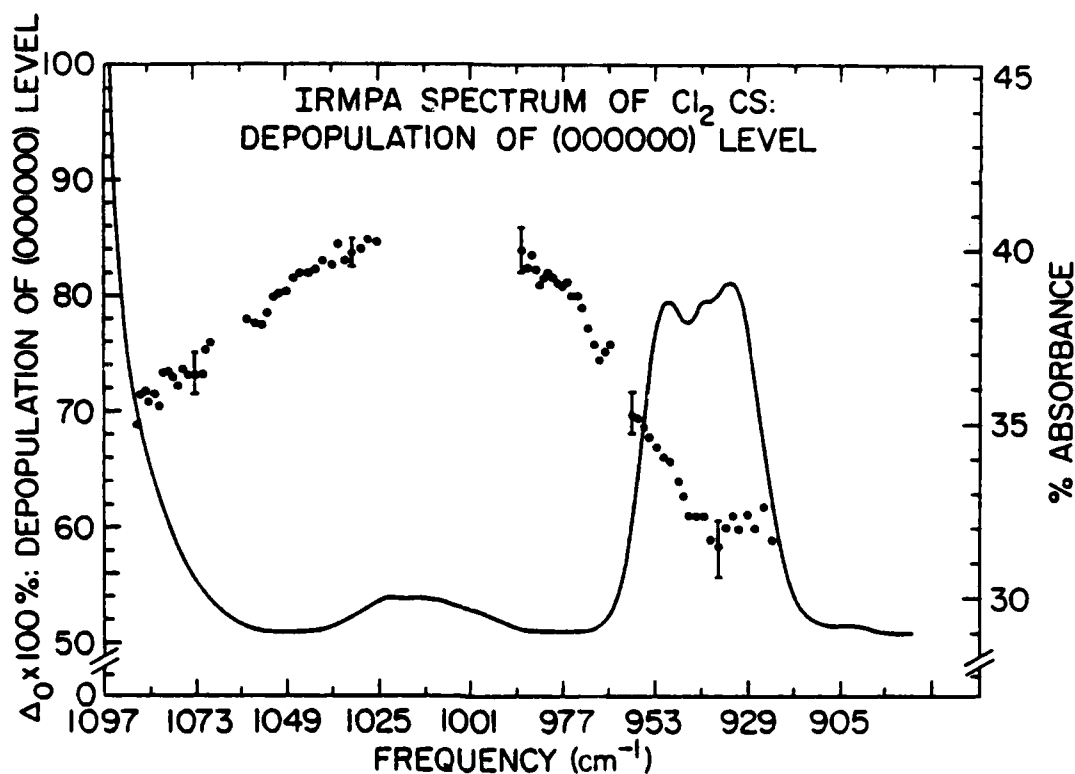


Figure 2. IR multiphoton absorption (IRMPA) spectrum (300°K) under collision free conditions at a fluence of 350 mJ cm^{-2} compared to the FTIR spectrum obtained with 30 Torr of Cl_2CS .

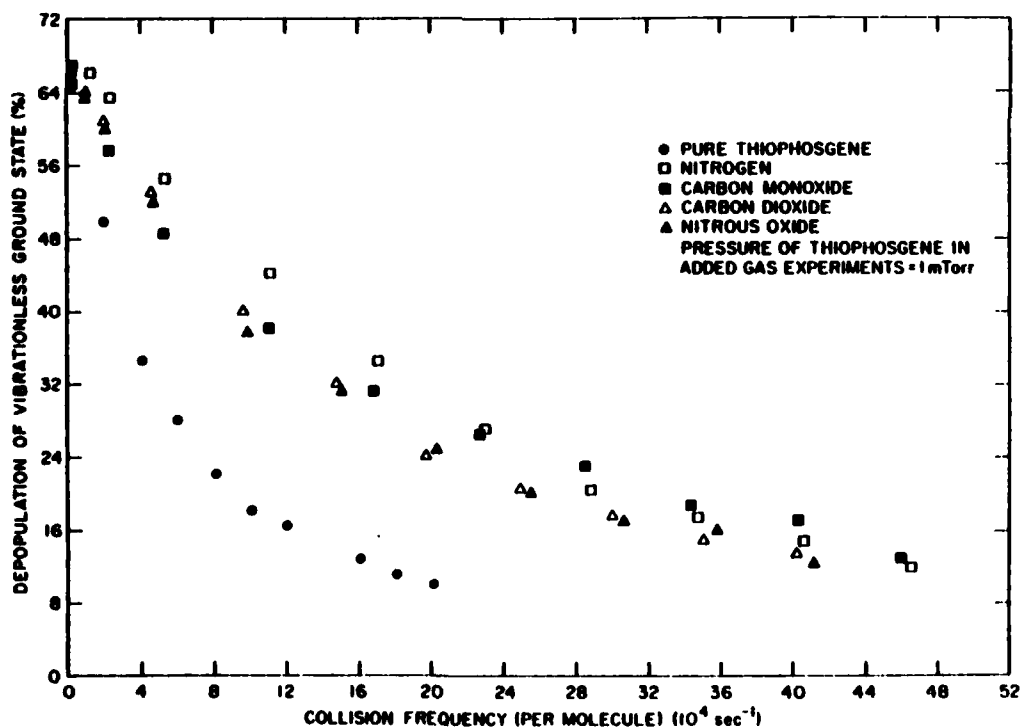


Figure 3. Dependence of ground state depletion of Cl_2CS on collision frequency with thiophosgene (\bullet), nitrogen (\square), carbon monoxide (\blacksquare), carbon dioxide (\triangle), and nitrous oxide (\blacktriangle). The thiophosgene pressure is 1.0 mTorr in the presence of mixed quenchers. The CO_2 laser fluence is 350 mJ cm^{-2} , the frequency, 944 cm^{-1} .

ABSTRACT M-5

Near threshold dissociation of tetramethyldioxetane (TMD)
using a TEA CO₂ laser

O. Aner, Y. Haas and S. Ruhman
Department of Physical Chemistry
The Hebrew University, Jerusalem

Measurements of the real time dissociation of TMD by a TEA CO₂ laser were extended to low fluences (5-10 J/cm²) and low pressures ($\sim 10^{-2}$ Torr). Under these conditions the risetime of the luminescence is much slower than the exciting laser pulse width. A strong dependence of both the rise and the decay times on the pressure is revealed. These results allow a direct comparison of multiphoton dissociation with the C-H overtone induced dissociation of Crim and Cannon [J. Chem. Phys. 75, 1752 (1981)]. Assuming that the reaction mechanism and rate is independent of the excitation mode, the overtone results can be used to "calibrate" the degree of excitation. This allows a quantitative determination of the average energy of the dissociating molecules.

ABSTRACT N-1

Vibrationally Excited Formaldehyde and Acetylene

E. Abramson, H.-L. Dai, R. W. Field, J. L. Kinsey,
C. Kittrell, D. E. Reisner, and P. H. Vaccaro

Department of Chemistry and George R. Harrison
Spectroscopy Laboratory, Massachusetts Institute
of Technology, Cambridge, MA 02139

The quest for mode selective photochemistry has stimulated intense interest in the structural and dynamical properties of excited vibrational levels of polyatomic molecules. A new spectroscopic and preparative technique, Stimulated Emission Pumping (SEP), has been applied to single rotation-vibration levels of $\text{H}_2\text{CO } \tilde{X}^1\text{A}_1$ and $\text{HCCH } \tilde{X}^1\Sigma_g^+$ at respective excitation energies up to 4600 and 9600 cm^{-1} . No other scheme (high overtone, IR multi-phonon, stimulated Raman) presently in use combines the characteristics of SEP: ability to prepare a chemically significant population, perfect rotation-vibration state selectivity, sub-Doppler resolution, double resonance elimination of rotational congestion, access to and recognition of unusual classes of highly distorted vibrational levels.

SEP introduces several unambiguous observables which are closely related to the vibrationally averaged structure of individual vibrational levels: the $2_{0,2}^{-1}0,0$ and

$2_{2,0} - 0_{0,0}$ rotational intervals (those least affected by Coriolis effects), the Stark coefficients of the $1_{1,0}$ and $1_{1,1}$ asymmetry doublet levels, Franck-Condon factors for transitions into each highly excited \tilde{X} -state vibrational level from several electronically excited vibrational levels of well-defined normal mode character, and total collisional removal rates from individual rotation-vibration levels.

Ab initio calculations show that the S_0 potential surface for the system $2H_2C,O$ supports at least three isomers (H_2CO , $HCOH$, and H_2+CO) which are so different structurally that chemically elastic collisions would not be expected to interconvert isoenergetic levels of these species at a rate competitive with chemically inelastic processes. It is anybody's guess whether the structural differences of two H_2CO levels, manifest through SEP as maximally different moments of inertia and electric dipole moments, will be robust enough to survive vibration relaxing collisions and thereby exhibit distinguishable chemical properties.

High overtone studies of acetylene suggest the existence of vibrational eigenstates of predominant C-H local mode character. SEP spectra sample levels of predominant C-C stretch and trans-bend normal mode character. It is reasonable to expect that if two isoenergetic levels are

ever found to be chemically distinguishable, they will be a normal mode and a local mode level. SEP and high overtone schemes are complementarily most sensitive to the two rarest and most different classes of vibrational eigenstates. This is the highly satisfactory situation where the proverbial needle jumps out of the haystack!

ABSTRACT N-2

VISIBLE ELECTRONIC ABSORPTION SPECTRUM OF VINYL RADICAL

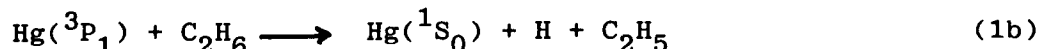
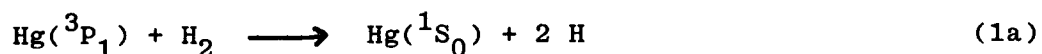
H.E.Hunziker, H.Kneppe, A.D.McLean, P.Siegbahn, and H.R.Wendt

IBM Research Laboratory, 5600 Cottle Rd., San Jose, California
95193, U.S.A.

It is surprising that a small hydrocarbon radical as common as vinyl, C_2H_3 , has not yet been detected optically. Observation of this species has previously been accomplished only by electron spin resonance and mass spectroscopy. We have predicted the lowest electronic transition of vinyl radical by ab initio calculation and detected the corresponding optical absorption spectrum by photochemical modulation spectroscopy.¹

SCF calculations show that the vinyl radical is planar in both its $^2A'$ ground state and $^2A''$ lowest excited state. The excitation moves one of the C-C π -bonding electrons into the in-plane orbital which is singly occupied and localized on the radical center in the ground state. In the isoelectronic formyl radical, HCO, an analogous excitation gives rise to the $\tilde{C}, ^2A''$ state. From calculations with a basis set of double-zeta quality the optimized geometries shown in Fig.1 were determined. The largest relaxation effects following excitation are the expected lengthening of the C-C bond and a contraction of the CCH angle at the radical center. Using these geometries and a basis set enhanced by polarization functions, a CI treatment incorporating all single and certain double replacements² yielded a vertical excitation energy of 3.24 eV and adiabatic excitation energy of 2.37 eV.

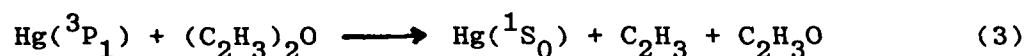
An experimental absorption spectrum corresponding closely with these predictions was obtained by photochemical modulation spectroscopy of the Hg-photosensitized reactions



Since HgH formed as an intermediate in reaction (1a) partially obscures the C_2H_3 absorption spectrum below 405 nm, the alternate H-atom source (1b) was used in this region. Experiments were carried

out at 1 atm. total pressure and 310°K, with 270 Hz modulation frequency. Fig. 2 shows the observed spectrum and Table 1 lists the observed band maxima. No clear evidence of rotational subband structure was obtained with .7 nm resolution in the 423.2 nm band. Experiments with deuterated reactants produced qualitatively similar spectra but due to various difficulties did not yield results good enough to establish isotope effects.

As an experimental check on the assignment of the observed spectrum the reaction



was investigated, since direct photolysis of divinyl ether is known to yield vinyl radicals.³ Several of the stronger bands of Fig. 2 were observed together with the spectrum of $\text{C}_2\text{H}_3\text{O}$ which starts at 348 nm.⁴ Other transients absorbing in the region of the vinyl spectrum are also formed in reaction (3).

From the equilibrium geometries of Fig. 1 we expect to see progressions of the upper state CC stretching and CCH bending vibrations in the $^2\text{A}'' - ^2\text{A}'$ electronic transition. Two progressions with $\nu_1' \approx 1200 \text{ cm}^{-1}$ and $\nu_2' \approx 920 \text{ cm}^{-1}$ are indeed observed, the ν_1' value being as expected for a C \equiv C bond. Both vibrational frequencies are close to those of the $\tilde{\text{C}}$ state of HCO where the corresponding modes give rise to intervals of 1200 cm^{-1} and 960 cm^{-1} .⁵ Whether the first band at 499.5 nm is the 0-0 transition cannot be ascertained from our results, but it is not far from the predicted, adiabatic excitation energy. Agreement is also good for the Franck-Condon maximum of the transition which occurs around 400 nm, near the predicted vertical excitation energy. Despite missing rotational and isotopic data we conclude that the evidence strongly favors assignment of the observed spectrum to the $^2\text{A}'' - ^2\text{A}'$ lowest electronic transition of vinyl radical.

REFERENCES

1. H.E. Hunziker, IBM J. Res. Develop. 15, 10 (1971)
2. A.D. McLean and B. Liu, J. Chem. Phys. 58, 1066 (1973)
3. K.O. MacFadden and C.L. Currie, J. Chem. Phys. 58, 1213 (1973)
4. H.E. Hunziker, H. Knepe, and H.R. Wendt, J. Photochem. 17, 377 (1981)
5. M.E. Jacox, Chem. Phys. Lett. 56, 43 (1978).

TABLE 1

Observed positions of band maxima, in cm^{-1} , with band spacings in parentheses. The v_1 numbering is arbitrarily started at the first band observed.

v_1	v_2	
	0	1
0	20020 (1202)	
1	21222 (1205)	22148 (1200)
2	22427 (1202)	23348 (1204)
3	23629 (1186)	24552 (1175)
4	24815* (1166)	25727 (1191)
5	25981 (1152)	26918
6	27137	

* Estimated position.

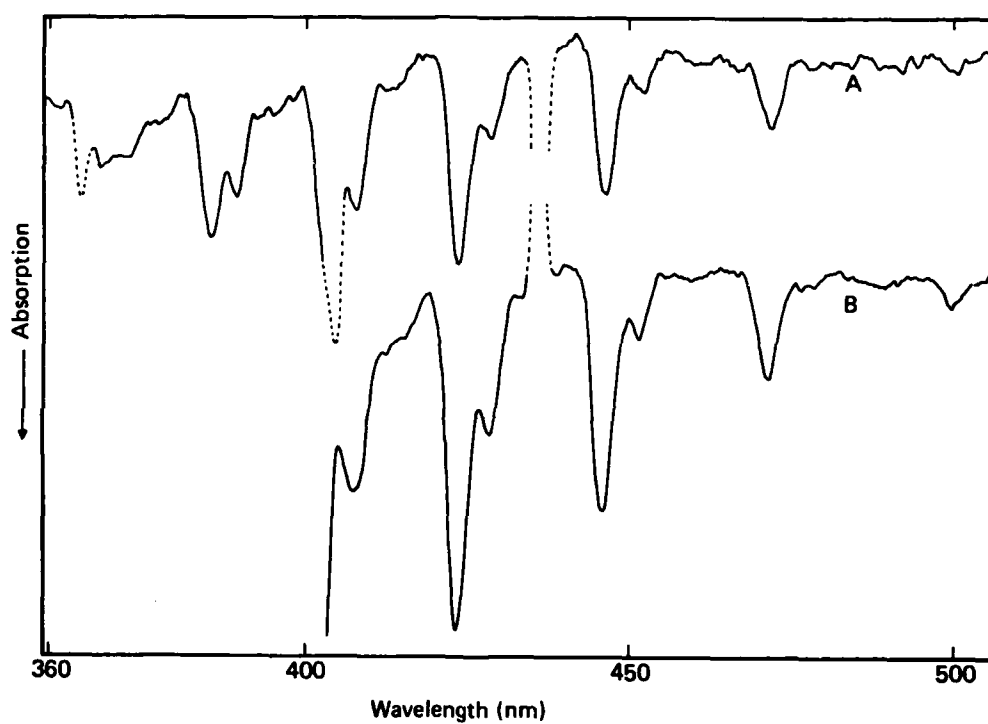
FIGURE 1

Qualitative electronic structures and computed SCF geometries of the $^2A'$ ground state and $^2A''$ first excited state of vinyl radical.

State	El. Structure	Geometry
$^2A''$		
$^2A'$		

FIGURE 2

Absorption spectrum of vinyl radical at 1.6 nm resolution. Reaction (1b) was the H-atom source for trace A, and reaction (1a) for trace B. Dotted regions indicate interference by HgH absorption bands and Hg I straylight lines.



ABSTRACT N-3

Spectral and kinetic study of rare gas/ Cl_2 mixtures excited with synchrotron radiation

M.C. Castex^(a), J. Le Calvé^(b), D. Haaks^(c), B. Jordan^(d), G. Zimmerer^(d)

(a) Laboratoire des Interactions Moléculaires et des Hautes Pressions, C.N.R.S., Centre Universitaire Paris-Nord, 93430 Villetaneuse, France.

(b) CEN/Saclay, DPC, 91190 Gif-sur-Yvette, France.

(c) Institut für Phys. Chemie, FB9, Gesamthochschule Wuppertal, D-5600 Wuppertal, Germany.

(d) II. Institut für Exp. Physik, Universität Hamburg, D-2000 Hamburg 52, Germany.

With the purpose to characterize fundamental processes involved in rare gas halides, we have undertaken at DESY a detailed study of spectral and kinetic properties of Cl_2 /rare gas (RG = Ar, Kr, Xe) mixtures excited by synchrotron radiation. After having shown that the fluorescence of the RGCl^* excimer ($\text{B} \rightarrow \text{X}$, $\text{C} \rightarrow \text{A}$ and $\text{D} \rightarrow \text{X}$) can be obtained not only from an initial excitation of the resonant states $^3\text{P}_1$ and $^1\text{P}_1$ of the rare gas (well known harpooning reaction) but also from the primary excitation of some excited states of Cl_2 above 9 eV (1) (2), we have exploited the advantages of this new formation channel : (i) large choice of possible entrance energies. (ii) possibility, under our experimental conditions (P_{Cl_2} 0.5 to 10 torr and $P_{\text{RG}} = 10$ to 1000 torr) to investigate the decay properties of the excimer states, and determine the radiative lifetimes and the quenching rate constants. This work has been closely connected to a detailed analysis of absorption and fluorescence spectra of pure Cl_2 itself (3) (4) and to the recent ab initio calculations of singlet and triplet excited states of Peyerimhoff (5).

Our kinetic study concerns mainly fast $\text{B} \rightarrow \text{X}$ emissions and try to take care of several difficulties inherent to these systems such as (i) the bound-free character of this emission with a long wavelength maximum containing contributions from all emitting vibrational levels v' (ii) the strong variation of lifetimes with v' (iii) vibrational relaxation and quenching.

The possibility to select both particular excitation and analysis wavelengths (band pass being respectively 4 Å and 12 Å) allows to disentangle some of the great variety of processes which are hidden in the time resolved spectra. For the two different cases XeCl and ArCl some results are reported here.

XeCl - When pumping Cl_2 , XeCl^* (B state) is formed in high vibrational levels ($v' \sim 120$ for 1350 Å excitation from Setser's calculation (6)) and so vibrational relaxation must occur to populate the lowest levels. This effect is illustrated by Fig (1) which shows, for nearly the same pressure conditions, the temporal behaviour of the $\text{B} \rightarrow \text{X}$ emission at two different analysis wavelengths following Cl_2^* excitation at 1350 Å.

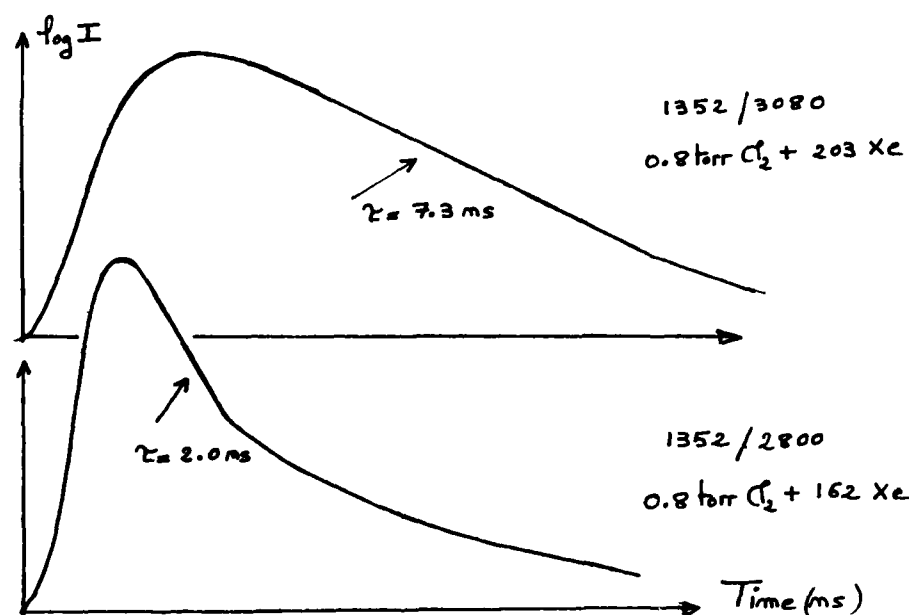


Fig. 1

When analyzing the fast decay component of the 2800 Å signal according to $1/\tau = 1/\tau_{\text{Rad}} + k_{\text{Relax}} [\text{Xe}] + k_{\text{Q}} [\text{Cl}_2]$, we measure a relaxation rate constant $k_{\text{Relax}} = 1 \times 10^{-10} \text{ cm}^3 \text{ s}^{-1}$, a quenching rate constant by Cl_2 $k_{\text{Q}} = 4.75 \times 10^{-10} \text{ cm}^3 \text{ s}^{-1}$ and a radiative lifetime $\tau_{\text{Rad}} \sim 40 \text{ ns}$ attributed to high vibrational levels. On the other hand, we put in evidence in the decay rate τ^{-1} , observed at 3080 Å and plotted as a function of rare gas pressure (fixed P_{Cl_2}), a two body term ($k_{\text{Xe}} \sim 10^{-12} \text{ cm}^3 \text{ s}^{-1}$, B/C mixing) and a three body term ($k_{\text{Xe}_2} = 1.3 \times 10^{-30} \text{ cm}^6 \text{ s}^{-1}$, Xe_2Cl formation). The radiative lifetime measured 16 ns, is characteristic of low levels.

ArCl - In contrast with the Xe/Cl₂ case, at rare gas pressure $P > 100$ torr the Cl₂* + Ar reaction gives rise to two competitive channels with production of ArCl* and Cl₂* (2580 Å) emissions. As illustrated by Fig (2), Cl₂ excitation allows the direct formation of ArCl* in low vibrational levels, with a determination of the excitation threshold at 1280 Å in agreement with theoretical prediction.

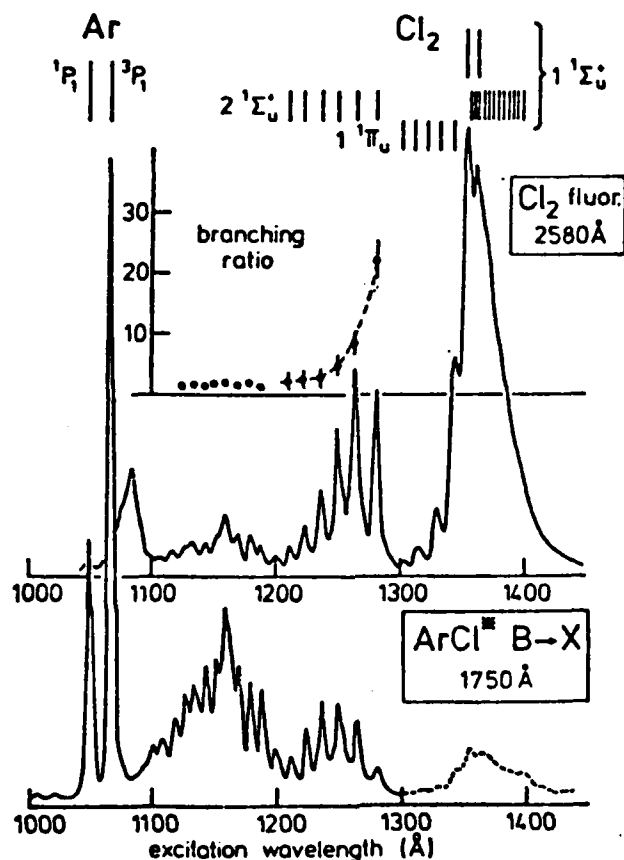


Fig. 2

References :

- (1) M.C. Castex, J. Le Calvé, D. Haaks, B. Jordan, and G. Zimmerer, Chem. Phys. Letters 70, 106 (1980).
- (2) J. Le Calvé, M.C. Castex, D. Haaks, B. Jordan and G. Zimmerer, Il Nuovo Cimento 63B, 265 (1981).
- (3) J. Le Calvé, M.C. Castex, E. Boursey and Y. Le Duff, European Conference on Atomic Physics, Heidelberg (1981).
- (4) T. Moeller, B. Jordan, P. Gürtler, G. Zimmerer, D. Haaks, J. Le Calvé and M.C. Castex, to be published.
- (5) S.D. Peyerimhoff and R.J. Buenker, Chem. Physics 57, 279 (1981).
- (6) T.D. Dreiling and D.W. Setser, J. Chem. Phys. 75, 4360 (1981).

ABSTRACT N-4

Multiphoton Excitation of Halogen Molecules

T. Ishiwata, T. Shinzawa, and I. Tanaka

Department of Chemistry, Tokyo Institute of Technology
Ohokayama, Meguroku, Tokyo 152, JAPAN

Recent years, much attention has been paid to the higher lying electronic states of halogen molecules in connection with the laser radiation in the vacuum ultraviolet and ultraviolet regions. The purpose of this work is to report the observation of new electronic states of halogen molecules by three-photon transition involving a sequential step from the ground state ($X^1\Sigma_g^+$) through the $B^3\Pi_{0u}^+$ state.

The properties of the higher lying electronic states of halogen molecules were investigated by an optical-optical double resonance (OODR) method. Radiation from a nitrogen laser was used to pump the two independently tunable dye lasers simultaneously through a beamsplitter.

The resultant OODR spectra showed that probe laser induced the three types of transitions to form the higher electronic states being resonant to the three photon energy.

- (I) $\nu_1 + (2\nu_2)$; Virtual two-photon transition with probe frequency ($2\nu_2$) following the excitation with pump frequency (ν_1).
- (II) $\nu_1 + (\nu_1 + \nu_2)$; Virtual two-photon transition with probe and pump frequencies ($\nu_1 + \nu_2$) following the excitation with pump frequency (ν_1).
- (III) $\nu_2 + (2\nu_2)$; Virtual two-photon transition with probe frequency ($2\nu_2$) accidentally induced from the rotational level in the B state pumped with probe frequency (ν_2).

Type (I) and (II) transitions showed three separate vibrational progressions consisting of O, Q, and S branches. These were represented by symbols α , β , and γ increasing energy in order in the case of molecular chlorine (Fig. 1). The molecular constants for these state are given in Table 1.

The effect of the incident light polarization on the two-photon transition from the B state was observed for the α , β , and γ series. For the type (I) transition, the ratio of two photon absorption cross sections (σ_{cc}/σ_{11}) was derived to be ~ 0.2 for Q branch and ~ 1.5 for O and S branches. These results are shown in Fig. 2 and Table 2, together with those for the type (II)

transition. According to the theoretical treatment on two-photon cross sections, the observed bands appeared to be Σ - Σ type transition.¹⁾ The symmetries of individual upper states would be then expected to be 0_u^+ in Hund's coupling case c.

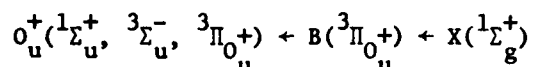


Fig. 3 shows the UV emission spectrum of Cl_2 from the γ state ($v'=0$) obtained by focussing the laser radiation at 501.89 nm. Due to the analysis using the molecular constants derived before, the excitation is performed by the visible transition of $B \leftarrow X$ ($12-0$ P_{11}) followed by the virtual two-photon transition ($0-12$ Q_{10}) from the B state. The emission spectrum consists of two types of transitions; (1) a line shaped system below 259 nm and (2) a broad band system around 259 nm, where no change in the spectral feature could be observed in the pressure range of $0.1 \sim 3$ Torr. Discrete emission around 235 nm can be assigned to the transition to the ground state using molecular constants characterizing²⁾ the ground state, as shown in Fig. 3. Since the intensities of predominant lines decrease monotonically on either side of a single intensity maximum, the fluorescence originates from the $v''=0$ level. Further, considering the Franck-Condon factor of this transition, the equilibrium nuclear distance of the γ state is roughly estimated to be ~ 3.0 Å from the outer turning point of ground state at the $v''=40$ level. It is clear that these facts are consistent with the OODR analysis.

The electronic transitions may be classified as intravalence-shell or Rydberg. Valence-shell states arise from the excitation of one or two valence electrons to outer valence orbitals. It is then reasonable to consider qualitatively that this change in the valence-shell configuration makes the bond length much larger and the vibrational frequency smaller than that of the ground state. According to potential curves calculated,³⁾ the valence-shell states of $^3\Pi_g$ and $^3\Pi_u$ lie at 57500 and 61000 cm^{-1} , respectively, while Rydberg states even converging to the lowest $^2\Pi_g$ state of Cl_2^+ do not exist up to 67000 cm^{-1} . The $^3\Pi_u$ state which dissociates to the ionic products, $Cl^+(^3P_g) + Cl^-(^1S_g)$, is consistent with our observed transition energetically or symmetrically (Fig. 4). The estimated nuclear distance (~ 3.0 Å) agrees with its theoretical value (~ 3.0 Å). Unfortunately, they did not treat the $^3\Sigma_u^-$ state which also converges to the ionic limit, $Cl^+(^3P_g) + Cl^-(^1S_g)$. Other electronic state being symmetrically acceptable is $^1\Sigma_u^+$ lying at 65500 cm^{-1} slightly

higher than our experimental values.

It should be noted here that the potential curves calculated, indicates some repulsive electronic states with the *gerade* symmetry converging to $\text{Cl}(^2\text{P}) + \text{Cl}(^2\text{P})$. The broad feature with a single intensity maximum at 259 nm strongly suggested that it can be assigned to the direct transition from the upper *ungerade* state mentioned before to the repulsive *gerade* states.

The new valence-shell state having 0_u^+ symmetry ($T_e \approx 54900 \text{ cm}^{-1}$ $\omega_e \approx 150 \text{ cm}^{-1}$ for bromine, $T_e \approx 51700 \text{ cm}^{-1}$ $\omega_e \approx 80 \text{ cm}^{-1}$ for iodine) observed by the virtual two-photon absorption from the B state in the cases of bromine and iodine molecules will be discussed.

References

- 1) A. E. Douglas and A. R. Hoy, Can. J. Phys., 53, 1965 (1975).
- 2) R. G. Bray and R. M. Hochstrasser, Mol. Phys., 31, 1199 (1976).
- 3) S. D. Peyerimhoff and R. J. Buenker, Chem. Phys., 57, 279 (1981).

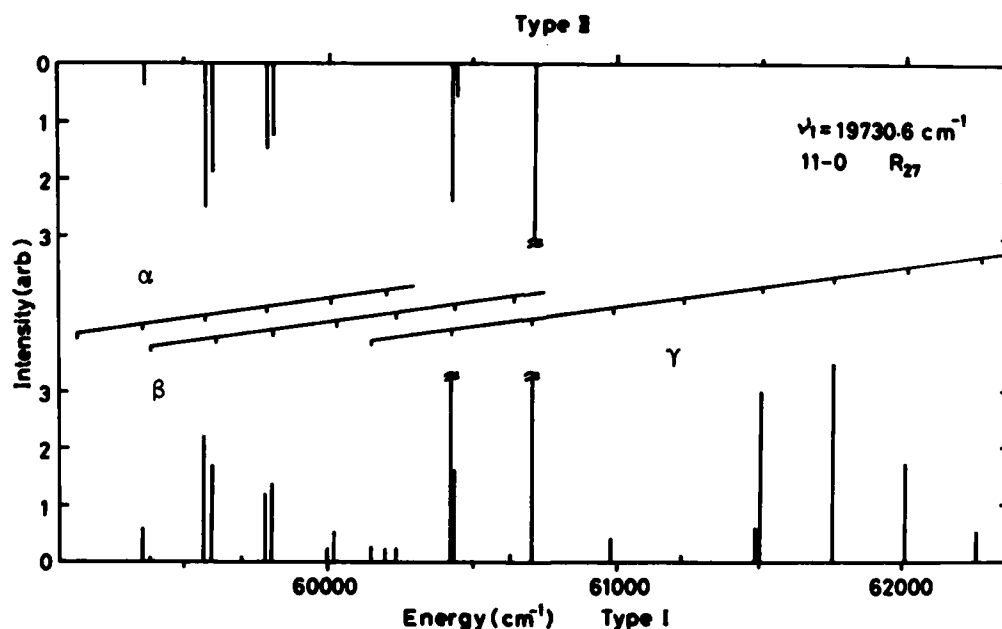


Fig. 1

	T_e	ω_e	$\omega_e x_e$	B_e	α_e	r_e^*
γ	59926.8	282.3	2.2	0.1112	0.0012	2.95
β	(58588)	210	—	0.1236	0.0010	2.79
α	58487.7	234.2	2.2	0.1201	0.0025	2.83
$B(^3\Pi_{ou}^+)$	17809	259.5	5.3	0.16256	0.00212	2.435
$X(^1\Sigma_g^+)$	0	559.7	2.7	0.24399	0.00149	1.988

(cm^{-1} , * \AA)

Table 1

$^{35}\text{Cl}-^{35}\text{Cl} \quad (B \ ^3\Pi_{ou}^+ + X \ ^1\Sigma_g^+)$
 $11 - 0 \ R_{35} \quad (19673.0 \text{ cm}^{-1})$

Type I $(\nu_1 + (2\nu_2))$

Branch	σ_{cc}/σ_{11}
O	1.3 (1.5)
Q	0.2
S	1.5 (1.5)

Type II $(\nu_1 + (\nu_1 + \nu_2))$

Branch	σ_{1c}/σ_{11}	$\sigma_{11}^*/\sigma_{11}$
O	0.9 (7/8)	0.7 (3/4)
Q	0.5 ($\sim 1/2$)	0.08
S	0.9 (7/8)	0.7 (3/4)

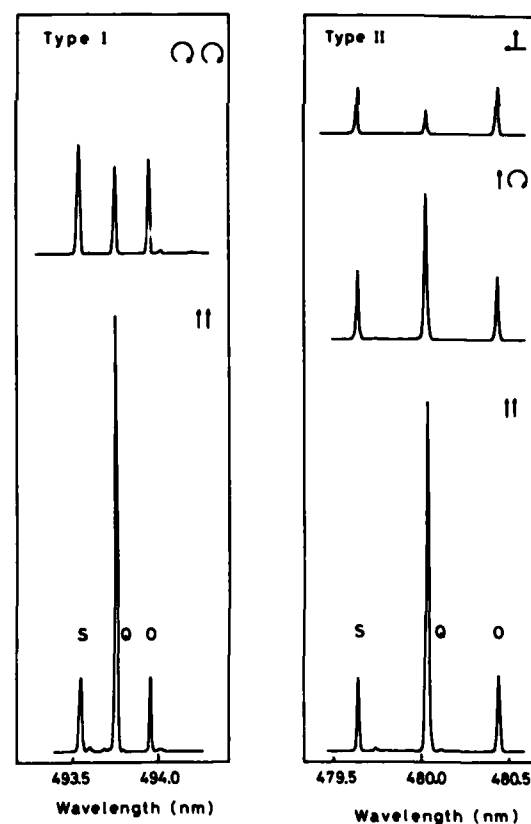


Fig. 2

Table 2

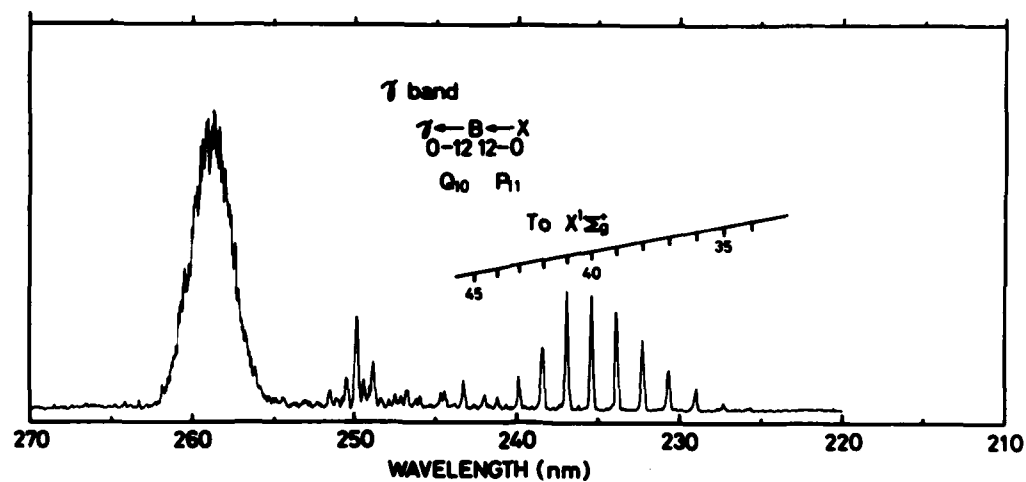


Fig. 3

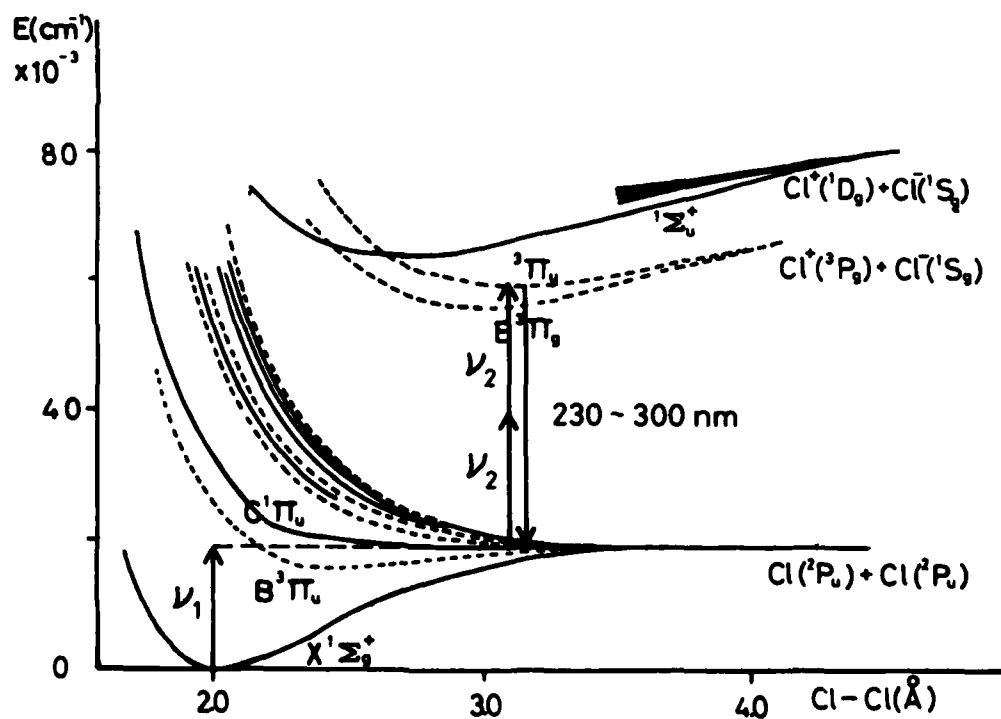


Fig. 4

ABSTRACT N-5

Vibration-Rotation and Pure Rotational Spectra of the CH₂ Radical in its Ground, \tilde{X}^3B_1 , Electronic State-Implications Regarding the Singlet-Triplet Splitting in CH₂.

Trevor J. Sears^a, P.R. Bunker^a, A.R.W. McKellar^a,
K.M. Evenson^b, D.A. Jennings^b and J.M. Brown^c

We report here the detection and assignment of vibration-rotation and pure rotational transitions in the methylene radical, CH₂, by laser magnetic resonance (LMR) spectroscopy¹. In a short communication of these results² we reported the observation and assignment of three rotational transitions in the ν_2 (bending) fundamental band; we have subsequently measured and assigned components of ten rotational lines in this band in the frequency range 880-1085 cm⁻¹ (11.36-9.23 μ m). Figure 1a shows an example of the spectra, obtained on the 931.001 cm⁻¹ 10P(34) CO₂ laser line. The saturation features evident on the doppler broadened line profiles show the positions of the three hyperfine components associated with each transition in the ortho-CH₂ species.

Analysis of the infrared spectra allowed the prediction of the frequencies of the pure rotational transitions in the ground (000) state of the radical and thirteen of these have now been detected and assigned in the far infrared between 681 and 63.1 μ m. Figure 1b shows the spectrum obtained on the 144.1 μ m CD₃OH laser line. The complete analysis yields a very precise determination of the rotational, fine structure and hyperfine parameters for methylene in the (000) and (010) levels of the ground state. An important result of the analyses is that the ν_2 fundamental frequency has been found to be 963.0986(3) cm⁻¹ which is much lower than previous theoretical³ and experimental^{4,5} estimates of the quantity.

The complete dataset was fitted to the semi-rigid bender model of Bunker and Landsberg⁶ in order to construct the effective bending potential function for the \tilde{X}^3B_1 (0 ν_2 0) state. The resulting potential function is:

$$V(\text{cm}^{-1}) = -7038.4(6.8)\rho^2 + 7566(20)\rho^4 - 2703(13)\rho^6 + 500\rho^8 \quad (1)$$

and the bond length is

$$R_{\text{CH}}(\text{\AA}) = 1.0745(14) + 0.0231(27)\rho^4, \quad (2)$$

where ρ is the supplement of the HCH bond angle (if has the value zero when the molecule is linear). The potential function is shown in fig. 2 with the positions of the lowest few bending vibrational levels.

^a Herzberg Institute of Astrophysics, National Research Council of Canada, Ottawa, Ont. K1A 0R6, Canada

^b National Bureau of Standards, Boulder, Colorado 80303 USA

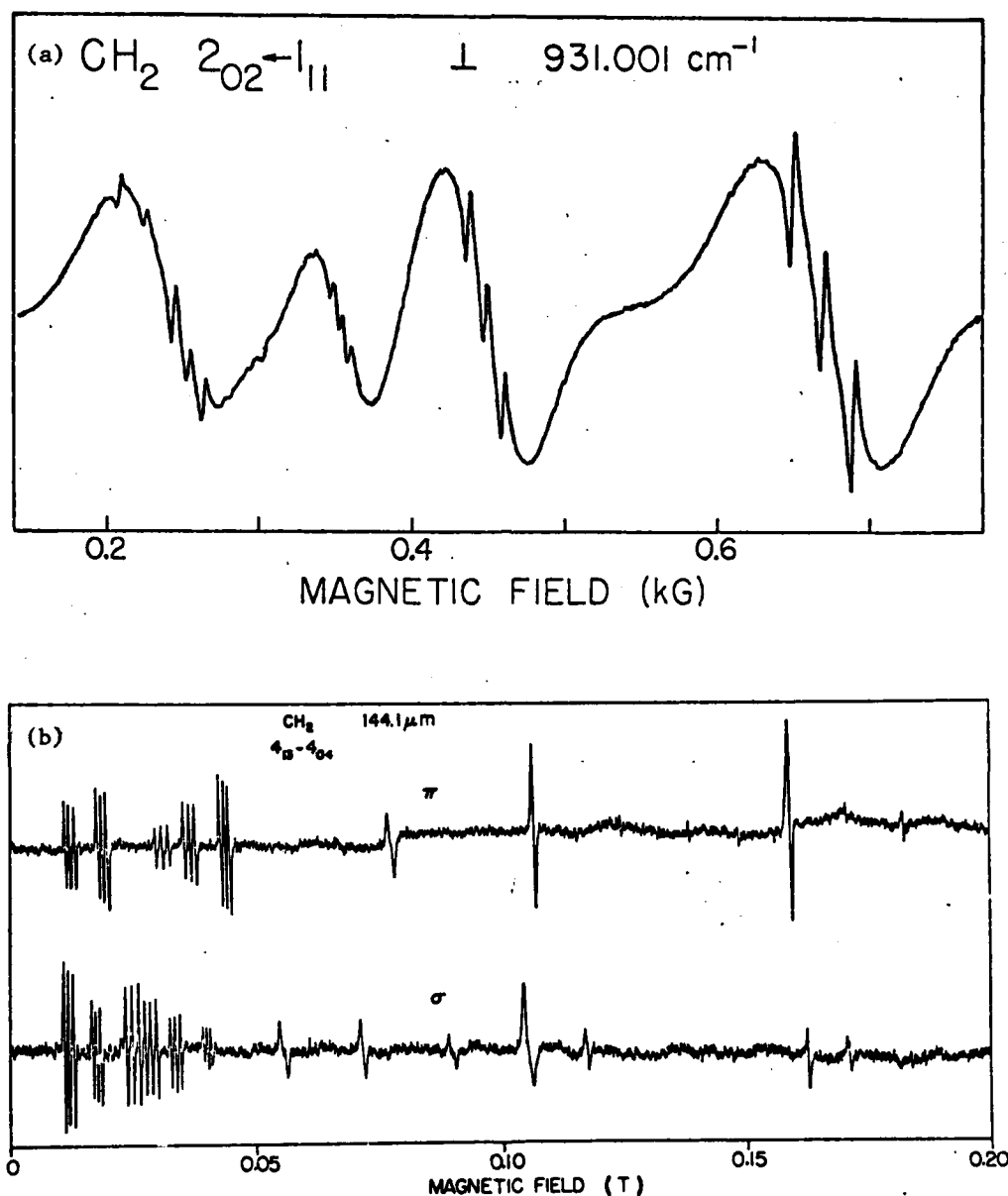
^c Dept. of Chemistry, The University of Southampton, Southampton SO95NH, England

These results together with the potential function for the \tilde{a}^1A_1 state derived from the electronic spectrum⁷ and the *ab initio* potential function for the CH_2^- ion form the basis for a realistic calculation of the expected photoelectron spectrum of the CH_2^- ion⁴. Previous assignments of this spectrum^{3,4,8} have been based on an assumed, harmonic, bending frequency of $\sim 1100\text{ cm}^{-1}$ for \tilde{X}^3B_1 CH_2 and have not fully allowed for the effect of rotational selection rules on the photoelectron band contours. These are important because very large shifts in the rotational contour can be introduced by transitions involving changes in K_a because of the very large values of the $A[v_2]$ rotational constants and the very large changes in $A[v]$ with v_2 . Rotational selection rules for the photodetachment process will be discussed and the results of the calculations outlined above presented.

References

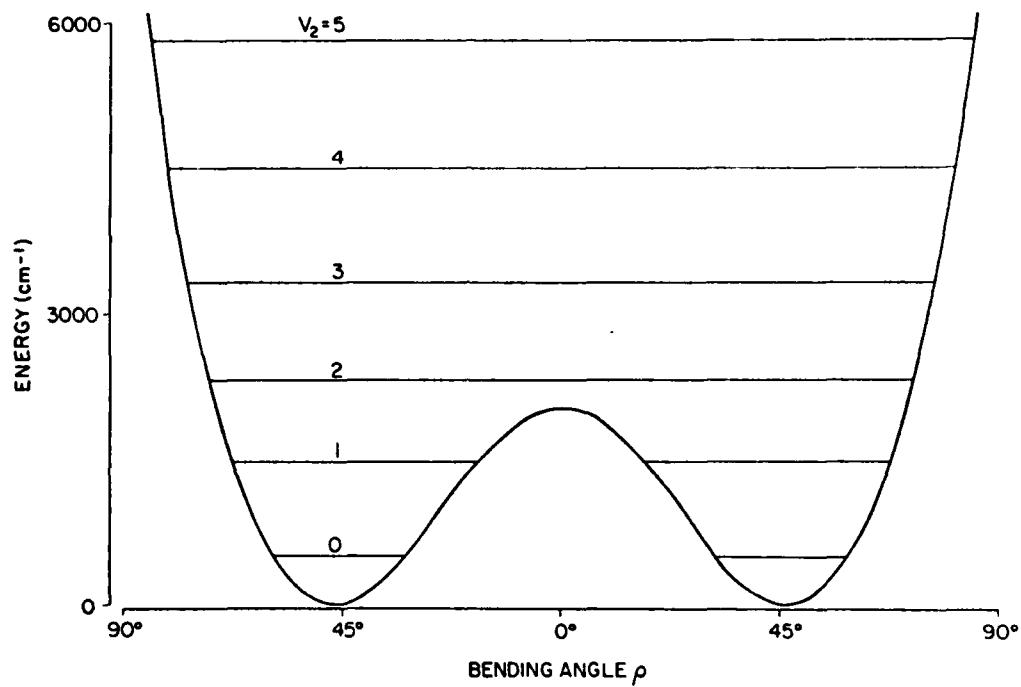
1. Reviews of the techniques are given in:
A.R.W. McKellar Faraday Disc. Chem. Soc. 71, 63 (1981);
K.M. Evenson, R.J. Saykally, D.A. Jennings, R.F. Curl and J.M. Brown. Chemical and Biochemical Applications of Lasers, ed. C.B. Moore Academic Press, New York, 1980), Vol. 5, p. 75.
2. T.J. Sears, P.R. Bunker and A.R.W. McKellar, J. Chem. Phys. 75, 4731 (1981).
3. L.B. Harding and W.A. Goddard III, Chem. Phys. Lett. 55, 217 (1978); J. Chem. Phys. 67, 1777 (1977).
4. P.C. Engelking, R.R. Corderman, J.J. Wendoloski, G.B. Ellison, S.V. O'Neil and W.C. Lineberger, J. Chem. Phys. 74, 5460 (1981).
5. Y.-P. Lee and G.C. Pimentel, J. Chem. Phys. 75, 4241 (1981).
6. P.R. Bunker and B.M. Landsberg, J. Mol. Spectrosc. 67, 374 (1977).
7. G. Herzberg and J.W.C. Johns, Proc. Roy. Soc. Lond., A295, 707 (1966).
8. S.-K. Shih, D. Peyerimhoff, R.J. Buenker and M. Peric, Chem. Phys. Lett. 55, 206 (1978).

Figure 1



(a) Components of the $2_{02} \leftarrow 1_{11}$ rotational transition in the ν_2 band of the CH_2 radical. In this slow sweep the saturation features representing the ^1H hyperfine splittings in ortho- CH_2 can be clearly seen. (b) Components of the $4_{13} \leftarrow 4_{04}$ pure rotational transition in $\tilde{\text{X}}^3\text{B}_1$ CH_2 observed using the $144.1 \mu\text{m}$ CD_3OH laser line. Due to the smaller doppler width at this frequency the hyperfine splittings are often greater than the Doppler profile and clearly resolved. In the upper trace the E-vector of the laser radiation is parallel to the magnetic field, in the lower it is perpendicular.

Figure 2



Experimentally determined bending potential energy function for \tilde{X}^3B_1 CH_2 in the $v_1=v_3=0$ state. The height of the barrier to linearity is 2032 cm^{-1} and the equilibrium bond angle $\alpha_e = 133.4^\circ$; the function is given in Eq. (1) and the energy origin in this figure is taken as the energy of the minimum.

ABSTRACT N-6

EXPERIMENTAL DETERMINATION OF ABSORPTION CROSS SECTIONS AND BAND
OSCILLATOR STRENGTHS OF THE SCHUMANN-RUNGE BANDS OF O_2 IN THE WAVELENGTH
REGION 175-205 NM

D.E. Freeman, K. Yoshino, and W.H. Parkinson

Harvard College Observatory
Cambridge, MA 02138

Cross sections of O_2 have been obtained from photoabsorption measurements at 300 K and at several pressures throughout the 175-205 nm region with a 6.65 m photoelectric scanning spectrometer¹ equipped with a 2400 lines/mm grating. For the Schumann-Runge (S-R) bands (12,0) through (1,0) spanning the wavelength region 179.3-201.5 nm, the instrumental width (HWHM = 0.00065 nm) is small enough for the measured cross sections to be absolute in the sense of their being independent of the instrumental width, a result not achieved by previous investigators working at lower resolution.^{2,3} Thus our measured cross sections are observed to be independent of oxygen pressure over a considerable pressure range. To maximize the accuracy of the cross section determined by combining sets of data points $\ln(I_0/I)$ obtained at the same wavenumber and at different pressures, only those points were selected for which the optical depth had values lying between preset upper and lower limits (usually 2.0 and 0.3, respectively). The absorption cross sections so obtained for the (12,0) through (1,0) bands are available as numerical compilations stored on magnetic tape and in two graphical formats, as linear or logarithmic plots of cross section against vacuum wavenumber. A representative example of the graphical results is shown in Fig. 1 for the (5,0) band.

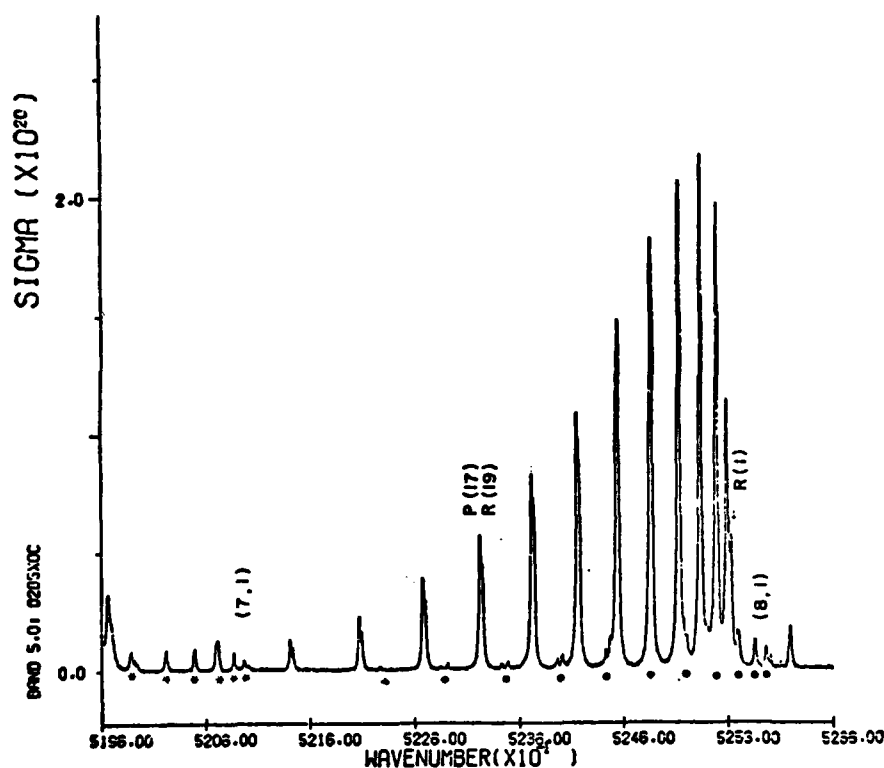


Fig. 1. A linear plot of absolute absorption cross sections (cm^2) against wavenumber in the region of the S-R band (5,0). The rotational assignments shown refer to lines of the (5,0) band. Lines belonging to the hot bands (8,1) and (7,1) are indicated by symbols # and *, respectively. In this case the absorption cross sections of the hot bands and the main band are absolute, i.e., independent of the instrumental function.

Band oscillator strengths $f(v',0)$ with $v' = 2-12$ have been determined by direct numerical integration of the measured cross section, $\sigma(v)$, over the relevant rotational lines,

$$f(v',0) = 1.127 \times 10^{12} \int_{\text{band}} \sigma(v) dv$$

and such a result does not invoke any modelling procedure requiring computed cross sections. At our resolution, lines belonging to hot bands can be excluded from the summation, as can lines belonging to any S-R band other than the one under consideration. Table 1 shows S-R band oscillator strengths determined by this method.

TABLE 1
Oscillator Strengths of Schumann-Runge Bands Determined
From Absolute Cross Section Measurements at 300 K^a

v'	$f(v',0) \times 10^5$ From integration ^b over lines $N \leq N_{\max}$	$f(v',0) \times 10^5$ From column 2, plus extrapolation for $N > N_{\max}$
2	0.0018 ₀ (27)	0.0018 ₉
3	0.0081 (23)	0.0084 ₅
4	0.026 ₉ (23)	0.028 ₂
5	0.072 ₈ (29)	0.074 ₂
6	0.158 (27)	0.162
7	0.33 ₄ (27)	0.34 ₃
8	0.60 ₈ (25)	0.63 ₁
9	0.88 ₄ (23)	0.99 ₇
10	1.36 (23)	1.54
11	1.98 (21)	2.26
12	2.19 (19)	2.43

^a Cross section measurements have been made for the (1,0) band which may be too weak for an accurate determination of $f(1,0)$.

^b The number in parenthesis in this column is N_{\max} where $R(N_{\max})$ and $P(N_{\max}-2)$ are the last lines included in the integration.

For the less predissociated sharper S-R bands ($v',0$) with $v' \geq 13$, between 179.2 and 175.0 nm, the cross sections measured with our 6.65 m spectrometer are dependent on the instrumental width and are therefore underestimates of the true absorption cross sections. In these cases computed cross sections incorporating the effects of convolution with the instrumental function are synthesized from the measured line center positions and from band oscillator strengths and predissociation line widths

which are treated as parameters to be determined simultaneously by the fitting of computed and measured cross sections; contributions to the cross section from nearby lines and from the measured continuum arising from $v'' = 1$ are also included in the comparison. Such modelling computations are also being used together with the definitive band oscillator strengths in Table 1 to obtain predissociation line widths for the S-R bands (12,0) through (2,0).

Acknowledgment: This work was supported by NASA under Grant NSG-5176.

-
1. K. Yoshino, D.E. Freeman, and W.H. Parkinson, Appl. Opt. 19, 66 (1980).
 2. J.E. Frederick and R.D. Hudson, J. Mol. Spectrosc. 74, 247 (1979).
 3. B.R. Lewis, J.H. Carver, T.I. Hobbs, D.G. McCoy, and H.P. Gies, J. Quant. Spectrosc. Radiat. Transfer 20, 191 (1978); 22, 213 (1979); 24, 365 (1980); 26, 469 (1981).

ABSTRACT N-7

PHOTOABSORPTION SPECTRUM OF OH IN THE VACUUM ULTRAVIOLET REGION*

R. L. Day and L. C. Lee

Department of Electrical and Computer Engineering

San Diego State University

San Diego, California 92182

The OH radical is very abundant in the interstellar medium and in the cometary and earth atmospheres. The photoabsorption spectrum of OH in the vacuum ultraviolet region is important information for understanding the OH roles playing in various environments, and also useful data for comparison with theoretical calculations of OH potential curves.

The OH radicals were produced by a pulse discharge of a few mtorr H_2O in 3 torr Ar inside a double wall glass tube. The tube (110 cm long) was made of a small glass tube (1.9 cm dia.) inside a large one (3.8 cm dia.). The inner tube was cut a slit of 1.2 cm wide. The radicals produced between the two glass tubes by electrical discharge flew through the slit into the light absorption path. The gas mixture was pumped at both ends of the tube, before the ends were sealed with two LiF windows.

The OH radicals were monitored by an $OH(A^2\Sigma^+ - X^2\Pi)$ resonance lamp. The resonance scattering signals were detected by a combination of a $3100 \pm 50 \text{ \AA}$ optical filter and a photomultiplier tube (PMT). A resonance scattering signal was observed when the H_2O/Ar gas mixture was discharged. This scattering signal ensures that the OH radicals were produced by the discharge.

The vacuum ultraviolet light source was produced by a microwave discharge of Ar, H_2 , or H_2O/Ar gas. The wavelength of light source passing through the gas medium was chosen by a vacuum monochromator, and its intensity was measured by a solar-blind PMT and accumulated by a multichannel analyzer.

After each discharge pulse ended, the gas medium shows an increase photoabsorption. The time durations of absorption increase linearly with Ar pressure, because of the radical diffusion time increasing with pressure. At an Ar pressure of 3 torr, the time duration is about 0.7 msec. The results indicate that the absorption is caused by the radicals produced by electrical discharge pulses. The electrons of energies higher than 11.5 eV will excite Ar into Ar^* metastables, which

then reacted with H_2O to produce $\text{OH} + \text{H}$.

At low H_2O concentration, the radicals are mainly OH and H . At high H_2O concentration, these radicals may react to produce other secondary radicals such as O , HO_2 , and H_2O_2 . These secondary reactions are noticed by the fact that the time dependence of absorption is greatly affected by H_2O concentration. In order to avoid the complication of secondary products, the OH absorption data were taken at low H_2O partial pressures (less than 10 mtorr).

The photoabsorption spectrum of OH was measured in the 1200-1370 Å wavelength region. The spectrum is consistent with previous observations¹ that OH has a high absorption at about 1200 Å and a small absorption at 1216 Å. The observed absorption spectrum is well correlated with the OH potential curves calculated by Dishoeck and Dalgarno.² The absorption peaks observed at 1354 and 1323 Å, at 1305 Å, and at 1223 Å correspond to the $\text{OH}(2^2\Sigma^-, 2^2\Pi, \text{ and } 3^2\Sigma^- \rightarrow X^2\Pi)$ transitions, respectively.

1) A. E. Douglas, Can. J. Phys. 52, 318 (1974).

2) E. Van Dishoeck and A. Dalgarno, private communication (1981).

* This work is based upon the work supported by NASA under contract no. NASW-3270. The data were taken at SRI International during the author's association with the Institute.

INDEX

Abramson, E. N1
 Adams, N. I1
 Anderson, J. G. D2, F3, F10, L1
 Anderson, L. G. I3

Barker, J. R. K1
 Baronavski, A. P. C2
 Bauer, R. K. M3
 Bayes, K. D. F15, L14
 Beck, W. F. I6
 Benson, S. W. G1
 Bércecs, T. B5
 Blickensderfer, R. P. I1
 Bondybey, V. E. C5, F4
 Breckrenridge, W. H. I1
 Bredohl, H. L2

Carrington, T. F2
 Castex, M. C. N3
 Carter, W. P. L. A1, H3, L13
 Chandler, D. W. C3
 Chou, J. S. A6
 Chu, J. K3

Dai, H. L. N1
 Day, R. L. F7, L8, N7
 DeGraff, B. A. F1
 DeKoven, B. M. C2
 de Mayo, P. M3
 Demas, J. N. F1
 Deraï, R. A4
 Deson, J. A5

Erler, K. A14
 Evans, D. K. L4
 Evenson, K. M. N5

Farneth, W. E. C3
 Ferris, M. J. L9
 Field, R. W. N1
 Filseth, S. V. F2
 Flynn, G. W. K3

Ghosh, S. D. K3
 Girardet, C. A5
 Gordon, R. J. H5

Aner, O. M5
 Apel, E. C. A9
 Aschmann, S. M. A1, H3
 Atkinson, R. A1, H3, L13

Breitenbach L. P. E4
 Brenner, D. M. M4
 Britt, P. F1
 Brown, J. M. N5
 Brudzynski, R. F8
 Brune, W. H. F3, L1
 Bunker, P. R. N5
 Burkhart R. D. A2
 Buss, R. J. A10, C4, F8
 Butler, L. J. C4, F8

Comes, F. J. M2
 Connell, P. S. E2
 Coveleskie, R. A. K4
 Crosley, D. R. A3
 Crutzen, P. J. E1

Diem, M. J4
 Doerr, F. L6
 Döhnert, D. F12
 Dolson, D. A. I4, K4
 Donohue, T. J3
 Dubois, I. L2
 Duignan, M. T. L3

Fournier, J. A5
 Fraser, M. E. H2
 Freeman, D. E. N6
 Frey, H. M. B1
 Friedl, R. R. F3

Grant, E. R. B2
 Gutman, D. G3, L5

Haaks, D. N3
Haas, Y. A6, M5
Halpern, J. B. F5
Heaven, M. C. C5, F4
Helvajian, H. C2, H4
Hepburn, J. W. C4
Ho, P. B3

Irwin, R. S. F11

Jackson, W. M. F5
Jennings, D. A. N5
Johnson, K. M. K5

Kaufman, F. G2
Kenner, R. D. K6
Keyser, L. F. A8
Killus, J. P. F6
Kinsey, J. L. N1

Laufer, A. H. G5
Le Calvé, J. N3
Lee, E. K. C. A9, J4
Lee, L. C. F7, L8, N7
Lee, Y. T. A10, C4, F8
Leone, S. R. I4

MacPherson, M. F15
Magnotta, F. E2
Maillard, D. A5
Maker, P. D. E4
Margitan, J. J. E3
Márta, F. B5
Marx, R. A4
Mauclaire, G. A4
Mautner, M. J2
McAlpine, R. D. L4
McDonald, J. R. H4
McGee, T. H. K3

Nee, J. B. F10
Nelson, H. H. H4, L5
Nicolet, M. E5

Ogryzlo, E. A. K6, L14
Okabe, H. B4

Houbrechts, Y. L2
Howard, M. J. A7
Hub, W. L6
Hudgens, J. W. L3
Hunyadi-Zoltán, Zs. B5
Hunziker, H. E. N2

Ishiwata, T. I

Johnston, H. S. E2
Jordan, B. N3
Jordan, K. D. I1

Kittrell, C. N1
Knepe, H. N2
Krajnovich, D. J. A10
Kurylo, M. J. I2

Leu, M. T. I5
Lewis, F. D. L6
Loge, G. F9, L9
Lorenz, K. G4
Lu, R. F5

McKellar, A. R. W. N5
McLean, A. D. N2
Melen, F. L2
Meyrahn, H. D4
Michl, J. F12
Miller, J. C. H5
Miller, T. A. C5, F4
Mohammed, H. H. A5
Moortgat, G. K. D4
Morris, P. F1
Morrison, R. J. S. B2
Munchak, S. C. K4

Niki, H. E4
Noble, M. A9

Osborn, M. K. A12
Oxman, F. L6

Paltenghi, R. L14
Paraskevopoulos, G. F11
Parkinson, W. H. N6
Parmenter, C. S. K4
Paschke, R. A14
Pasternack, L. H4

Qiu, L. X. G2

Ravishankara, A. R. D1, L12
Reisler, H. A13, A6, M1
Reisner, D. E. N1

Sadowski, C. M. F2
Savage, C. M. E4
Schneider, S. L6
Schuh, M. D. I6
Schultz, E. A. F15
Schwab, J. J. L1
Schwarz, F. P. J2
Sears, T. J. N5
Semmes, D. H. L12
Shinzawa, T. N4
Shokoohi, F. A13
Siegbahn, P. N2
Simons, J. P. K5
Simpson, F. T. L6
Singleton, D. L. L7
Slagle, I. R. G3

Tanaka, I. N4
Thomas, M. P. I6
Tlee, J. J. F13, L9
Toby, F. S. F14
Toby, S. F14

Umemoto, H. I1

Vaccaro, P. H. N1

Pease, R. K5
Penn, J. H. F12
Penner, J. E. D3
Pilling, M. J. F15
Pitts, Jr., J. N. A1, L13
Prasad, S. S. D5

Quick, Jr., C. R. F13, K3

Rentzepis, P. M. J1
Rossi, M. J. J5
Ruhman, S. M5

Smith, A. V. B3
Smith, G. P. A3
Smith, I. W. M. A7, A12, K2
Smith, M. F15
Spencer, M. N. M4
Sridharan, U. C. G2
Stedman, D. H. H2
Steinfeld, J. I. M4
Stephan-Rosbach, K. H. M2
Stephens, R. D. I3
Stimpfle, R. M. D2
Sullivan, B. J. A3
Sumida, D. A6
Sutoh, M. F7, L8
Swanson, D. E2

Tokumura, K. L10
Troie, J. C1
Trout, T. J. I6
Tso, T. L. J4

Wagal, S. S. F2
Wagner, G. A14
Wampler, F. B. L9
Ware, W. R. M3
Warneck, P. D4
Watson, T. A. A13
Wendt, H. R. N2
Weston, Jr., R. E. K3

Yoshino, K. N6

Zalotai, L. B5
Zare, R. N. C3
Zellner, R. A14, G4

Whitten, G. Z. L11
Wine, P. H. L12
Winer, A. M. A1, L13
Wittig, C. A6, A13, M1
Wolfrum, J. H1
Wrigley, D. J. A12
Wu, K. C. M3
Wyatt, J. R. L3

Zetzsch, C. A11
Zimmerer, G. N3
Zipf, E. C. D5